Investigation of Different Techniques to Upgrade Legacy WDM Communication Systems

Mousaab Nahas

Doctor of Philosophy

ASTON UNIVERSITY

July 2006

Aston University

Investigation of Different Techniques to Upgrade Legacy WDM Communication Systems

Mousaab Nahas

Doctor of Philosophy

May 2006

This thesis presents experimental investigation of different effects/techniques that can be used to upgrade legacy WDM communication systems. The main issue in upgrading legacy systems is that the fundamental setup, including components settings such as EDFA gains, does not need to be altered thus the improvement must be carried out at the network terminal.

A general introduction to optical fibre communications is given at the beginning, including optical communication components and system impairments. Experimental techniques for performing laboratory optical transmission experiments are presented before the experimental work of this thesis. These techniques include optical transmitter and receiver designs as well as the design and operation of the recirculating loop.

The main experimental work includes three different studies. The first study involves a development of line monitoring equipment that can be reliably used to monitor the performance of optically amplified long-haul undersea systems. This equipment can provide instant finding of the fault locations along the legacy communication link which in turn enables rapid repair execution to be performed hence upgrading the legacy system. The second study investigates the effect of changing the number of transmitted 1s and 0s on the performance of WDM system. This effect can, in reality, be seen in some coding systems, e.g. forward-error correction (FEC) technique, where the proportion of the 1s and 0s are changed at the transmitter by adding extra bits to the original bit sequence. The final study presents transmission results after all-optical format conversion from NRZ to CSRZ and from RZ to CSRZ using semiconductor optical amplifier in nonlinear optical loop mirror (SOA-NOLM). This study is mainly based on the fact that the use of all-optical processing, including format conversion, has become attractive for the future data networks that are proposed to be all-optical. The feasibility of the SOA-NOLM device for converting single and WDM signals is described. The optical conversion bandwidth and its limitations for WDM conversion are also investigated.

All studies of this thesis employ 10Gbit/s single or WDM signals being transmitted over dispersion managed fibre span in the recirculating loop. The fibre span is composed of single-mode fibres (SMF) whose losses and dispersion are compensated using erbium-doped fibre amplifiers (EDFAs) and dispersion compensating fibres (DCFs), respectively. Different configurations of the fibre span are presented in different parts.

Key words and phrases

Fibre-optics, optical transmission, legacy WDM communication systems and networks, submarine cable networks, long-haul undersea systems.

Acknowledgments

First of all, I would like to thank Prof Keith Blow who has been my supervisor during my three years PhD programme and has provided me with much appreciated help and advice.

Secondly, I would like to thank Azea Networks for the financial support, technical help and advice during my research. This thank should include: Dr Stuart Barnes (the director of engineering), Steve Webb, Steve Desbrulais, John Ellison and Joerg Schwartz. I also thank Wai Wong who has provided me with the simulation results for the LME work presented in chapter 3.

I would also like to thank Robin Ibbotson for his practical assistance during my experiments especially in the first year when I was developing my experimental skills. I should not forget to thank Paul Harper for the valuable assistance he has given me in the last year which helped me completing my experimental work on time. Paul's help has also included providing the software codes for generating different PRBS data and loading them to the pattern generator/BERT for the work of chapter 4.

I would also like to acknowledge Mohammad Halim Wahid who I have worked closely and collaborated with in the work shown in chapter 5.

I would also like to take this opportunity to thank all other members of the Photonics Research Group of Aston University who I have not mentioned here.

I would also like to acknowledge the financial support of the EPSRC.

Finally, I would like to give very special acknowledgment to my wife Hazar Monla for her patience and strong support during my PhD research. This special acknowledgment should also extend to my parents for their great encouragements during the research as well.

Contents

List of Figures

List of Tables

Chapter 1

Introduction to optical fibre communications

Optical fibre communication systems have been deployed worldwide since 1980 and have indeed revolutionised the technology behind communications. The main advantage of using optical fibre channels in data transmission is that the bandwidth is very large, compared to that in conventional coaxial copper cables used in telephone networks. In addition, the loss in the signal can be minimised by using a suitable wavelength in the optical source. For instance, today's standard single-mode fibre (SMF) has an attenuation of approximately 0.2dB/km at a wavelength of 1550nm. In fact, optical fibre channels can provide the fundamental backbone of the world's communications networks since they can carry high bit-rates of information over tens of kilometres before amplification is required [1]-[4]. This allows data transmission over point-to-point lines with several hundreds of kilometres for terrestrial links and several thousands of kilometres for trans-oceanic links using large spacing between optical repeaters. Such large spacing can indeed minimise the initial cost of installing the transmission links specially that of the trans-oceanic systems. Trans-oceanic systems are usually referred to as undersea or submarine systems because fibre cables were designed for deep-water operation (up to 8km depth). In addition, these undersea systems can also be referred to as legacy systems as over 600,000km of fibre cables have already been installed across the world's oceans since 1990. The first undersea fibre systems were installed across the Atlantic and the Pacific oceans in 1988 and 1989 respectively where the capacity was 280Mbit/s [5]. These systems employed electro-optic repeaters along the fibre cables where the incoming signal was converted from optical to electrical, regenerated and then reconverted to optical for transmission. The transmission capacity was then increased from 280Mbit/s up to 2.5Gbit/s with more repeater spacing by using lasers with 1550nm wavelength in place of 1300nm. However, utilising the large bandwidth of the optical fibre was limited in these systems by the capacity of the electronic repeaters. Therefore, undersea optical fibre systems started to employ optical repeaters in the mid of 1990s where the demand for large bandwidth increased due to the dramatic growth of the data communication services, such as the internet, e-mail...etc. Today's optical repeaters use erbium-doped fibre amplifiers (EDFAs) whose bandwidth is sufficient to support many optical signals, hence large capacity. However, transmitting many optical signals through the fibre simultaneously required multiplexing at the transmitter. Nowadays' optical fibre communication systems use two multiplexing techniques: Wavelength-division multiplexing (WDM) and optical time-division

multiplexing (OTDM). In WDM, different data channels with different wavelengths are combined in a single stream and transmitted together along the fibre cable [6]-[8]. Therefore for N channels, the aggregate system is transmitting at N times the individual laser speed, providing a significant capacity enhancement. The channels are separated at the receiver by demultiplexing where each channel is sent to its own destination. The spacing between the adjacent channels has to be large enough to avoid channel overlapping during multiplexing/demultiplexing process. In OTDM, channels are spaced apart in time domain to form the composite bit stream. Therefore, all channels are carried by the same optical wavelength but share the time [9]-[10]. This can only be achieved with return-to-zero format (RZ), which is discussed in the next section.

As this thesis will investigate different techniques to upgrade legacy optical communication systems, this chapter is designated to give an overview of the main aspects of such systems including components and system impairments.

1.1 Optical fibre communication system components

Similar to all communication systems, optical fibre communication system consists of three main components: transmitter, communication channel, which is a fibre cable, and receiver. The transmitter and receiver are designed to meet all of the needs of optical communications channels. This section provides general overview on each of the above components individually.

1.1.1 Optical transmitter

The optical transmitter converts the electrical signal into an optical form and then launches the resulting signal into the transmission fibre. The major component of the transmitter is the optical source, which is often a semiconductor source such as semiconductor laser or light emitting diode (LED) [11]. These semiconductor sources have several advantages like: compact size, high efficiency, long life hence good reliability and small emitting area compatible with the fibre core size. Semiconductor laser emits light through stimulated emission while LED uses spontaneous emission. As a result of stimulated emission, the semiconductor lasers can provide an intense, coherent and quasi-monochromatic source of light [12]. This allows emitting light with high power (up to 10mW), high coupling efficiency into the fibre and relatively narrow spectral width. The latter (narrow spectrum) allows operation at high bit-rates with less significant dispersion (discussed in 1.2) and high spectral efficiency. In general, most of optical fibre communication systems use semiconductor lasers due to their superior performance compared with LEDs. The experimental work of this thesis will therefore employ semiconductor

lasers at transmitters. However, the output wave of the optical source is modulated by applying electrical data signal either directly to the optical source or indirectly using an external modulator. Obviously, direct modulation simplifies the transmitter design thus it is cost-effective choice. Nevertheless, indirect modulation is commonly used with high bit-rates (≥10Gbit/s) giving that the modulator is another major component of the transmitter for those systems operate at high bit-rates. In fact, intensity modulation is commonly used in optical communications systems, where there are two types of optical modulators: the electro-absorption modulator (EAM) and lithium niobate ($LiNbO_3$) Mach-Zehnder modulator. The EAM modulator is a bulk layer device based on the principle of Franz-Keldysh effect [13] i.e. changing the absorption spectra near the bandgap of the semiconductor by applying an electric field. This effect is enhanced by using multi-quantum well structure where the effect is called Stark effect [14]. Such electro-absorption effect is used to perform intensity modulation where the applied electric field shifts the band-edge hence increasing the absorption of light. In other words, as the field is reverse-biased, the absorption edge broadens inducing attenuation or absorption [15]-[19]. An advantage of this modulator is that it is made from the same semiconductor material that is used for the laser, thus the two can be integrated on the same chip.

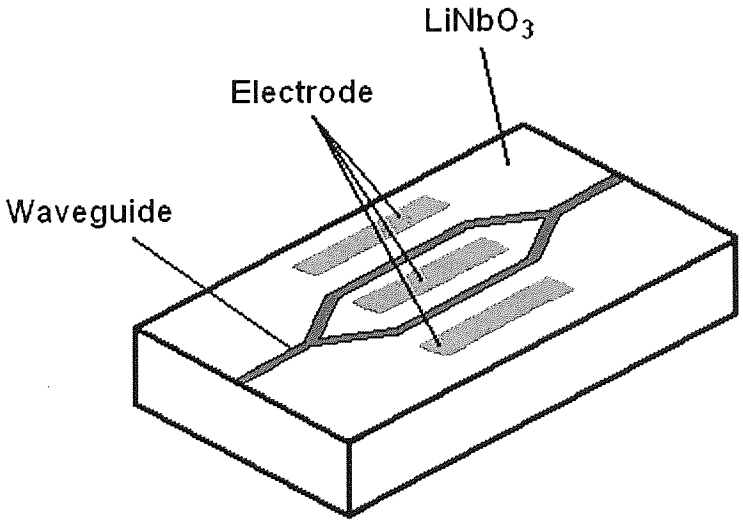

Figure 1.1 $LiNbO_3$ Mach-Zehnder modulator.

$LiNbO_3$ Mach-Zehnder modulator makes use of the electro-optic $LiNbO_3$ material and Mach-Zehnder (MZ) interferometer [20]-[25]. Figure 1.1 shows a diagram for this type of modulators; the MZ interferometer is composed of two arms which are titanium-diffused $LiNbO_3$ waveguides. The input light splits into two parts that propagate through the MZ arms with

identical phase shift. Thus at the output of the MZ interferometer, the two signals interfere constructively. A phase shift is introduced in one arm by applying an external voltage that changes the refractive index of the $LiNbO_3$ material thus destroys the constructive interference. This basically results in reducing the transmitted intensity. For instance, if the phase difference between the two arms is π, no light will be transmitted. However, if electrical bit stream is applied to the modulator, it will produce an optical replica of the bit stream. This results in optical data stream at the modulator output. The performance of the modulator is characterised through the extinction ratio, which is the on-off ratio, and the modulation bandwidth. Recent $LiNbO_3$ modulators can provide extinction ratio of more than 20dB and bandwidth of 75GHz [21]. $LiNbO_3$ modulator has been chosen as amplitude (or intensity) modulator for the experimental work of this thesis since it provides stable operation over a large range of temperatures, very low bias-voltage drift rates and very high intrinsic modulation bandwidth [25].

At the modulator it is necessary to decide how the electrical signal would be converted into an optical bit stream, i.e. which modulation format is required. There are two conventional modulation formats; return-to-zero (RZ) and non-return-to-zero (NRZ) formats [26]-[27]. In RZ, the amplitude returns to zero before the bit duration expires. Therefore, the pulse representing bit 1 is shorter than the bit slot [28]. In NRZ, the amplitude does not return to zero between two successive 1-bits but remains on throughout the bit slot. This causes a variation in the pulse width depending on the bit pattern whereas it is still the same for all pulses in RZ format.

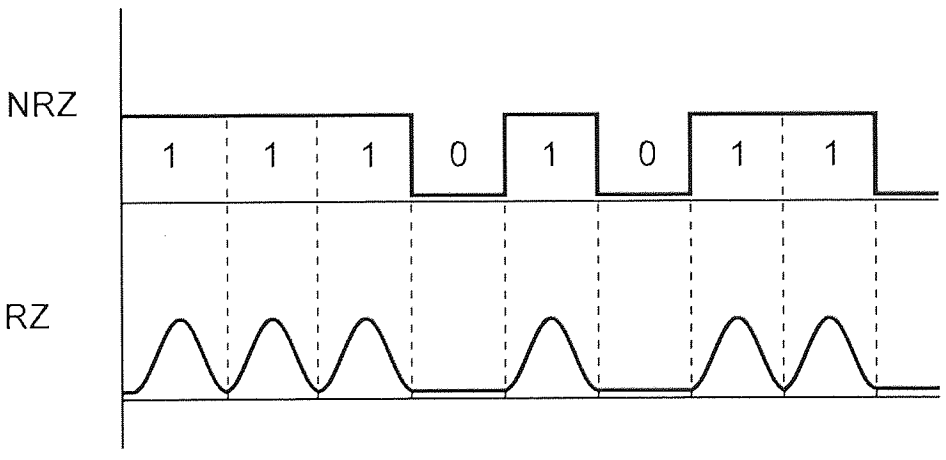

Figure 1.2 Schematic representation of the NRZ and RZ formats.

Example of bit stream using NRZ and RZ is shown in figure 1.2. The advantage of NRZ format is that it has smaller bandwidth than that of the RZ format basically because the on-off transitions occur fewer times. However, RZ pulses are used in most optical communication

systems since they are more tolerant to chromatic dispersion as well as the inter-symbol interference (ISI). It is found that RZ pulses can be used in the design of high-capacity communication systems using WDM and OTDM techniques [29]. For these reasons, RZ format will be used in most of the transmission experiments in this thesis. In general, there are different factors to be considered in choosing the format such as spectral efficiency, power margin and tolerance to fibre dispersion and nonlinear effects (the latter are discussed in section 1.2).

As alternatives to RZ and NRZ, several other modulation formats have been proposed such as chirped return-to-zero (CRZ), carrier-suppressed return-to-zero (CSRZ), single-sideband RZ (SSB-RZ) and duobinary modulation formats [30]-[38]. CRZ and CSRZ have been evolved from RZ format. In CRZ the optical pulses in each bit slot are chirped before they are launched into the optical fibre. Therefore, the signal can propagate through the fibre in presence of dispersion, nonlinearity and accumulated noise with more tolerance than the original un-chirped RZ. CSRZ is discussed in chapter 5, where the main carrier component is suppressed and spectral width narrows thus the system is also more tolerant to dispersion and nonlinearity impairments compared to the original RZ. In both CRZ and CSRZ, phase modulation is required in addition to amplitude modulation, which in turn increases the transmitter complexity.

At the output of the modulator, transmitters usually have optical amplifier (referred to as *booster*) to ensure sufficient power at the input of the fibre. This power is called launch power which is an important parameter as it can increase the repeater spacing if it is increased but is also limited by the nonlinear effects induced during transmission.

1.1.2 Optical fibre

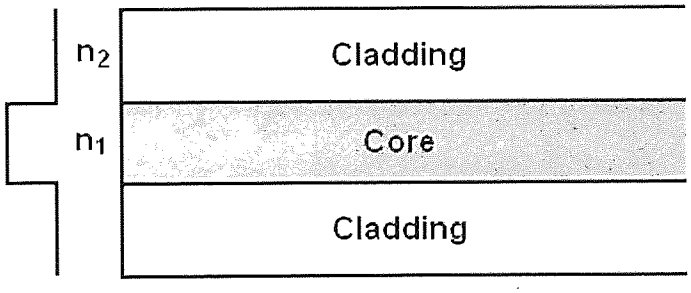

Figure 1.3 Schematic diagram of step-index fibre.

Optical communication systems use optical fibre as a communication channel that transports the optical data from transmitter to receiver. Optical fibres are classified into several

types according to their refractive index profiles, where the most common type used in communication systems is called *step-index fibre*. Figure 1.3 shows the schematic of this type; the fibre consists of a cylindrical core surrounded by a cladding. Both the core and the cladding are made form transparent silica glass but the refractive index of the core is greater than that of the cladding. Therefore, step-index fibre transports the optical signal by using the principle of total internal refraction, i.e. the incident ray is refracted away from the normal if the incident angle does not exceed the critical angle [39]. In fibre, the light will be totally internally reflected when it hits the core sides, and thus is guided along the fibre core. Step-index fibres can support number of propagation modes determined by a parameter called *normalised frequency* (V) and defined as:

$$V = \frac{2\pi}{\lambda} a(n_1^{\,2} - n_2^{\,2})^{1/2} \tag{1.1}$$

where a is the core radius, n_1 and n_2 are the refractive indices of the core and cladding respectively and λ is the wavelength of the optical source. If $V < 2.405$; the fibre can support only one propagation mode, which is called fundamental mode of the fibre, and the fibre is referred to as *single-mode fibre* (SMF). Otherwise the fibre will support many modes and referred to as *multimode fibre*. The approximate number of propagation modes can be given by $V^2/2$ [11]. Practically, single-mode fibre is designed such that all higher-order modes are cut-off at the operating wavelength. This is done by choosing a core diameter in the region between 5 and 10μm. Such small core makes it difficult to couple the light into the fibre which adds more complexity and cost to the system. Nevertheless, single-mode fibre is being used in this thesis experiments since its loss can be as small as 0.2dB/km if the wavelength is around 1550nm, and can also reduce the effect of dispersion.

1.1.3 Optical receiver

The optical receiver converts the optical signal received at the output end of the fibre into the original electrical signal to recover the data transmitted through the system [40]. The main component of the optical receiver is a photodetector, which detects the light and converts it back into electricity through the photoelectric effect. Photodetectors usually use semiconductor photodiodes due to their capability with the whole system. The main advantages of the

semiconductor photodiodes are that they have high sensitivity, fast response, low noise, low cost, high reliability and small size compatible with the fibre core size. The most common semiconductor photodiodes used in optical communication systems are PIN and Avalanche (APD) photodiodes. PIN photodiodes use the PIN structure where the depletion region of the semiconductor material is made as large as possible. This is achieved by having a lightly-doped intrinsic layer between the heavily-doped p-type and n-type materials, thus most of the photons are absorbed within the depletion region. Each absorbed photon ideally produces one electron-hole pair i.e. one electron flowing in the external current produced. The detection process within the PIN photodiode is characterised by quantum efficiency which is the probability that each photon will generate an electron-hole pair. In APD photodiodes, a few incident photons result in many carriers being produced and an increased external current. To achieve this, the APD relies on the phenomenon of avalanche multiplication where each primary electron-hole pair is accelerated in a strong electric field which can cause the generation of several secondary electron-hole pairs through the effect of impact-ionisation. This results in amplifying the produced photocurrent [41]-[42]. In general, the APD photodiodes are faster than the PIN photodiodes and have higher sensitivity but they are more expensive and require much higher bias voltage. However, PIN photodiodes are used in the experimental work of this thesis.

The second major component of the receiver is the demodulator which is used to recover the original data bit sequence. The design of the demodulator depends on the modulation type, e.g. FSK, PSK ...etc, used at transmitter. As most optical communication systems use intensity modulation, the whole modulation/demodulation scheme is referred to as *intensity modulation with direct detection* (IM/DD). In this scheme, the demodulator has an electric decision circuit which simply identifies the 1 and 0 bits according to amplitude of the received electrical signal.

After demodulation, the performance of the system can be quantified by the following parameters: bit-error-rate (BER), Q-value or the opening of eye diagram. BER can be defined as the average probability of incorrect bits detected at the receiver. This means that a BER of 10^{-6} corresponds to one error per million bits. Real optical communication systems operate at BER much lower than 10^{-9}, where this value is commonly used as a reference level for acceptable performance. Practically, an advanced digital bit-error-rate tester (BERT) can be used at the receiver for direct BER measurements.

Q-value (also called Q-factor) measures the quality of the received signal and is related to the BER as [43]:

$$BER \approx \frac{\exp(-Q^2/\ 2)}{Q\sqrt{2\pi}} \tag{1.2}$$

Figure 1.4 shows the variation of the BER with the Q-value. The BER improves as Q increases where BER $=10^{-9}$ is corresponding to $Q = 6$, which thus can be the minimum acceptable Q-value.

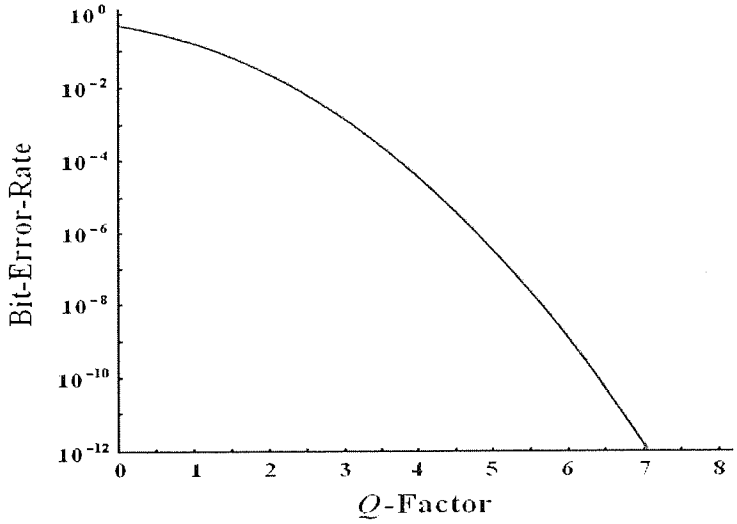

Figure 1.4 The variation of bit-error-rate with Q-value

Practically, Q is measured from the eye diagram displayed on a sampling scope. The eye diagram provides a visual way of quantifying the system performance. It is formed by superposing number of bit sequences in the bit stream on the top of each other. Therefore, the more eye opening observed; the better performance achieved. Figure 1.5 shows examples of the eye diagrams for both optical RZ and NRZ signals. Q-value measurement is then performed by measuring the mean values and standard deviations of the 1 and 0 levels and by using the following formula:

$$Q = \frac{\mu_1 - \mu_0}{\sigma_1 + \sigma_0} \tag{1.3}$$

where μ_1 and μ_0 are the mean values of the 1 and 0 bits respectively, and σ_1 and σ_0 are the standard deviations of the 1 and 0 bits respectively. More details are presented in chapter 2.

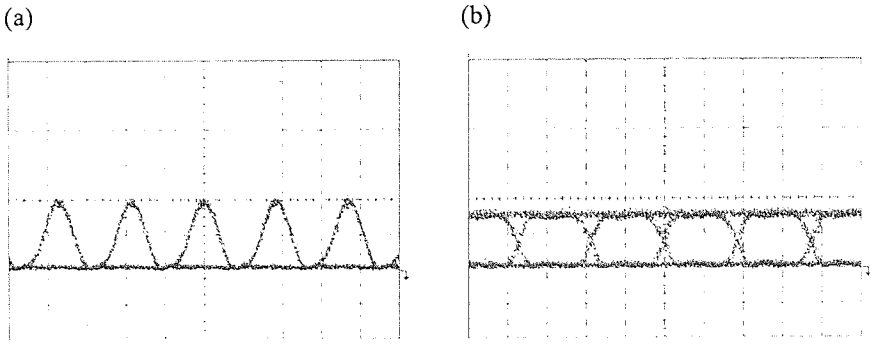

Figure 1.5 The eye diagram: (a) RZ; (b) NRZ.

The system performance can also be characterised through the optical signal-to-noise ratio (OSNR) measurement, which is the ratio of the received optical signal power to the noise signal power. Therefore, OSNR measurement must be performed before demodulation where the signal is still in the optical domain. Knowledge of the OSNR is important because it provides information of the received noise that is mostly generated by the optical amplifiers used along the communication channel. OSNR is also related to the BER in digital communication systems, thus it can indicate the quality of the overall system. Practically, OSNR can be measured directly on an optical spectrum analyser (OSA) - details are in chapter 2.

An important parameter associated to receiver performance is the *receiver sensitivity*, which is defined as the minimum average received optical power required for BER = 10^{-9} or Q = 6. Receiver sensitivity depends on the received electrical signal-to-noise ration (SNR) which in turn depends on various noise sources. In addition to the amplifier noise generated during transmission, other noise sources are imposed by the receiver itself such as quantum noise (or shot noise) that is introduced by the photodetection process, and thermal noise. The receiver sensitivity is therefore determined by the accumulative effect of all possible noise mechanisms that degrade the SNR at the decision circuit of the receiver [43].

1.2 Optical communication system impairments

1.2.1 Fibre loss

Fibre loss is one of the main factors that limit the performance of the optical communication system. It reduces the average power reaching the receiver, thus decreasing the OSNR and also limits the maximum repeater spacing along the fibre channel. The loss can be determined by using the following relation:

$$Loss = \alpha L = -10\log\left(\frac{P_{out}}{P_{in}}\right) \tag{1.4}$$

where α is the fibre attenuation (or loss) coefficient measured in dB/km, L is the fibre length in km, P_{in} and P_{out} are the fibre input and output powers, respectively. If the fibre attenuation coefficient is known, equation (1.4) can be used to calculate the attenuation limit of the fibre length (L), hence the amplifier spacing. In fact, fibre loss depends on the wavelength used at the optical source. Figure 1.6 shows the loss as a function of the wavelength for the conventional single-mode fibre [43].

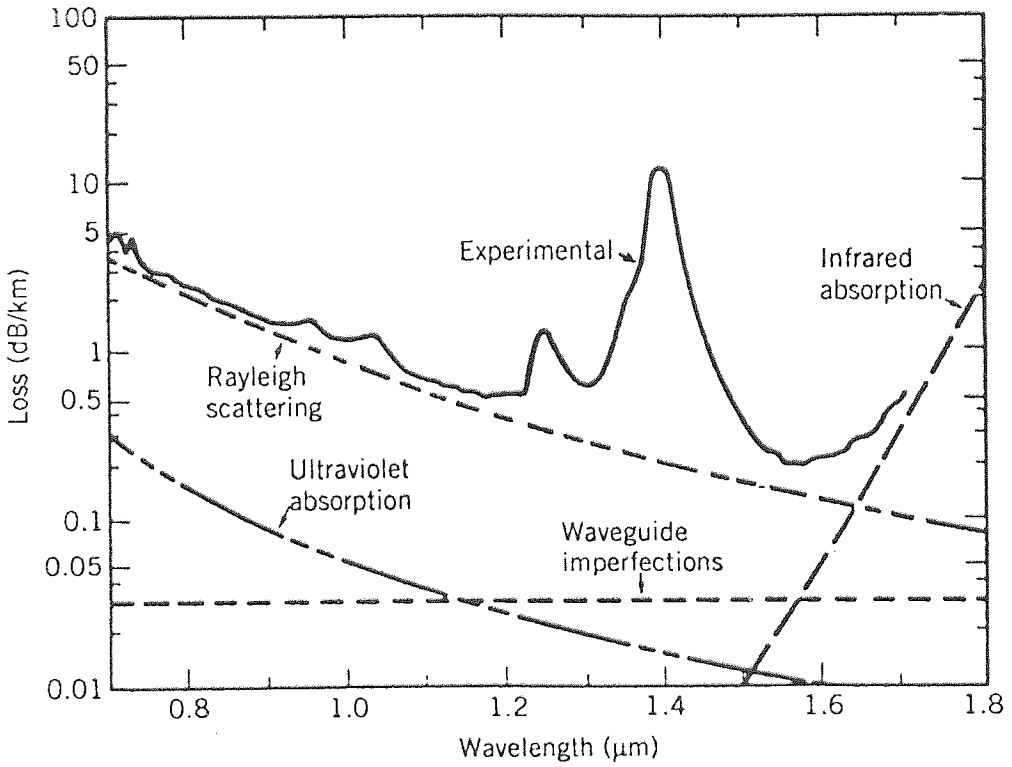

Figure 1.6 Loss spectrum of a single-mode fibre. Curves of several loss mechanisms are shown.

There are several mechanisms that contribute to the overall losses where the most important two among them are material absorption and Rayleigh scattering [39]. Material absorption can be divided into two types: intrinsic and extrinsic absorption. In intrinsic absorption, the light is absorbed by fused silica (the material used to make the fibre) at certain wavelengths. In extrinsic absorption, the light is absorbed by the impurities of the OH ions within the silica. The fundamental absorption peak of these OH ions is near 2700nm but its harmonic and combination

tones with silica produce another absorption peaks at 950, 1240 and 1400nm. Rayleigh scattering originates from the variation in the glass structure as it is not a uniform structure and has local fluctuations in density. These fluctuations lead to fluctuations in the refractive index on a scale shorter than the wavelength of the signal light thus incident light scatters inside the fibre. Rayleigh scattering is actually proportional to λ^{-4} and dominates at shorter wavelengths. However, if all of the above mechanisms are incorporated, the overall loss curve, denoted in figure 1.6 as experimental, can identify three traditional operating widows for optical communications. Each of these windows is related to different generation of the optical fibre communication systems. The first window is at 850nm where the loss is ~10dB/km. The second window is at 1300nm where the loss is 0.5dB/km and dispersion is zero. Finally, the third window, which is used in most recent communication systems, is at 1550nm where the loss is 0.2dB/km but dispersion is high (solving dispersion problem is discussed in the next section).

Additional extrinsic losses are introduced from launching light into the fibre, bending the fibre and splicing fibres together. Bending the fibre changes the angle of the incident ray which in turn destroys the total internal reflection if it exceeds the critical angle. This results in that the light will be reflected out of the fibre core, introducing considerable loss. Bending is normally avoided by surrounding the fibre by a strong layer so that large bending is impossible. Furthermore, the connectors used between fibres and other components to form the overall fibre link also introduce additional losses to the system. Fibre losses are basically compensated by the in-line optical amplifiers using either semiconductor optical amplifiers or EDFAs. EDFAs (which are discussed in section 1.3) are more commonly used because they are all-optical and bit-rate independent as apposed to semiconductor optical amplifiers.

1.2.2 Fibre dispersion

Dispersion is another limiting factor in optical communications as it leads to a considerable broadening of optical pulses after long propagation distance. This broadening will cause the adjacent data bits to overlap thus corrupting the data signal. There are two main types of dispersion: intramodal and intermodal dispersion. Intramodal dispersion is also known as chromatic dispersion since no source is truly monochromatic and is introduced because different spectral components of the pulse travel at slightly different group velocities. Thus it can also be referred to as group-velocity dispersion (GVD). Intermodal dispersion is related to the different mode indices hence group velocities associated with different propagation modes. It can appear only in multimode fibres since only one mode is guided in a single-mode fibre. This is the main

advantage of single-mode fibres. However, there are two sources of fibre dispersion: material dispersion and waveguide dispersion. Material dispersion manifests itself through the frequency dependence of the refractive index $n(\omega)$ of the material. As the propagation velocity is determined by the refractive index, different frequency components will suffer different delays as they propagate through the fibre. Waveguide dispersion is the dispersive contribution of the waveguide structure. It occurs as a result of light distribution between the core and cladding. This can be realised as not all light propagating in the fibre is confined to the core thus the light travelling in the cladding will have slightly different velocity due to a slightly different refractive index. Waveguide dispersion depends on the refractive indices and the dimensions of the core and cladding. Therefore, by altering these parameters waveguide dispersion can be adjusted thus improving the resultant dispersion characteristics of the fibre.

As a result, chromatic dispersion can be the total of both material dispersion and waveguide dispersion. In general, waveguide dispersion is relatively small in comparison with material dispersion contribution. Therefore, the total dispersion which is expressed by a dispersion parameter D and measured in ps/(km-nm) can be described in the following equation:

$$D = -\frac{\lambda}{c}\frac{d^2 n}{d\lambda^2} \tag{1.5}$$

where λ is the source wavelength, c is the speed of light and n is the core refractive index which is wavelength dependent. Figure 1.7 shows the variation of the dispersion parameter D with wavelength for standard single-mode fibre. It can be seen that $D = 0$ at a wavelength of 1300nm, which is the second operating window and is called zero-dispersion wavelength (λ_{ZD}). At the third window i.e. 1550nm, the dispersion is approximately 17ps/(km-nm) which is reasonably high but the loss is at minimum. Therefore, to operate the system at such window, dispersion can be compensated by adding a new fibre with negative dispersion of 17ps/(km-nm) to the conventional single-mode fibre. The length of this new fibre can be determined by using:

$$D_1 L_1 + D_2 L_2 = 0 \tag{1.6}$$

where D_1 and L_1 are dispersion and length of the conventional SMF fibre, respectively, and D_2 and L_2 are the same for the additional fibre. Such additional fibre is called *dispersion-compensating fibre* and denoted by DCF [44]-[47].

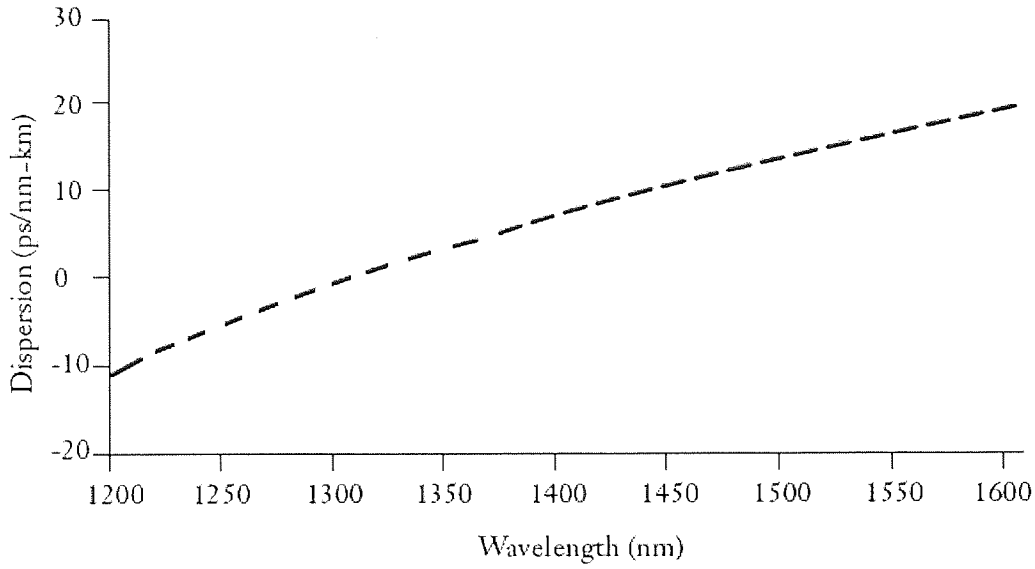

Figure 1.7 Dispersion versus wavelength for standard single-mode fibre.

In fact, it is possible to design a fibre such that λ_{ZD} is shifted into the 1550nm region rather than 1300nm as in the SMF, and such fibre is called *dispersion-shifted fibre* (DSF). This fibre has been developed for use of 1550nm without need of the DCFs along the fibre link. Another solution for dispersion can be implemented by tailoring the waveguide contribution such that the total dispersion D is relatively small over a wide wavelength range extending from 1300 to 1600nm. Such fibre is referred to as *dispersion-flattened fibre* [43].

In this thesis, transmission experiments will use SMFs and DCFs due the availability of these fibres that are used in most legacy systems.

1.2.3 Fibre nonlinearity

Dielectric materials, including optical fibres, suffer from nonlinearity as their response to light becomes nonlinear for intense electromagnetic fields [48]. Although silica is not highly nonlinear material, the waveguide geometry that confines light inside a small cross section over long length of fibre makes nonlinear effects very important to take into account in designing and operating systems. There are three nonlinear phenomena that are most relevant to optical fibre communications: stimulated light scattering, nonlinear phase modulation and four-wave mixing.

Stimulated light scattering can be understood as an interaction between the electric field of the optical signal and the silica molecules of the fibre during propagation. This results in inelastic scattering effects such as stimulated Raman scattering (SRS) and stimulated Brillion scattering

(SBS). SRS occurs due to the photons interaction (hence scattering) with the medium while SBS is due to the interaction between the acoustic properties of photons (called phonons) with the medium. Both scattering processes result in a loss of power at the incident frequency where the electric field transfers part of its energy to the medium. Although SRS and SBS are similar in the origin, a main difference between them is that SRS in optical fibre occurs in both the forward and backward directions while SBS occurs only in the backward direction. This is related to the dispersion properties of the optical photons (associated with SRS) and acoustic phonons (associated with SBS). However, simulated light scattering effects can be negligible at low power levels but are important at high powers as they lead to a considerable degradation in the system performance.

Nonlinear phase modulation originates as the refractive index of silica becomes intensity dependent at high incident powers and can be described as the following [49]:

$$n(I) = n_0 + n_2 I \tag{1.7}$$

where n_0 is the linear refractive index of the core, n_2 is the nonlinear coefficient ($\sim 2.6\times10^{-20}$ m^2/W for silica fibre) and I is the intensity which is related to power as $I = P/A_{eff}$ (A_{eff} is the effective area of the fibre core $\sim 80\mu m^2$ for SMF and $\sim 50\mu m^2$ for DSF). This intensity dependence of the refractive index is referred to as *Kerr-nonlinearity* (or *Kerr-effect*) which results in induced-phase shifts in the propagating signal, and hence spectral broadening. This can be understood as the phase of the optical signal is dependent on the refractive index of the fibre hence the intensity according to (1.7). As the intensity is time dependent for data signal, the phase will thus be time dependent, i.e. the optical phase will change with time in exactly the same manner as the intensity of the signal. Since the frequency is the rate of change of the phase with time, the frequency spectrum will change as the signal propagates along the fibre, leading to considerable spectral broadening after long distance. This effect is called self-phase modulation (SPM) where the phase shift is self-induced i.e. by the optical field of the propagating signal. The nonlinear phase shift induced by SPM is given by:

$$\phi_{NL} = \gamma P_{in} L_{eff} \tag{1.8}$$

where $\gamma = 2\pi n_2/(A_{eff}\lambda)$ is an important nonlinear parameter measured in W^{-1}/km, P_{in} is the incident power and L_{eff} is called the effective interaction length defined as $[1-\exp(-\alpha L)]/\alpha$ and can be approximated as $1/\alpha$ where $\alpha L >> 1$ in practice [48]. Another type of phase modulation is called cross-phase modulation (XPM), and occurs when two or more channels are transmitted simultaneously inside the fibre using the WDM technique. The nonlinear phase shift of each channel will therefore depend not only on its power but also on the power of other channels [50]. The phase shift for the *i*th channel is given by [48]:

$$(\phi_{NL})_i = \gamma L_{eff}\left(P_i + 2\sum_{m\neq i} P_m\right) \tag{1.9}$$

where the sum is taken over the number of channels. The factor of 2 indicates that XPM is twice as effective as SPM for the same amount of power. The total phase shift therefore depends on the power in all channels and also varies from bit to bit depending on the bit pattern of the adjacent channels. The worst case is when all channels carry 1-bits simultaneously, assuming equal channel powers. However, since the nonlinear phase shift proportionally depends on the nonlinear parameter γ which inversely depends on the effective area, nonlinear effects can be reduced considerably by increasing A_{eff}. A new type of fibre known as *large effective-area fibre* (LEAF) has been developed for reducing the effect of nonlinearities [51]-[52].

Four-wave mixing (FWM) originates when three optical fields with different carrier frequencies propagate inside the fibre simultaneously. A fourth field is generated with a new frequency depending on those three frequencies. If three optical signals have carrier frequencies ω_1, ω_2 and ω_3, the new frequency ω_4 will be related to the original frequencies as:

$$\omega_4 = \omega_1 \pm \omega_2 \pm \omega_3 \tag{1.10}$$

Therefore ω_4 can have several values corresponding to different combinations of pluses and minuses in (1.10) where the most troublesome combination in practice is $\omega_1 + \omega_2 - \omega_3$ if the channel wavelengths are close to zero-dispersion wavelength [48]. Obviously, FWM never appears in single-channel transmission systems, but it becomes a limiting factor in multiple-channel systems using WDM technology. The effect can be understood as significant amount of

channel power transfers to adjacent channels and such an energy transfer can lead to an inter-channel crosstalk in addition to the power loss results in each individual channel.

However, it is difficult to determine the effect of the XPM and FWM on the performance of WDM communication systems because the above discussion assumed that they act in isolation without dispersive effects. Practically, pulses of different channels travel at different speeds due to the presence of dispersion. The XPM-induced phase shift and FWM effect can occur only when two pulses overlap in time. For high dispersion i.e. widely separated channels, pulses overlap for such a short time that XPM and FWM effects are virtually negligible. Modern WDM systems avoid XPM and FWM by using fibres with high local dispersion such as SMFs and DCFs. It is found that at least 4ps/nm/km dispersion can be enough to suppress FWM [43].

1.2.4 Fibre birefringence

Single-mode fibre actually supports two orthogonally polarised modes that correspond to the two orthogonal electrical and magnetic field components of the propagating signal. If the fibre is ideal, i.e. has perfectly cylindrical core with uniform geometry, these modes must have the same propagation speeds hence no polarisation dependence. In practice, it is impossible to manufacture such perfect fibre where real fibres have non-uniform geometry due to unintentional variation in the fibre core structure and anisotropic stresses along the fibre length. This results in a difference in the refractive indices for the two modes hence difference in propagation velocities. This phenomenon is known as birefringence and is defined as:

$$B = \left| n_x - n_y \right| \tag{1.11}$$

where n_x and n_y are the indices of the orthogonally polarised fibre modes. In conventional SMF, birefringence is undesirable because it is not constant along the fibre thus leads to a random power exchange between the different modes during propagation. Therefore, the linearly polarised launched light will quickly reach a state of arbitrary polarisation. Moreover, birefringence leads to dispersion called *polarisation-mode dispersion* (PMD) where different frequency components of the pulse acquire different polarisation states. This type of dispersion becomes a limiting factor for optical communications operate at high bit-rates. In fact, birefringence problem of the SMF can be minimised by using in-line polarisation controllers in the system. Furthermore, it is possible to make fibres with nearly constant birefringence over the length that allows signal to propagate without variation in the polarisation state. These fibres are

referred to as *polarisation-maintaining fibres* and can be manufactured by changing the structure of the fibre core to elliptical shape or by introducing stress into the fibre [43]. Polarisation-maintaining fibres actually have large degree of birefringence such that small random birefringence fluctuations do not affect the light polarisation significantly [48].

1.3 Erbium-doped fibre amplifiers (EDFAs)

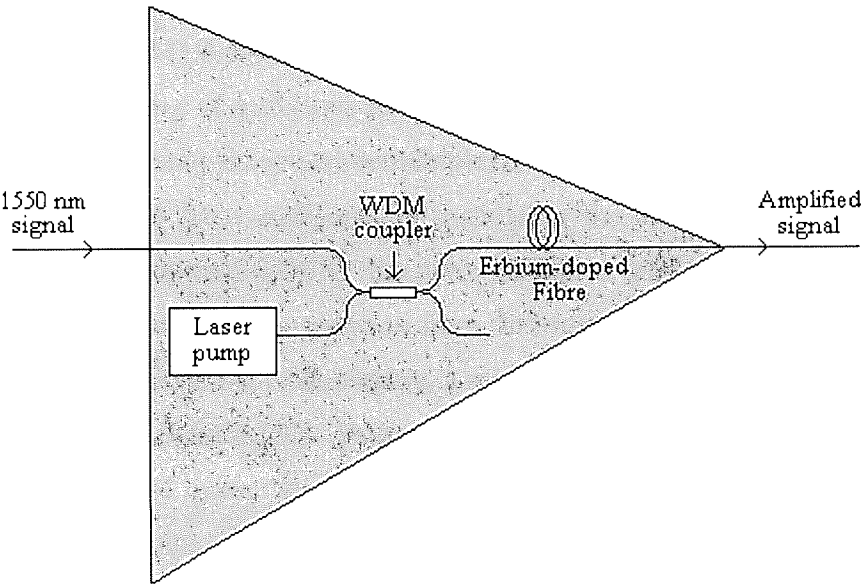

Figure 1.8 Erbium-doped fibre amplifier (EDFA).

Erbium-doped fibre amplifiers (EDFAs) are all-optical repeaters that amplify the optical signal directly, without opto-electronic and electro-optical conversion. They were first reported in 1987 and the first commercial amplifiers were available in 1990 [53]. The design of EDFA is simple where it uses a short length of optical fibre doped with the rare-earth element erbium. The typical configuration of an EDFA can be shown in Figure 1.8; it consists of a laser pump, WDM coupler and erbium-doped fibre. Amplification is implemented as the laser pump couples light into the fibre at wavelengths of either 980 or 1480nm. This light excites the atoms in the erbium-doped section of the fibre hence exciting the electrons into higher energy state so that they can decay to release photons at different wavelengths. When the incoming signal in the region around 1550nm passes through the fibre, it stimulates the excited erbium atoms thus the electrons emit photons at the same wavelength of the incoming signal during the transition from high energy state back to the ground level. As a result, the incoming optical signal is amplified as it

propagates through the erbium-doped fibre. In fact, using 980nm pump can excite the electrons into energy state higher than that reached by 1480nm pump, hence provides larger gain. At the output of the erbium fibre, the amplified signal is usually passed through an optical isolator which prevents any reflected light from entering the erbium fibre. EDFAs are used in the experimental work of this thesis since they can have high gain over large optical bandwidth in the region around 1550nm (the third communication window) [54]-[55]. This region is referred to as conventional or central wavelength band (C-band) which extends between 1530-1570nm. EDFAs can also be made to support longer wavelengths from 1570 up to 1610nm which is then referred to as long wavelength band (L-band). Furthermore, it is possible to design a C+L band amplifier through the parallel coupling of a C-band EDFA with an L-band EDFA [56]. In this way, the C+L band amplifier must have an optical demultiplexer at its input port which separates the C-band from the L-band and feeds each spectral band into the appropriate EDFA. Then, after passing through the appropriate EDFA, the two multiplex are recombined by an optical multiplexer and launched into the transmission fibre. In order to avoid crosstalk between the C- and L-bands during demultiplexing/multiplexing, a mid-point guard band of a few nanometres is required between the two bands [57]. However, amplification process within the EDFA is accompanied by a backward noise, which is generated through amplified spontaneous emission (ASE) [43], [53]. ASE noise originates as not all the erbium atoms are stimulated by the incoming signal thus they emit light through spontaneous transition from higher to lower energy states. Since the optical fibre link has a chain of concatenated amplifiers, ASE noise accumulates over distance and thus limits the performance of long-haul optical communication systems. Normally, optical filters are used within the system to remove unwanted noise components hence to minimise the overall ASE noise built up during transmission.

1.4 Thesis overview

Given a general introduction to the optical fibre communications as shown in this chapter, the next chapters can present the experimental work of this research. Since the research is experimental in nature, it is necessary to introduce the fundamental techniques that are used in the laboratory to set up an entire optical fibre communication system. This is done in chapter 2, which discusses the main components and techniques used in the experiments of this thesis. The chapter therefore includes experimental methods of setting up an optical transmitter that produces the optical data including all: single, WDM and OTDM channels. It also presents the components used in the optical receiver to detect and examine the received signal. The chapter also presents a

practical method used to simulate long-haul optical fibre link by setting up short fibre span and using a recirculating loop to multiply the propagation distance. Different measurement techniques for characterising the system performance are also presented. The actual experimental work is covered in chapters 3, 4 and 5. These chapters use the techniques shown in chapter 2 to set up WDM communication systems operating at 10Gbit/s and using dispersion managed SMF-DCF spans in the recirculating loop. Losses of the fibre spans of the loop are compensated by EDFAs due to the advantages discussed in section 1.3. The systems use intensity modulation with direct detection (IM/DD) scheme at their transmitter and receiver.

In specific, chapter 3 is designated to demonstrate an advanced line monitoring technique that can be used to monitor the signal through the entire long-haul undersea system. The proposed line monitoring equipment is used to find the fault location along the fibre link by specifically monitoring the signal at the output of every repeater. This is assuming that the fibre spans are well-protected so that the only reason for fault is a fail in the optical amplifier. The proposed monitoring equipment is actually simple, cheap and can provide instant fault finding which is therefore useful for instant repair or upgrade of a legacy undersea fibre cable.

Chapters 4 and 5 involve different studies as they, respectively, investigate the effects of changing the shape of the transmitted data pattern and the modulation format on the overall performance of the optical fibre system. These studies can also be useful for improving the performance of the legacy systems. However, chapter 4 in particular presents the effect of changing the number of transmitted 1s and 0s in the data sequence. The experiment of this chapter uses 5×10Gbit/s WDM signals in RZ format driven by random data sequences as long as 2^{15}-1 and 2^{31}-1. The effect is investigated for two different regimes: linear where the launched power is sufficiently low; and nonlinear where the power is reasonably high. The importance of this study can be thought as a simulation of what is happening in coding systems where some encoders change the ratio of the 1s by adding extra bits to the original bit sequence. An example of this is forward-error correcting (FEC) codes that add redundant information to the data for error detection and correction at the receiver. Chapter 5 presents the effect of changing the modulation format of the transmitted signal from NRZ to CSRZ and from RZ to CSRZ using all-optical conversion. The use of all-optical conversion in place of normal electro-optic conversion is based on that all-optical devices will become the main key factors for the future all-optical networks. However, the converter uses semiconductor optical amplifier in nonlinear optical loop mirror (SOA-NOLM) which has already been shown elsewhere for single-channel conversion. The chapter presents the feasibility of such all-optical device in converting single and WDM

signals at 10Gbit/s data rate. It then presents the transmission results of the converted CSRZ signals against the original un-converted NRZ and RZ signals using long distance through recirculating loop and short distance through in-line fibre span. In the case of WDM, a back-to-back conversion is run over the whole C-band in order to explore the optical conversion bandwidth of the device.

Finally, chapter 6 gives overall conclusions and suggested future work.

Chapter 2

Experimental techniques for optical fibre communications

2.1 Intensity modulation and optical data signal generation

Modulation is the most important process carried out by the optical transmitter, where the electrical data is converted into an optical bit stream to be transmitted over the fibre link. The optical signal can be modulated directly, by applying an electrical signal to the optical source which can also be called internal modulation, or indirectly, by using an external modulator. Direct modulation can be cheaper as well as the output spectrum can be broader due to a frequency chirp imposed on the modulated signal [58]-[59]. At high-bit rates such as 10Gbit/s or higher, such frequency chirp becomes considerably large resulting in huge chromatic dispersion induced during transmission. Therefore, an external modulator is commonly used at 10Gbit/s or more to avoid such broadening penalty [43], [60]. Note that the penalty of direct modulation can be reduced by reducing the laser current albeit at the expense of the extinction ratio (the on-off ratio) where the output signal has less power. In high speed transmission systems using indirect modulation, the laser is biased at a constant current to produce a continuous wave (CW) and the external optical modulator is placed next to the laser to convert the CW light into a bit stream with the required modulation format. Such arrangement is used in the experiments of this thesis as all the transmission systems investigated operate at 10Gbit/s. $LiNbO_3$ Mach-Zehnder modulators are used as external intensity modulators due to the advantages mentioned in chapter 1. Moreover, $LiNbO_3$ modulators in general have low insertion loss and can provide high electro-optic effect, i.e. the change in refractive index of the material with an applied electric field.

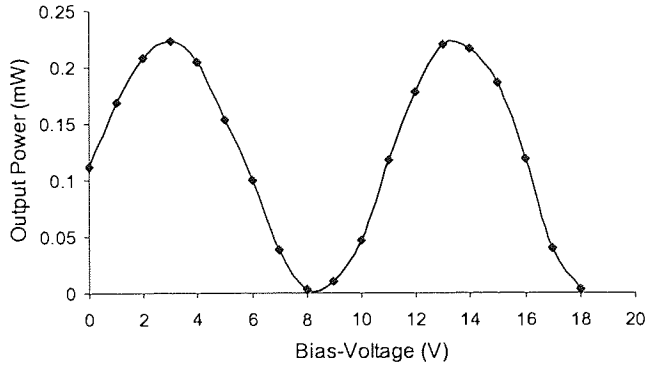

Figure 2.1 The output signal power variation with modulator bias-voltage for 1mW input power.

If a light signal passes through $LiNbO_3$ modulator, its output power changes as a function of the modulator bias-voltage and has a sinusoidal shape, as shown in figure 2.1. The light signal can be modulated if an electrical signal is applied to the modulator, hence superimposed onto the bias-voltage of the modulator. If the input electrical signal has sinusoidal shape, the optical output signal will also be sinusoidal with different frequencies corresponding to different bias-voltage points. Figure 2.2 compares different output signals obtained for different bias points, using 10GHz electrical signal.

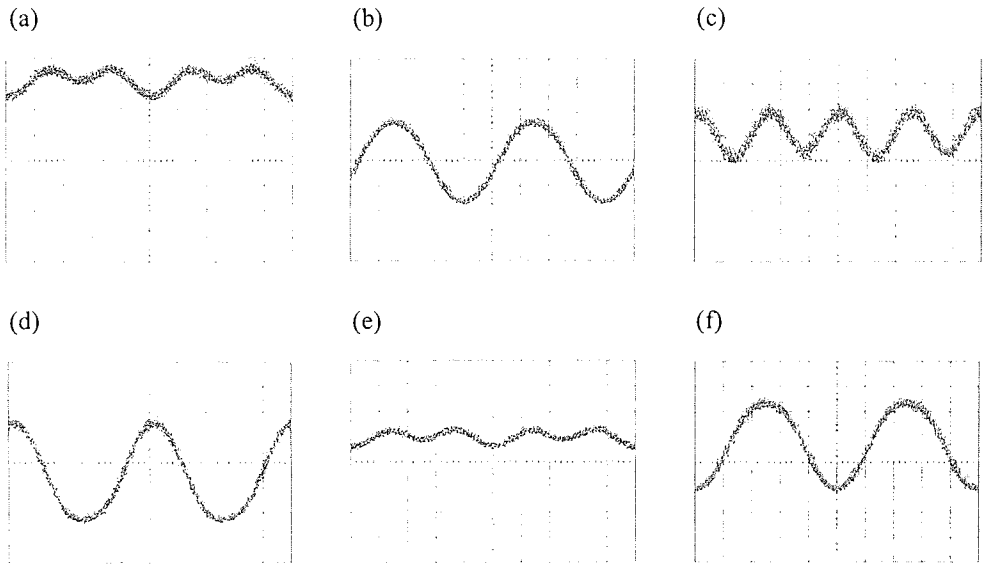

Figure 2.2 Optical output modulated signals obtained for: (a) 2.5V; (b) 5V; (c) 8V; (d) 11V; (e) 14V; (f) 16V. (Time scale: 20ps/div).

It can be seen that the output signal has full-wave shape, i.e. 10GHz frequency, for bias at 5, 11 and 16volts. These points are corresponding to power values seen in the linear range (i.e. between the maximum and minimum) of the modulator curve shown in figure 2.1. These results can be understood using figure 2.3. If the bias point is corresponding to the midpoint of the linear region of the modulator curve and the electrical signal has amplitude of V_π, the optical output signal will have the same shape and frequency of the electrical signal. If the amplitude of the input electrical signal is reduced from V_π, the extinction ratio of the output signal will be reduced. On the other hand, if the amplitude is larger than V_π, the modulator is overdriven, hence distorting the output signal. In contrast, the output signal will have half-wave, i.e. twice as the frequency of the electrical signal, if the bias points are corresponding to the maximum or minimum powers of the modulator curve. This is clearly shown in figure 2.2 (a), (c) and (e).

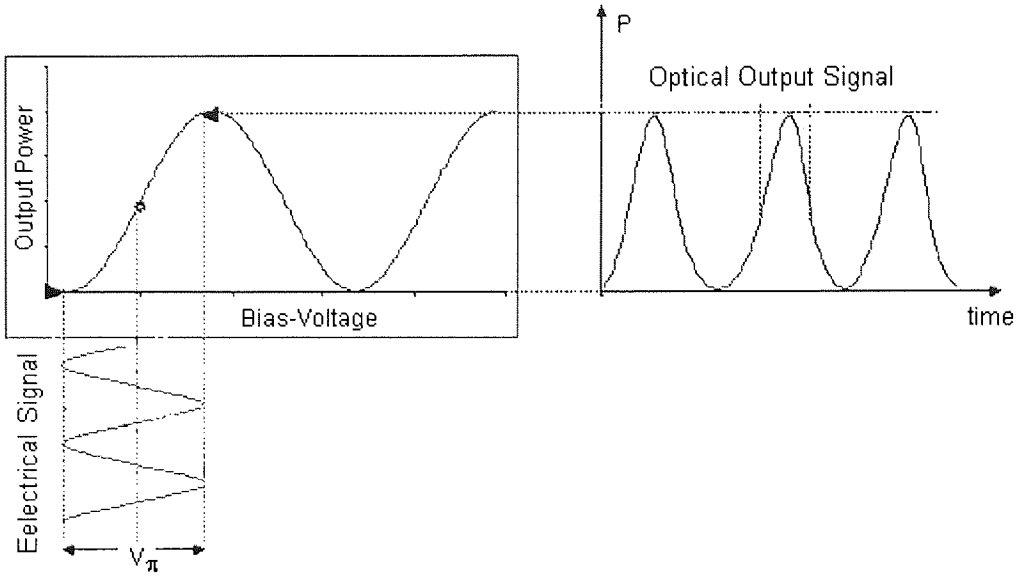

Figure 2.3 Electrical signal modulation.

Unfortunately, the performance of the $LiNbO_3$ modulator is polarisation-sensitive, where any change in the state of polarisation will affect the phase shift between the two Mach-Zehnder arms (recall figure 1.1). Therefore, the state of the input light must be carefully maintained in order to maximise the performance. This can be done by either using a polarisation controller (PC) before the modulator, or using a polarisation-maintaining fibre at the modulator input. Having considered this, the signal shapes in figure 2.2 (a) and (e) can be improved as well as the insertion loss in figure 2.1.

2.1.1 Optical PRBS data signal generation

PRBS, which stands for *Pseudo Random Bit Sequence*, is commonly used as a random data pattern and can be useful for experimental purposes. It can be generated electrically by the pattern generator. Pattern generators can typically produce long bit patterns up to 2^{31}-1 bits, where PRBS can produce all possible combinations of ones and zeros for a given pattern length. For example, a 2^9-1 PRBS pattern produces all possible combinations of 9-bit binary numbers from 000000001 to 111111111 [61]-[62]. Electrical PRBS data signal is converted into optical through optical modulation, where both NRZ and RZ data signals can be generated. To generate NRZ data, the modulator is biased in the linear range and the electrical PRBS modulation signal is applied to the modulator. This can be shown in figure 2.4; since the PRBS data is NRZ with amplitude of V_π, the optical output signal will be PRBS with NRZ format as well.

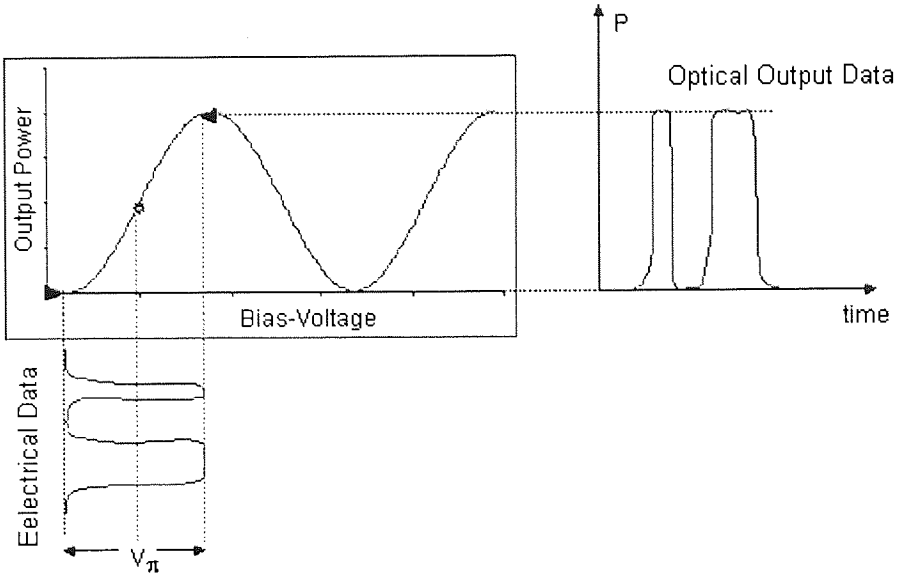

Figure 2.4 NRZ data modulation.

If RZ data is required, it is necessary to have two cascaded optical modulators. A clock signal is applied to the first modulator to produce an optical carrier at the required frequency, as shown earlier in figure 2.2, and then the electrical PRBS is applied to the second modulator to produce the optical RZ data signal [63]. At the first modulator, the clock signal is considered as an RZ bit pattern with all 1-bits and a bit-rate equals to the clock frequency if biased in the linear region, and twice as the clock frequency if biased at the maximum or minimum points. The second modulator must also be biased in the linear region, where the best performance can be achieved at the midpoint of the linear range.

In this thesis, optical RZ data are preferred in most of the transmission work for the reasons discussed in section 1.1.1. Figure 2.5 shows the experimental setup used for optical RZ data generation using two $LiNbO_3$ modulators, where NRZ data can be achieved simply by removing the first modulator. Electrical amplifiers (denoted as RF Amp) are used to amplify the electrical clock and data signals so that they have amplitudes close to V_π as in figures 2.3 and 2.4. Again, if the power is too large, i.e. larger than V_π, the modulators are overdriven, hence degrading the output signals. Electrical attenuators are usually used in association with the RF amplifiers to adjust the electrical signals powers.

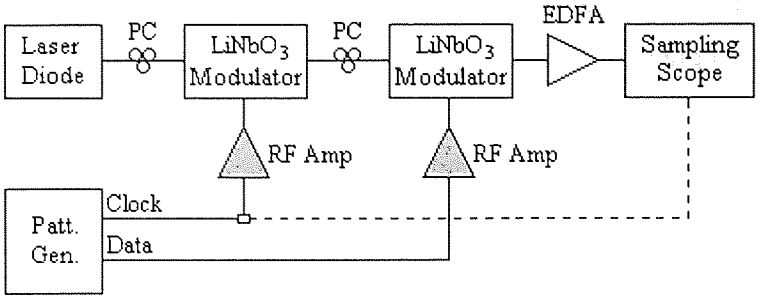

Figure 2.5 The experimental setup for generating optical RZ data.

The resultant optical RZ signal can then pass through erbium-doped fibre amplifier (EDFA) for pre-amplification before being displayed on the optical sampling scope. Note that the clock signal produced at the pattern generator is split into two signals; one for modulation at the first modulator and the other is used for clock recovery (or trigger) at the optical sampling scope. Figure 2.6 (a) shows the output signal from the first modulator, while (b) shows the eye of the output RZ data signal from the second modulator. Each modulator was biased at the midpoint of its linear range. The frequency of the electrical clock used in this experiment was 10GHz resulting in an RZ optical data signal with 10Gbit/s speed.

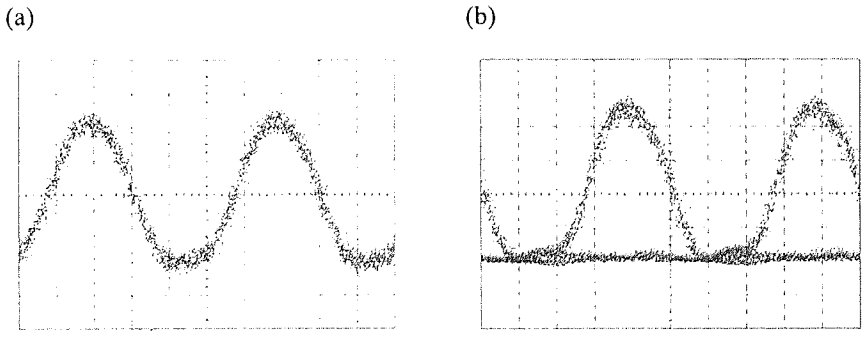

Figure 2.6 Optical output signal: (a) from the 1st modulator; (b) from the 2nd modulator. (Time scale: 20ps/div).

Optical NRZ and RZ data can also be generated and detected by optical transponder, which is highly integrated electro-opto-mechanical device, used in optical networking equipment. Optical transponder, in which both optical transmitter and receiver are packaged within the same device, can be useful for optical transmission experiments if it is designed so that signal is generated by transmitter and detected by receiver. In networking equipment, it is designed to be used as a regenerator where the signal is detected by receiver, amplified and then retransmitted

[64]-[65]. In this thesis experiments, the two optical modulators shown in figure 2.5 are sometimes replaced by an optical transponder, whose transmitter section (Tx) consists of two optical $LiNbO_3$ modulators with their drivers and one phase modulator that can be used to control the chirp on the output signal. The input of each modulator is spliced by polarisation-maintaining fibre, so polarisation is always maintaned in the device. The receiver section (Rx) is composed of a PIN photodiode which detects the optical signal and converts it back into an electrical signal, pre-amplifiers for increasing signal strength, and a clock recovery unit, which extracts the clock signal and recovers the original data stream. All transmitter and receiver parameters, such as modulators bias-voltages, receiver decision level ...etc, can be controlled through a software programme which is accompanied with the transponder module. This in turn makes the optical transponder easy and more practical to utilise in the laboratory experiments.

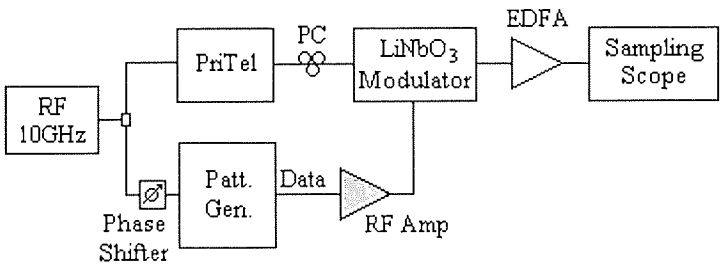

Figure 2.7 The experimental setup for generating narrow optical RZ data pulses.

So far, the laser source used to produce the optical signal is called *distributed feedback* (DFB) laser, which was developed in the 1980s and is now used in optical fibre communication systems operate at more than 2.5Gbit/s and use wavelengths near 1550nm [12], [63], [65]. DFB lasers are able to produce pulses at width of about 25ps. In some experiments, a very narrow optical pulses (as narrow as 2ps) are required and this can be achieved by using special optical sources. One of these sources is referred to as *PriTel mode-locked laser*, where PriTel is the name of the manufacturer [66]. PriTel module has an internal mode-locked laser that is normally driven by an external frequency reference so that it can generate optical pulses at the required repetition rate and frequency, rather than CW. PriTel laser has the ability to produce extremely narrow optical pulses that can reach 1.6ps. In fact, this laser is ideal for use in ultra-high-speed optical fibre communications at bit rates of 2.5, 10, 40, and 160Gbit/s. The output of the PriTel laser can be used to generate narrow optical RZ data signal if it is modulated by electrical data. Figure 2.7 shows the experimental arrangement used to generate a narrow optical RZ signal at 2.8ps pulse-

width and 10Gbit/s speed. The RF source produces 10GHz electrical clock signal that is used to drive both the PriTel laser and the pattern generator. The pattern generator produces a PRBS data signal, which is used to modulate the PriTel output signal at a $LiNbO_3$ amplitude modulator. It is essential to have a phase shifter to match the phase between the PriTel and the pattern generator. The 2.8ps signal produced by the PriTel laser can be shown in figure 2.8 (a), and the resulting 10Gbit/s RZ signal generated through modulation can be shown in (b). Note that the pulse width measured directly on the sampling scope is not accurate where it is limited by the sampling scope resolution, which is rather limited by the speed of the input photodiode. The detected signal can be synchronised either by triggering the sampling scope with the clock signal used at the RF source, or by using a built-in clock recovery unit, which is available in the most modern sampling scopes. The clock recovery unit recovers the frequency of the received signal thus the BERT can be used to detect errors on the received data using the recovered clock frequency (this is explained later in this chapter with more details).

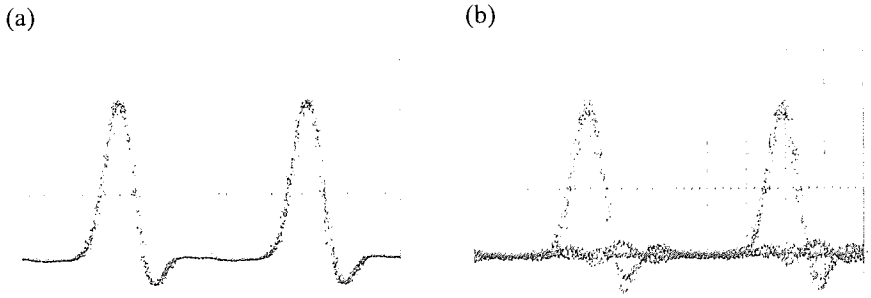

Figure 2.8 Optical output signal: (a) from the PriTel laser; (b) from the $LiNbO_3$ modulator. (Time scale: 20ps/div).

2.1.2 WDM data signal generation

As mentioned before, high-capacity optical communications require transmitting many data channels over the optical fibre link simultaneously. Therefore, different channels from different nodes are multiplexed through WDM or OTDM technologies before being transmitted over the fibre. If WDM is used, different optical sources produce light signals with different wavelengths and each signal is modulated individually, as different data are carried over different channels. The modulated signals are then multiplexed by WDM multiplexer to produce the composite WDM bit stream. Obviously, this requires one modulator for each data channel if NRZ data is employed and two modulators for each channel if RZ data is used. For instance, it is necessary to

have eight optical modulators in order to produce 4×WDM data signal using RZ format, which is too expensive to be setup in the laboratory for test purposes. Having considered this in addition to the fact that most test experiments use PRBS in all data channels, it is possible to simulate WDM transmission system as shown in figure 2.9, where four optical signals with different wavelengths are WDM multiplexed and then modulated by only one clock and data signal using two $LiNbO_3$ modulators to produce RZ data signal. The resulting signal can be transmitted as a 4×10Gbit/s WDM signal. However, the problem of this configuration is that all the channels have the same bit stream whereas ideally they would all be different. This results in a potential interaction between the simultaneous pulses due to the effect of XPM and FWM during transmission. Again, this effect can be avoided if data signals propagate through fibres with high dispersion so that pulses of different WDM channels have different group velocities. This causes separation of the pulses for more than one bit period after short distance hence the interaction is negligible. As this thesis uses high dispersion fibres, i.e. SMFs and DCFs, the setup shown in figure 2.9 can still be used for WDM transmission experiments.

At the receiver, the four WDM signals are demultiplexed by using a tunable band-pass optical filter that enables detecting and testing the individual channels by single receiver. In real system, channels are demultiplxed by WDM demultiplexer that sends each channel to an individual receiver, which recovers the original data signal and then allocates it to its destination. This indeed requires number of receivers equals to the number of channels which can also be saved in laboratory experiments. The band-pass filter is preferred to be as narrow as possible for proper separation of the different WDM channels.

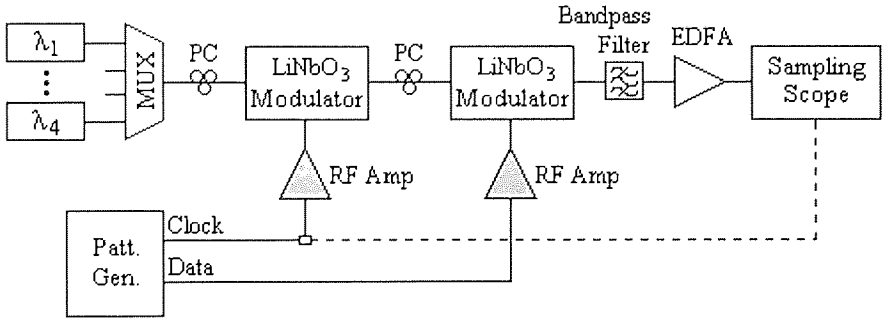

Figure 2.9 The experimental setup for generating and detecting WDM RZ data.

2.1.3 OTDM data signal generation

The capacity of the fibre link can also be increased by multiplexing different channels through OTDM, where all channels have the same carrier wavelength but share the time. This means that the time is divided into time slots where each channel is transmitted within its allocated time slot. To achieve that, all different data channels are used to modulate one light signal and pass through an OTDM process where bits belong to different channels are delayed by different amount of time so that they are transmitted at different times. The adjacent channels are usually spaced apart by small guard-band to avoid any bit interference.

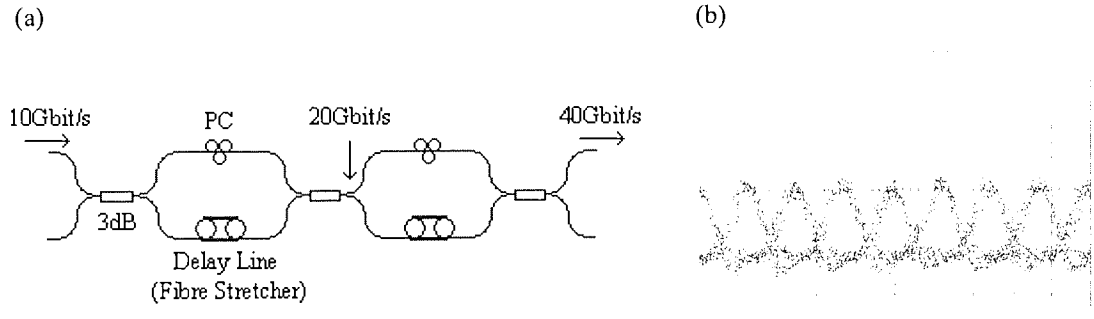

Figure 2.10 (a) Mach-Zehnder OTDM stage. (b) 40Gbit/s output signal (Time scale: 20ps/div).

For experimental purposes, where PRBS data can be used for all channels, OTDM signal can be generated from single-channel by using Mach-Zehnder OTDM stage as shown in figure 2.10 (a) [67]. If light signal is modulated at 10Gbit/s, the time window of the pulse is 100ps. If this signal is split into two signals; one is delayed by 50ps, using fibre stretcher, and then couples back with the other signal, the resultant is 20Gbit/s signal. If this stage is repeated with 25ps delay, the output signal is then 40Gbit/s. In practice, such delays are insufficient for adequate mixing of bits as they would result in sequential bit repetition within the combined 40Gbit/s PRBS data. Therefore, larger delays are used instead to avoid this effect. For example, the pulses are delayed by 100ps (one time window) in addition to the 50ps and 25ps mentioned above. Polarisation controller is used in one arm of the Mach-Zehnder to ensure that the output bits have the same polarisation. Figure 2.10 (b) shows the output 40Gbit/s signal using an input 10Gbit/s signal generated by modulating a PriTel signal as described in figures 2.7 and 2.8. Note that OTDM cannot be performed unless the input pulses are sufficiently narrow.

At the receiver, an individual 10Gbit/s OTDM channels must be separated from the 40Gbit/s bit stream for error detection. Since each pulse occupies a 25ps window in the 40Gbit/s

signal, it is required to create a 25ps switching window every 100ps to extract a 10Gbit/s channel. To achieve this, an electro-absorption modulator (EAM) is used to absorb the unwanted three channels and leave only one channel in the time window [68]-[70]. Figure 2.11 shows the OTDM receiver setup. The EAM is initially driven by a 10GHz electrical signal generated by clock recovery unit (CRU) to enable modulation of the first arrived bits, and then driven through feedback clock recovery for the next coming bits. The phase of the 10GHz signal can be adjusted using a phase shifter which enables sliding the switching window in the time domain, giving the ability to select which of the four OTDM channels to be detected. The output 10Gbit/s signal is isolated and pre-amplified before being detected by the BERT.

Although OTDM will not be used in this thesis work, it was still useful to discuss it here as part of the context of data signals generation and detection.

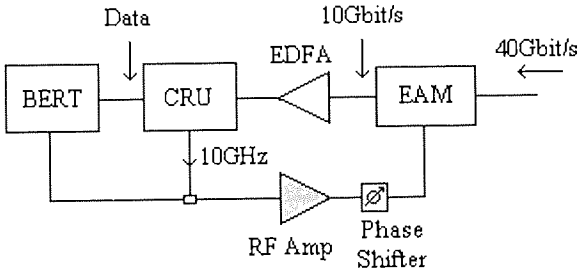

Figure 2.11 OTDM receiver setup.

2.2 Transmission through recirculating loop

Having generated the required optical data signal as discussed so far, an optical fibre link can be setup for transmission experiment. The fibre link consists of number of fibre spans and corresponding number of optical amplifiers to compensate for fibre losses in each span. In general, the fibre spans can have any types of fibres such as DSFs or SMFs accompanied by DCFs such that the overall dispersion is compensated at the end of the fibre link. However, in real undersea systems where transmission distance reaches thousands of kilometres, the fibre link requires large number of fibre spans and optical amplifiers in addition to the other components such as filters. This indeed costs a lot of money and is impossible to design and setup in the laboratory for test experiments. In fact, long-haul transmission systems can be simulated by setting up a recirculating loop, in which optical signal is allowed to propagate many times around short fibre link. Therefore, recirculating loop can be described as a simplified transmission

system that consists of few fibre spans and a corresponding number of amplifiers (typically up to 4), and can act as a long distance transmission medium. Obviously, the cost of using recirculating loop can be a small fraction of that for the whole transmission system exists in reality. In addition, the loop configuration can be easily changed for another experimental setup due to a limited number of components exist in the system.

The recirculating loop was first used in 1977 to simulate long transmission system using electronic repeaters [71]. After the development of all-optical repeaters, e.g. EDFAs, recirculating loop has become common and is being extensively used in nowadays' experiments [72]-[77]. Although the recirculating loop is used to give a prediction of the real in-line system performance, it is important to know that its performance is different because signal propagates through the loop components periodically, while in real system it propagates through different components in each span. Such difference in performance can be minimised by reducing the periodicity which can be achieved by extending the loop length. This of course requires more components to be setup in the loop, which increases the complexity, thus adds more cost to the experiment. As a result, designing a recirculating loop experiment is a compromise between these effects and it is up to the engineer to decide which effect is to be eliminated.

Since this work investigates different effects in legacy long-haul transmission systems, the experiments discussed in the following chapters use recirculating loop. The loop has been configured so it has no more than four spans (or sections) in all experiments, although single span loop is never used. Details of loop setups are discussed later, while the remaining of this chapter covers the design and operation of the recirculating loop in general.

2.2.1 Recirculating loop design and operation

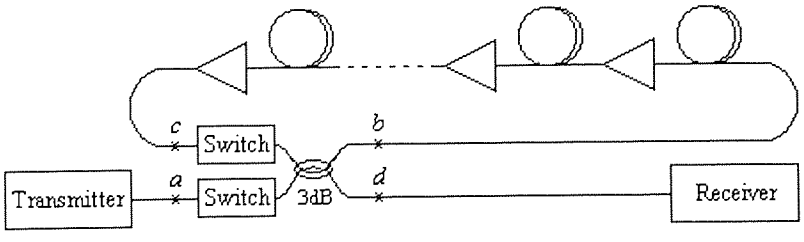

Figure 2.12 Schematic diagram of the recirculating loop.

The schematic diagram of the recirculating loop system is shown in figure 2.12. This diagram can be used to explain the main principle of operation for any arbitrary loop setup, which can be a series of fibre spans and EDFAs in addition to other components such as filters. The recirculating loop system consists of two switches and 3dB fibre coupler. One switch is placed outside the loop (as the bottom switch in figure 2.12) to allow a burst of data to pass into the loop, and can be referred to as *input switch* (or *load switch*) [5]. The other switch (the top one in figure 2.12) is placed inside the loop to define the number of the recirculations, which corresponds to the transmission distance, and can be referred to as *loop switch*. Data can enter the recirculating loop as the input switch closes to let the data burst through, while the loop switch is open. At the fibre coupler, the signal splits into two equal parts: one enters the loop and the other passes through the output arm. The data that enters the loop can propagate through the fibre spans till it reaches the loop switch after it has filled the loop length. The input switch must then open to stop data passing into the loop, while the loop switch closes to allow data to propagate around the loop. The input and loop switches are controlled by a digital delay generator that tells each switch when to open and close using timing states as shown in figure 2.13.

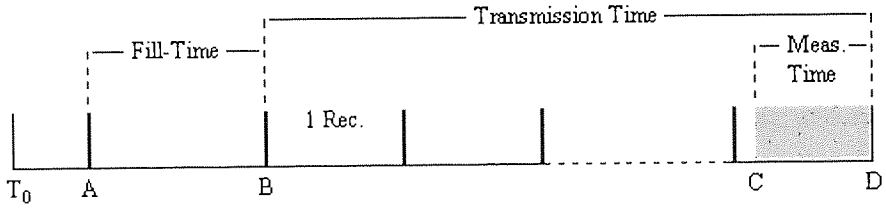

Figure 2.13 Timing states of the recirculating loop.

There are four timing states in the digital delay generator: T_0-A, A-B, B-C and C-D. T_0-A is set to define the starting time, which is used to introduce a guard-band between the two successive cycles. A-B is set to define the fill time of the loop which can be calculated by using:

$$T_{round-trip} = \frac{n \times l}{c} \tag{2.1}$$

where n is the refractive-index of the fibre core, l is the total length of the fibres in the loop and c is the speed of light. It is always recommended to set the fill-time at more than one round-trip time so that the EDFAs in the loop stabilise. B-C is set for transmission or propagation time,

which can be a multiple of the round-trip time. C-D is the measurement time which sets the sampling scope and error detector to carry out measurements. In fact, the measurement time has to be maximised to allow the largest data length in measurement, but should not exceed the round-trip time. It is also important to note that the measurement time C-D is set to include data in the last recirculation time, thus B-C time is a multiple of the round-trip time minus the measurement time, where the actual transmission time can be considered as B-D. For example, the loop used for the experiment discussed in chapter 4 has 52.8km SMF with $n = 1.46$. Using the equation (2.1), the round-trip time is 257μs. A-B is set to be 512 μs, which is twice as the round-trip time. For ten recirculations test (528km), B-C is 2.32ms if the measurement time is set at 250μs.

Actually, high extinction is required at the input and loop switches so if a switch is opened to stop passing data through, there is no leakage at the output of the switch. Suck leakage is undesirable because it results in an additional noise in the system. To meet this requirement, an acousto-optic modulator (AOM) is commonly used as a switching device in the recirculating loop system, as it can provide an extinction of more than 50dB [78]-[79].

The insertion loss of the AOM used in this thesis is around 3dB. So in addition to the 3dB loss of the fibre coupler, an additional attenuation of 6dB is added to the input signal and another 6dB to the signal recirculating or departing the loop. This requires increasing the power at the input of the recirculating loop to compensate for the loss of the input signal, and increasing the amplification in the loop EDFAs to compensate for the loss of the recirculating or departing signal. Practically, the loop is balanced if the power at point *a* shown in figure 2.12 is equal to the power at point *c*, and the power at *b* is equal to that at *d*. This can be understood as the loss on *a*-*b* bath is the same as that on *c*-*b* and *c*-*d* path. Normally, an EDFA is used before the input switch (or input AOM) to increase the loop input power, where this EDFA is referred to as a *booster*. This enables the signal to launch into the loop fibre at point *b* at the required power level. In the loop, each fibre span is followed by an EDFA to compensate for the loss of the span, and the final amplifier can compensate for the losses of the loop AOM and the coupler. If a component such as filter is set up somewhere in the loop, its insertion loss is compensated by the following amplifier. The AOM is commonly followed by an isolator to avoid impairments caused by backward reflection.

2.2.2 Dispersion measurements

Having compensated the losses in the recirculating loop, it is important to measure the total dispersion of the loop. For transmission experiments, it is necessary to make sure that dispersion is minimised at the operating wavelength. Dispersion of the individual fibre (in ps/(nm-km)) can be measured by measuring the exact length of the fibre and its dispersion at a chosen wavelength. This enables calculating the total dispersion of the combined fibres that are set up in the loop. For WDM systems, where many channels are transmitted using different wavelengths, it is important to measure the dispersion slope by measuring the dispersion over a wide range of wavelengths. Therefore, a method is used to measure both dispersion and dispersion slope of the combined fibres while they are in the loop. Such method can be referred to as *laser cavity method*, where the loop is set up so that it looks like a laser cavity ring and its EDFAs are used to provide a CW lasing within the loop [80]. This can be shown in figure 2.14.

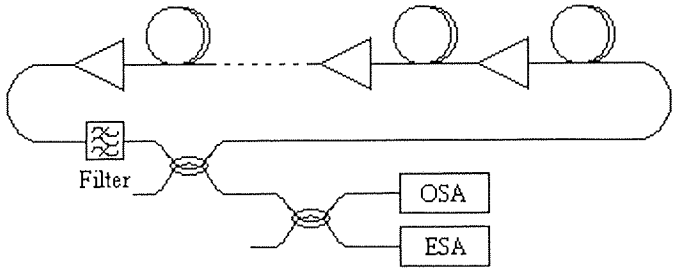

Figure 2.14 Schematic diagram of the cavity ring used for dispersion measurements of recirculating loop.

The cavity lasing wavelength is defined by a tunable band-pass filter and the frequency modes generated by the cavity ring can be observed on the electrical spectrum analyser (ESA). The operating wavelength can also be monitored using an optical spectrum analyser (OSA). The fundamental mode has a period which is the same as the round-trip time of the loop. If the lasing wavelength is altered by the tunable band-pass filter, the mode frequency will change thus the round-trip time will change due to dispersion effect. This change in the frequency can be seen as a shift in the harmonics observed on the ESA thus the round-trip time variation can be calculated by using:

$$\Delta T_{round-trip} = -\frac{m\Delta\nu}{\nu^2} \tag{2.2}$$

where m is the mode number of the observed harmonic, v is the harmonic frequency and Δv is the frequency change. The average dispersion in ps/(nm-km) is then calculated by dividing this time variation (or delay) by the product of wavelength change and loop length. Plotting the dispersion measurements versus wavelengths, the dispersion slope is achieved. This method has the advantage that the dispersion of the entire loop can be measured, including all components not only that of the transmission fibres. On the other hand, this method assumes that the loop length remains constant during the whole experiment. Temperature fluctuation results in slight variation in the loop length while taking measurements thus dispersion values show large fluctuations between the different measurements. Therefore, dispersion curve can be achieved by taking the average (or trend-line) of the measured values.

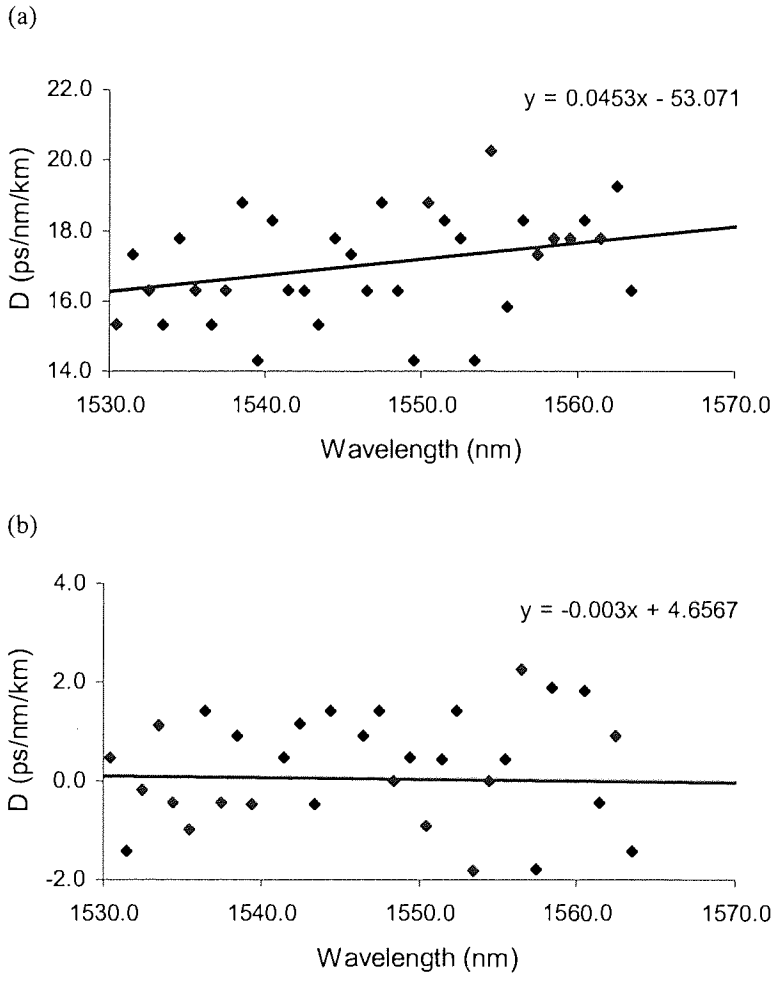

Figure 2.15 Dispersion measurements of a recirculating loop consists of: (a) two 80km SMF spans; (b) two 80km SMF spans with two 15km DCF modules; each has negative dispersion of ~ 87ps/(nm-km).

Example of this can be shown in figure 2.15 where (a) presents the results of a loop consists of two symmetric spans; each has 80km SMF and EDFA. Obviously, the average dispersion measured at 1550nm is approximately 17ps/(nm-km), which is standard for SMF, and the dispersion slope can be seen in the equation appears on the right top of the figure. Again, such high dispersion of the SMFs can be compensated by adding DCFs in the loop. Figure 2.15 (b) shows the same sort of results obtained after adding a DCF module with negative dispersion of approximately 87ps/(nm-km) and 15km length in each span. It is seen that dispersion and dispersion slope are improved, where the average dispersion measures approximately 0 at around 1550nm. However, the fluctuations in the measurement values due to temperature instability can be minimised by placing the fibres inside an isolated cupboard and performing measurements as quickly as possible. Ideally, a straightforward method can be used instead to measure the dispersion and dispersion slope using *network analyser* or *lightwave component analyser* [81]. This equipment has input and output ports which are simply connected to the two ends of the loop. By running the analyser, the dispersion curve over the whole wavelength range is being displayed on the screen. Measurement taken by this method is more accurate than that by the laser cavity method that is used in this thesis work due to unavailability of the network analyser.

2.2.3 *Q*-value and BER measurements

As mentioned before, the transmission system performance is characterised through the measurements of Q-value or BER as a function of transmission distance. Q measurement can be taken from the eye diagram displayed on the sampling scope. Most of the recent sampling scopes have a function of building up a histogram for sampled points within a chosen time window. They also have a statistic facility that allows measuring the mean and standard deviation of the 1 and 0 levels directly from the histogram. This indeed enables calculating the Q-value by using equation (1.3), which is recalled here as follows:

$$Q = \frac{\mu_1 - \mu_0}{\sigma_1 + \sigma_0}$$

Example of such measurement is shown in figure 2.16, where the measurement window is set to measure the mean and standard deviation for the 1 level in (a) and for the 0 level in (b). For accurate measurement, it is necessary to set the time window around the peak of the pulse and keep it small so measurements are restricted to the samples within the peak time. It is also

important to set a decision level in the vertical dimension so all sampled points above this decision level can be included in the 1 level measurement and those below the decision level are included in the 0 level measurement. The decision level is ideally chosen as the halfway between the 1 and 0 levels. The distribution of the samples used in the measurement is plotted in the histogram appears on the left of the sampling scope picture. Basically, the displayed mean and standard deviation values (as circled in (a)) can be directly substituted in the equation (1.3) to give the Q-value measurement. Using the values displayed in figure 2.16 gives a Q-value of 13, which represents a high quality signal with approximately 10^{-30} BER according to equation 1.2. However, from the definition of the Q-value, it is obvious that any increase in the standard deviation values due to an ASE noise, timing jitter or amplitude jitter will degrade the Q-value of the detected signal. Also, any decrease in the mean value of the 1 level due to loss or even dispersion, where broadening lowers the peak of the signal, will degrade the Q-value.

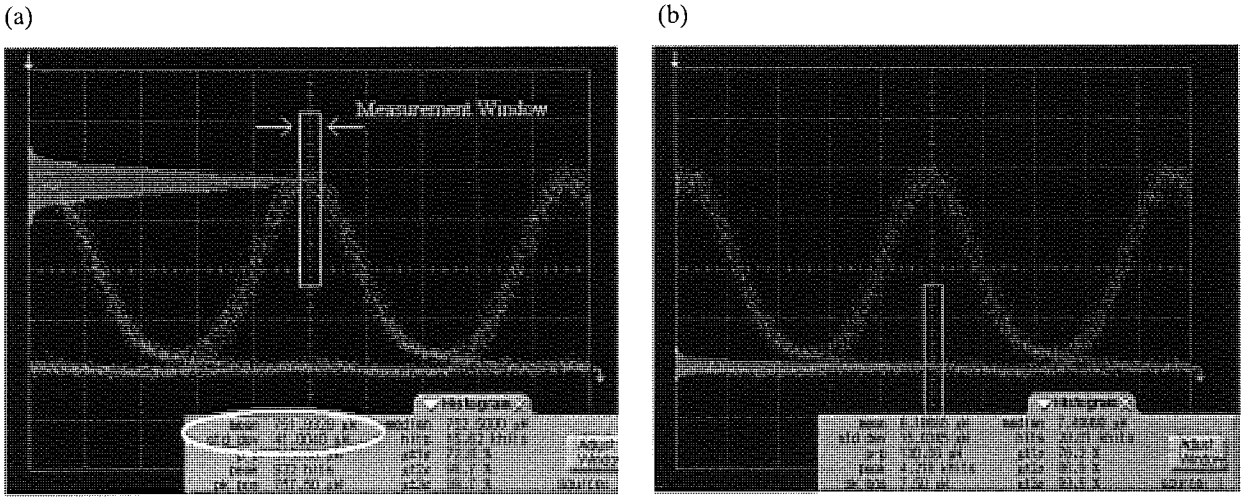

Figure 2.16 Example of Q-value measurement. (a) The mean and standard deviation measurements for the 1 level. (b) The same measurements for the 0 level. (Time scale: 20ps/div).

Although the Q-value measurements provide good analysis of the system performance, it is more practical to evaluate the performance through BER measurements. The main problem in measuring Q value is that it varies with any small change in the position of the measurement window as it is based on statistical distribution of the samples contained within the window. This may require repositioning the measurement window quite frequently as the pulse position changes in time due to a phase variation caused by transmission. Moreover, most of the sampling scopes do not have a facility to display the Q measurement but only the mean and standard deviation values which can be used for calculating the Q-value, as done above. This indeed

disables the engineer from being given an instant performance while playing around with system parameters or adjusting setup. Using BER measurement can be more practical, since the BERT displays the instantaneous error-rate which enables making adjustments while the experiment is running. BER measurement is based on setting a decision level and phase decision either manually or automatically on the BERT. Automatic setting is normally preferred as it chooses the optimum position of the decision level and phase decision. To perform the error measurements, the BERT is directly connected to the data and clock signals that have already been separated at the clock recovery unit of the receiver. The clock signal provides a time reference for the arriving bits in the data signal. In the recirculating loop experiment, it is important that both sampling scope and BERT carry out measurement within the C-D timing state as in figure 2.13, otherwise the measurement is incorrect. This can be achieved through specific connection between the sampling scope/BERT and the C-D output of the digital delay generator used with the AOMs. In this case, the scope/BERT equipment is externally triggered using the so-called *gated* triggering mode. This is also required with the optical spectrum analyser measurements discussed in the next section.

2.2.4 Optical signal-to-noise ratio measurements

Optical signal-to-noise ratio measurement (OSNR) is also important when performing a recirculating loop experiment. It provides a good optical performance monitoring as it gives the ratio between the signal power and the ASE noise introduced by EDFAs. In fact, OSNR degrades as the number of recirculations increases, and that is basically because the ASE noise accumulates over an increased number of EDFAs. OSNR is normally measured as a function of propagation distance by using an optical spectrum analyser (OSA). To keep monitoring the OSNR and spectrum during the experiment, a fibre coupler with 90/10 coupling ratio can be placed at the output of the recirculating loop. This allows 10% of the signal to be observed on the OSA, while the remaining 90% can proceed onto the receiver.

OSNR measurement can be related to BER performance where there is a minimum acceptable OSNR value that corresponds to the BER reference level 10^{-9} or $Q = 6$. This value depends on the resolution bandwidth of the OSA. For instance, by using 0.1nm resolution bandwidth which is very common, the minimum acceptable value is ~13dB in logarithmic scale. In this case, the measurement can have a unit of (dB/0.1nm). Note that it is always more convenient to use logarithmic scale in the OSNR measurements rather than linear scale. Practically, the single OSNR measurement is obtained directly from the OSA by setting two

markers: one to read the level of the signal and the other to read the level of the noise, and then subtracting the two readings. Actually, the OSA does automatically calculate the difference between the two markers thus the result is immediately obtained on the screen.

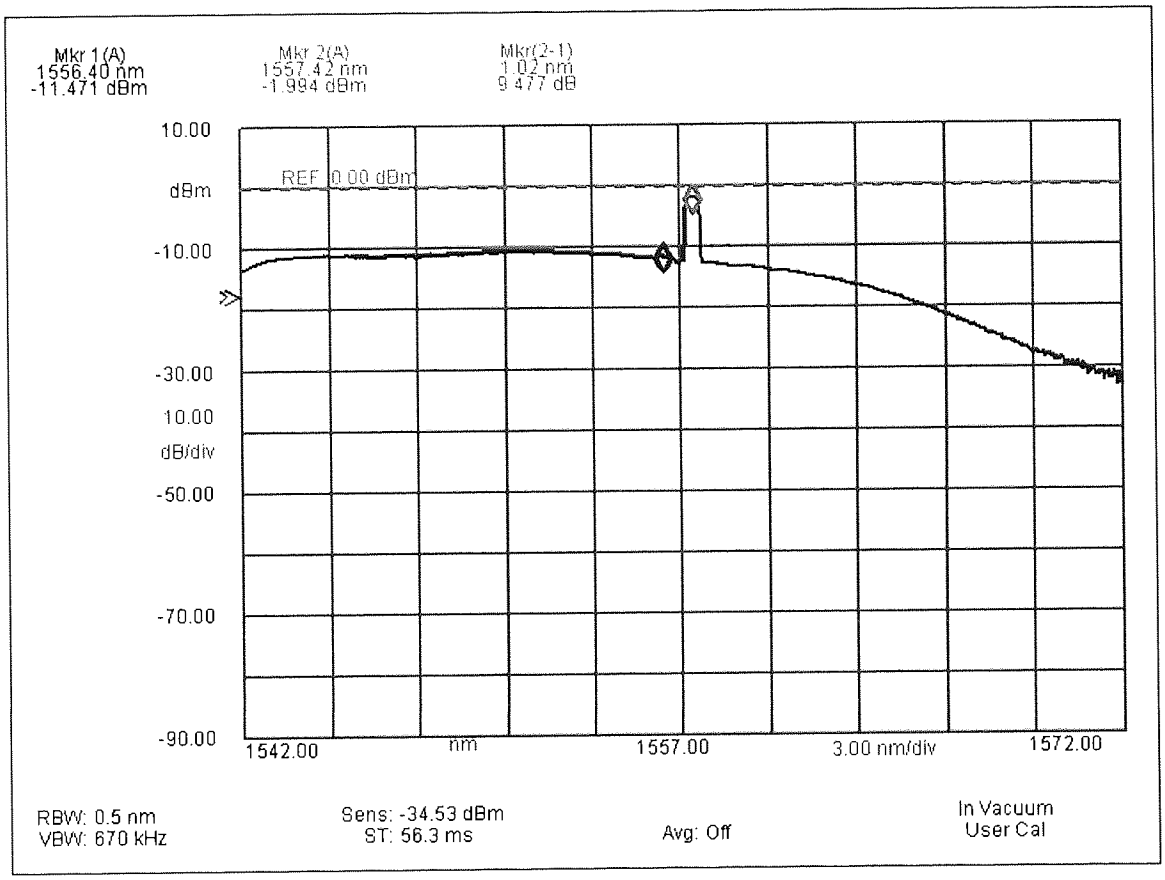

Figure 2.17 Example of OSA picture and OSNR measurement.

Figure 2.17 shows an example of OSA picture using 0.5nm resolution bandwidth as displayed on the left bottom of the picture. The OSNR measured on this picture is obviously 9.48(dB/0.5nm). It is important to realise that the marker on the signal reads the total power including both signal and noise within 0.5nm under the marked wavelength. This results in an output OSNR measurement as $(S+N)$-N, where S is the signal power and N is the noise in dBm. Although this result is acceptable as an OSNR measurement in the most cases, it can be corrected to the accurate ratio, S-N, by using the following formula:

$$S - N = 10\log(10^{X/10} - 1) \tag{2.3}$$

where X is the measured OSNR. For example, the accurate OSNR measurement of the signal in figure 2.17 is 8.96(dB/0.5nm). This value can also be converted into a (dB/nm) unit if it is offset by -3dB, giving an OSNR of 5.96(dB/nm). If this unit is used, the OSNR has to be larger than 0, at which the receiver starts to count errors on the received signal. In general, the unit of the OSNR measurement is not a big issue as long as it is the same in all measurements, where the main objective is to compare the relative performance for different number of recirculations.

2.3 Summary

This chapter started with introducing the principles of generating and detecting different optical data signals experimentally, including single-channel, WDM and OTDM. It then has presented the main principles of designing and operating the recirculating loop experiment which is used to simulate long-haul optical transmission link. This has included the main design issues in the recirculating loop system such as power and dispersion management. All measurements techniques and methods used for analysing the performance of the recirculating loop system have also been demonstrated. The chapter has provided few examples in the different sections for more clarification.

Chapter 3

Line monitoring equipment for optically amplified long-haul undersea systems

3.1 Introduction

Having presented the experimental method used to simulate long-haul optical fibre communication link as in previous chapter, it is possible to introduce a line monitoring technique that can be used to diagnose the location of faults along such fibre link [5]. The demand for line monitoring has greatly increased due to a high capacity and long distances of the current undersea transmission links. These transmission links require continuous monitoring that should be carried out at the network terminal. Such remote monitoring enables instantaneous determining of any degradation along the fibre link which in turn allows rapid maintenance execution to be performed. In fact, the main problem with monitoring the legacy optically amplified links is that the system gives limited information about what is happening along the fibre link, which has not been the case in electrical systems or even regenerative optical systems. Those systems have much more complex electrical regenerators that carry out huge amount of processing, thus they can give very detailed monitoring information (e.g. error-rates on individual channels). In general, regenerative systems typically use information derived at the regenerators to monitor link performance where these information get multiplexed onto the data stream and can be used at the network terminal to determine the fault location. On the other hand, the main requirement of the line monitoring equipment (abbreviated as LME) is that it should have a much lower cost than the transmission link itself; otherwise it is not a cost-effective solution. To meet such requirement, several optical line monitoring techniques have been developed, where the most famous technique was based on the coherent optical time domain reflectometry (COTDR) [82]-[88]. In this technique, the Rayleigh backscattered light from an optical probe pulse propagating down the fibre is detected and examined at the transmit terminal. The level of the detected signal is displayed as a function of fibre distance which, in normal case, shows linear degradation due to constant fibre loss. If the signal is lost due to a cable fault, it can be seen as a sudden drop in the signal level. The main advantage of the COTDR is that it can define the fault at any part of the system rather than just the output from the repeaters as in other techniques. Nevertheless, this method has a cost problem, since it performs an optical coherent detection, which is relatively expensive, rather than electrical coherent detection. It also has another drawback that it becomes

difficult to measure for a very long fibre span as well as in the presence of optical isolators located in the optical amplifiers, although optical isolators can be bypassed by couplers which transfer power between fibres [83]. Moreover, COTDR tends to be used out-of-service in the case of a fibre break because it needs high optical power levels which affects the in-service channels - the backscattered power is typically 34dB down on the forward signal if integrated over a whole span length, but the power returned from a fibre segment will of course be far lower, especially for the backscatter from the remote parts of the fibre. Another line monitoring methods have been demonstrated in [89]-[91] but the main disadvantage of these methods is that they can only provide an in-service monitoring, which means that if the link is out-of-service and there is no signal propagating through, the fault location cannot be determined.

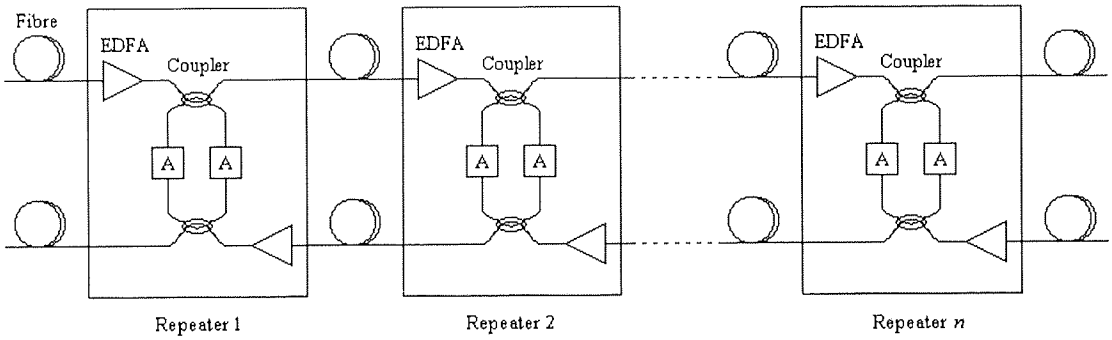

Figure 3.1 Schematic diagram of the transmission fibre pair showing the high-loss loopback circuits

Therefore, in addition to the cost requirement, it is important to develop an LME that can be used in both in-service and out-of-service cases, providing a continuous monitoring of the transmission fibre link. These requirements have been met since 1996 by designing a relatively simple, low cost LME which is particularly applicable to undersea optical transmission systems [92]. This method is based on the fact that the optical transmission system contains at least one optical fibre pair extending between two terminals. Each fibre has a sequence of fibre spans and optical repeaters (i.e. EDFAs). Each repeater can have a simple high-loss optical loopback circuit which provides a connection between the existing two fibres and can be used to define fault location. The loopback circuit taps off a portion of the optical signal propagating through one of the fibres, attenuates this portion and then returns it back to the terminal via another tap in the other fibre. This can be shown in figure 3.1. Obviously, the loopback circuit can be very simple as it is composed of passive components which are two fibre couplers and two optical attenuators. All spans are assumed to be identical and the system is assumed to be symmetrical with respect

to direction of propagation. Fault location can be determined by launching a supervisory signal into the fibre from one of the terminals, and return the attenuated part of this signal to the terminal through the loopback circuit used at each repeater. Since the loopback circuit is passive, the repeaters do not return any information, where all information must be gleaned from the returned signal levels and delays. Details of this are explained in the following sections. This method assumes that the main origin of the faults in the fibre link comes from impairments in the optical repeaters, specifically due to a failure of the pump laser diodes of EDFAs. This of course assumes that the other components including fibre spans are well-protected against all degradation factors.

3.2 LME system transmitter and receiver

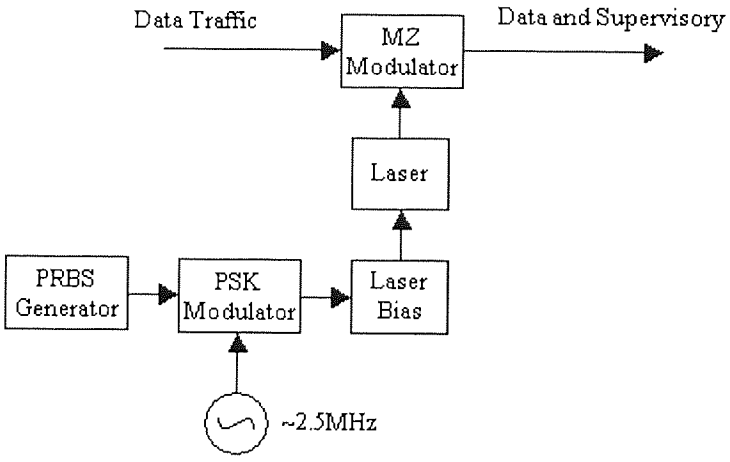

Figure 3.2 Block diagram of the transmitter of the in-band LME system.

LME system is composed of a transmitter, in which a supervisory signal is generated and transmitted along with the original data signals, and a receiver to detect the returned signals form the loopback circuits and examine the received supervisory signals. Both transmitter and receiver are located at the same terminal. This section presents two LME approaches. The first approach has a transmitter as shown in figure 3.2 [93]. It consists of a laser source, whose output is modulated at an optical MZ modulator by a single data traffic signal. The laser bias is also modulated by an RF supervisory signal with a sub-carrier frequency at ~2.5MHz. The supervisory signal itself is encoded electrically using PSK but the sub-carrier is intensity modulated. Thus the supervisory signal is a PRBS, whose bit-rate is typically between 10 to 100kbit/s. For instance, if 50kbit/s is used, one supervisory bit occupies a distance of 6km of

fibre. However, the output from the optical MZ modulator comprises the intensity modulated data traffic over which is superimposed the supervisory RF amplitude modulation. Therefore, as the supervisory signal exist within the data signal band it can be referred to as *in-band LME signal*, and the whole system can be called *in-band LME system*.

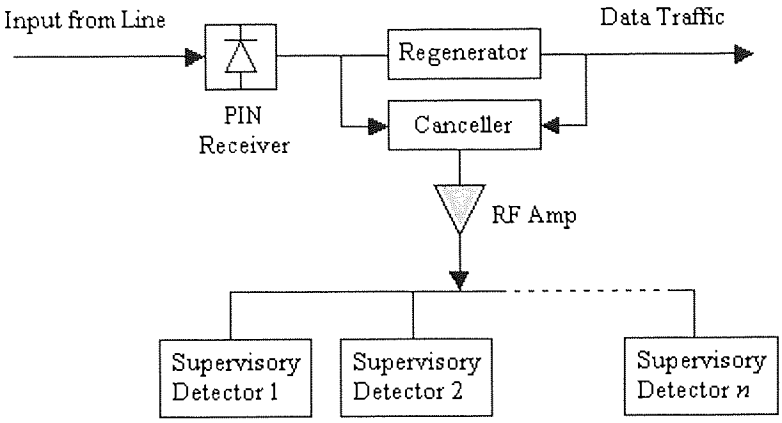

Figure 3.3 Block diagram of the receiver of the in-band LME system.

The LME receiver of this system can be shown in figure 3.3 [93]. It detects both the traffic and the supervisory signals looped back from each repeater. The supervisory modulation is sufficiently small that the regenerator can recover the data traffic without excessive penalty. The regenerator output then has essentially no supervisory content. If the input from the transmission line is not too distorted, then the input and output of the regenerator can be subtracted to yield the supervisory signals together with any residual noise and distortion. Since the supervisory signal has a much narrower bandwidth than the traffic, it is not necessary to cancel the signal at all frequencies. Typically, the cancellation is performed after low-pass filtering to 20MHz. The output of the canceller passes through an RF amplifier that provides a band-pass filtering in addition to amplifying the supervisory signal. Since a supervisory signal is returned from every repeater, a supervisory detector is provided for each repeater. Each of the supervisory detectors must be able to discriminate between the signals returned from the required repeater and all other repeaters. This is essentially achieved from knowledge of the round-trip delay for the required repeater. Each supervisory detector includes a PRBS generator which is identical to that used at the transmitter, but is delayed by the round-trip time of the *i*th repeater. The delay of each detector is adjusted for a specific repeater. The looped back signals are correlated with the local PRBS signal by multiplying the digital local PRBS sequence with the noisy received PRBS. Note

that the noise from the unwanted returned signals is normally expected to increase with the square root of time and hence the OSNR to do the same. However, by integrating the output of the multiplier in time, the noise contributions average to zero yielding a ramp, i.e. a signal which increases linearly with time, at the output of the integrator. The output of the integrator divided by the duration of the ramp gives the returned supervisory signal level. The received supervisory signal also includes the sequences returned from all the other repeaters. These contributions will average to zero in a similar manner to the noise. Although the noise sources average to zero, this is only true after an infinite integration time. However, the average still approaches zero. A pertinent performance measurement is then the time required to achieve a given degree of confidence in the output of the integrator. The integrator is reset to zero periodically so that changes in loopback loss can be recorded. Given these changes for each repeater in the system, the health of the system can be deduced on a span-by-span basis [93]. In figure 3.3, it is possible in practice to have an optical pre-amplifier before the PIN photodetector to raise the signal level well above the noise sources within the receiver.

A key feature of the receiver of the in-band LME system is a cancellation circuit which subtracts the data signal from the small supervisory signal. In out-of-service case, the cancellation unit is not used. The dominant degradation mechanism after cancelling the signal is beat noise between the traffic and ASE noise which falls within the supervisory frequency band. The contributions from the beat noise arise from the whole traffic spectrum, so engineering a notch in the optical spectrum for the supervisory signal would be ineffective as the traffic spectrum would be changed little.

As a summary, the production of the supervisory signal is simplified and there is no command information as a part of the supervisory signal. Degradation of signals through the optical transmission system is easily detected in a reasonable amount of time at the terminals of the system via the correlation technique. Therefore, the correlation technique allows identifying the location of the fault in the transmission line, where basically the degradation in the *i*th signal corresponds to impairment in the *i*th repeater. In this approach, the in-service measurement times for a typical system were of the order of 3.1 hours [93]. The principal degradation mechanisms for the returned signal from a given repeater were firstly counter-propagating traffic and secondly spontaneous-spontaneous beat noise between the traffic signal and ASE noise. Of these, the counter-propagating traffic can be nulled by a data cancellation scheme, but because the beat noise occurs before the cancellation circuit is affected, the traffic can not be completely suppressed using this technique.

In another LME approach, the counter-propagating signal is avoided by utilising a dedicated supervisory wavelength between traffic wavelengths in a WDM system. The supervisory signal of this approach can thus be referred to as *out-of-band LME signal*, and the whole system can be called *out-of-band LME system*. In addition, crosstalk can be avoided by transmitting a pulse which is sufficiently short such that when looped back from each repeater, there is no overlap. The returned signals are then integrated to obtain the signal level. The integration of each returned pulse is accounted sequentially so the integration is a serial rather than a parallel process, thus a set of parallel detectors is not required. Furthermore, the in-service measurement time of a typical system is reduced from an order of 3 hours to 1 minute [94]. This system therefore avoids the PRBS generator, the correlators and the data cancellation unit. Given these advantages, the LME system demonstrated in the following sections will use out-of-band LME signal. The system will therefore require its own wavelength, a small bandwidth PIN detector and a tunable optical filter locked to the supervisory signal wavelength at the receiver. Note that it might be more convenient at this point to refer to the supervisory wavelength as LME wavelength.

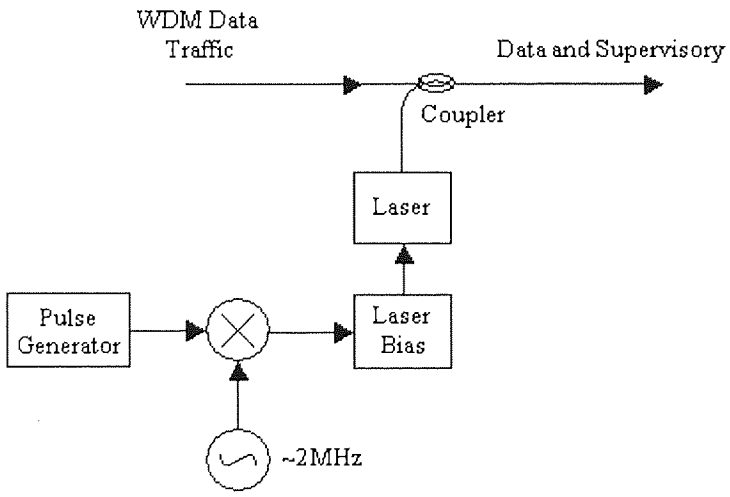

Figure 3.4 Block diagram of the transmitter of the out-of-band LME system.

The transmitter block diagram of the out-of-band LME system is shown in figure 3.4 [94]. It comprises WDM traffic signals over a given set of wavelengths. An LME wavelength is coupled into the aggregate traffic signals. The LME wavelength is chosen to be midway between two adjacent traffic wavelengths of the counter-propagating traffic. No restrictions are placed on the location of the LME wavelength with respect to co-propagating traffic, but performance is

improved if it can also be placed between co-propagating traffic wavelengths. The LME channel comprises a pulsed laser. The pulse duration is chosen to be as long as possible, but sufficiently short such that returned signals from each repeater do not overlap. Since the duration of a pulse is greater than the Er^{3+} metastable life-time (τ), the pulse must be modulated to prevent attenuation by a saturated EDFA. This can be achieved using a sub-carrier of the order of 1MHz [94]. The idea is that the EDFA acts like a high-pass filter to the modulation with a cut-off frequency of about 10kHz. If a CW LME signal is applied with very short rise-time for a duration of 1 second (for instance) so that the total power increased by 10%, then the output power would increase by ~10% initially (because of the high frequency content of the leading edge) and then decay back to a value close to the original power level with a time constant of ~1/(10kHz). If the mean input power of a saturated EDFA increases by 10% the output power would increase by far less than 10%. Over a number of EDFAs, a low speed or DC modulation would be lost. When modulation is applied at >>10kHz (e.g. 1MHz), the mean output power will stay about the same as it was before the modulation since the power of all the other channels will tend to reduce. Therefore, the modulation would not be lost.

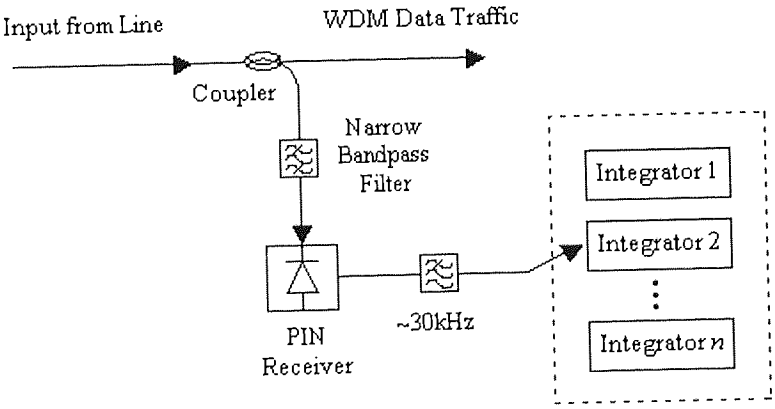

Figure 3.5 Block diagram of the receiver of the out-of-band LME system.

The receiver block diagram of this system can be shown in figure 3.5 [94]. Again, it detects both the traffic and the LME signals looped back from each repeater. The LME optical band-pass filter must be as narrow as possible (typically ~0.2nm) to minimise crosstalk from adjacent traffic channel and to minimise ASE noise incident on the PIN. The filter is locked to the LME signal wavelength to achieve maximum transmission. The detected signal from the PIN is passed through a low-pass filter of a few kHz bandwidth and then integrated. Integration is performed

sequentially and the output from the *i*th integrator represents the LME signal level returned from the *i*th repeater.

The out-of-band LME can also be referred to as *pulsed LME* because it uses an LME pulse on an unused wavelength, while the in-band LME can be referred to as *passive LME* as a PRBS signal is superimposed on an existing traffic channel [93], [94]. Again, this chapter will consider the out-of-band LME system.

3.3 Performance degradation mechanisms

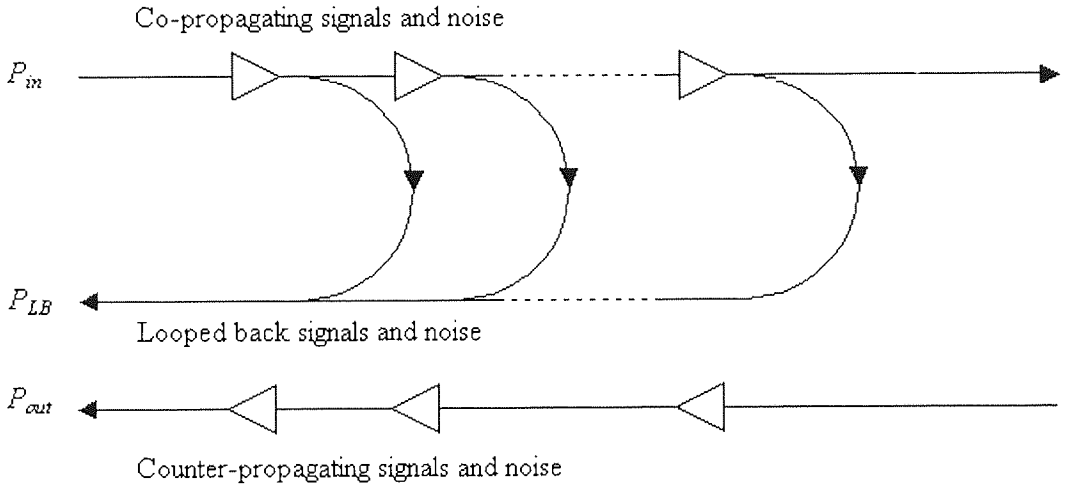

Figure 3.6 Representation of signal flows.

Data traffic and LME signals have different performance degradation mechanisms; therefore they are discussed separately. Starting with data traffic signals, it is important to know first that they have no modulation penalty from the LME signal since it is carried on an independent wavelength. However, a number of other penalties still persist which are discussed here. Referring to figure 3.6, the counter-propagating traffic is affected by the proportion of the co-propagating traffic that is looped back at every repeater. Moreover, the traffic signal power is attenuated by the tap coupler of every loopback circuit, effectively increasing the span losses. Additional penalties are caused by the ASE noise, which is added by each repeater and by the transmitter post amplifier, and the beat noise arises due to the presence of LME wavelength within the traffic filter band. If the LME signal is outside the traffic optical filter bandwidth, then this penalty can be avoided. Four-wave mixing between the traffic and LME signals as well as

the SBS penalties also degrade the data traffic performance. These can be avoided by ensuring the LME signal power is sufficiently small compared with the traffic signal power, and there is enough spacing between the LME signal and the adjacent data signals.

From figure 3.6, the returned LME signal can have a set of penalties, which are due to: the counter-propagating traffic at the skirts of the LME optical filter, the looped-back traffic from every repeater - can be negligible due to the high-loss in the loopback circuit, counter-propagating ASE noise and looped back ASE noise. The receiver also generates thermal noise and the signals are subject to shot noise.

3.4 LME pulse performance analysis

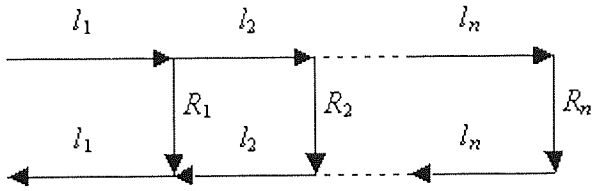

Figure 3.7 Signal paths of a launched LME pulse.

Figure 3.7 shows the signal paths of the launched LME pulse. If the distance between repeaters $i-1$ and i is l_i, then the total loopback distance z_i for repeater i is:

$$z_i = 2\sum_{j=1}^{i} l_j \ , \ i = 1...n \tag{3.1}$$

and the path difference Δz_i between repeaters $i-1$ and i is:

$$\Delta z_i = z_i - z_{i-1} = 2l_i \tag{3.2}$$

The time required for a signal to return from repeater i is:

$$T_i = \frac{n_r z_i}{c} \tag{3.3}$$

where $n_r = 1.46$, which is the refractive index of the transmission fibre. The difference in loopback time between adjacent repeaters $i-1$ and i is then:

$$\Delta T_i = \frac{n_r \Delta z_i}{c} = \frac{2n_r l_i}{c} \tag{3.4}$$

To prevent the overlap of the returned signal from adjacent repeaters, the LME pulse duration must be no greater than $\Delta T_i\big|_{\min}$, $i = 1...n$, where the *min* subscript refers to the minimum repeater spacing $l_{\min}$. To allow for switching time between returned LME pulses, a guard-band should also be provided of duration T_G. The pulse duration is then shortened according to:

$$\begin{aligned} T_p &= \frac{2n_r l_{\min}}{c} - T_G \\ &= \frac{2n_r l_{\min}}{c}(1-\beta) \end{aligned} \tag{3.5}$$

where $\beta = \dfrac{cT_G}{2n_r l_{\min}}$ is the proportion of $T_p + T_G$ reserved for the guard-band.

After an LME pulse has been launched, a second cannot be transmitted until all the loopback pulses have arrived. From (3.1) and (3.3), the time for the leading edge of the pulse to return from the *n*th repeater is:

$$T_n = \frac{2n_r}{c}\sum_{j=1}^{n} l_j \tag{3.6}$$

where $\sum_{j=1}^{n} l_j$ is the length of the system, excluding the last, $(n+1)$th, span. The trailing edge of the pulse arrives after a time $T_n + T_p$ and the pulse repetition time T_R, allowing for the guard-band, is then:

$$T_R = T_n + T_p + T_G$$
$$= \frac{2n_r}{c}\left(l_{\min} + \sum_{j=1}^{n} l_j\right), \tag{3.7}$$

where $T_n + T_p$ is substituted from (3.5).

Figure 3.8 illustrates the LME pulse propagation and return times. The guard-band T_G is the time between the closest arriving pulses.

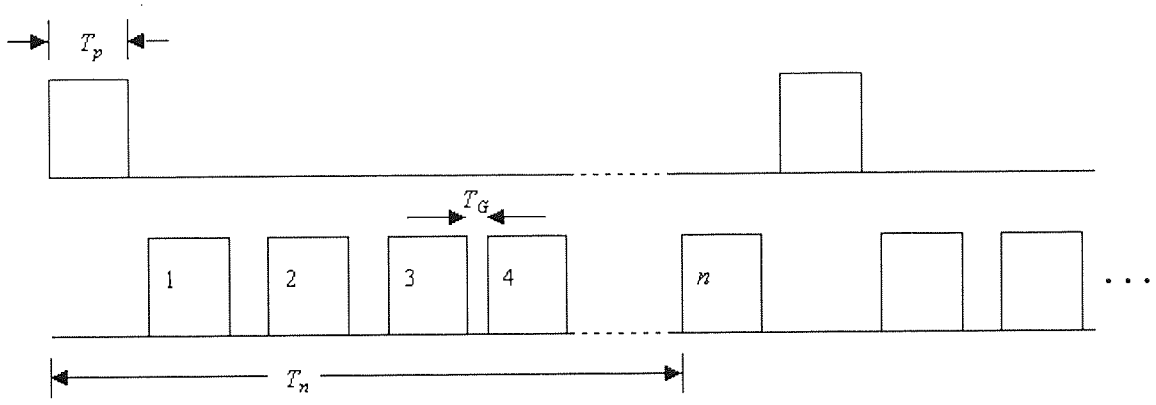

Figure 3.8 Launched and returned pulses

For example, a system with 140 repeaters, whose spacing is 45km and total length is 6345km will require an LME pulse duration of no greater than 0.45ms. The pulse repetition time is 63.45ms, which corresponds to a rate of 15.76 pulses/s.

3.4.1 OSNR analysis

If the launched power during the LME pulse is S_{in}^{cw}, then the received loopback power from any repeater is:

$$S_{out}^{cw} = A_{LB} L S_{in}^{cw} \tag{3.8}$$

where A_{LB} is the total loopback transmittance due to a single repeater and L is the transmission fibre transmittance. The noise within an optical bandwidth B_o incident with the counter-propagating signal is given by:

$$N_{out} = nFh\nu B_o \tag{3.9}$$

where N_{out} is the received line amplifier noise, n is the number of line amplifiers, F is the noise figure and ν is the carrier frequency. The transmitter and receiver noise have been neglected. After detection by the PIN, the electrical signal power is given by:

$$i_{out}^2 = \left(R_s S_{out}^{cw}\right)^2, \tag{3.10}$$

and the electrical signal-spontaneous and spontaneous-spontaneous noise powers are:

$$i_{s-sp}^2 = N_{s-sp} = 2R_s^2 S_{out}^{cw} N_{out} \frac{B_e}{B_o} \tag{3.11}$$

$$\begin{aligned} i_{sp-sp}^2 = N_{sp-sp} &= N_{out}^2 R_s^2 \frac{B_e}{B_o}\left(1 - \frac{B_e}{2B_o}\right) \\ &\approx N_{out}^2 R_s^2 \frac{B_e}{B_o} \end{aligned} \tag{3.12}$$

where R_s is the responsivity and it is assumed the electrical bandwidth $B_e << B_o$.
The electrical signal-to-noise ratio is then given by:

$$\text{eSNR} = \frac{\left(S_{out}^{cw}\right)^2}{N_{out}\left(2S_{out}^{cw} + N_{out}\right)} \frac{B_o}{B_e} \tag{3.13}$$

Because the input signal power suffers from high attenuation through the loopback circuit, therefore $S_{out}^{cw} << N_{out}$ and (3.13) can be approximated by:

$$\text{eSNR} \approx \left(\frac{S_{out}^{cw}}{N_{out}}\right)^2 \frac{B_o}{B_e} = \text{OSNR}^2 \frac{B_o}{B_e} \tag{3.14}$$

3.4.2 Measurement time

Given a minimum required electrical signal to noise ratio eSNR_{req} to achieve the desired repeatability, the number of samples required is:

$$n_s = \frac{\text{eSNR}_{req}}{\text{eSNR}} \tag{3.15}$$

If the sample rate is $2B_e$ (which is the Nyquist rate), then the number of samples per pulse is:

$$n_{sp} = 2B_e T_p \tag{3.16}$$

and so the number of transmitted pulses required is:

$$n_p = \frac{n_s}{n_{sp}} = \frac{1}{2B_e T_p} \frac{\text{eSNR}_{req}}{\text{eSNR}} \tag{3.17}$$

Given the pulse repetition rate $1/T_R$ the measurement time T is then given by:

$$T = n_p T_R = \left(1 + \frac{1}{l_{min}} \sum_{j=1}^{n} l_j\right) \frac{B_o \text{eSNR}_{req}}{2(1-\beta)} \left(\frac{nFh\nu}{A_{LB} LS_{in}^{cw}}\right)^2 \tag{3.18}$$

where (3.5), (3.7), (3.8), (3.9) and (3.17) have been used.
In the case of equal span lengths, $l_{\min} = l_j$, and (3.18) reduces to:

$$T = \frac{n^2(n+1)}{2(1-\beta)} \left(\frac{Fh\nu}{A_{LB} LS_{in}^{cw}}\right)^2 B_o \text{eSNR}_{req} \tag{3.19}$$

The required eSNR for a measurement repeatability (R_p) of ±0.5dB to within a $\pm t\sigma$ confidence interval is given by [93]:

$$\text{eSNR}_{req} = \left[\frac{tr_p}{(r_p - 1)}\right]^2 \tag{3.20}$$

where r_p is the linear repeatability and related to the measurement repeatability as $R_p = 10\log_{10}(r_p)$.

The measurement time then becomes:

$$T = \frac{n^2(n+1)}{2(1-\beta)}\left(\frac{tr_p}{(r_p - 1)}\right)^2\left(\frac{Fh\nu}{A_{LB}LS_{in}^{cw}}\right)^2 B_o \tag{3.21}$$

From (3.21), it can be seen that the measurement time increases as the cube of the number of repeaters and inversely as the square of the supervisory signal receiver input powers LS_{in}^{cw}. For a typical 100 repeater system, T is approximately 1 minute for a measurement repeatability of 0.5dB to within a $\pm 3\sigma$ confidence interval [94].

3.4.3 Example

Consider a 100 repeater system with a 45dB loopback loss and a pulse launch power of -7dBm. The parameters of the entire system are given below:

Transmitter	
LME signal input power (single pulse)	-7 dBm
Wavelength	1558 nm
Frequency	192.55 THz
Quantum efficiency	0.85
Responsivity (R_s)	1.07
Guard-band β factor	5 %

Line	
Span loss	15 dB
loss coefficient (α)	0.2 dB/km
Span length	75 km
Tap coupler ratio	10 dB
Tap coupler loss	0.4 dB
Tap coupler through loss	0.82 dB
Tap coupler drop loss	10.4 dB
EDFA gain	15.82 dB
EDFA noise figure	5.5 dB
Loopback pad loss (A)	25 dB

Total loopback loss (A_{LB})	44.98 dB
Number of repeaters	100
System length	7575 km

LME receiver

Optical filter bandwidth (B_o)	0.25 nm
LME filter bandwidth	30 kHz
Sample rate	60.0 kHz
Required repeatability (R_p)	0.5 +/- dB
Confidence limits index (t)	3
Confidence limits	99.8650 +/- %
Confidence level (γ)	0.99865
Required eSNR for signal measurement	28.814 dB
pulse duration without guard-band (T_p+T_G)	0.750 ms
pulse duration (T_p)	0.713 ms
Guard-band duration (T_G)	0.038 ms
Return time from nth repeater (T_n)	75.000 ms
pulse repetition time (T_R)	75.750 ms
samples per pulse (n_{sp})	

By using equations (3.8)-(3.21), the]

as the following:

S_{out} (LME pulse)	
N_{out}	
$N_{s\text{-}sp}$	
$N_{sp\text{-}sp}$	
Thermal noise	-100.02 dBm
Shot noise	-169.33 dBm
Total noise (σ)	
eSNR	10.94 dB
Samples required to measure LME pulse (n_s)	37653
Number of pulses required to measure LME level (n_p)	881
Pulse repetition rate ($1/T_R$)	13.20 /s
Time (T) to measure repeater level	1.11 mins

It can be seen that for such 100 repeater system, the receiver needs only 1 minute to measure the in-service returned LME pulse using the 881 averages of the received LME pulse.

3.5 LME system prototype

3.5.1 LME transmitter and receiver architecture

As explained before, the method of operation relies on a high-loss loopback path being available at every repeater. A probe (or supervisory) signal of dedicated wavelength is launched into the system at low level, and narrow band receiver is used to pick off the weakly returned signals from each repeater. Due to the high-loss of the loopback path, the returned signal is extremely weak and heavily swamped by amplifier noise of the returned path. Hence the receiver has to operate well under heavily noise loading. The prototype transmitter and receiver of such in-band LME system are shown in figure 3.9 [95]. At the transmitter, gated pulses from oscillator X_1 are amplified, shaped and applied to the bias PIN of laser diode D_1. The resulting optical LME pulse from D_1 has a burst duration T_p, repetition rate T_r and modulation frequency f_s.

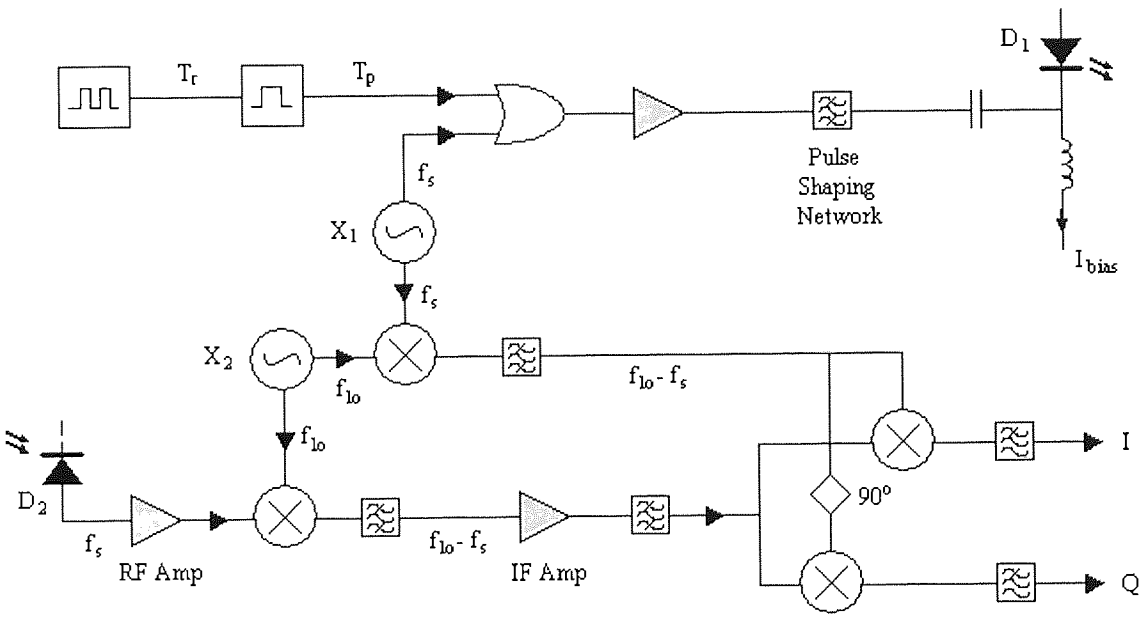

Figure 3.9 In-band LME transmitter (top section) and receiver (bottom section) architecture.

At the receiver, the returned signal with carrier frequency f_s is coupled into detector D_2, amplified by the RF amplifier and fed to one arm of a mixer. The other arm of the mixer is driven by local oscillator X_2 at the frequency f_{lo}, generating at the output of the mixer the sum and difference frequencies $f_{lo} \pm f_s$. The difference frequency is selected by the band-pass filters and amplified by the intermediate frequency (IF) amplifier, as in a conventional heterodyne receiver. Most of the gain of the receiver is present in this stage. Detection of the carrier envelope is accomplished through the IQ demodulator at the output of the IF amplifier. The reference

frequency for the IQ demodulator is obtained by mixing the local down-conversion oscillator X_2 with the transmit carrier oscillator X_1, resulting in a DC output at the I and Q ports of the demodulator. The amplitude of the received carrier is then proportional to $\sqrt{(I^2+Q^2)}$. Figure 3.10 shows the transmitted optical pulse in (a) and the corresponding electrical output of the receiver for a back-to-back measurement with no fibre in the system in (b). The carrier or modulation frequency is ~2MHz and the optical power into the receiver is approximately -50dBm.

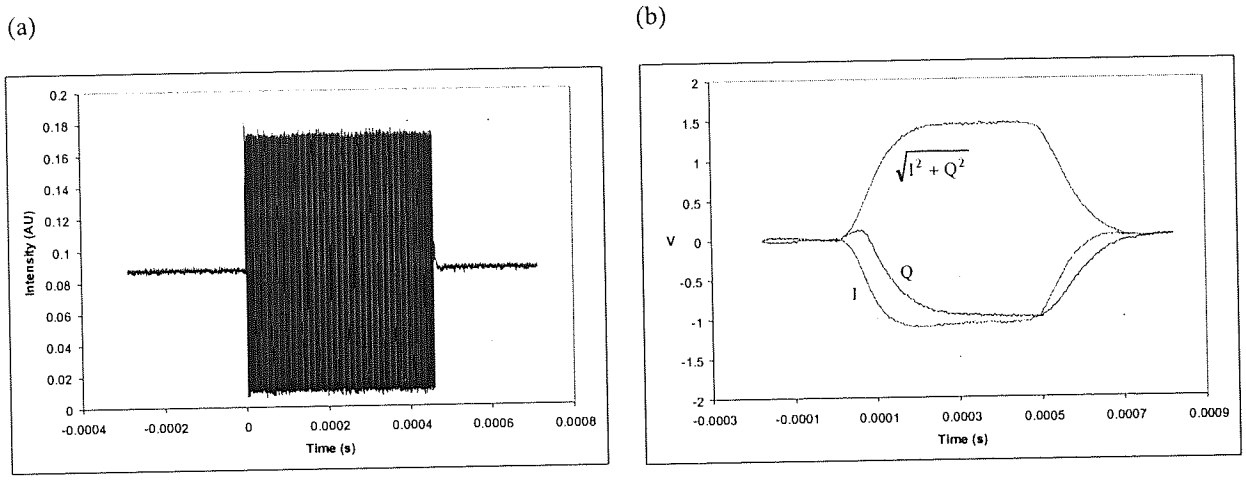

Figure 3.10 (a) Transmitted optical LME pulse. (b) Receiver output for back-to-back measurement.

3.5.2 High-loss loopback system setup

High-loss loopback system can be simulated in the laboratory as shown in figure 3.11, which is used to monitor one direction of the fibre pair. As in figure 3.4, a WDM data signals are coupled with an LME signal that was generated by the LME transmitter described in figure 3.9, to give the composite forward or co-propagating traffic. The co-propagating path is basically simulated by using a recirculating loop, in which a single loopback circuit with variable attenuators is placed to monitor the performance at the output of the last EDFA. This of course provides one repeater monitoring where further repeaters can be monitored by increasing the number of recirculations. Therefore, using different number of recirculations enables simulating different repeater loopback circuits. In fact, the recirculating loop has to be set up such that its length is larger than the LME pulse-width to ensure full propagation of the LME pulse in the loop. Also, the loop should have one LME pulse propagating in every recirculation. This can be achieved by triggering the loop with the LME pulse, and setting the fill-time such that the next LME pulse appears in the next propagation cycle.

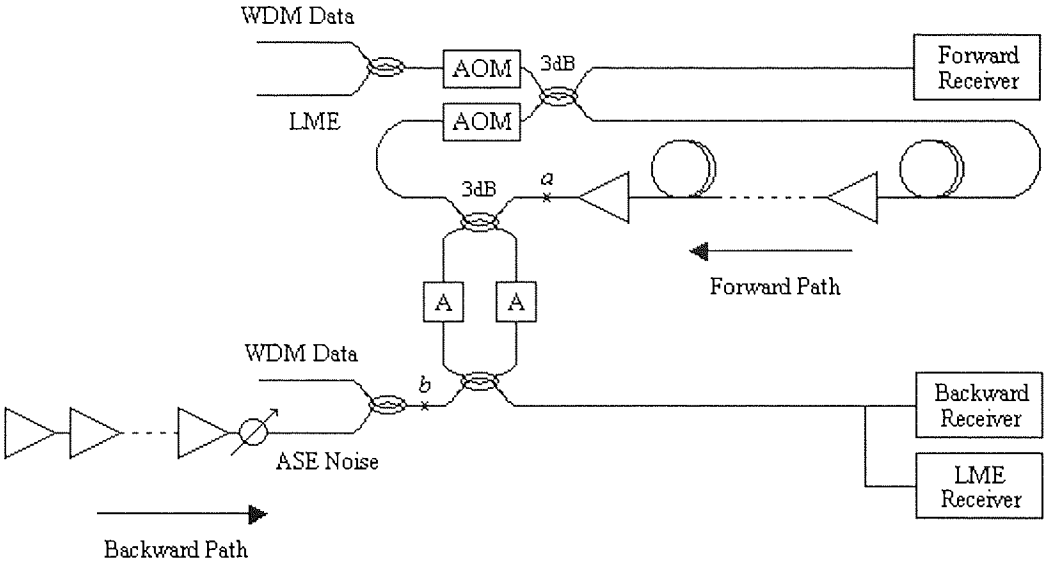

Figure 3.11 Loopback system setup.

In the counter-propagating direction, by referring back to figure 3.6, the backward path includes the counter-propagating data traffic signals and ASE noise. This indeed gives the ability to simulate the backward path by setting up a WDM data source and an ASE noise source, as appears in figure 3.11. The ASE noise source is composed of a chain of cascaded EDFAs followed by variable attenuator that is used to match the noise signal level to that in the co-propagating path. Therefore the noise at point *b* in the figure must be equal to the noise at point *a*. The data signals are coupled with the noise signal by fibre coupler to give the composite backward traffic, which allows simulating the backward path without setting up fibre spans. Even though the system setup is not identical to a full dual path system, it can still be usable for this experiment. The key idea is that the returned signal has to be swamped by the noise of a backward path which is in real system identical to that of the forward path, assuming that the system is symmetric. Setting up a full dual path system will require two identical recirculating loops; one for forward direction and the other for backward as discussed later in chapter 6.

3.6 LME experiment

In this section, an LME experiment is demonstrated using the LME system prototype discussed in previous section. The objective of this experiment is to test the feasibility of an LME transmitter and receiver on long-haul optical transmission system. This includes the recovery of a

weak LME pulse that is returned by the high-loss loopback circuit and swamped by the backward noise. The typical loss of the loopback circuit is 45dB; including all the combined losses of the attenuator and the two tap couplers [92]. Therefore, the main aim of the experiment is to achieve an LME detection and recovery after 45dB loopback attenuation and over long distance. The experiment will start testing the LME pulse recovery at different amounts of loopback attenuation and transmission distance. It is indeed a big challenge to achieve an LME recovery after long distance where the backward noise level is expected to be much higher than the returned LME signal. Therefore, LME recovery will be further examined by investigating different parameters such as LME signal launch power and optical bandwidth of the filter used prior to the LME receiver. Having achieved this, it is then possible to look at the effect of the LME signal to the forward data traffic signals. This includes the effect of the LME power increase as well as the decrease in spacing between the LME and the adjacent data channel. Furthermore, it is also important to look at the effect of the forward data signals to the LME signal at different spacing.

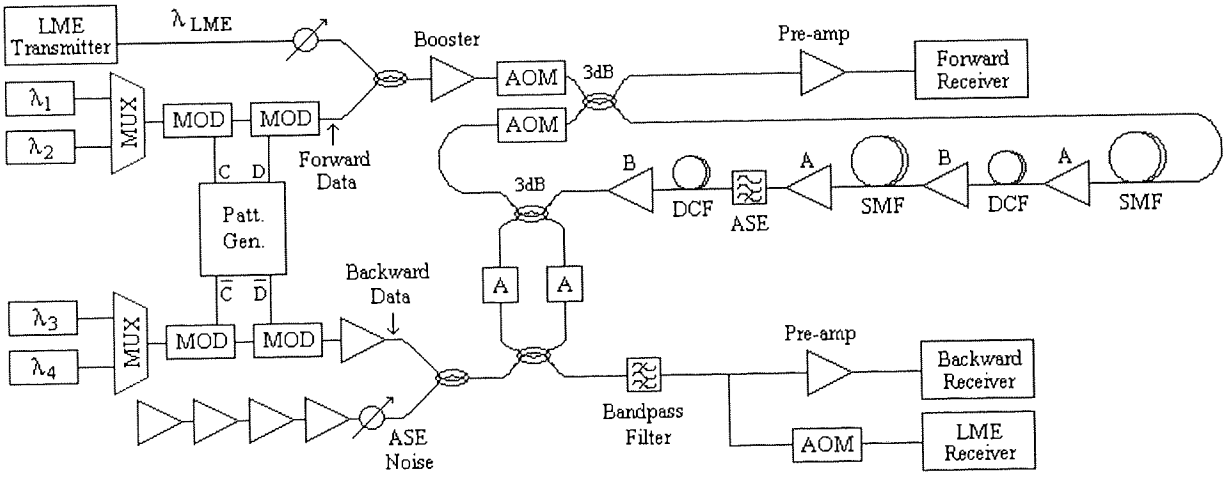

Figure 3.12 The whole LME experimental setup.

The whole setup for this experiment is shown in figure 3.12. In the forward path, an LME transmitter has been set up as shown in figure 3.9 to produce optical LME pulses with duration (T_p) of 500μs, repetition rate ($1/T_r$) of 8Hz, and carrier frequency (f_s) of 2MHz. The LME signal is then coupled with two WDM data signals in RZ modulation format and 10Gbit/s bit-rate. These data signals were generated by using two $LiNbO_3$ modulators driven by clock and data signals of a pattern generator with 10.709GHz frequency and $2^{31}-1$ PRBS data. The wavelength of the data signals λ_1 and λ_2 are 1556.4 and 1557.4nm, respectively, while the LME wavelength is 1558.4nm, using DFB lasers in all channels. The reason for choosing such wavelengths is that the

maximum backward noise from the noise source (discussed later) was achieved at around 1558.4nm, and the data signals are firstly intended to be 1nm apart from the LME signal and from each other. A variable optical attenuator follows the LME transmitter to adjust the LME signal level, which is supposed to be much lower than the data signals levels, typically 10dB lower. The resultant data and LME signals are amplified to the required level and then propagated through a 200.9km recirculating loop. The experiment starts with low power levels, which are 0dBm in each data signal and -10dBm in LME signal at the input of the load AOM (or input AOM). The launch powers into the fibre are hence lower by 6dB due to the insertion losses of the AOM and coupler. These powers were measured on an Agilent multi-wavelength meter - model 86120C [96], which reads the power of every wavelength within 10GHz resolution bandwidth. The total average power can be measured on the power meter (e.g. Newport) that reads the average of the power over the whole band, including ASE noise. However, starting the experiment with low LME power enables defining the minimum power that can be used with this system for LME recovery after 45dB loss in the loopback path. This may perhaps require increasing the LME power until the 45dB is achieved.

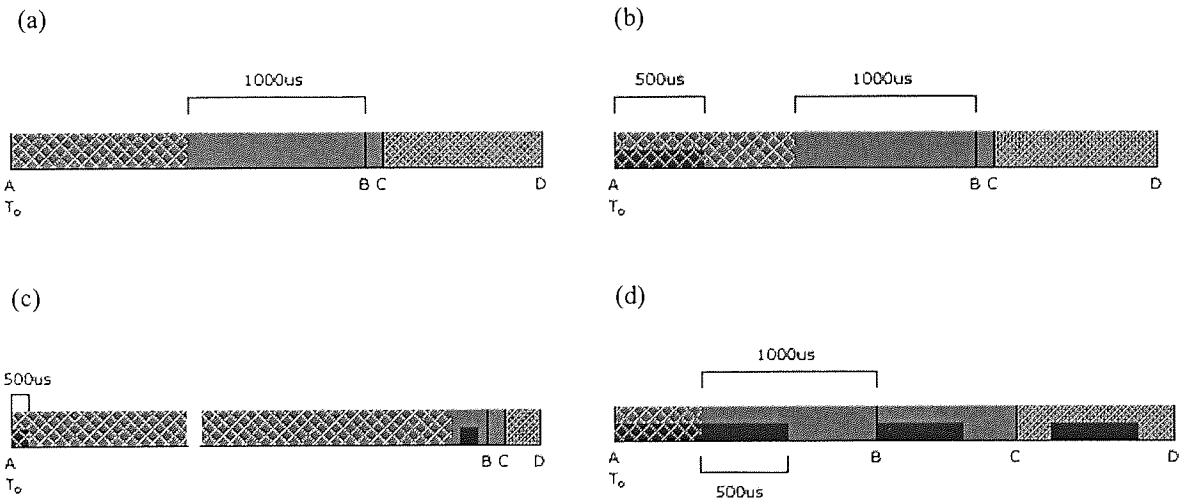

Figure 3.13 Recirculating loop timing for LME experiment.

Triggering the recirculating loop by the LME pulse is not straightforward as it is necessary to make sure that the LME pulse is fully propagated around the loop and there is one LME pulse in each recirculation. In fact, there are three timing possibilities for triggering the loop as shown in figure 2.13. (a) shows the normal operation of the recirculating loop, where the fill-time is twice as the round-trip time of the loop which is 1000μs for 200km. The first triggering

possibility is shown in (b); the loop is triggered by the start time of the LME pulse, thus the whole LME pulse is not filled within the loop as it is lost by the AOM. This is basically because the first 1000μs is lost while the second 1000μs fills the loop. Another possibility is shown in (c), where the loop is also triggered by the LME pulse but the fill-time is set to wait for the next LME pulse. In this case, the next LME pulse will reset the time T_0 and re-start the triggering; giving that the LME pulse will never propagate around the loop. As a result, the best way to trigger the loop can be done as shown in (d) by extending the LME pulse from 500μs up to 1000μs at the LME source, and reducing the fill-time till the next pulse appears in the next cycle. In this way, the first 500μs of the LME pulse is lost by the AOM while the remaining 500μs is propagated through the loop. Doing this, the LME pulses at the output of the recirculating loop can be displayed on a real-time oscilloscope as shown in figure 3.14. It is obviously shown that 1000μs pulse enters the loop but only 500μs of it recirculates around the loop. This gives that each pulse appears in the figure corresponds to one recirculation.

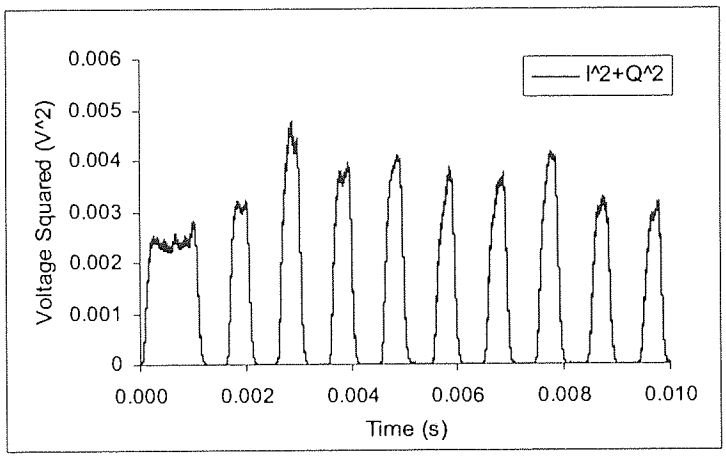

Figure 3.14 LME pulse propagation in the loop.

The recirculating loop itself consists of two SMF-DCF fibre sections. The first section is consisting of 82.5km of SMF with 0.2dB/km attenuation coefficient and dispersion of 17ps/nm/km at 1550nm, and 15.2km of DCF with attenuation of 0.5dB/km and a negative dispersion of 1387ps/nm. The second section is consisting of 86.7km of SMF with the same attenuation coefficient and dispersion of that in the first section, and 16.5km of DCF with attenuation of 0.5dB/km and a negative dispersion of 1387ps/nm. The losses of these fibres were compensated by using two C-band EDFAs in each section. The EDFAs denoted A in the figure 3.12 had a 30dB maximum small signal gain and ~13dBm maximum output saturation power,

while the EDFAs denoted B had a 40dB maximum small signal gain and ~15dBm maximum output saturation power. The gain of each amplifier was set to compensate for the loss of the previous span, except for the last amplifier whose gain was increased to further compensate for the losses of the loopback tap coupler as well as the loop AOM and following coupler. All EDFAs had a noise figure of approximately 5. An ASE filter with an insertion loss of 3dB was used before the last amplifier to remove the accumulated ASE gain peak at 1530nm. This 3dB loss was compensated by the third amplifier, so power at the input of each fibre is constant. The reason why the ASE filter is not set up after the last EDFA is basically to reduce the amount of losses being compensated by that EDFA, thus reducing the gain of the EDFA. This of course results in the ASE peak at 1530nm of the last EDFA, only in the last recirculation not being removed, which is alright as long as all the accumulated peaks from the previous amplifiers have already been removed.

In the backward path, two WDM data signals with wavelengths λ_3 and λ_4 of 1559.4 and 1560.4nm, respectively, are generated in the same way of those in the forward direction, using the same pattern generator but with the inverse clock and data signals. This was due to the unavailability of another pattern generator. Four cascaded EDFAs; each with noise figure of approximately 5 are set up to produce the backward noise. The gains of the EDFAs are set at the maximum where a variable attenuator is used to adjust the noise level corresponding to the transmission distance used in the forward direction. The noise signal is then coupled with the backward data signals to give the composite backward traffic that passes through the tap coupler of the loopback circuit. Remember that the power of the backward traffic must be similar to that of the forward traffic, i.e. each backward signal has a power of -10dBm after the loopback coupler. Before the receiver, a tunable band-pass filter with 0.24nm bandwidth and 7dB insertion loss is used to extract the wanted wavelength to be detected. The filter can then be used as a demultiplexer for the backward data signals that can be therefore pre-amplified and detected by the BERT/sampling scope, or to extract the LME signal that can be detected and examined by the LME receiver. By the way, for examining the forward traffic, the band-pass filter and the pre-amplifier are also required at the output of the recirculating loop as shown on the top of figure 3.12. However, the LME signal has to pass through an AOM, which is triggered by the C-D time of the digital delay generator used for the recirculating loop (recall figure 2.13), before being detected by the LME receiver. This is to ensure that the receiver will detect the LME pulse of the last recirculation, while the other recirculated pulses are eliminated. This implies that the different LME pulses that correspond to different repeaters are detected and examined

individually, not like the real system in which they are detected and displayed serially as shown in figure 3.8. This is understood as there is only one loopback circuit in the experiment which is used to monitor one repeater at a time. The LME receiver is similar to that shown in figure 3.9, where the local frequency (f_{lo}) is 2.455MHz and receiver sensitivity is about -60dBm. The electrical bandwidth of the receiver (B_e) is 6.3kHz, determined by the IF filter bandwidths and the low-pass filter at the output of the IQ demodulator. The full description of the device used at the heart of the receiver, which is referred to as a 3 V low power receiver IF subsystem (AD607), can be found in the datasheet shown in appendix A.

3.6.1 Recirculating loop measurements

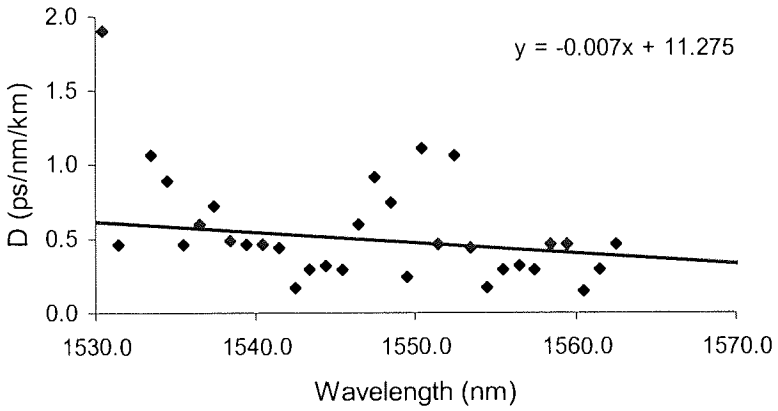

Figure 3.15 Dispersion measurements of the 200km loop.

Before running the LME experiment, it is essential to examine the performance of the recirculating loop, by performing dispersion measurements as well as BER/Q or OSNR over transmission distance of the forward data signals. This can all be done as long as the losses of the fibre spans and components of the loop are compensated by the EDFAs. As mentioned before, the gains of the EDFAs are set such that the total average power into the input of each fibre span is constant; giving that the loop is balanced with respect to the losses. However, figure 3.15 shows the dispersion measurements of the loop by using the laser cavity method discussed in previous chapter. It is seen that the total dispersion measures ~0.5ps/nm/km in the operating wavelength region giving that the dispersion of the current loop is not properly managed.

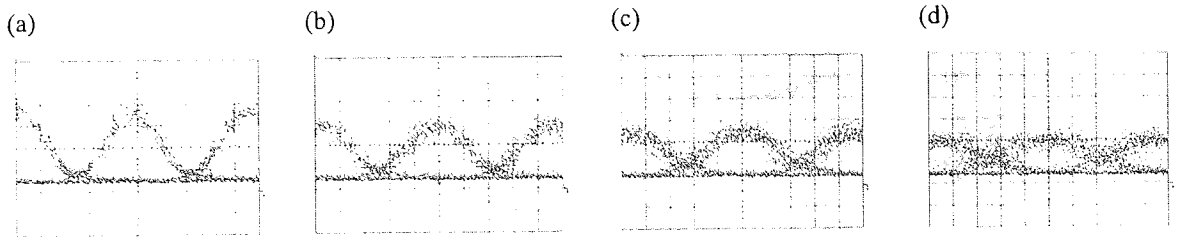

Figure 3.16 Signal shape for the first data signal (λ_1=1556.4nm) after: (a) 200km; (b) 400km; (c) 600km; (d) 800km. (Time scale: 20ps/div).

The result would be that the data signals will be considerably broadened after long distance, but for the LME signal whose pulse duration is 500μs, the broadening effect can be negligible. This would imply that the first part of the experiment, which examines the detection and recovery of the returned LME signal, can still be performed with such loop configuration. Furthermore, the BER/Q measurements of the forward data signals cannot be taken at this stage, since the broadening will distort the signals after few recirculations, as shown in figure 3.16. This requires that the dispersion must be fully compensated at the next stage which will investigate the effect of the LME signal to the data signals and vice versa. Certainly, such investigation cannot be performed without optimising the forward traffic performance. Nevertheless, the OSNR measurements for the forward signals can still be taken for the current loop as they provide performance with respect to the noise accumulation and are not affected by the dispersion. Moreover, noise measurements over distance are important at this stage where they give indication of how much ASE noise is to be generated in the backward direction. Figure 3.17 presents the OSNR and noise measurements as a function of transmission distance for the forward data signal (λ_1=1556.4nm) using OSA resolution bandwidth of 0.5nm. The figure also shows the results obtained by simulation using VPI*. It can be seen that data signals can propagate over ~4600km with acceptable OSNR performance. This would imply that the objective of this stage is to get the LME receiver detecting and recovering the LME signal after 4600km if 45dB loopback attenuation is used.

* All simulation results shown in this chapter have been provided by Dr Wai Wong, Azea Networks. For information about VPI simulator, see appendix B.

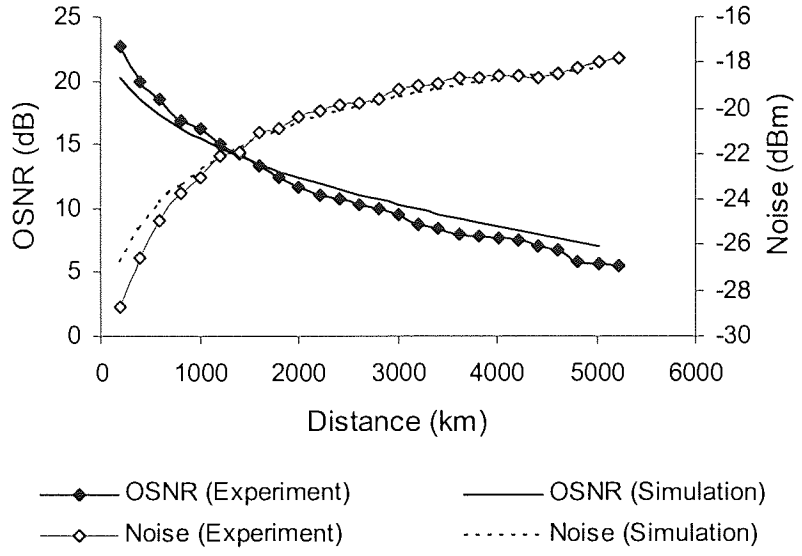

Figure 3.17 OSNR and noise versus transmission distance for data signal (λ_1=1556.4nm).

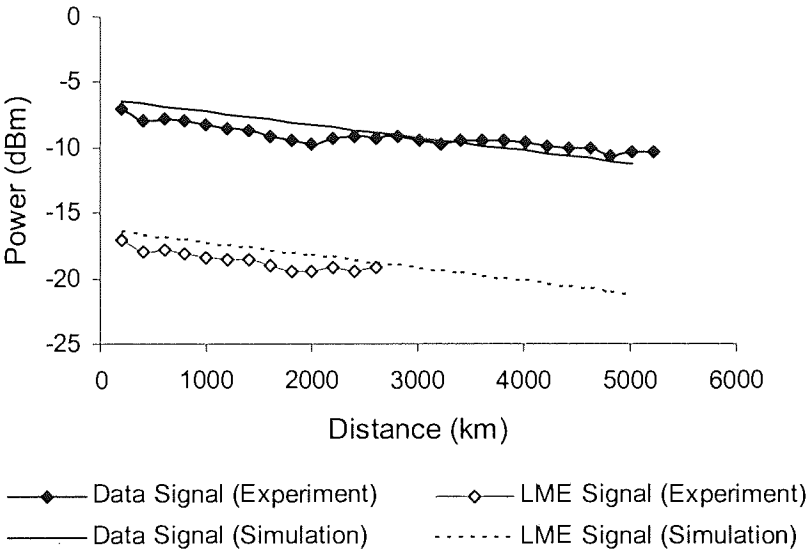

Figure 3.18 Power versus transmission distance for the data signal (λ_1=1556.4nm) and the LME signal.

The power evolution of the data and LME signals over transmission distance can be shown in figure 3.18. Since the power was measured at the output of the loop, it was attenuated by 6dB through the loop AOM and the coupler. However, it is seen that the power level of both signals drops down as the distance increases, where it reduces by almost 3dB after 4600km. This can be understood as the ASE noise builds up while the total average power should remain constant. It is also noticed that the LME signal becomes below the noise level after ~2600km and cannot be measured but can be extrapolated as in the simulation curve.

3.6.2 Backward noise

The level of the backward noise that is generated by the four cascaded EDFAs, as in figure 3.12, must be varied for different number of recirculations according to the noise level in the forward direction. The amount of the backward noise that is required for a transmission distance can be therefore obtained from figure 3.17. It is important to remember that these noise measurements were taken at the output of the recirculating loop, which means that they have already been attenuated by the losses of the loop AOM and the 3dB coupler. Referring to figure 3.11, since the noise at point *b* must equal the noise at point *a*, the noise values of figure 3.17 must be offset by +9dB. This amount includes the 3dB loss of the loopback coupler in the forward direction in addition to the 6dB of the AOM and its following coupler. Given this, the backward noise can be simply achieved by setting the four EDFAs at their maximum gain, and varying the optical attenuator to produce the required amount of noise. It is therefore useful to define the amount of attenuation in the optical attenuator that is required for each number of recirculations as shown in figure 3.19. This allowed rapid adjustment of the noise level for different propagation distance while the experiment is running. Note that the noise level refers to the level of the ASE noise that is observed at around the LME wavelength on the OSA screen.

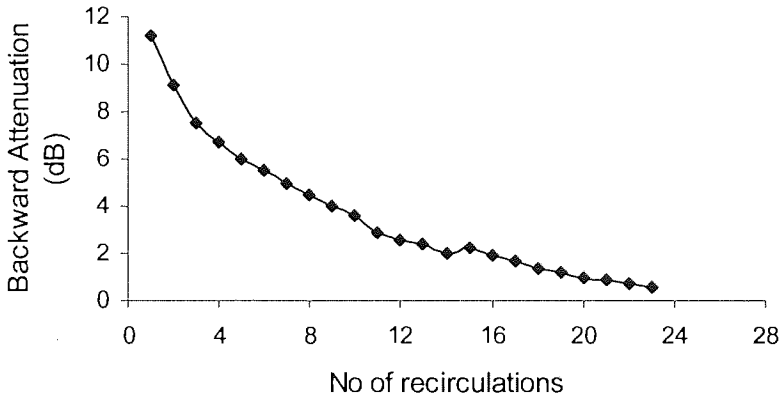

Figure 3.19 Backward noise attenuation required for different number of recirculations.

The maximum noise level from the cascaded EDFAs was achieved at around 1558.4nm as shown in figure 3.20, which explains the reason behind using such wavelength for the LME signal. This picture was taken just before the loopback coupler in the backward path, i.e. at point *b* in figure 3.11.

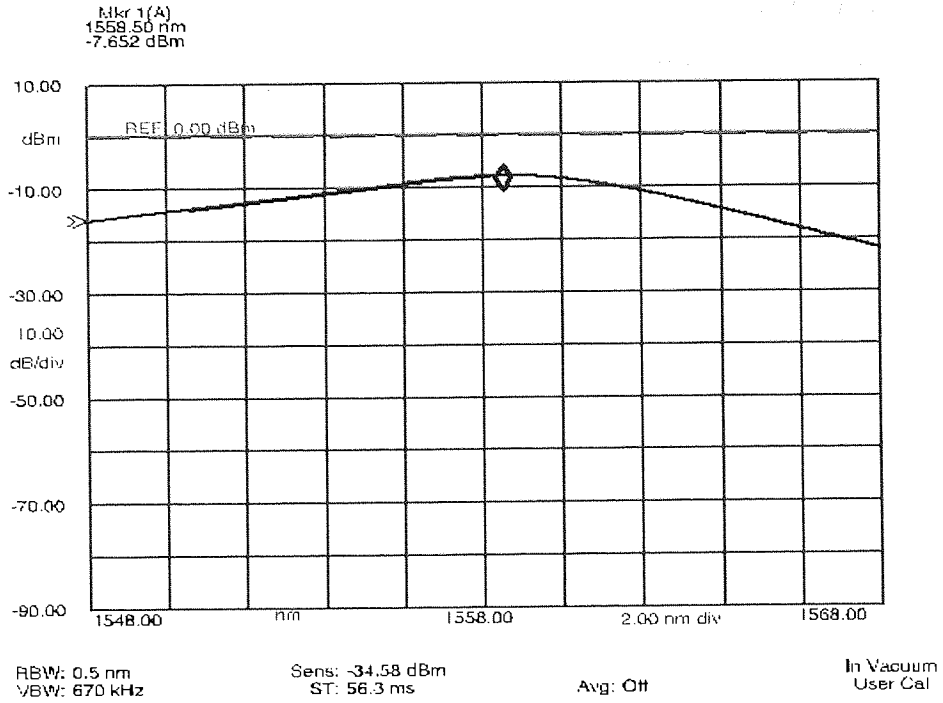

Figure 3.20 ASE noise profile of the backward EDFAs; the marker defines the maximum noise point.

3.6.3 LME pulse recovery after high loopback attenuation

Having set up both forward and backward paths, the first part of the LME experiment can be performed. As mentioned above, the main aim of this part is to test the feasibility of the LME receiver in detecting and recovering the attenuated LME pulse that is also overflown by the high noise of the backward traffic. Before running such experiment, a quick test was performed to check the ability of the LME receiver to detect a pulse which is swamped by noise. This test was done using a simple setup as shown in figure 3.21, where an optical LME signal was coupled with noise signal such that the noise level was much higher than the LME signal. The composite signal was then sent directly to the LME receiver that must recover the original LME pulse. Figure 3.22 (a) shows the optical spectra of the LME and noise signals before the receiver, where the noise signal was set to be higher than the LME signal by almost 11dB. Figure 3.22 (b) shows the $\sqrt{(I^2+Q^2)}$ curve of the received signal, which is proportional to the LME amplitude. Note that the signal was arbitrarily attenuated before the receiver to prevent photodiode saturation. However, as long as the $\sqrt{(I^2+Q^2)}$ curve is visible on the oscilloscope, it means that the receiver has been successful in recovering the LME pulse. Otherwise, the LME signal is lost or the receiver cannot extract it from the noise signals that are received with the LME signal. It can

be noticed that the LME pulse had 1000μs as it was taken straight from the LME source and not being recirculated around a loop. It is also important to remember that the LME pulse of different repeater will be displayed with different time (T_i) according to the repeater distance. The pulse displayed in figure 3.22 (b) is therefore corresponding to 0th repeater, i.e. back-to-back.

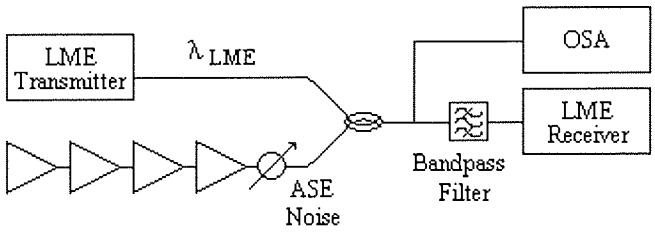

Figure 3.21 Setup for LME pulse recovery test.

(a) (b)

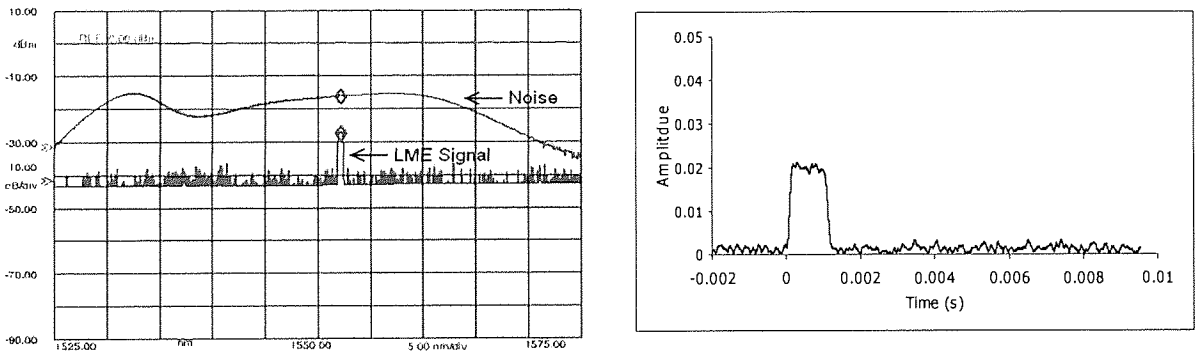

Figure 3.22 (a) OSA picture shows an LME signal swamped by a noise signal. (b) The pulse recovered by the LME receiver.

Back to the LME experiment which has, in summary, a forward and backward traffic. The forward traffic has two data signals and LME signal propagating around the recirculation loop. The backward traffic has two data signals, which are analogous to those in the forward direction but at different wavelengths, coupled with a noise signal that is also matching the noise of the forward traffic. An LME receiver then receives the returned portion of the forward traffic through a high-loss loopback circuit as well as the whole backward traffic. The receiver should recover the LME pulse that can be observed on the oscilloscope. In order to check the LME recovery after 4600km with 45dB loopback attenuation, the results shown in figure 3.23 were required. The figure shows a plot of the maximum transmission distance, at which the LME pulse is still being recovered, versus loopback attenuation. This graph means that, for instance, if the loopback

attenuation is set at 40dB, the LME pulse can still be observed until the propagation distance reaches 2800km. Beyond this distance, the LME pulse is no longer visible on the oscilloscope.

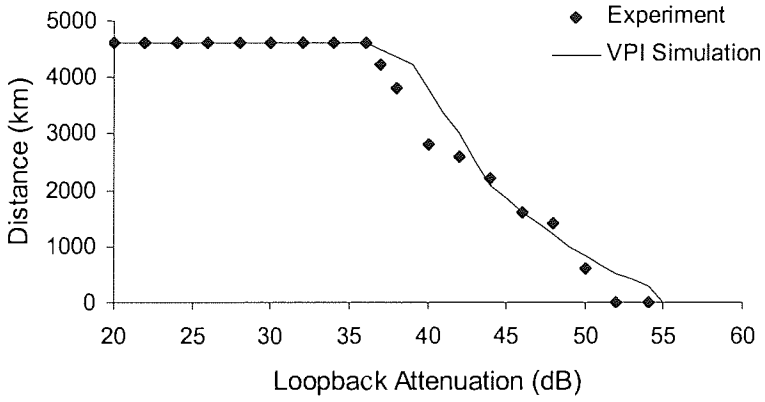

Figure 3.23 Maximum transmission distance at which LME signal is being recovered versus loopback attenuation

Obviously, the results are limited by a distance of 4600km which is the maximum propagation distance for this system. This can be shown in the figure as a straight line of dots for the loopback attenuation values less than 36dB. This 36dB is an interesting value as it defines the maximum loopback attenuation that can be achieved for this system. The next value is referred to as *turning point* and can be defined as the loopback attenuation value at which the curve starts to drop below 4600km. Therefore, a big challenge would be that the curve is shifted upward until the turning point becomes >45dB loopback attenuation. There are different possible ways to do so, where one can be using a narrower bandwidth in the optical filter that is located before the LME receiver. This requires a filter bandwidth which is less than 0.24nm in the operating wavelength region. Unfortunately, such filter was not available in the laboratory at the time of this experiment. On the other hand, if the filter bandwidth is larger than 0.24nm, the results are expected to degrade; hence the turning point will shift downward. This can be proven in figure 3.24, where the 0.24nm filter was replaced by another filter with a bandwidth of 1.1nm. The turning point was degraded by 4dB. It was largely important to make sure that the insertion loss of the new filter was similar to that of the original one for correct comparison. The insertion loss of the original filter was 7dB while the loss for the new filter was 2.5dB. The losses were equalised by adding an optical attenuator of 4.5dB at the output of the new filter.

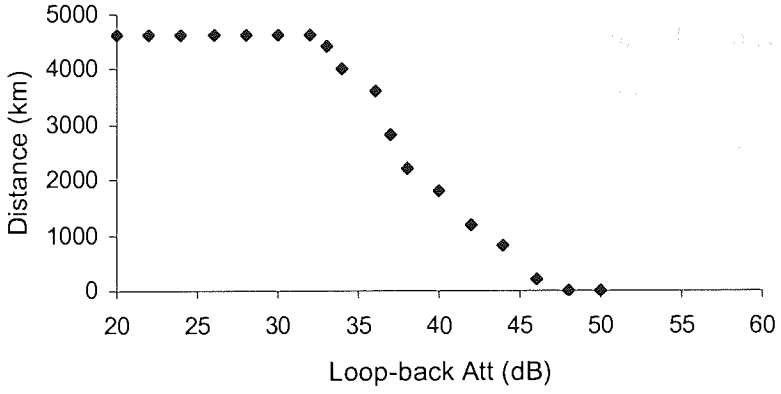

Figure 3.24 Maximum transmission distance versus loopback attenuation, using 1.1nm filter bandwidth.

Back to figure 3.23, while the LME signal had -10dBm entering the load AOM, the power after the loopback coupler of the forward direction is also -10dBm when the loop is balanced. This basically gives that the power is -7dBm before the loopback coupler, i.e. at point *a* in figure 3.11, which will enter the loopback circuit. From the signal evolution measurements presented in figure 3.18, the LME power drops by approximately 3dB after 4600km. Having attenuated this signal by 36dB, which is the maximum loopback attenuation achieved for this system, the power of the looped back LME pulse becomes -46dBm. This weak signal is swamped by the backward noise signal with -12.4dBm power according to the noise measured at 4500km in figure 3.17, which was offset by +9dB but then attenuated by the loopback coupler of the backward path. Therefore, the LME signal that is received is lower than the backward noise signal by ~34dB, although the composite signal is further attenuated by the band-pass filter and the final AOM. In addition, the LME signal is also accompanied by a portion of the forward noise signal which is also higher than the LME signal by about 2dB at 4600km. If the loopback attenuation is increased by 1dB, the LME pulse cannot be seen on the oscilloscope at 4500km as in figure 3.23. It is then possible to be seen at a distance that is shorter by almost two recirculations (i.e. 400km). In fact, this discussion can lead to one other possible way that can also be used to improve the turning point. This way is simply implemented by increasing the LME power into the system until the 45dB loopback loss is achieved over 4600km. This would hence allow defining the minimum acceptable LME power for this system which can be used to obtain the aimed loopback attenuation. Theoretically, the increase of the loopback attenuation is linearly proportional to the increase in the LME power. This can practically be proven by plotting the propagation distance versus the loopback attenuation, similar to that in figure 3.23, for increased LME power levels. It is always important that the difference between the LME and the data signals is kept constant

(~10dB), as well as the backward data signals have the same power as in the forward signals. From the propagation distance versus loopback attenuation graph, the maximum loopback attenuation versus the LME power can be plotted as shown in figure 3.25. The figure shows experimental results as well as simulation results obtained by two different simulators. It is clearly seen that the simulation curves have different slopes hence different improvement of loopback attenuation with LME power. The Excel curve shows perfectly linear improvement with slope 1, i.e. 1dB increase in the LME power results in 1dB improvement in the loopback attenuation. However, the experimental results lie in between the two simulation curves, where linear improvement with slope 1.15 has been shown.

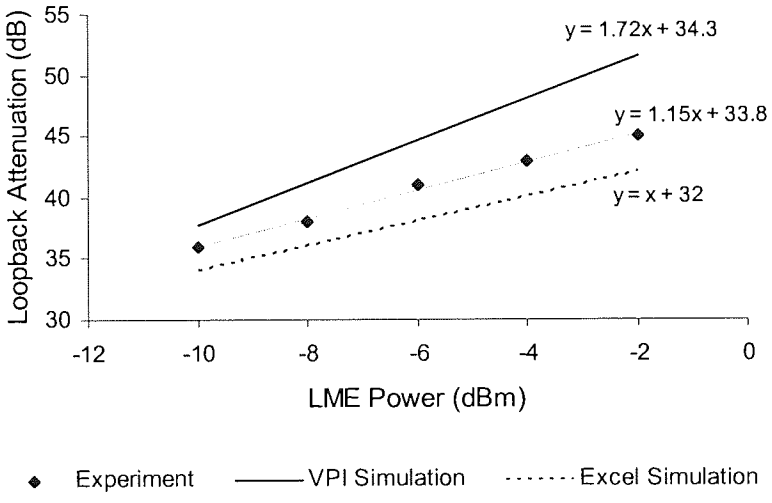

Figure 3.25 The loopback attenuation versus LME power over 4600km propagation distance.

As a result, the loopback attenuation of 45dB has been achieved experimentally when the LME power was increased up to -2dBm at the input to the load AOM. This gives that the LME power launched into the fibre span of the loop is -8dBm and the data signal powers are 2dBm, keeping 10dB difference. Typically, the LME power into the fibre is preferred not to exceed -10 dBm, assuming that the data signals operate at around 0dBm. If the LME power is higher than -10dBm as in this case (-8dBm), the difference between the LME and the data signals will be no longer 10dB. This might be undesired for the general context of the LME system. To check the minimum acceptable difference between the LME signal power and the data signals for this system, it is then important to study the effect of increasing the LME power on the performance of the data signals if their power is fixed. This will be discussed in section 3.6.5.

Another possible way to improve the turning point can be thought as if an EDFA is placed before the LME receiver as a pre-amplifier for the received signal that has already passed through a band-pass filter and an AOM. In this case, it should be born in mind that this EDFA will amplify the whole signal including the backward noise and the returned portion of the forward noise that are received in association with the LME signal. The EDFA will also produce an additional noise to the entire signal that will be detected. However, the experiment was intended to be performed without using such EDFA due to the above effects as well as the receiver was planned to be examined with an extremely low LME signal level.

Another method can also be used, in which the LME signal performance is improved through averaging which in turn improves the turning point of the loopback attenuation. This method will be discussed later in 3.6.6.

3.6.4 Electrical signal-to-noise ratio (eSNR)

The received OSNR at the input to the LME receiver will be in the region of -34dB as obtained in previous section. In this regime, the electrical signal-to-noise ratio (eSNR) is mostly dictated by the optical noise rather than electrical receiver noise. The eSNR can be theoretically obtained by using:

$$\text{eSNR} = \frac{P_{Sig}}{P_{Noise}} = \frac{\left|A_{Sig}\right|^2}{\sigma} \tag{3.22}$$

where A_{Sig} is the amplitude of the LME pulse and σ is the standard deviation. Since the received LME pulse has amplitude proportional to $\sqrt{(I^2+Q^2)}$, the numerator can be achieved through the peak of the I^2+Q^2 curve. The denominator can be achieved through the variance between I and Q. Therefore, the measurement of the eSNR can be approximately obtained by:

$$\text{eSNR} = \frac{\text{Ave}(I^2+Q^2)}{\text{Var}(I,Q)} \tag{3.23}$$

where the I^2+Q^2 peak is averaged over a small region around the maximum value, and the I and Q variance is measured over a wider region in the zero level. This all can be dipected in figure

3.26. The measured eSNR out of this method is linear and can be simply converted into logarithmic by:

$$\mathrm{eSNR(dB)} = 10\log(\mathrm{eSNR}_{\mathrm{measured}}) \tag{3.24}$$

Practically, the I, Q and I^2+Q^2 curves are displayed on the oscilloscope and can be converted into an Excel spreadsheet, which has a function of calculating the average of a curve as well as the variance between two curves over a chosen measurement region. This indeed makes the eSNR measurement straightforward once the LME pulse is detected and observed. The change in the measurement region will definitely change in the eSNR, but can be negligible with small changes. Thus the eSNR measurements can be useful if the measurement region is fixed for a series of measurements.

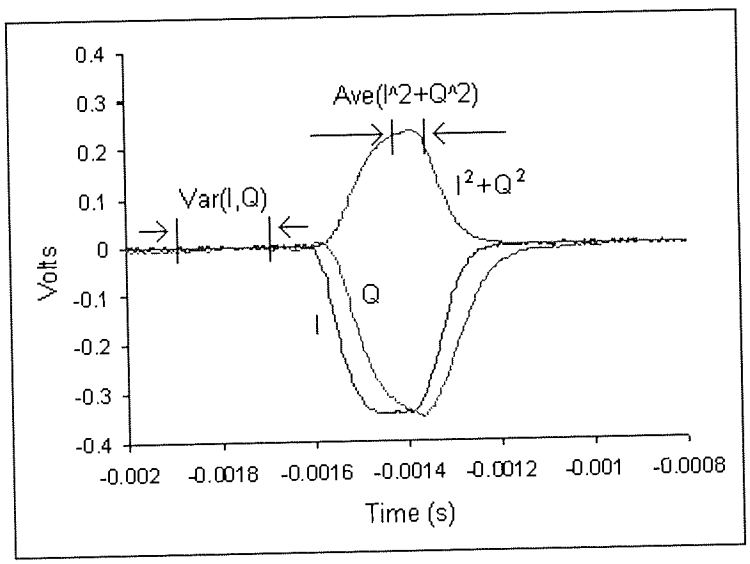

Figure 3.26 eSNR measurements method.

Using the above method, the eSNR measurements (in dB) versus distance for the received LME signal of the current system (using -2dBm LME power into the system and 45dB loopback attenuation) are shown in figure 3.27. The eSNR reduces over distance and becomes ~14dB at 4600km. The eSNR calculated by equation (3.14) for this regime is -1.2dB using OSNR=-34dB, B_o=0.24nm and B_e=6300Hz. Actually, the measured value is much better due to the effect of averaging which will be discussed later in section 3.6.6. This is based on the fact that equation (3.14) assumes that the number of averages taken for measurements is zero, while the experiment

used 10,000 averages. Moreover, it can be noticed that the simulation curve had much higher eSNR values at the start, and that is because the simulator provides perfect performance for the LME signal at short distance. Any other discrepancy is due to the error between experiment and simulation.

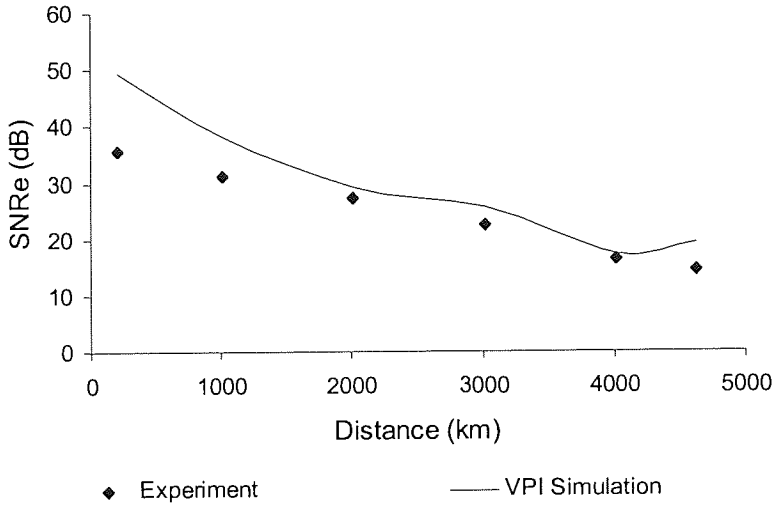

Figure 3.27 eSNR measurements versus propagation distance using LME power = -2dBm into the system and 45dB loopback attenuation.

3.6.5 Studying the effect of the LME signal on the data signals

Referring back to figure 3.6, the co-propagating traffic was expected to be affected by the amount of the looped back signals and noise of the counter-propagating traffic. In fact, this amount is no longer affecting the co-propagating traffic if 45dB loopback attenuation is used on both arms of the loopback circuit. (Recall that the loopback system must be symmetric, i.e. both arms have 45dB). Moreover, the co-propagating signals also suffer from extra losses through the loopback couplers along the forward path. These losses have already been compensated by the loop EDFAs as stated before. As a result, the main degradation mechanisms for the co-propagating traffic which were listed in section 3.3 have been solved. Nevertheless, these mechanisms were discussed as if they would affect the whole co-propagating traffic that includes both LME and data signals. However, since the LME signal is a supervisory signal that carries no information and is accompanied by the data traffic signals, it is important to study the effect of such LME signal to the co-propagating data signals. This section is therefore dedicated to investigate the effect of the LME signal if its power increases or its wavelength shifts towards the

neighbouring data signals. The later is important as it defines the minimum acceptable spacing between the LME signal and the adjacent data signals.

To study the effect of the LME signal on the data signals, the performance of the forward data traffic must be optimised. This can basically achieved by improving the recirculating loop behaviour. The main problem of the recirculating loop so far is that the dispersion is not fully compensated, where the total dispersion is ~0.5ps/nm/km in the operating wavelength region. This requires more dispersion management to be implemented on the loop. Theoretically, the 0.5ps/nm/km, i.e. 100ps/nm in every recirculation, can be reduced down to zero if the total length of the SMFs in the loop is shortened by ~6km. This can simply be worked out where the SMF has approximately 17ps/nm/km, giving that removing 6km will save up to 100ps/nm dispersion. Practically, the last SMF span was replaced by another span which is shorter by 6km, thus the total length of the loop has become 194.9km. The dispersion measurement over wavelength has been performed for the new loop using the ring cavity method discussed earlier. The results are shown in figure 3.28. It can be seen that the overall dispersion measures approximately 0ps/nm/km over wide spectrum including the operating wavelengths, giving that the dispersion is now fully compensated.

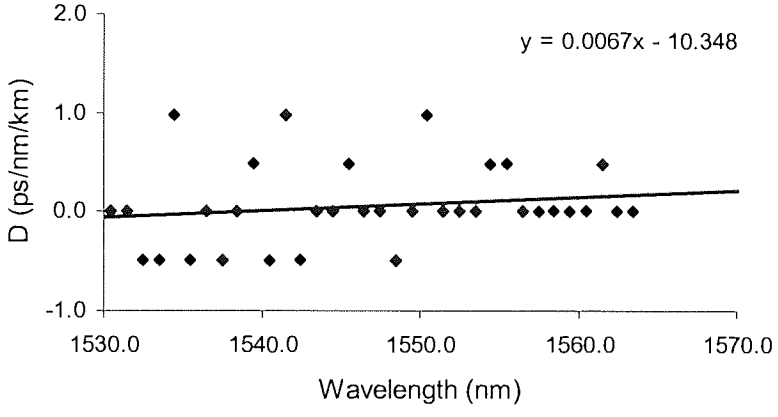

Figure 3.28 Dispersion measurements of the 194km loop.

Having achieved that, the forward traffic performance test can be performed. The performance can be characterised through the BER or Q-value measurements as a function of transmission distance. Due to unavailability of bit-error-rate tester (BERT) at the time of this stage, the performance was examined by the Q-value measurements. The experiment started with using an LME power of -4dBm at the input to the system while the data signals are 10dB higher.

This gives that the data signals had 0dBm power launching the SMF in the loop and the LME signal had -10dBm at the same point. The reason for choosing such values is that the data signals were intended to be at around 0dBm at the input to the fibre with keeping 10dB difference to the LME signal. This was also good choice since the minimum LME signal power for 45dB loopback attenuation was obtained at -8dBm into the fibre, giving the ability to test the effect of the LME power increase from -10dBm up to -8dBm and higher. The total average power measured on a Newport power meter was ~6.2dBm. Therefore, the EDFAs of the loop need to set such that 6.2dBm is ensured at the input of each fibre. However, the performance of the forward data traffic can be examined on the data signal that is adjacent to the LME signal (i.e. λ_2 =1557.4nm in this system). This is due to the fact that the adjacent signal in particular is most affected by the change in the LME signal. Therefore, the Q-value versus distance for this data signal has been measured as shown in figure 3.29.

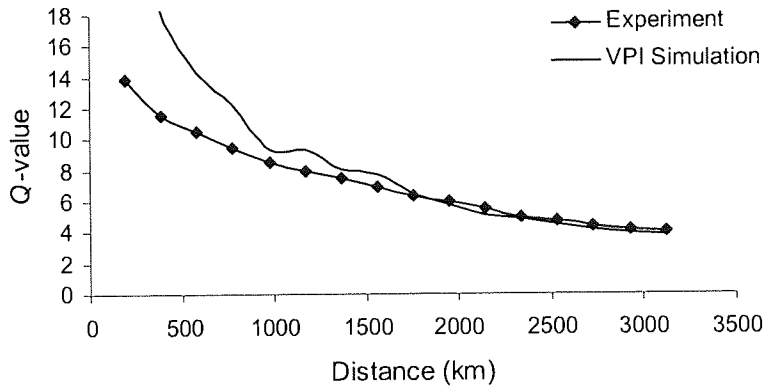

Figure 3.29 Q-value versus distance for the SMF-DCF configuration.

The disagreement between the experimental and simulation results for distances less than 1000km came from the difference in the way of measuring Q. Again, in simulation, signal was assumed to be extremely perfect at the start, so Q measured infinity at 0km. This is absolutely impossible to be obtained in experiment. However, the results are still useful where both curves agreed that the performance was limited to a transmission distance of only 1800km, after which Q started to drop below 6.

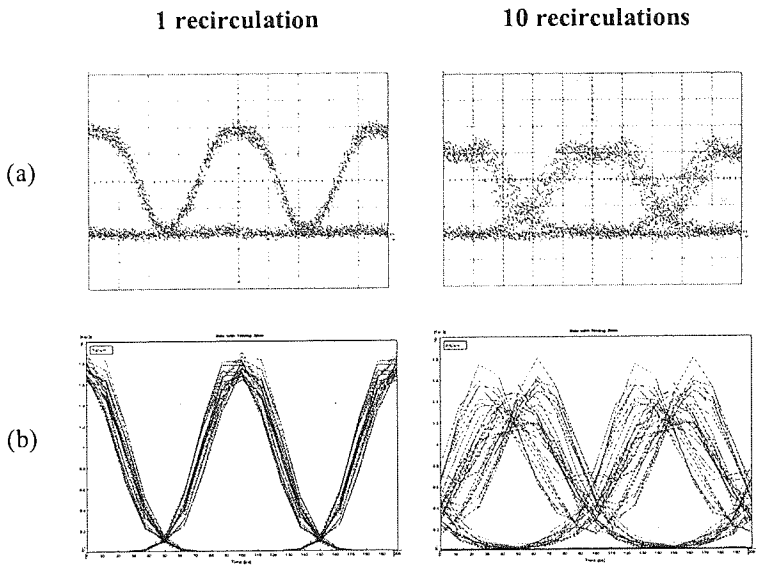

Figure 3.30 Eye diagram after 194km and 1940km: (a) experimental results (Time scale: 20ps/div); (b) VPI simulation results.

Figure 3.30 shows the eye diagram after 1 recirculation and 10 recirculations respectively; it is clear that the signal shape is distorted after 10 recirculations. This kind of distortion is normally induced by the self-phase modulation (SPM) within the propagating signal. SPM, which was discussed in chapter 1, usually appears after long propagation if the launch power is high. Since the launch power into the SMFs is not too high, i.e. power is not sufficient to show large SPM over such distance for SMF, there should be another reason for this effect. In fact, SPM-induced pulse distortion can also appear if there is large accumulative dispersion along the fibre span. This can apply to the current loop, where a relatively long SMF span (~80km) with large local dispersion is followed by another large dispersion DCF module but in the opposite sign, so that the overall dispersion in the section is approximately zero. Figure 3.31 (a) shows the dispersion profile for this loop configuration as applies to 1550nm. The signal has large positive dispersion accumulation over the SMF span - reaches 1400ps/nm - and then large negative dispersion over the DCF length to compensate for such 1400ps/nm in each section. This gives that the zero-dispersion point (that is corresponding to zero-chirp) is reached only twice in each recirculation. To improve this, the SPM-induced pulse distortion can be minimised by reducing the accumulative dispersion over the fibre spans [57], [97]. This can be achieved by changing the dispersion map from SMF-DCF in each section into SMF-DCF-SMF map, while the total length remains constant. This means that each SMF span in the current loop is divided into two shorter spans where the DCF is placed in the middle.

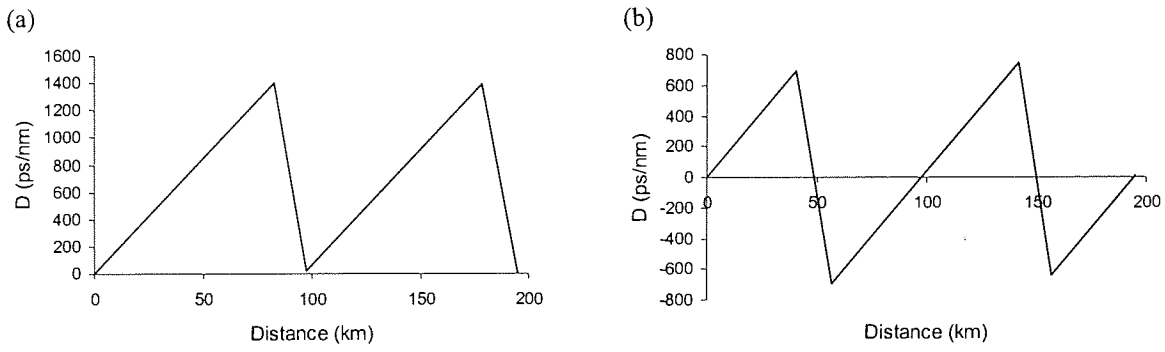

Figure 3.31 Dispersion accumulation over distance for: (a) SMF-DCF configuration, (b) SMF-DCF-SMF configuration.

The dispersion profile of this configuration can be shown in figure 3.31 (b). In this way, the dispersion accumulates over the first SMF and reaches 690ps/nm, which is half of that reached in previous configuration, and then reduced down to -690ps/nm over the DCF, crossing the zero-dispersion point. It then accumulates over the second SMF until reaching the zero-dispersion level again. As this is repeated again over the second section, the zero-dispersion can be reached four times in each recirculation. With such configuration, the system can be referred to as symmetric dispersion-managed system, while with the previous configuration it can be referred to as periodic dispersion-managed system [97].

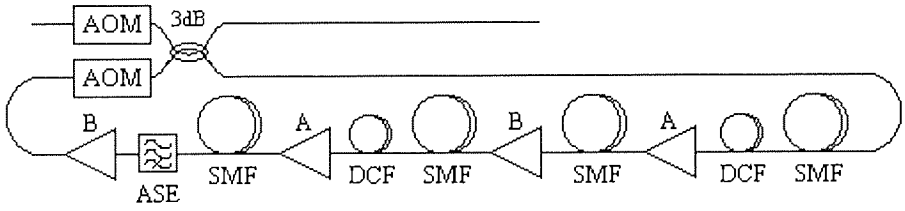

Figure 3.32 The new loop setup based on symmetric dispersion management.

The new loop configuration is shown in figure 3.32. It has in the first section: 40.7km SMF followed by 16.5km with -1383ps/nm DCF, which is then followed by another SMF with 41.8km. In the second section, it has 42.9km SMF followed by 15.2km DCF with -1387ps/nm, and then 38km SMF. The EDFAs denotes A and B are similar to those in previous setup. This setup obviously requires adjusting the EDFAs gains as the lengths of the fibre sections have changed. Moreover, it can be noticed that the DCFs are no longer placed after EDFAs in this setup, which means that the power into the DCFs has reduced due to the attenuation in previous SMF. This

power decrease should further reduce the effect of SPM which can also arise due to high power being launched into the DCF that has very small effective area (typically ~30μm^2).

Figure 3.33 shows the new Q-value measurements versus propagation distance for the same data signal (λ_2). Obviously, the performance has been reasonably improved where the maximum transmission distance that is corresponding to $Q = 6$ is now ~3300km.

The effect of the LME signal can be tested at this stage by simply increasing the power of the LME signal and observing the effect on the Q-value of the data signal. This must be performed while data signal power is fixed as well as the propagating distance. The data signals power is fixed at 0dBm and the propagation distance is at maximum, i.e. 3300km. Note that increasing the LME power will increase the total average power launched into the fibre, which needs re-adjusting the gains of the loop EDFAs for each measurement.

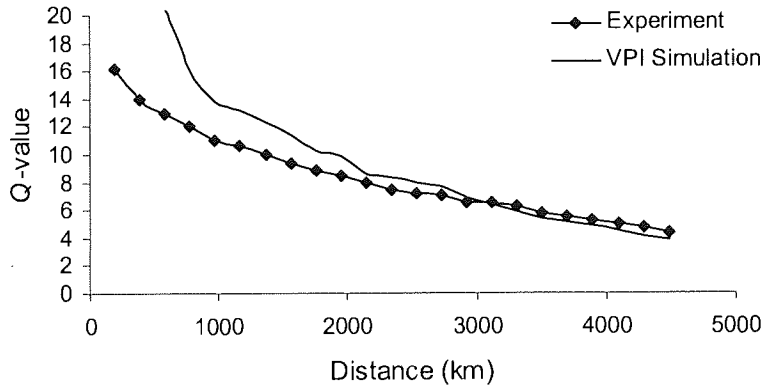

Figure 3.33 Q-value versus distance for the SMF-DCF-SMF configuration.

Figure 3.34 presents the Q-value as a function of the LME power measured at the input to the first fibre. It can be seen that the forward data signal is only affected if the LME signal's power becomes higher than the data signal by 4dB. This can simply be obtained from the turning point of both experimental and simulation curves in the figure. This can be realised as the inter-channel interaction between the data and the LME signals appears when the LME signal exceeds the adjacent data signal by 4dB or more. However, this case should never occur as the LME signal is intended to be much lower than the data signals. In addition, this can be a good news, as the data traffic will not be affected by the increase in the LME power even when its power becomes comparable to the data signals power. Moreover, the same kind of results has been achieved for different position of the LME signal, i.e. LME signal being placed in the middle of the two forward data signals, keeping 1nm spacing between the adjacent signals. It was found

that both signals were affected in the same way, where the turning point for each signal was still around 4dBm.

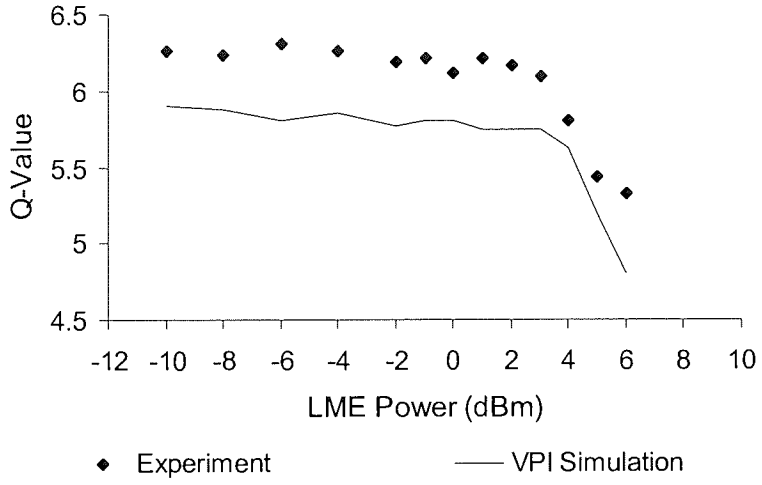

Figure 3.34 Q-value of the forward data signal versus LME power at the input to the loop fibre, measured with the maximum distance ~3300km.

The above results were all obtained with 1nm (125GHz) spacing between the LME and data signals. Therefore, the performance for different spacing must be presented by plotting the LME power at which the data signals start to be affected (i.e. the turning point of figure 3.34) versus spacing. The experimental results of this can be shown in figure 3.35. The turning point degrades as the LME signal gets closer to the data signals, but the LME signal still requires high power (-2dBm) to start affecting the data traffic performance.

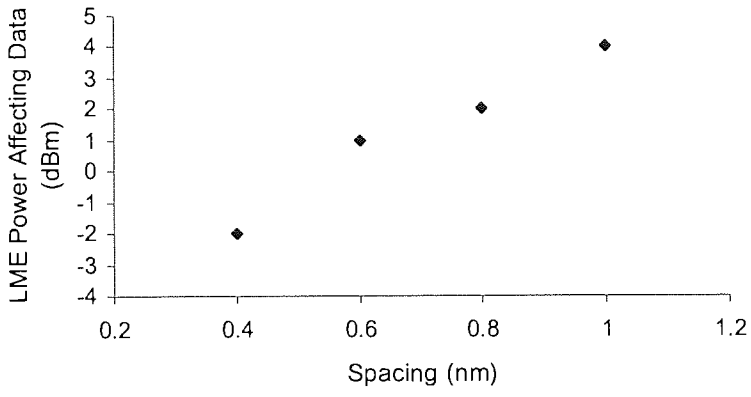

Figure 3.35 LME power turning point versus spacing between the LME signal and adjacent data signals.

As a result, the LME signal will have no considerable effect to the accompanied data signals as in practice its power is always much lower than that of the data signals. This obviously allows using higher LME power if necessary to achieve higher loopback attenuation, as done earlier, in which the LME power increased from -16 up to -8dBm at the input to the loop fibre. This can also be done with smaller spacing, e.g. 0.4nm, thus the LME signal can be placed in the halfway between any data signals that are spaced apart by 0.8nm. This is all true assuming that there is no effect from the data signals themselves to the LME signal, i.e. on the other way around. Figure 3.36 shows the eSNR measurement of the returned LME signal versus spacing to the adjacent data signals when the LME was on the side, and when it was in the middle. It can be seen that the penalty on the LME signal performance becomes most considerable at 0.4nm in both cases. It is thus recommended to use any spacing $\geq$ 0.6nm for acceptable performance penalty. Moreover, the eSNR measurements for the LME in the middle are worse, and that is basically due to the double-side interaction from the data signals. (Note that simulation results have not been provided since figures 3.35 to the end of the chapter).

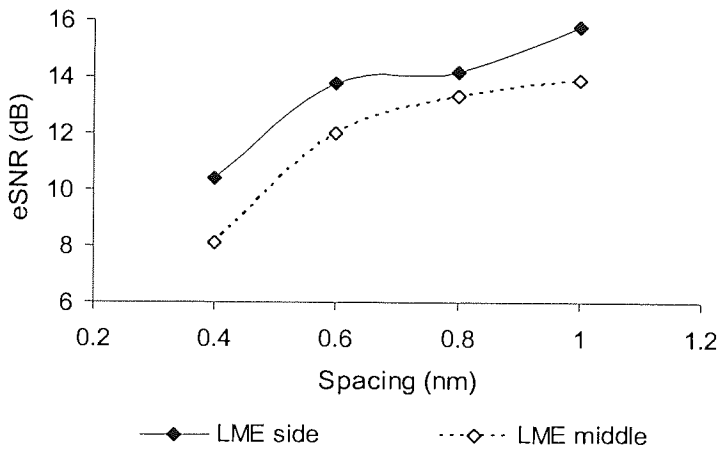

Figure 3.36 eSNR of the LME signal versus spacing between the LME signal and adjacent data signals.

3.6.6 Studying the effect of averaging

The quality of the eSNR measurement of the LME pulse is proportionally dependent on the number of samples taken for the measurement. This implies that the performance of the LME signal can be improved by increasing the number of samples; hence the turning point of the loopback attenuation of figure 3.23 can also be improved. The eSNR improvement is given by (3.15)-(3.17):

$$\mathrm{eSNR}_{ave} \approx n_p \mathrm{eSNR} \tag{3.25}$$

where n_p is the number of averages. Practically, the number of averages can be set directly on the measuring equipment (i.e. oscilloscope) which therefore takes the average of n_p samples of the received LME signal. The effect of averaging on a back-to-back LME pulse can be shown in figure 3.37, where (a) shows the received signal with no averaging and (b) shows the received signal after 4096 averages. It is obvious that the pulse is not discernible by eye until averaging is applied, where with 4096 averages; the noise amplitude is reduced by roughly two orders of magnitude.

(a) (b)

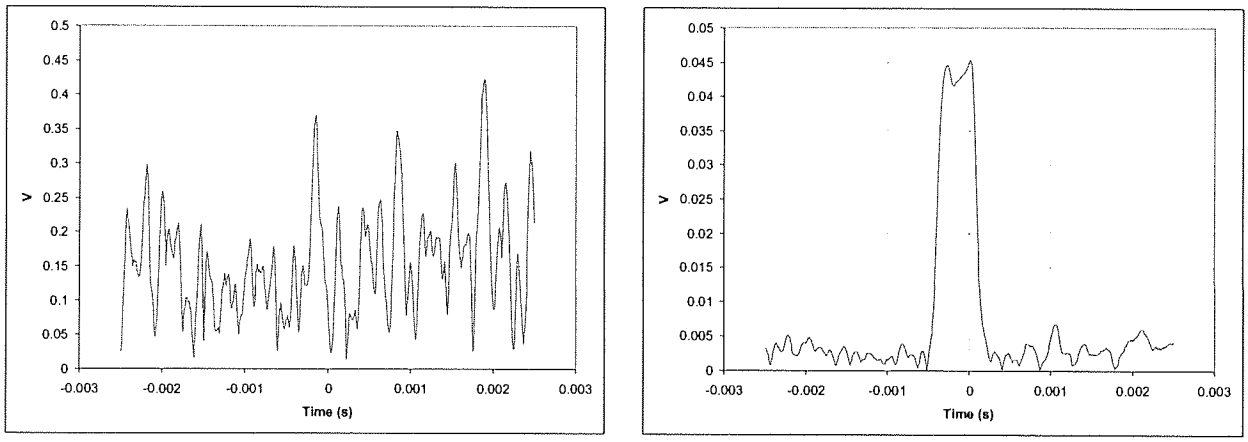

Figure 3.37 Received LME pulse with: (a) no averaging; (b) 4096 averages.

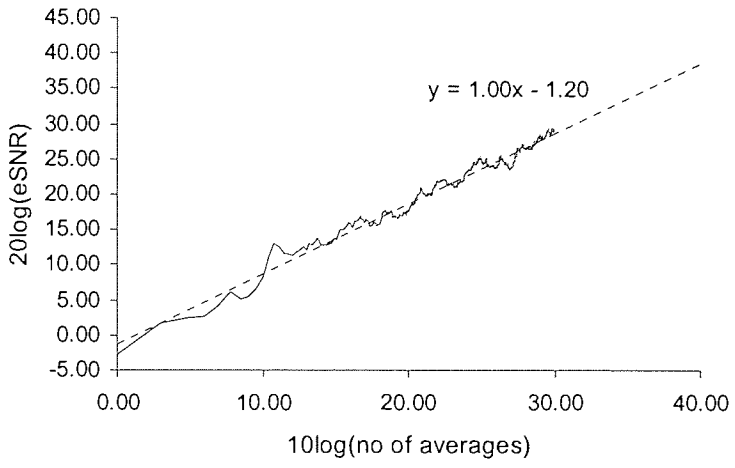

Figure 3.38 VPI simulation results of eSNR versus number of averages for received OSNR = -34dB.

To better quantify the signal improvement through averaging, the eSNR must be plotted as a function of the number of averages, where linear improvement is expected. Figure 3.38 shows the simulation results of the resulting eSNR improvement for the regime discussed in section 3.6.3 and 3.6.4 where the received OSNR was ~-34dB. The gradient of the trend-line of the eSNR curve is 1 if [20×log($eSNR_{Linear}$)] is used on the y-axis, giving that equation (3.25) holds for this receiver. Moreover, according to equation (3.14), the calculated eSNR at the output of the receiver before averaging is -1.2dB using B_o=0.24nm and B_e=6300Hz. If this value is doubled (i.e. becomes in [20×log] scale) it will be in a reasonable agreement with the eSNR shown in figure 3.38 for 0 averages.

This section is actually dedicated to prove the above improvement practically. The number of averages used in all previous work was fixed at 10,000 averages. It is therefore essential to run the experiment with more averages in the oscilloscope and examine the performance of the received LME signal. In fact, the system was intended to be optimised at this stage for another experiment which will be covered in the next chapter. Optimisation was encouraged as a new gain-flattening filter (GFF) had become available, as well as the BERT. This allowed using an optimised system for the rest of this chapter. However, the GFF is used to provides an in line compensation of the spectral gain profile of cascaded EDFAs. In other words, since EDFAs have a wavelength-dependent gain; i.e., some wavelengths are amplified more than others, the GFF restores all wavelengths to approximately the same intensity. The GFF has several advantages like: wide operating wavelength range, low insertion loss, flat spectral gain and high stability and reliability. Furthermore, the GFF has variable extinction as well tunable wavelength. In fact, the less extinction; the wider flattening range achieved, which can be useful for systems with large number of channels. In the current experiment, where the number of channels is small, i.e. two data channels and one LME channel, the extinction is preferred to be set at high over the operating wavelength region. This in addition to the ASE filter of the loop results in high amplification in the operating region, so the ASE accumulation outside this region is minimised. This can be understood from figure 3.39, which shows the spectral evolution of 5-WDM channels (space by 0.8nm) with different number of recirculations. This test was performed on the current 194.9km recirculating loop for the experiment covered in the next chapter, using a GFF after the second EDFA (EDFA 'B' in the first section). Thus the insertion loss of the GFF which is 2dB must be compensated by this particular EDFA so the total input power to the following fibre remains the same. The extinction of the GFF was set at maximum and centred at the middle of the data signals; hence most of the amplification is carried out in the data signals region. This is

realised as the data wavelengths suck the power of the ASE wavelengths outside the operating band.

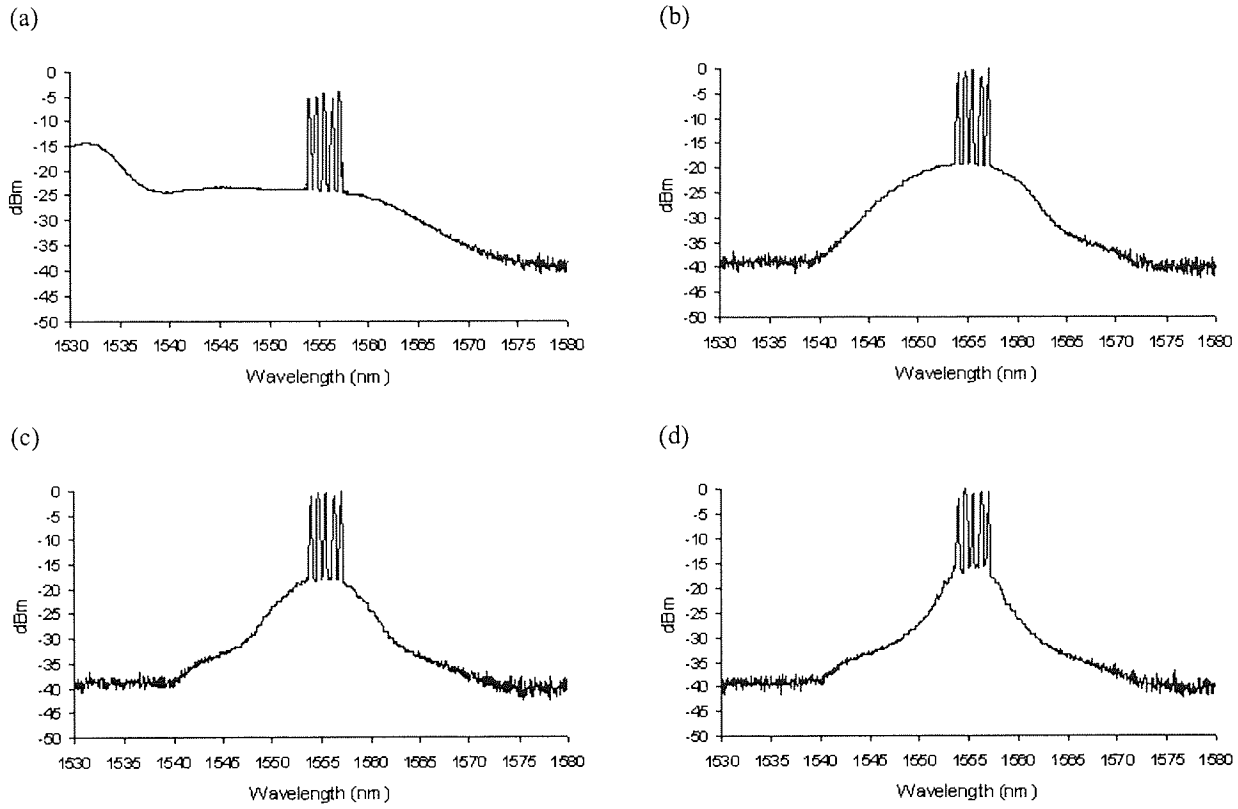

Figure 3.39 Spectrum of 5-WDM channels after: (a) 0 recirculation; (b) 1 recirculation; (c) 3 recirculations; (d) 10 recirculations; if GFF is used in the recirculating loop.

As a result, the majority of the total average power measured on the power meter exists within the data signals region, giving that large amount of ASE power has been saved. Moreover, the peaks of the data signals increase over the first few recirculations then start to drop as in the normal case, i.e. without GFF. In the normal case, the peak of the signal is expected to drop in distance due to the ASE accumulation where the total average power is constant. With the GFF, as the amplification builds up over short wavelength region compared to the overall C-band, the power within the signal band builds up more, resulting in more amplification within the signals band. After few recirculations, the overall amplification of the loop reaches saturation, where the peak of the signal starts to drop while ASE noise keeps accumulating over the operating band.

Having used the GFF for LME experiment, a new set of results can be obtained. For optimisation purpose, in addition to the GFF being set up in the loop, the system was intended to operate at the optimum data signal power as well as optimum LME power. The optimum data

signal power can be achieved by plotting the performance of the loop versus the data signal power. The optimum LME power is referred to as the power used in previous work to achieve 45dB loopback attenuation, i.e. -8dBm into the loop fibre. Figure 3.40 shows the maximum distance achieved with error = 10^{-9} as a function of the data signal power measured at the input of the first loop fibre. It can be seen that the optimum power is found at around -1dBm, where the maximum propagation distance reached ~5400km. The distance is obviously reduced by almost four recirculations and became 4600km at 0dBm power. As a result, the GFF improved the propagation distance by more than 1000km, and the optimum power further improved the performance by almost 800km.

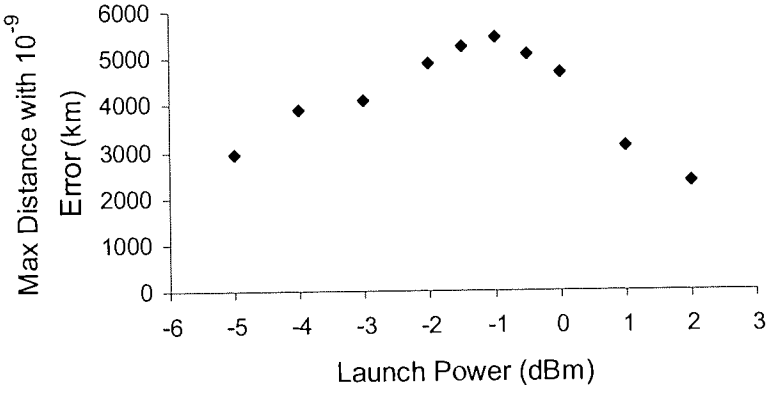

Figure 3.40 Maximum transmission distance with error = 10^{-9} versus data signal launch power.

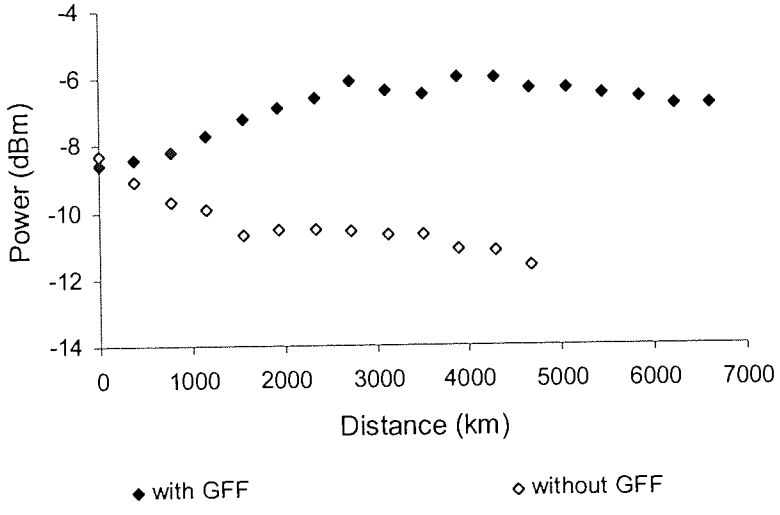

Figure 3.41 LME signal power evolution with distance for loop setup with GFF and without GFF. (RBW=0.5nm).

The GFF improvement can be justified by figure 3.41 which shows a comparison between the LME power evolution for the setup with GFF and that without GFF. In the case of no GFF, the power drops down in distance where it becomes lower by more than 3dB after 4500km. With GFF, the power increases and becomes higher by almost 3dB at 3000km; it then fluctuates and then starts to drop very slowly after 4000km. The result is that the power is still reasonably high after 4500km, and have a huge difference to that measured without GFF (>5dB). This will absolutely result in an improvement in the eSNR of the returned LME pulse, examined later.

However, the backward noise has been set in the same way used for the old setup, so it matches the forward noise at different number of recirculations. The noise measurements for the new setup are shown in figure 3.42 using the optimum power. It can be seen that the noise curve is higher than previous by almost 2dB.

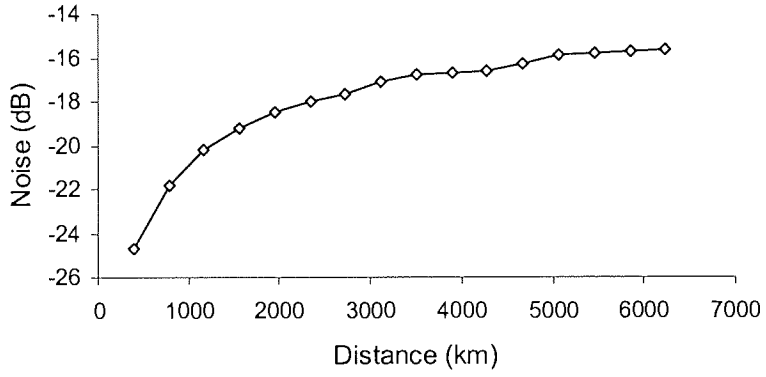

Figure 3.42 Noise versus distance for the setup with GFF (RBW=0.5nm).

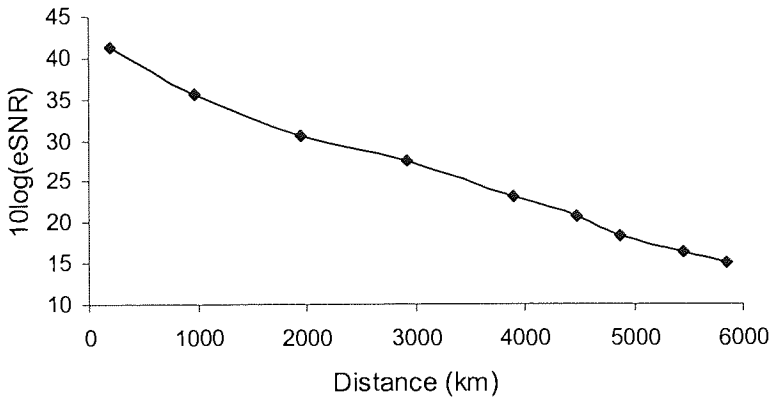

Figure 3.43 LME signal eSNR versus distance using 10,000 averages.

As a result of running the new experiment, the LME receiver has been successful in detecting and recovering the returned LME signal after 5400km with 45dB loopback attenuation. The eSNR measurements for the LME signal as a function of propagation distance are shown in figure 3.43, using 10,000 averages. It is seen that the LME signal can still be recovered till ~6000km distance. Moreover, these results must be compared to the experimental curve in figure 3.27. The comparison shows that the LME performance has considerably improved due to the several changes that have been made to the system. These changes can be summarised as: the dispersion of the loop has been optimised by reducing the lengths of the fibre, the SPM effect has been avoided by changing the loop configuration and finally the GFF has been set up in the loop.

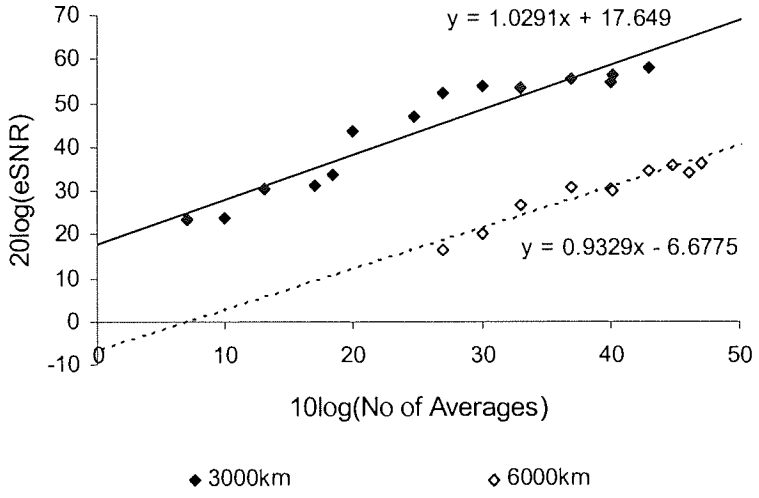

Figure 3.44 eSNR as a function of the number of averages.

The effect of averaging can be examined by measuring the eSNR of the received LME pulse for different number of averages at fixed propagation distance, i.e. in the similar way of figure 3.38. Figure 3.44 shows the results for 3000km and 6000km. Obviously, the measurements have shown linear improvements in the eSNR as a function of the number of averages, where the slope was always close to 1. This behaviour can match that obtained by simulation in figure 3.38, although the system has been modified. This gives that the LME pulse can be considerably improved by using large number of averages at the receiver. Otherwise, the LME pulse may not be visible on the oscilloscope. This can be realised in the case of 6000km in figure 3.44, where the eSNR could not be measured for number of averages less than 500. However, from equation (3.25), the $eSNR_{ave}$ required for such number of averages is ~20dB using eSNR = -6.68 for no

averages (obtained from the y-intercept of the curve). This calculated value does agree with the measured value shown on the curve for 500 averages. Moreover, the time required by the oscilloscope to recover the LME signal is also proportional to the number of averages. Figure 3.45 shows the measurement time required for different number of averages. This time was measured manually. It can be seen that the measured time is in good agreement with that described in equation (3.18). For example, the time required for 8000 averages is 1000 seconds using equation (3.18), which is almost the same in the figure. It is also seen that the receiver needs 40 minutes to recover LME signal if 20,000 averages are used. This time will basically double with 40,000 averages, giving that a balance between the time and performance is required. Note that the minimum time required for good quality measurement after 6000km was corresponding to 500 averages which was still in the order of 1 minute in our measurements.

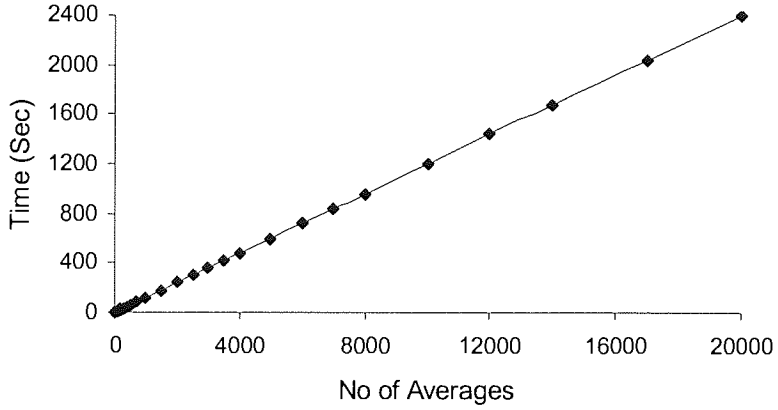

Figure 3.45 Measurement time versus number of averages.

However, the OSNR for the returned LME signal can be approximately worked out for the above system. The LME had -2dBm into the load AOM which implies that it had ~1dBm before the loopback coupler if the loop is balanced. From figure 3.41, the LME power improved over distance where it increased by roughly 2dB after 5400km (the maximum distance). The resulting LME signal with 3dBm was then attenuated by 45dB through the loopback circuit and became -42dBm. This signal was swamped by the backward noise of -9.8dBm (-15.8 at the loop output after 5400km, offset by +9 and attenuated by 3 of the backward loopback coupler). The received OSNR was therefore ~-32dB. In fact, it was shown earlier that the LME receiver had the ability to detect and recover the LME pulse in the region of -34dB. This implies that the power used for the LME signal (-2dBm into the system) might not be the minimum power to achieve 45dB in

this system. This of course requires defining the minimum power for the system, by simply reducing the LME power and checking whether the LME pulse is visible on the oscilloscope or not. There is a chance to increase the number of averages if the LME signal is not recovered with low power. Defining the minimum power is actually important although it has been proven that the LME signal would have no effect to the co-propagating data signals using high power. In fact, a difference of 10dB between the data signals and the LME is still desired in the main context of the LME system. In the above experiment, the LME signal was lower than data signals by 7dB. Having run the experiment with lower LME power, it was found that the LME signal can still be recovered if its power dropped by 1 and 2dB, i.e. difference became 8 and 9 respectively. This was actually obtained by using 10,000 averages or more. If the LME signal dropped by 3dB, i.e. the difference becomes 10dB; it was found that it could not be seen on the oscilloscope unless the number of averages is $\geq$20,000.

As a conclusion, the number of averages has reasonably improved the eSNR performance of the LME signal. This has led to an LME signal recovery after the maximum propagation distance (5400km) using 45dB loopback attenuation and LME signal power lower than the optimum data signal power by 10dB.

3.7 Summary

This chapter has demonstrated a line monitoring equipment (LME) suitable for optically amplified long-haul undersea systems. It is based on setting up a simple, passive, low cost high-loss optical loopback circuit at each repeater. This loopback circuit provides a connection between the existing two undersea fibres and can be used to define fault location. Fault location can be defined by transmitting a supervisory signal (referred to as LME signal) along with the WDM data signals where a portion of the overall signal is attenuated and returned to the transmit terminal by the loopback circuit. An LME receiver must then extract the weakly returned LME signal and display it on the oscilloscope. The oscilloscope will then show different LME pulses which correspond to different optical repeaters. Therefore, the degradation in any repeater will appear on its corresponding LME signal level.

The chapter started by giving examples of other line monitoring techniques that have already been demonstrated. It has also discussed the advantages of the proposed high-loss loopback LME system in comparison with the other techniques. Then, the chapter has presented two different approaches for the high-loss loopback LME system; in-band and out-of-band LME systems where it has concentrated on the second approach i.e. the out-of-band LME systems.

This system, which was also referred to as "pulsed high-loss loopback LME system", has actually been chosen for the LME experiment demonstrated in the chapter. The performance analysis of this LME system has then been presented. After that, the chapter has demonstrated the LME system prototype, including the LME transmitter and receiver architecture as well as the setup of the high-loss loopback circuit in the laboratory. Then the whole LME experiment has been demonstrated. It began with defining the experimental transmitter, fibre link (which was a recirculating loop) and receiver. The recirculating loop measurements, such as dispersion and OSNR performance have been presented. It was found that the dispersion of the loop was not fully managed, but it was still usable for the LME signal recovery experiment. The objective of the LME signal recovery experiment was to test the feasibility of the LME receiver in recovering the LME signal after 45dB attenuation over the loopback circuit and after long transmission distance. The experiment started with low LME power that was then increased until the aimed 45dB loopback attenuation was achieved. The effect of the optical notch filter bandwidth to the LME performance has also been presented. Then the eSNR measurements of the recovered LME signal have been shown. After this, the chapter has shown a study of the effect of the LME signal to the co-propagating data signals. This stage included optimising the recirculating loop by fully compensating the dispersion and minimising the SPM effect on the propagating signals. It was found that the LME signal would have no considerable effect on the adjacent data signals even when its power is comparable to the data signals power. It was also important to present the opposite effect, i.e. the effect of the data signals to the accompanied LME signal. It was found that a considerable effect would appear if the spacing is less than 75GHz. The chapter has then ended by studying the effect of averaging on the eSNR performance of the returned LME signal. This stage has included further optimisation on the system where a gain-flattening filter (GFF) has been added to the recirculating loop. It has been proven that the LME signal performance improved linearly as the number of averages increased at the receiver.

As an overall conclusion, the proposed high-loss LME system has been successful in providing a supervisory signal recovery after long distance, i.e. ~5400km, if it was attenuated by high-loss, i.e. ~45dB, in the loopback circuit that connects between the two undersea fibres. This has all been achieved while the supervisory signal was much lower than the WDM data signals (by ~10dB).

Chapter 4

WDM transmission performance using different proportions of 1s and 0s in random data

4.1 Introduction

The previous chapter has presented a line monitoring method that can be used to monitor legacy optical fibre links. In particular, the scheme can find the location of a fault along the optical fibre link which in turn can be useful for maintaining and upgrading the existing WDM communication systems. This chapter presents another study that can also be used to upgrade legacy optical fibre systems. It investigates the effect of the data pattern on the performance of the WDM system, specifically the effect of the number of 1s and 0s in the transmitted data. However, from information theoretic perspectives, the transmitted data is simply a combination of 1s and 0s. This implies that if the bit sequence has all 1s or all 0s, there is no information transmitted. Therefore, the maximum information can be achieved by the largest possible combination, i.e. if the bit sequence has half 1s and half 0s. This, in fact, can be the ideal proportion of 1s and 0s in transmission as well [98]. However, it has already been shown that in some systems particular bit sequences can result in a worse performance than others due to some effects such as ISI and nonlinearities [99]. It has been found that patterning effects that occur in high bit-rate dispersion managed systems, resulting from bit overlapping, can increase the probability of errors. This may lead to saying that the 50% 1s and 0s can be ideal selection for systems operate in linear regime, assuming that the system performance is dominated by noise in the electrical receiver which simply adds equally to the 1s and 0s. Thus the probability of errors in the received 1 and 0 bits is almost the same, which indeed makes the receiver design simple as the threshold can be set at half the average power. In practice, in optically amplified transmission systems, the noise contributions for the 1 and 0 bits are different where the 1 is dominated by signal-spontaneous beat noise while the 0 is dominated by the spontaneous-spontaneous beat noise [54], [65]. The signal-spontaneous beat noise that is induced on the 1-bit has larger contribution than the spontaneous-spontaneous beat noise of the 0-bit. Thus the probability of errors in the 1 is larger than that of the 0. In this case, the BER for the received data is expected to be affected by the proportion of 1s. The usual approach in this case is to bias the receiver threshold so that the error-rate for the 1s is equal to the error-rate for the 0s. Figure 4.1 shows

example of two systems; the first assumes equal error probability distributions of the 1s and 0s where the threshold can be set in the midpoint between the 1 and 0 amplitudes. The second assumes larger error probability distribution for the 1s thus the threshold must be set below 1/2 so that errors in the received 1s are avoided.

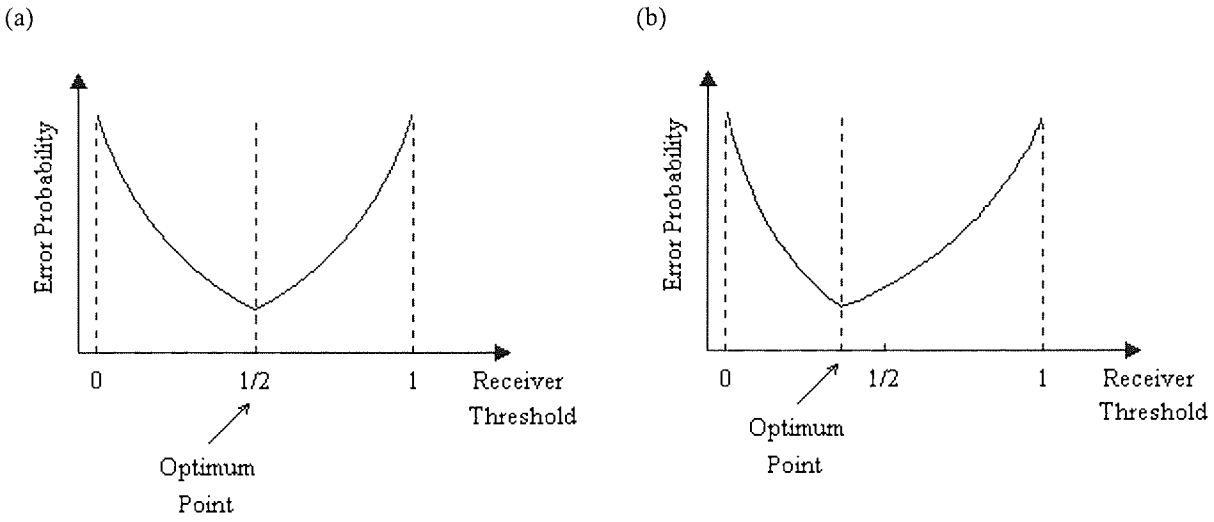

Figure 4.1 Receiver threshold bias for: (a) System with equal error probabilities for the 1s and 0s; (b) System with unequal error probabilities.

What about those systems operate in nonlinear regime? Actually, systems operating in the nonlinear regime are often limited by nonlinear interactions, where the noise effect can be neglected. Since the nonlinear effect is induced only on the 1-bit, where there is a pulse (assuming RZ modulation), the probability of errors for the 1-bit is much larger than that of the 0-bit. Thus the BER performance of the system can be a function of the proportion of 1s. This actually can be understood as in real systems, where all amplifiers operate at saturation, the amplifiers output powers are always constant giving that changing the number of 1s at transmitter will keep the average power constant at the input of each fibre span. In this case, the change in the proportion of 1s at the transmitter will only change the individual pulse energy at the input of the fibre spans. This consequently can affect the whole system performance. For instance, if the number of 1s increases, the pulse energy decreases which in turn can reduce impairments induced by nonlinearity, with the net effect being an improvement in the performance. This enables reliable communication at reduced energy levels, where this margin in power can be spent to improve the bit-rate distance product, i.e. by allowing the signal to propagate for longer distance with acceptable BER [5], [43]. In contrast, if the number of 1s decreases, the pulse energy will

increase and therefore the nonlinear effect will increase thus the performance degrades. This is all assuming that the system allows for high nonlinearity i.e. the power is far higher than the optimum power. In other words, the system performance, in general, is anticipated to show BER drop as power increases from zero and then increases as we enter the nonlinear regime. Therefore, the performance can go both ways, better and worse, even in the nonlinear regime, where the effect of changing the proportions of 1s and 0s depends on where on that BER curve we set the optimum condition and how far we operate the system from that point. However, if the pulse energy is kept constant, i.e. average launch power varies; the performance will therefore depend on the optical signal-to-noise ratio (OSNR) of the signal. For instance, if the number of 1s increases, the signal power increases and, therefore, the system performance is expected to improve due to an improvement in the OSNR. Note that in order to implement this; the gain of each amplifier on the fibre link needs to be set for different proportion of 1s such that the output pulse energy is at required level. This cannot actually be the case in investigating legacy system where the amplifier gains are constant. Thus it can only be performed in experiment for comparison purposes.

The above argument leads to carefully studying the effect of patterning with respect to the proportion of 1s and 0s to the performance of WDM communication systems working in both linear and nonlinear regimes. Again, since the receiver can be biased to equalise the probabilities of the received 1s and 0s in the linear system, the effect is not expected to be as strong as that for the nonlinear, in which the total BER is a more complicated function of the proportion. However, any improvement of the system performance achieved by such effect can be useful for the application discussed in the next section.

4.1.1 Forward error correcting codes

Studying the effect of different proportions or fractions of 1s and 0s in the transmitted data can be useful for some applications related to coding. Forward error correction (FEC) codes can be good examples to consider in this study. FEC is a technique used in communication systems by which redundant information is transmitted along with the data that can be exploited by the receiver to correct errors incurred during transmission [100]-[102]. Recently, FEC has been deployed in communication systems using WDM fibre-optic channels [5], [65]. Since new bits are added to the original bit stream, which are referred to as *overhead*, the bit-rate of the data changes. For instance, if the FEC adds 20% overhead to a 10Gbit/s data, the bit-rate becomes 12Gbit/s after the FEC encoder. In addition, if the data is originally balanced, i.e. has the ideal

50% 1s and 0s, the data at the output of the FEC encoder is no longer balanced depending on the ratio of the 1s in the overhead. In fact, the FEC encoder is conventionally followed by a scrambler which is used to rebalance the data, i.e. to ensure a proportion of 50% before transmission. This is traditionally based on the assumption that the system operates in the linear regime and the error probability for the 1s and 0 is almost equal. The scrambler operates on the input data using a primitive polynomial and is implemented using XORs and shift registers [103]. The original intention of the scrambler was basically to remove long sequences of 1s or 0s, which would make timing extraction difficult, so that the decision circuits at the receiver could function properly. The scrambler does not actually add any overhead, and an identical polynomial is used at the receiver to descramble. In fact, the probability of having 1s and 0s is equal at the output of the scrambler when averaged over many bits. The maximum length of a sequence of 1s or 0s is given by the order of the polynomial.

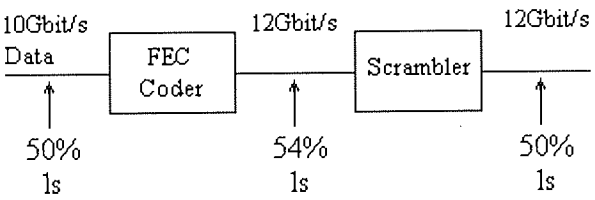

Figure 4.2 FEC encoder and the following scrambler.

Figure 4.2 shows a simple diagram of the FEC system used at the transmitter. It shows an example of balanced 10Gbit/s data that is encoded by the FEC encoder with 20% overhead. The resulting 12Gbit/s data stream is unbalanced where the encoder adds more 1s to the data such that the output fraction of 1s is 54%. The scrambler basically brings the fraction back to 50% for transmission. A comparison can be therefore implemented between the balanced and unbalanced data in the way discussed in previous section. Theoretically, the more 1s in the data; the better BER performance if the system operates in the nonlinear regime. If such effect has been proven practically with considerable improvement, FEC systems can be operated without requiring the additional scrambler. This would consequently save electronic component from the system, where the improvement is achieved simply by operating at high power. This is true as long as the transmitted data has larger number of 1s, hence lower individual pulse energy. On the other hand, if the encoder adds more 0s so the resulting data stream has less 1s, the performance is theoretically expected to degrade. This allows using the inverse of the overhead bits, or even the

inverse of the whole data stream, which can be inversed back at the receiver. In this case the fraction of 1s would be large over the transmission fibre so nonlinear effects are avoided. This would also enable saving the scrambler.

The following sections investigate the above patterning effect on a 5×10Gbit/s WDM transmission system. The work is divided into two parts; low power operation which simulates linear system, and high power operation to simulate nonlinear system. The experiments will simulate the effect by simply changing the fraction of the 1s and 0s in a PRBS data using a function on the pattern generator. The experiments will use a recirculating loop for long-haul transmission.

4.2 Low-power operation

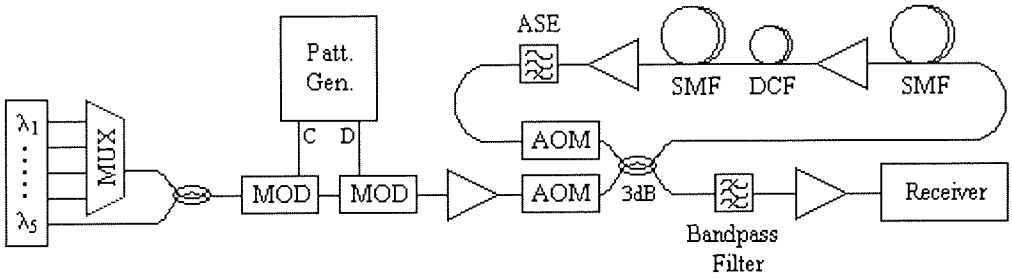

Figure 4.3 Experimental setup.

This section examines the effect of changing the fraction of 1s and 0s on a system operating in linear regime. This means that the power of the individual data signals is relatively low so that the pulse energy is sufficiently small. The experimental setup for this system can be shown in figure 4.3. The system uses five lasers; four wavelengths are WDM multiplexed and coupled with the fifth wavelength through a 3dB fibre coupler. The whole WDM signals are then modulated indirectly via two $LiNbO_3$ modulators that are driven by a pattern generator of 10.7GHz frequency and PRBS data pattern with 2^{31}-1 word length, respectively. The resulting 5×10Gbit/s WDM signals that have RZ modulation format are then amplified to the required launch power and enter a 52km recirculating loop. The wavelengths used are: 1553-1557nm with an even separation of 125GHz. Each channel has -7dBm launch power (measured on the multi-wavelength meter) at the input of the fibres in the recirculating loop.

The recirculating loop consists of two SMF spans; each has 21km length with ~0.2dB/km attenuation coefficient and ~17ps/nm/km dispersion at 1550nm. The whole dispersion is

compensated by using one 9.8km DCF unit, with a negative dispersion of 685ps/nm at 1550nm and 4dB insertion loss, between the SMF spans. Thus the loop has symmetric dispersion configuration. Two C-band EDFAs, each with 5dB noise figure and 30dB maximum small signal gain, are used to compensate for losses of the loop as shown in the figure. The maximum output saturation power of each EDFA is ~12dBm. Although the length of the loop fibre is short, two amplifiers are used because the total loss over the whole recirculating loop system, including the AOM's, the 3dB coupler and an ASE filter, is large that cannot be compensated by a single amplifier. An ASE filter with 5dB loss is used at the end of the loop to remove the ASE noise that would build up at 1530nm. At the receiver, a narrowband optical band-pass filter with 0.24nm bandwidth and 7dB insertion loss is used to demultiplex the WDM channels, which are then pre-amplified and detected by the receiver.

4.2.1 Recirculating loop performance

As mentioned before, it is necessary to make sure that the recirculating loop is fully compensated with respect to loss and dispersion before running the experiment. The losses are assumed to have been compensated by the loop EDFAs, where the total average power at the input to the input AOM is equal to that at the input to the loop AOM, or the power at the output of the loop is equal to that at the input to the first fibre span in the loop. Again, the dispersion of the loop can be examined using the ring cavity method discussed earlier. Remember that this measurement method can tell if the dispersion and dispersion slope of the system are fully compensated or another dispersion management is required.

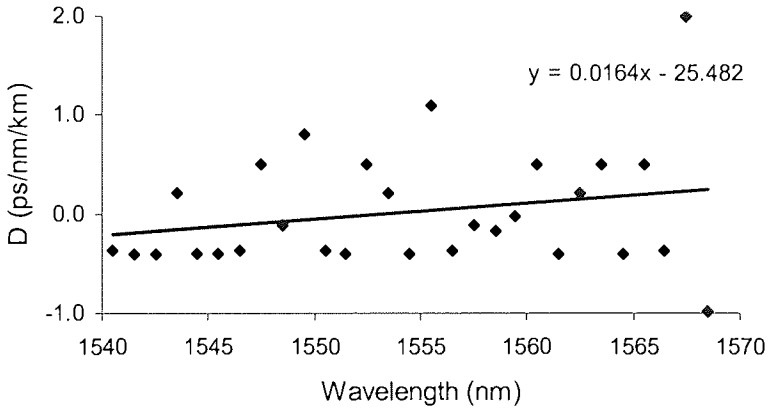

Figure 4.4 Dispersion measurements for the 52km recirculating loop.

Figure 4.4 shows the dispersion measurements of the current 52km recirculating loop. It can be seen that the dispersion is almost around zero over the operating wavelength region (around 1555nm), thus no more dispersion management is required on the system.

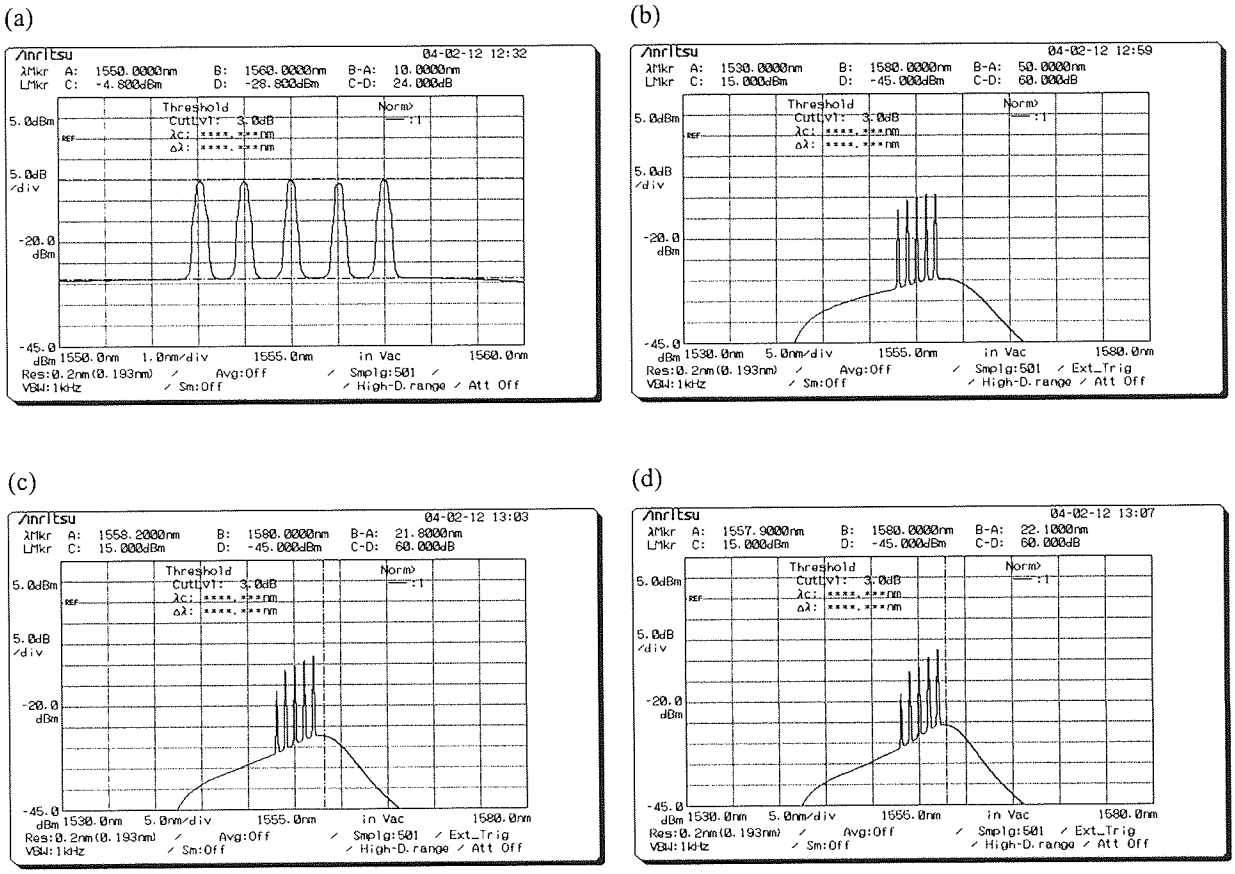

Figure 4.5 Spectrum after (a) 0 recirculations; (b) 2 recirculations; (c) 6 recirculations; (d) 10 recirculations.

The 5×10Gbit/s WDM transmission experiment can be described now. Since the system uses multiple signals that are separated by relatively large spacing (1nm), it is necessary to ensure equal gain over the whole WDM signals after long distance. Figure 4.5 shows the spectral evolution of the signals with the number of recirculations. The signal peaks are equalised at the transmitter, while each has ~-7dBm into the fibre. In transmission, the signals are getting un-equalised as the distance increases, where longer wavelengths have larger gain. This is due to the overall gain profile of the loop which depends on the individual gain profile of each EDFA in the loop. However, this will result in large difference in the OSNR at the receiver, hence different BER performance for the different channels. Such effect is of course undesired in WDM systems where all signals are supposed to have almost the same quality when received after long distance.

The system therefore requires gain equalisation which can be attained by gain equalisers, such as the gain-flattening filter (GFF) that was discussed in previous chapter. In fact, such filter was not available at the time of this experiment; therefore another method must be used to solve the problem. Commonly, the signals are pre-emphasised [104] at the transmitter, i.e. they have different peaks, such that the resulting OSNR after long distance is almost the same for all signals. For this system, for instance, this means that the peaks of the signals must have a slope at the opposite of the gain slope. Therefore, the first channel (from left) must have the largest peak and the last channel must have the lowest peak at the transmitter. Pre-emphasis can also be done where all the WDM signals are shifted upward and become around the maximum gain peak, which is observed at 1557.5nm in this system. In this case, the lowest peak must be on the central channel while the highest must be on the two side channels. This can be shown in figure 4.6.

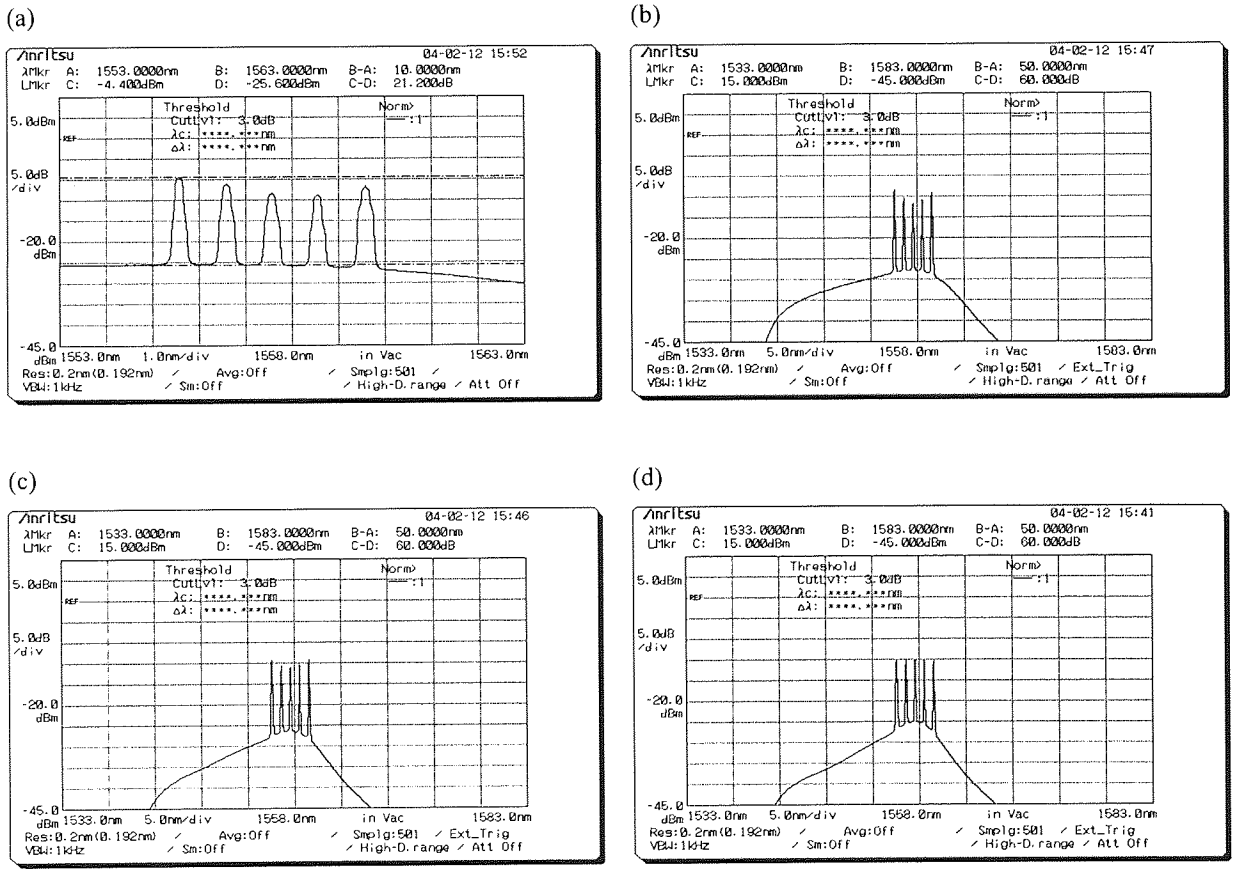

Figure 4.6 Spectrum after (a) 0 recirculations; (b) 2 recirculations; (c) 6 recirculations; (d) 10 recirculations, using pre-emphasis at the transmitter.

The wavelengths of the signals are now: 1555.5-1559.5nm. The launch power is no longer -7dBm in all channels, but the total average power is measured at around 1dBm. As a result, it is

seen that the OSNR of the WDM signals is nearly equalised after long transmission distance, hence the BER/Q performance must not have considerable difference. The OSNR and Q-value measurements versus transmission distance for the central channel (λ_3=1557.5nm) are shown in figure 4.7 (note that BERT was not available here). The system performance is obviously limited by the noise where the OSNR becomes considerably small after long distance as shown in (a). This is expectable as the system operates at low power that the noise effect is dominant. This gives that the maximum propagation distance with acceptable Q for this system is achieved at around 1300km as appears in (b). Actually, it was found that the performance of the whole WDM signals is almost equalised after 1300km, where all other channels have acceptable Q-value at that particular distance. Figure 4.8 shows a comparison between the eye diagram of the central signal at back-to-back and after 1300km. Apparently, the eye is much more closed at 1300km due to the noise accumulation, while the shape of the signal is not distorted.

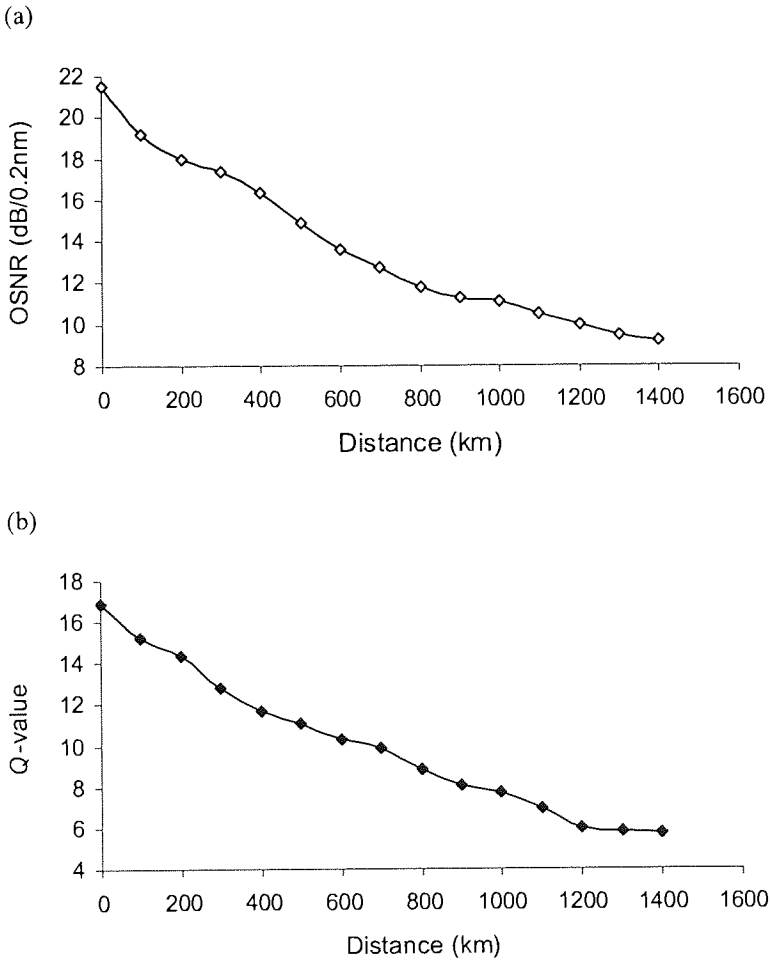

Figure 4.7 (a) OSNR (using 0.2nm RBW); (b) Q-value versus transmission distance for the central channel (λ_3=1557.5nm).

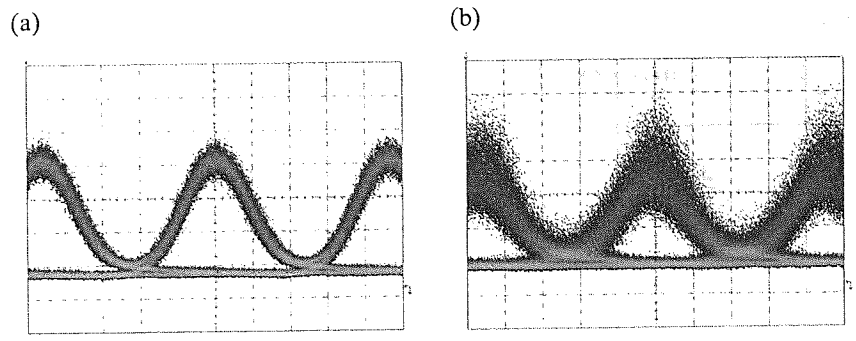

Figure 4.8 Eye diagram for the central signal after (a) 0km; (b) 1300km. (Time scale: 20ps/div).

4.2.2 Results of different fractions

The performance shown in previous section is based on using PRBS data with the ideal fraction of the 1s and 0s, i.e. 50% (note that a PRBS does not always have exactly 50%, even a maximal length sequence has a very slight bias of 1s over 0s). This fraction can now be varied directly from the pattern generator in order to simulate the effect of unbalancing the data. In fact, the fraction is initially intended to be widely varied, i.e. by ±25%, for simulating highly unbalanced data. Such high unbalancing may not happen in FEC coding process as the length of the overhead is usually a small fraction of the data word length, e.g. 20%. However, examining the performance with large variation in the fraction can provide the extremist effects that can be considered as boundaries or limits for this study. This means that smaller variation effects that can occur in coding process should not exceed these limits. In practice, the fraction of the 1s at the pattern generator used here can only be changed from 50% by ±25 or ±37.5, other fractions can be set by loading an external pattern into the pattern generator. However, changing the fraction by ±37.5 will not be used in this experiment as the fraction would be extremely unbalanced (i.e. data would have 12.5% 1s or 0s) that we believe is not significant for this study. The experiment will therefore compare the performance of the system using 25% and 75% 1s with that shown in previous section for the more ideal 50%.

Again, the total average power must remain constant at the input to the fibres in the loop while using different fractions assuming that the EDFAs operate in saturation where their output power is always constant. Practically, the gain of the EDFAs are set such that they work in saturation region where each EDFA is followed by a variable optical attenuator (VOA) that can be initially used to adjust the power level into the fibre. This implies that changing the fraction of

1s at the pattern generator will keep the total average power fixed at the fibre inputs. This in fact results in a change in the pulse energy of the 1-bits in the data stream.

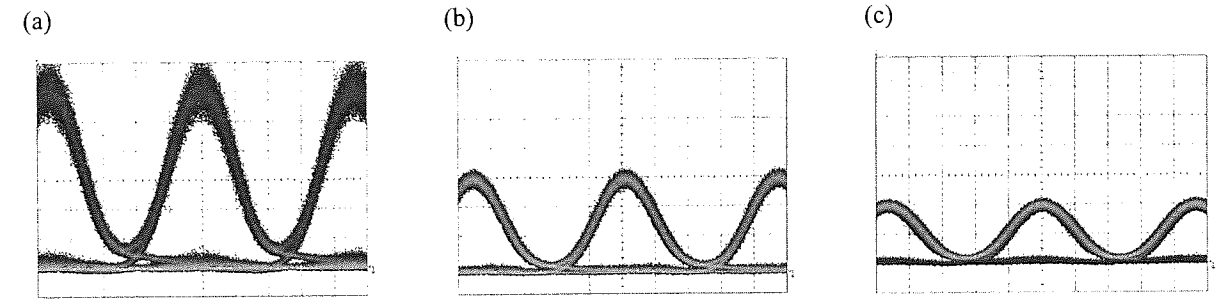

Figure 4.9 Back-to-back eye diagram for (a) 25%; (b) 50%; (c) 75% of 1s in the data. (Time scale: 20ps/div).

Figure 4.9 shows the pulse shape for different fractions of 1s in the data. These pictures were actually taken at back-to-back for the central channel. Note that all signals were equally attenuated by arbitrary value before being displayed to avoid photodiode saturation or damage. It is clearly seen that the pulse energy increases with 25% and becomes almost twice as that of the 50%, and reduces with 75%.

Table 4.1: OSNR and Q-value after 1300km for different fractions.

	Central signal λ=1557.5nm		Right-side signal λ=1559.5nm	
Fraction (%)	OSNR (dB/0.2nm)	Q-value	OSNR (dB/0.2nm)	Q-value
25	8.8	5.3	9	5.5
50	9.1	5.9	9.5	6.2
75	9.6	6.3	10.1	6.7

Table 4.1 shows the results obtained after long distance for the different fractions of 1s and 0s. The table shows the OSNR and Q-value after 1300km distance. Results for the central channel and the right-side channel (λ_5=1559.5nm) are compared here. It is seen that the OSNR is better for more 1s in the data; hence the Q-value is also better. This can be understood as the second modulator at the transmitter receives more electrical power from the pattern generator for more 1s which seems to improve the OSNR at the output of the transmitter, hence after transmission. It is however noticed that the improvement in performance is small for high

unbalancing, which gives that the effect would be negligible in systems use FEC codes, where the unbalancing is much smaller. This would imply that for such linear system, the ideal fraction of the 1s and 0s can still be around 50%.

For comparison purposes, the above experiment can be run where the pulse energy is fixed. In this case, the total average power will increase for more 1s and decrease for more 0s. To work out how much power is required in the channel for each fraction, the pulse energy needs to be calculated by using the following formula:

$$E(J) = \frac{P_{ch}(W)}{\nu \times fraction} \tag{4.1}$$

where P_{ch} is the channel power and ν is the frequency which is 10.7GHz here. For example, the pulse energy of the central channel that uses -8dBm (0.000158W) is 2.96×10^{-14}J for 50% 1s. From this value, the channel power for the other fractions can be calculated for this particular channel by using:

$$P_{ch}(W) = E \times \nu \times fraction \tag{4.2}$$

This gives that the power required in the central channel for 25% is 0.000079W, i.e. -11dBm, which is basically half the power of 50%. This in fact must be done for all other channels, so that the amplifier gains can be adjusted to give the required power for each channel at different fraction. Simply, the total average power must be offset by -3dB if the fraction decreased to 25% and offset by +1.8 if the fraction increased up to 75%. This can be achieved through adjusting the VOAs that follow the EDFAs. Having performed this, the results of different fractions of 1s for the central signal can be shown in figures 4.10. It is seen from (a) that the OSNR improves with more 1s and degrades with more 0s. This is realised as the signal power, hence the total power increases for more 1s and reduces for less 1s, where the system is dominated by the noise impairments. This in turn affects the quality of the signal which shows better behaviour for more 1s and worse behaviour for more 0s. As a result, the maximum transmission distance increases from 1300km up to ~1600km with 75% and reduces down to ~800km with 25%.

As a summary, it was found that different performance can be obtained by transmitting different fractions of 1s and 0s in the data. If the launch power is small i.e. not sufficient to hit a

nonlinear interaction (as in the above experiment), the effect of different fractions can be negligible in the case of FEC coding assuming that the total average power is constant along the fibre link and the encoder does not produce highly unbalanced data. This consequently means that 50% can be the ideal proportion for the 1s and 0s in linear operation. For comparison, if the power does not remain constant over the fibre link, the performance improves with more 1s and degrades with more 0s. This is due to the fact that the signal has larger average power with more 1s hence larger OSNR, and smaller power with more 0s hence smaller OSNR.

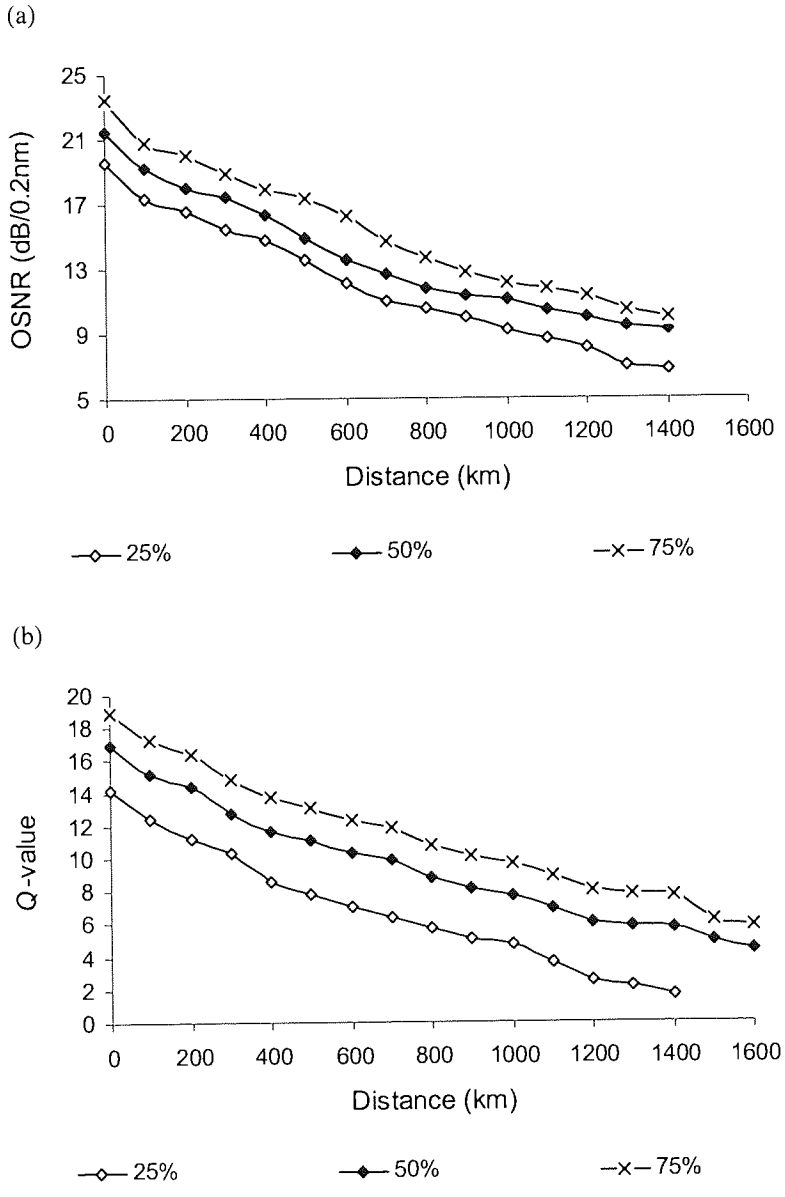

Figure 4.10 (a) OSNR (using 0.2nm RBW); (b) Q-value versus transmission distance for the central channel (λ_3=1557.5nm) using fixed pulse energy.

4.3 High-power operation

In this section we now investigate the effect of changing the fraction of the 1s and 0s on a system operating in the nonlinear regime. The main difference in the results would be that the performance must be affected by the variation of the pulse energy when the fraction changes, while the power is still constant over the fibre link. Theoretically, the nonlinear effects are proportionally dependant on the pulse energy of the signal rather than the total average power. Practically, if the total average power increases with constant fraction of 1s, the pulse energy for each 1-bit increases as well. By keep increasing the power, hence the pulse energy, the performance of the system will increase until the pulse energy becomes sufficient to introduce nonlinear interaction. At that point, the system performance will stop improving and then starts to degrade proportionally with the increase of the pulse energy. This point in fact can be defined as the optimum power for the system, i.e. the maximum power at which the nonlinear interaction has not yet started to degrade the performance. Simply, the optimum power is the power value that corresponds to the minimum BER or maximum Q-value after long propagation distance. However, the system can be referred to as nonlinear system if the operating power is larger than the optimum power, where in linear system the operating power is smaller than the optimum power. The optimum power can be defined as the total average power that is normally measured on the power meter or the individual signal power that is measured on the multi-wavelength power meter. For large number of channels, the individual signal power is commonly defined by dividing the total average power over the number of channels. This is based on that the signals are distributed over wide wavelength band, i.e. the majority of the power over the band is used by the signals. Although this method gives an approximate value, it can still be valid specifically for comparison purposes.

To run a nonlinear system, the same loop setup that was used for linear system (figure 4.3) can be used but the power launched into the fibres must be increased. This in fact requires defining the optimum power of the system by plotting the Q-value performance versus launch power after long distance. The system must then operate at a power larger than the obtained optimum power. In fact, the nonlinear operation experiment discussed here was performed after the 194.9km loop that was used for LME experiment and shown in figure 3.32 became available. That setup in addition to a GFF that was also available at the time of this experiment was used to improve the 5×10Gbit/s WDM system performance. Figure 4.11 shows the whole new experimental arrangement of this experiment.

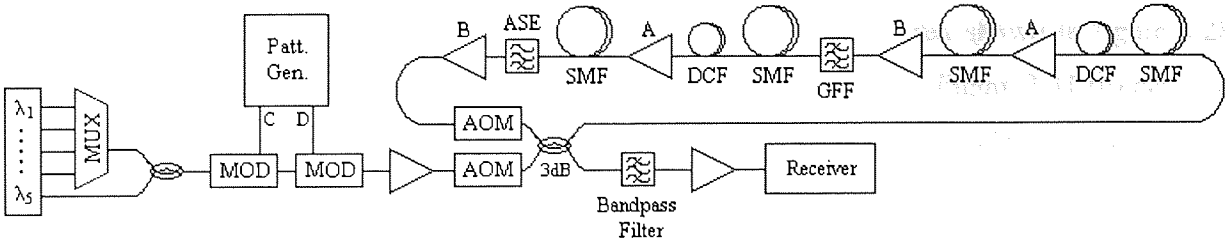

Figure 4.11 Experimental setup.

The system uses the same transmitter as that in the linear experiment which again has five WDM wavelengths modulated via two $LiNbO_3$ modulators that are driven by a pattern generator of 10.7GHz frequency and PRBS data pattern with 2^{31}-1 word length, respectively. The resulting 5×10Gbit/s WDM signals with RZ modulation format are then amplified to the required launch power and enter the 194.9km recirculating loop. The system actually uses wavelengths between 1553.9-1557.1nm with the standard separation of 100GHz rather than 125GHz.

The recirculating loop consists of two fibre sections; the first section has 40.7km SMF, 16.5km with -1383ps/nm DCF, and then another SMF with 41.8km. In the second section, it has 42.9km, 15.2km DCF with -1387ps/nm, and then 38km SMF. The attenuation coefficients of the SMFs and the DCFs are 0.2dB/km and 0.5dB/km, respectively. These losses are compensated by using two C-band EDFAs in each section. The EDFA denoted A in the figure has a 30dB maximum small signal gain and ~13dBm maximum output saturation power; while the EDFA denoted B has a 40dB maximum small signal gain and ~15dBm maximum output saturation power. The gain of the EDFAs is set to operate in saturation where each EDFA is followed by a VOA, as in linear experiment, to adjust the power into the next fibre span. All EDFAs have a noise figure of approximately 5. A GFF with 2dB insertion loss is setup after the second EDFA, and an ASE filter with an insertion loss of 3dB is used before the last EDFA to remove the accumulated ASE gain peak at 1530nm. Each loss of these filters is compensated by the previous EDFA so that the power into each fibre is constant.

The receiver is similar to that used in the linear experiment, where a narrowband optical band-pass filter with 0.24nm bandwidth and 7dB insertion loss is used to demultiplex the WDM channels. The individual channels are then pre-amplified and detected by the receiver.

4.3.1 Recirculating loop performance

The dispersion measurements of the current loop have already been shown in figure 3.28 which has shown approximately zero dispersion over the 1550nm region. Figure 3.31 (b) has also shown how the dispersion evolves with distance for the 1550nm wavelength using such symmetric dispersion configuration. Before presenting the OSNR and *Q*/BER performance of the loop, the optimum power of the system is defined. Again, the optimum power can be either the total average power or the individual signal power. For signal power, the performance must be plotted as a function of the signal power measured on the multi-wavelength meter. Actually, although the number of channels is not large in this experiment, the power per channel can still be obtained by dividing the total average power over the number of channels. This can be understood by referring back to figure 3.39. The figure tells that in addition to having an ASE filter, if the extinction of the GFF is set at maximum and centred in the middle of the data signals, the majority of the total average power will exist within the data signals band. For this experiment where there are five channels, the total power measured on power meter can be therefore divided by 5 to give an approximate power per channel. Figure 4.12 shows the BER measured for the central channel (1555.5nm) versus the total power after 23 recirculations (~4500km). Since the measurements were performed in dB, the power values must be subtracted by 7 to give the power per channel. (Note that since the BERT is available here, there is no need to measure *Q*-value as done in the linear experiment).

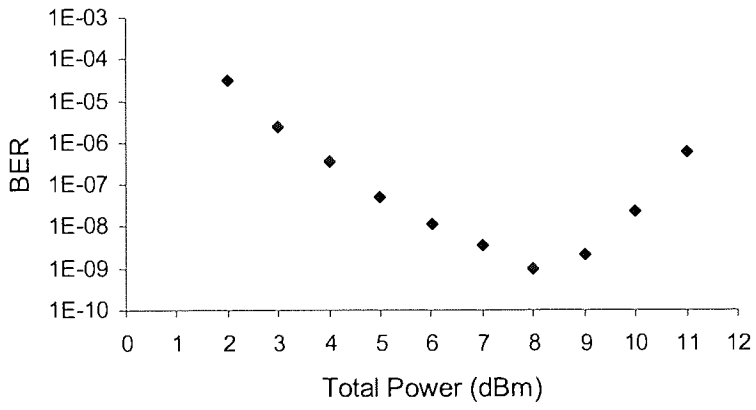

Figure 4.12 BER (measured for the central channel) versus total power after 4500km.

From figure 4.12, it is shown that the optimum total power is around 8dBm, i.e. 1dBm per channel. This basically means that if this system operates at power less than 8dBm, it is classified

as linear regime, and if it operates at power larger than 8dBm it is then classified as nonlinear regime. Ideally, systems are intended to operate at the optimum power where the BER is at minimum. In fact, the signals are initially pre-emphasised at the transmitter although the loop has a GFF. This is important as the GFF is not perfectly flat so some wavelengths have more gain than others. Figure 4.13 shows the pre-emphasised signals at the back-to-back in (a) and how they look after 4000km in (b). The signals are shown almost equalised with respect to the OSNR after long distance thus the demultiplexed channels can have almost the same BER performance at the receiver.

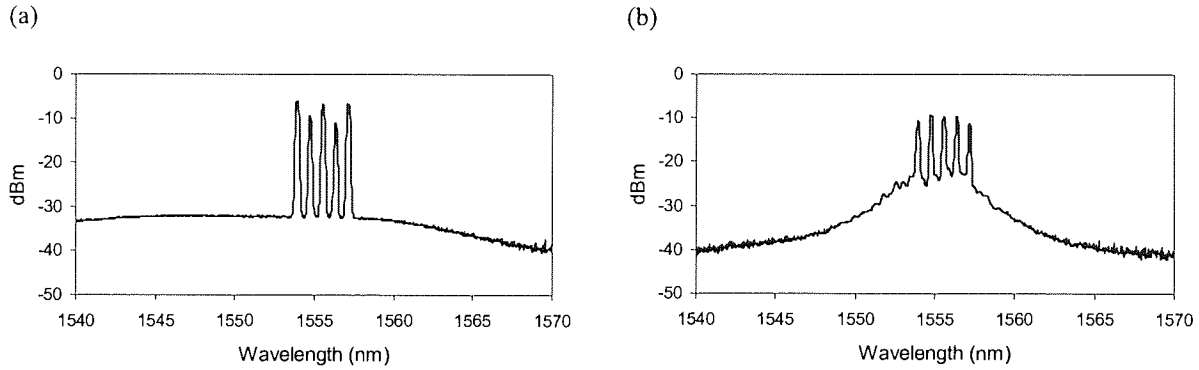

Figure 4.13 Spectrum (a) at back-to-back; (b) after 4000km, using 0.2nm RBW.

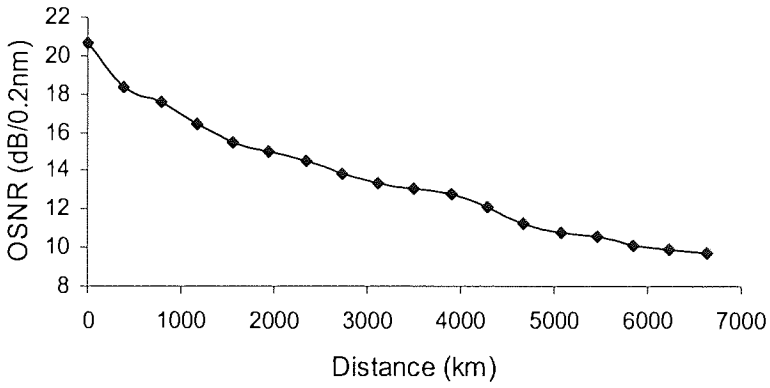

Figure 4.14 OSNR versus transmission distance for the central channel using 0.2nm RBW.

The OSNR measurements for the central channel versus transmission distance using the optimum power are shown in figure 4.14. It can be seen that the signal can propagate over ~6000km with an acceptable OSNR. Nevertheless, it is not necessary that the signal has acceptable BER after such distance, where nonlinear effects may appear. Therefore, it is useful to

present the BER performance as a function of transmission distance for the optimum power as shown in figure 4.15. The curve shows the performance for the whole five WDM signals; the maximum distance achieved with BER = 10^{-9} is around 4600km for most of the channels. This basically gives that the nonlinear effects limit the performance of the system to a distance of 4600km.

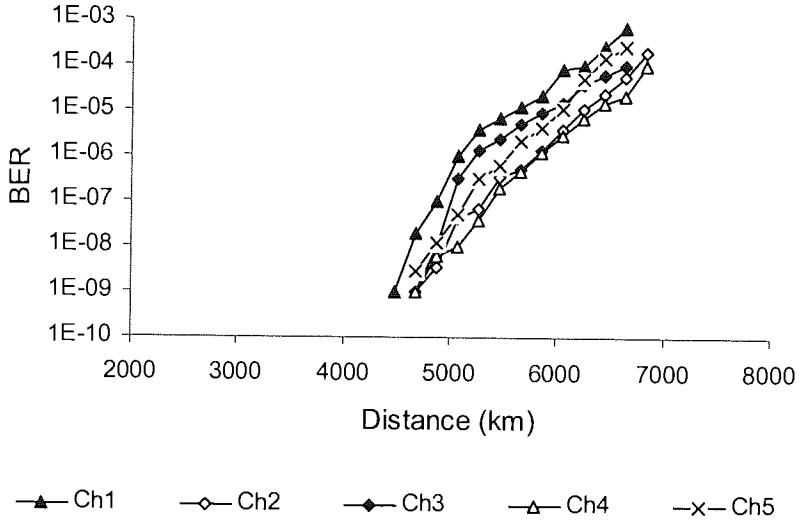

Figure 4.15 BER versus transmission distance for the whole WDM signals. (Ch1: 1553.9nm, Ch2: 1554.7nm, Ch3: 1555.5nm, Ch4: 1556.3nm and Ch5: 1557.1nm).

4.3.2 Results of different fractions

If the system is allowed to operate at optimum power, unbalancing the fraction of the 1s and 0s will however degrade the system performance. This is basically because the optimum power is corresponding to the optimum pulse energy of the 1-bits that will be changed by changing the fraction. This implies that the ideal fraction of the 1s and 0s is 50% for optical transmission systems that work near the optimum power. This in turn requires that the encoder that is used for FEC must be followed by the scrambler to ensure the 50% fraction before transmission. What if the system operates in the nonlinear regime? In fact, operating in the nonlinear regime means that the launch power is larger than the optimum power, hence larger pulse energy. Since the nonlinear penalty is proportional to the pulse energy, the main problem with nonlinear operation would be that the system is limited to a distance which is shorter than that obtained with the optimum power according to [48]:

$$L_{NL} = \frac{1}{\gamma P_0}; \tag{4.3}$$

$$\gamma = \frac{n_2 \omega_0}{c A_{eff}} \tag{4.4}$$

where L_{NL} is the maximum distance limited by nonlinearity (called nonlinear length), P_0 is the peak power (related to pulse energy), γ is called nonlinear parameter measured in (m^2/W), n_2 is the nonlinear coefficient of the fibre which is ~ 2.6×10^{-20} m^2/W for silica fibres, ω_0 is the signal frequency, and A_{eff} is the effective area of the fibre, which is 80μm^2 for the SMFs of this experiment. Theoretically, the nonlinear length L_{NL} can be increased by reducing the pulse energy, which can be achieved through increasing the fraction of the 1s in the data. This is again based on that the power remains constant over the fibre link where the EDFAs operate in saturation. As mentioned before, if the above is proven practically, it can be useful for systems use FEC, where unbalancing the fraction through coding process can be an advantage if the encoder adds more 1s to the data. In other words, the system with FEC can operate at high power where the nonlinear penalty can be compensated through the existing coding process adding more 1s, thus an additional scrambler may not be required.

This section investigates the effect of unbalancing the fraction of the 1s and 0s on the system shown in figure 4.11 by allowing nonlinear operation. Again, the system can operate in nonlinear regime if the total launch power is larger than 8dBm according to figure 4.12. The launch power used here is 3dB higher, i.e. 11dBm in total or 4dBm per channel, to allow for high nonlinearities. Having run the experiment, the BER results versus transmission distance for the whole five channels are shown in figure 4.16.

(a)

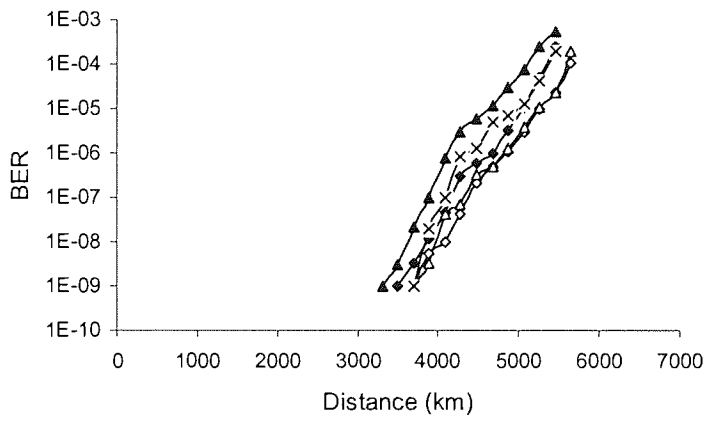

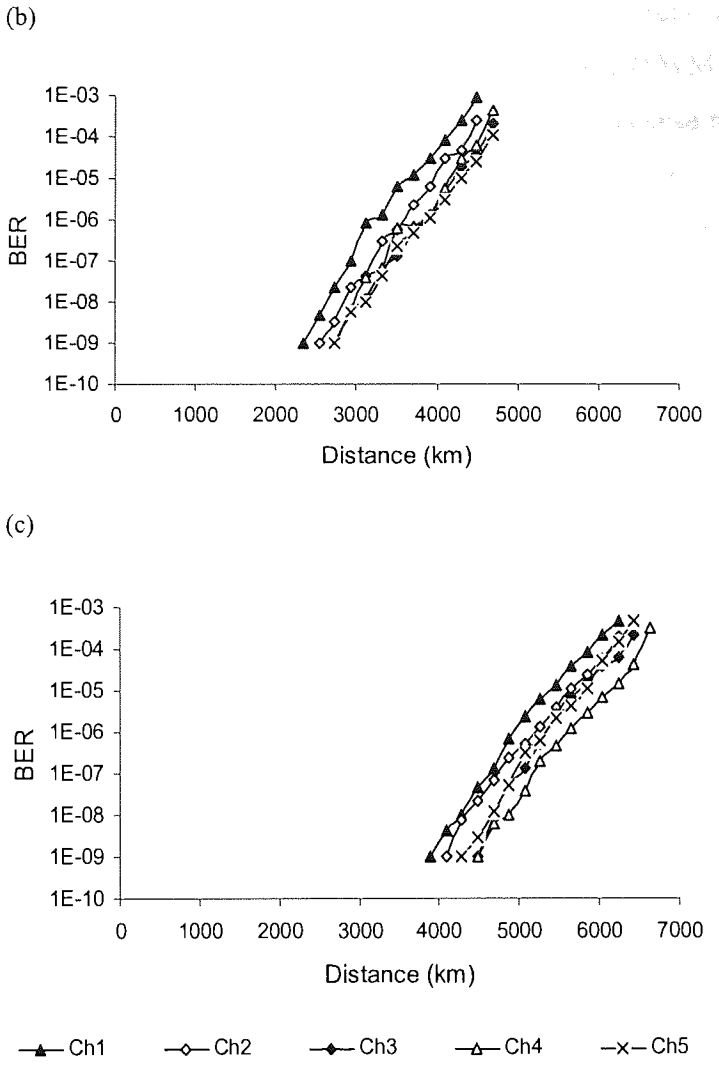

Figure 4.16 BER versus transmission distance for the whole WDM signals using: (a) 50% 1s; (b) 25% 1s; (c) 75% 1s. (Ch1: 1553.9nm, Ch2: 1554.7nm, Ch3: 1555.5nm, Ch4: 1556.3nm and Ch5: 1557.1nm).

In (a), when the data comprises of 50% 1s, the maximum transmission distance achieved with 1×10^{-9} BER is around 3500km. This distance can be compared to that obtained with the optimum power, giving that the nonlinear length has reduced with large power. In (b), when the fraction of 1s is reduced to 25%, the pulse energy increased in the 1-bits (recall figure 4.9), introducing greater nonlinear interaction thus the whole performance degraded. In this case, the maximum distance with BER of 1×10^{-9} is shifted down by nearly five recirculations, i.e. 1000km. In (c), when the fraction of 1s is increased up to 75%, the pulse energy reduced; hence the nonlinear interaction decreases thus the overall performance improved. A propagation distance of ~4000km with BER of 1×10^{-9} is attained in this case. Obviously, the performance of the system is limited by the nonlinear impairment rather than noise. However, since the loop uses fibres with

high local dispersion, e.g. SMF (D ~ 17ps/km/nm at 1550nm), and relatively large channel separation, both cross-phase modulation (XPM) and four-wave mixing (FWM) would not have a large contribution to the overall nonlinear impairment. This is again because the bits of different signals have different group velocities when propagate through the fibre. Thus they will be separating from each other and after short distance they will have a time separation larger than one bit period. This results in that the interaction between them can be very small during transmission. As a result, the most contribution to the nonlinear effect in this experiment can be the self-phase modulation (SPM) in addition to SBS. Moreover, the overall nonlinear interaction is further increased due to using amplifiers at the chirp-free points, i.e. after the second and the fourth SMFs, where the dispersion is compensated hence the peak power is at a maximum.

Back to figure 4.16 (c), it can be seen that the 75% has improved the propagation distance of the nonlinear regime up to ~4000km, while figure 4.14 has shown that the ideal 50% had ~4600km at the optimum power. This can be more realised by working out the pulse energy of each case using equation (4.1). The equation gives that the pulse energy for 75% using 4dBm/ch is 3.13×10^{-13}J, while for 50% using the optimum power (1dBm/ch) the pulse energy is 2.35×10^{-13} J. This theoretically implies that the pulse energy of the 75% must be reduced to 2.35×10^{-13} to achieve 4600km distance. This in fact can be attained by reducing the power of the channel, where the exact power can be calculated by (4.2) that gives 2.8dBm/ch. This means that the system can work in nonlinear regime using 2.8dBm/ch or 9.8dBm total average power and 75% 1s to achieve similar performance to that operating at optimum power with standard 50% 1s.

As assumed before, the FEC codes cannot reach 75% 1s where the overhead is small fraction of the total length of the data sequence. This assumption in addition to the results obtained here, which show that large variation in the fractions causes considerable effect in the nonlinear system, can lead to investigating the effect with small variations as presented below.

4.3.3 Small variation results

To better simulate the effect of unbalancing data by the FEC codes, it is necessary to use small variation in the fraction, e.g. 47%, 53%. Since the pattern generator used in this experiment does not have a function of producing data with such fractions, it is necessary to load external data patterns to the pattern generator. The external patterns are generated by a software programme (based on Excel) and transferred to the pattern generator by using a Labview code*.

* The Excel and Labview codes have been provided by Dr Paul Harper, Photonics Research Group, Aston University.

Note that the same pattern should be loaded on the BERT for error detection. Although the software code used here is able to generate PRBS data with a pattern length of up to 2^{31}-1, the pattern generator/BERT have a limit of 2^{15}-1 bits for user programmable data. This implies that the system described here can use data words with length of 2^{15}-1 at maximum instead of 2^{31}-1.

The experiment must be performed in the same way presented in previous section. Initially, the optimum power and the maximum propagation distance for the system must be defined for 50% 1s. As a result, it was found that the optimum power did not change from previous results (with longer data word), where it is still at around 1dBm per channel. The signals can still propagate to a transmission distance of 4600km with acceptable BER. Again, if the system is allowed to operate in the nonlinear regime at an average power of 4dBm/ch, the results for the new fractions can be shown as in figure 4.17. The figure shows the BER performance versus transmission distance for the central channel using different fractions as appear on the bottom of the graph.

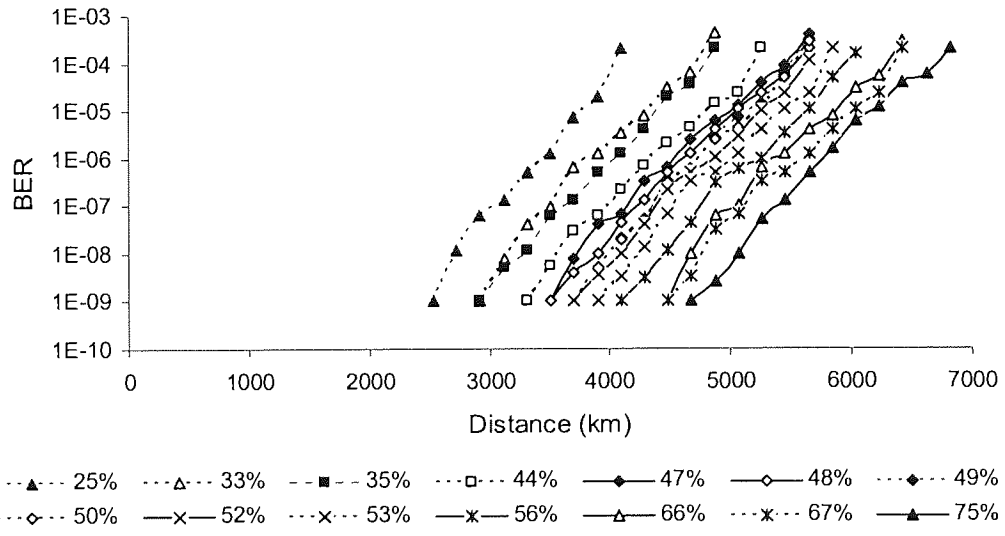

Figure 4.17 BER versus transmission distance for the central channel using different fractions of 1s.

For comparison purposes we performed a separate experiment in which the input was a single-channel using 1555.5nm and 4dBm power. Figure 4.18 shows the maximum transmission distance achieved with error = 10^{-9} for different fractions. The figure has the results of both WDM and single-channel transmission, where the WDM results can be obtained from figure 4.17. It is seen that the performance of the system has improved for more 1s and degraded for more 0s in both cases. This can prove that the majority of the nonlinear impairment comes from the SPM induced on every signal rather than inter-channel interaction.

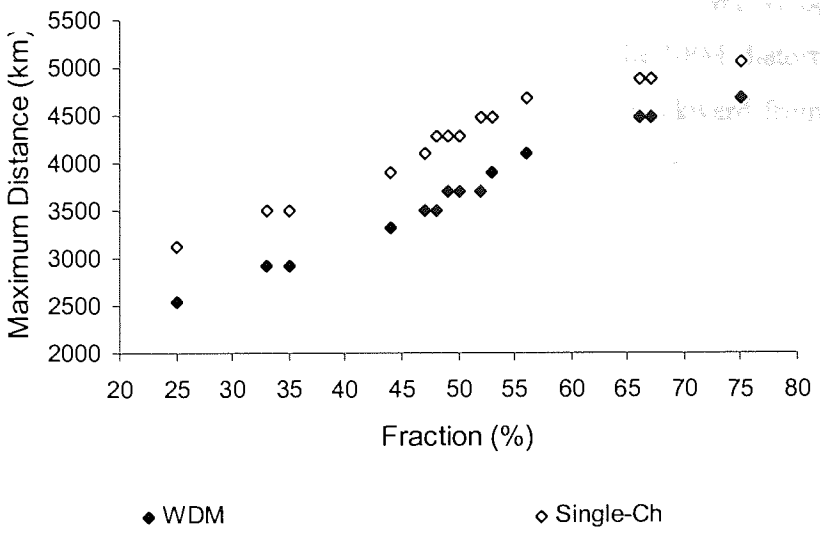

Figure 4.18 Maximum propagation distance with error = 10^{-9} versus fraction for the central channel.

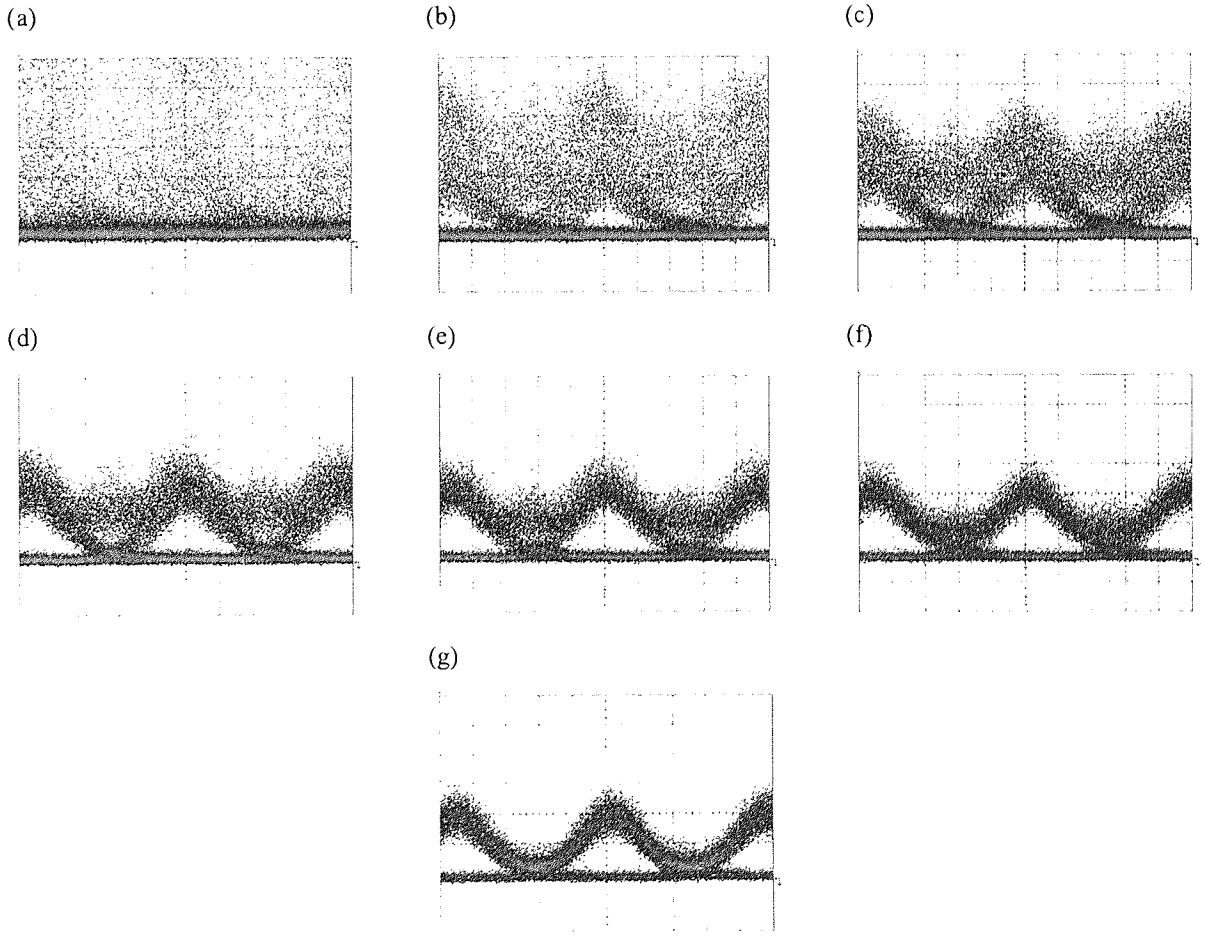

Figure 4.19 Eye diagram for the central channel after 22 recirculations (~4200km) using fractions: (a) 25%; (b) 35%; (c) 44%; (d) 50%; (e) 56%; (f) 65%; (g) 75%. (Time scale: 20ps/div).

Figure 4.19 shows the eye diagram of the central channel in WDM operation after 22 recirculations (~4200km) for different fractions. It shows that the SPM distorts the signal with lower fraction due to the increase in the pulse energy. Working backward from 75%, the signal starts to have considerable distortion at 56% (in (e)), thus the receiver counts considerable number of errors as shown earlier in the BER curve of figure 4.17. This kind of distortion that arises due to nonlinear effects, specifically SPM, causes an induced spectral broadening in the signal. Figure 4.20 shows the spectral shape of the central channel after 22 recirculations for different fractions. It can be clearly seen that more 1s in the data results in narrower spectrum. Note that the spectrum is asymmetric in all cases where this asymmetry is caused by modulation at the transmitter. The pulse broadening versus fraction is shown in figure 4.21 for the central channel in both WDM and single-channel transmission, measured at -10dB bandwidth point on the OSA.

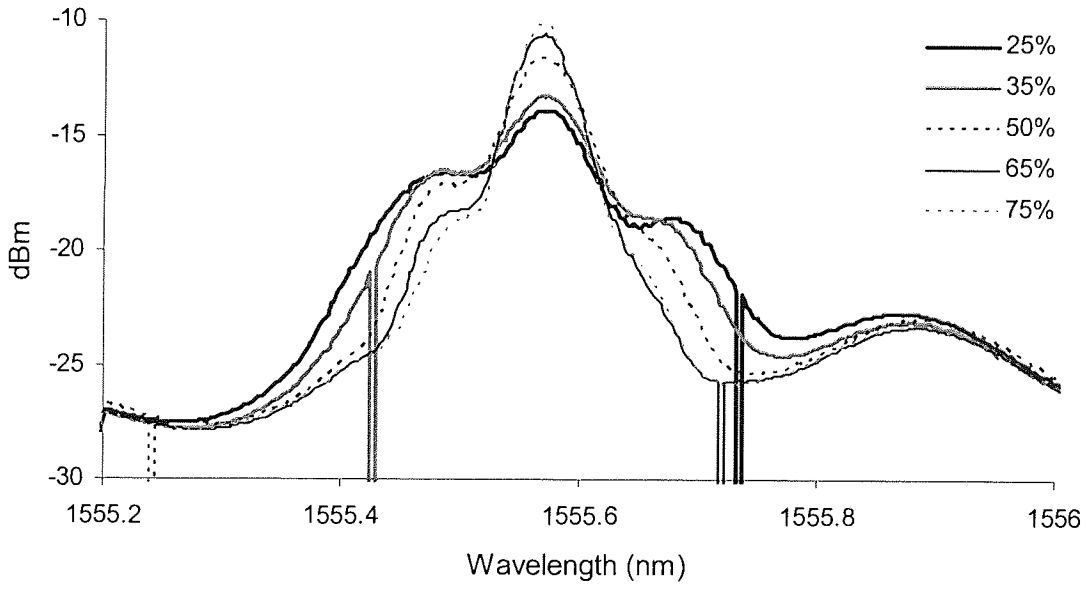

Figure 4.20 Spectral shape of the central channel after 22 recirculations (~4200km) for different fractions, using 0.07nm RBW.

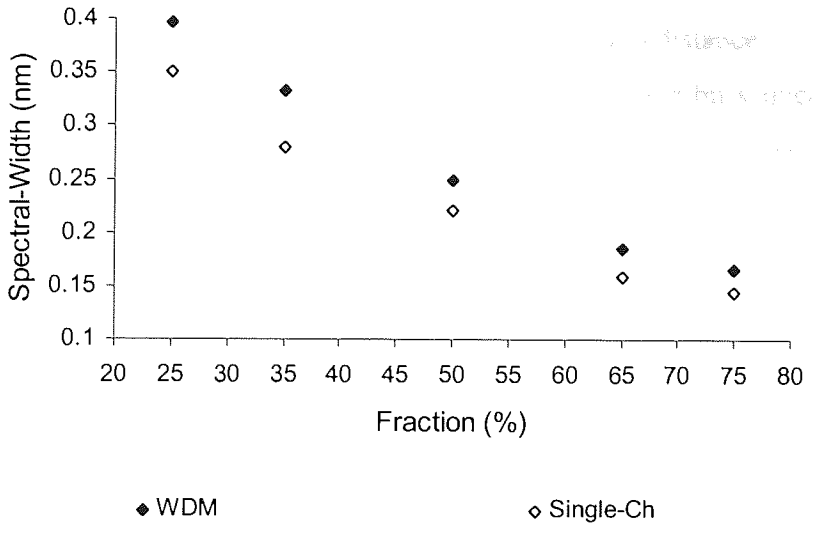

Figure 4.21 Spectral-width versus fraction after 22 recirculations for the central channel.

Back to figure 4.18, it is shown that the propagation distance of the fraction 50% is improved by increasing the fraction of the 1s. For instance, the 56% has improved the distance of the 50% by two recirculations, i.e. ~400km. The pulse energy of the 1-bits in 56% can be calculated from (4.1) which gives 4.19×10^{-13}J using 4dBm/ch power. Remember that the optimum pulse energy for 50% is 2.35×10^{-13}J using 1dBm/ch. This implies that the pulse energy of the 56% must be reduced to 2.35×10^{-13} to achieve the optimum performance of this system. Therefore, the power required for 56% to attain such pulse energy is 1.49dBm/ch from equation (4.2). This means that the system can work in nonlinear regime using 1.49dBm/ch or 8.49dBm in total if the encoder output has 56% 1s, where the performance can be similar to that of the ideal 50% operating at optimum power. Again, this gives the ability of saving the additional electronics required by the scrambler to rebalance the fraction.

Table 4.2: Power required per channel for different fractions to achieve optimum pulse energy in the 1-bits.

Fraction (%)	Power (dBm/ch)
50	1.00
52	1.16
53	1.25
56	1.49
65	2.13
75	2.76

Table 4.2 shows the power per channel that is required for different fractions to achieve the optimum pulse energy in the 1-bits, hence the maximum transmission distance.

If the encoder adds less 1s, hence the overall fraction of 1s in the bit sequence is less than 50%, the inverse of the bit sequence can be transmitted which is then re-inversed at the receiver. This is based on the fact that less 1s in the data results in worse performance in nonlinear operation due to higher pulse energy. In fact, it is possible to reduce the pulse energy by decreasing the launch power where the power required to achieve optimal pulse energy can be worked out in the same way used in table 4.2. For instance, the power required per channel for fraction 44% to achieve 2.35×10^{-13}J is 0.44dBm. This power can actually be used if the encoder's output is around 44% so that the system can still propagate for long distance. But it is important to notice here that the OSNR will reduce where the power is less than the optimum power (1dBm/ch), thus the performance cannot be similar to that of the optimum case.

In general, if the output fraction of a specific code is known by the engineer, the system can be allowed to operate at the required power level for optimum pulse energy as done above. This requires that the EDFAs gains or their associated VOAs are set to provide that power level at the input of each fibre.

For comparison, the nonlinear system is also allowed to operate with fixed pulse energy as done in linear system. Therefore, the pulse energy is fixed at sufficiently high to ensure nonlinear operation with all fractions. Actually, the system uses launch power of 4dBm/ch which gives pulse energy of 4.7×10^{-13}J in the case of 50%. All other fractions should then use this pulse energy where the required power for the different fractions can be obtained by using (4.2). Theoretically, the required power will increase with more number of 1s, thus the performance will improve as the OSNR improves while the pulse energy is constant. Figure 4.22 shows the maximum transmission distance achieved with error = 10^{-9} versus fraction for the central channel in both WDM and single-channel transmission. The figure also shows the OSNR versus fraction for the central channel in WDM transmission after 4000km. It can be seen that the propagation distance improves with more 1s for the fractions less than 65%. The distance improvement is almost proportional to the OSNR improvement. At high fraction, i.e. 65% and more, the performance degrades as the fraction of 1s increases, and that can be understood as the number of successive 1s increases thus the interaction between pulses increases as well. This is based on that the pulse energy of the 1-bits was sufficiently high, i.e. 4.7×10^{-13}J. Figure 4.23 shows the eye diagram of the central channel after 3000km for different fractions. It is clear that the signal distorts with large fractions as noticed in the 65% and 75% cases.

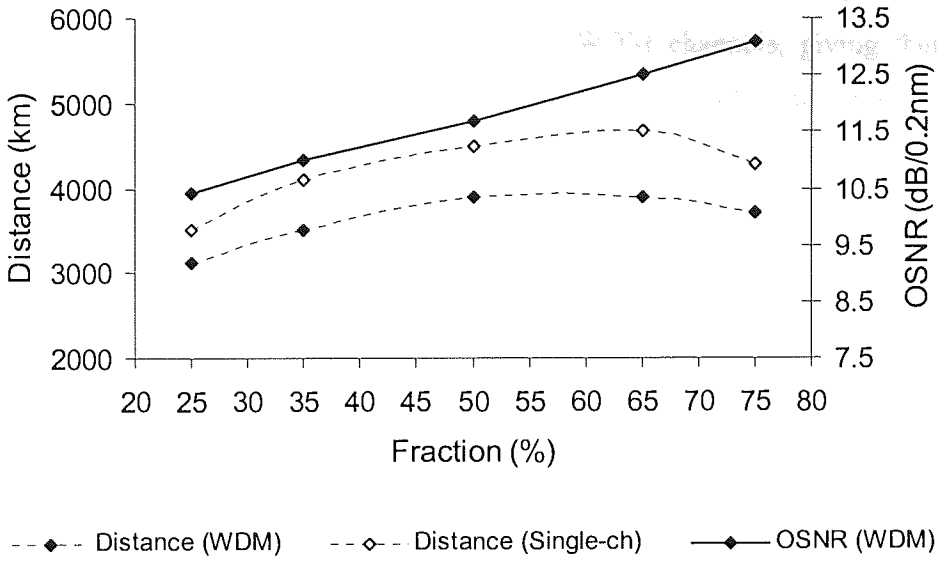

Figure 4.22 Maximum distance with error=10^{-9} versus fraction for the central channel in both WDM and single-channel transmission; and OSNR versus fraction after 4000km for the central channel in WDM transmission.

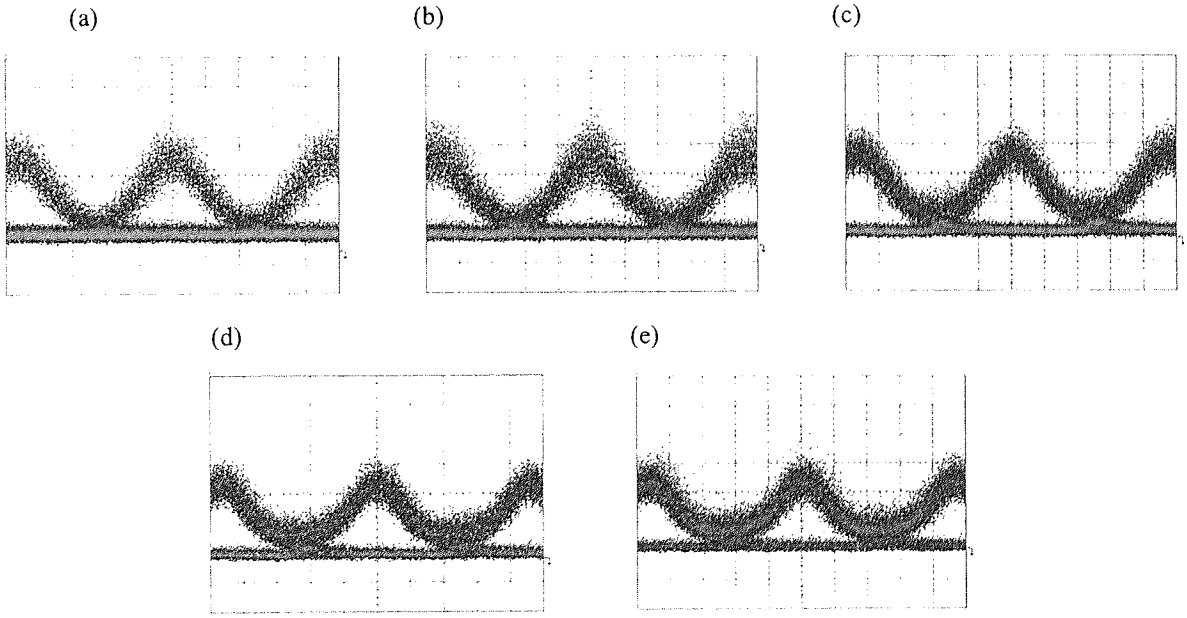

Figure 4.23 Eye diagram for the central channel after 3000km using fractions: (a) 25%; (b) 35%; (c) 50%; (d) 65%; (e) 75%, and constant pulse energy. (Time scale: 20ps/div).

So as a summary of the above, if the pulse energy is constant, the performance changes with unbalancing the fraction of the 1s in the data. With smaller fractions; the OSNR is worse

after long distance, but there is no distortion noticed on the signal. With larger fractions; the OSNR is better after long distance, but signal distorts due to more interaction between 1s. Furthermore, the single-channel seems to perform similar to WDM channels, giving that the majority of the distortion for large number of 1s comes from the pulse interaction rather than WDM interaction. This is because the channels were spaced by 100GHz. If the spacing is reduced to allow more inter-channel interaction, different results will be expected.

4.4 Summary

This chapter has investigated the effect of varying the fraction of the 1s and 0s in random data on the performance of a WDM communication system. The chapter started by giving an introduction that was important to understand the reason for this study. It was all based on a discussion about the probability of errors in the 1 and 0 bits in both linear and nonlinear optical transmission systems. The introduction also had a general discussion about the forward error correction (FEC) as an application that can use the advantage of this study. After the introduction, the experimental work has been demonstrated. In fact, the work was divided into two parts; low power (linear) operation and high power (nonlinear) operation, where each part was presented separately. Both experiments used 5×10Gbit/s WDM signals propagating through SMFs and DCFs in a recirculating loop.

The first experiment which was designated for linear operation used 52km fibres in the recirculating loop. The total average power was sufficiently low to ensure linear operation. The performance of this loop, i.e. the dispersion, OSNR and Q-value, have been first presented using 50% 1s. After that, the system was examined with the fraction being varied by ±25% from the pattern generator. The total power was kept constant over the loop since loop EDFAs operated at saturation. This means that the pulse energy of the 1-bits decreases for more 1s and increases for less 1s. As a result, it has been found that the performance of the system changed little with such high unbalancing. This gave that in FEC coding, where the unbalancing is small, there would be no considerable effect to the system performance, and thus the ideal fraction can be 50%. For comparison, the system was allowed to operate while the pulse energy was constant. This means that the total average power is larger for more 1s and smaller for less 1s. It has been found that the transmission distance improved for more 1s due to an improvement in the OSNR hence Q-value, and degrades for less 1s due to a degradation in the OSNR.

For nonlinear operation, the loop used 194.9km fibres in the recirculating loop. The experiment started by defining the optimum power of the system, thus the nonlinear region was

defined. The OSNR and BER performance of the loop have been presented using 50% 1s and optimum power. Then, the system was allowed to operate at high power, 3dB higher than the optimum power, to ensure high nonlinearity. The performance was then compared for 50% and 50±25% fractions where the total power is constant over the loop. It has been shown that the performance considerably improved for 75% 1s due to a decrease in the pulse energy hence less nonlinear interaction, and degrades for 25% 1s due to an increase in the pulse energy hence more nonlinear impairments. This has actually led to investigating the effect of small unbalancing, e.g. ±3%, ±5%, which can better simulate the effect of the FEC encoder unbalancing. The experiment was run with different small-unbalanced fractions and the transmission distance performance was compared. The signal shape as well as the spectrum has been compared for different fractions after long distance; it has been shown that the signal distorted and the spectrum broadened with reducing the fraction of 1s. As a result, it has been advised that the scrambler which conventionally follows the FEC encoder to rebalance the data can be saved if the encoder adds more 1s to the data while the system operates at high power. If the encoder adds more 0s, the inverse of the data can be transmitted and then inversed back to its original sequence at the receiver. This would still allow saving the additional scrambler in the FEC system. The system was also allowed to operate at fixed pulse energy for comparison; it has been shown that the performance improved with the fraction increase due to an OSNR improvement until 65%, at which the performance started to degrade although the OSNR keeps improving. This was because the interaction between the 1s in the signal increased due to having more successive 1s in the data signal.

Chapter 5

Single and WDM transmission after all-optical NRZ to CSRZ and RZ to CSRZ format conversion using an SOA-NOLM

5.1 Introduction

As the previous chapter has investigated patterning effect whose advantages can be used in improving the performance of legacy WDM communication system, this chapter presents another possible way to improve the performance of such optical system. This technique is actually based on choosing an appropriate modulation format for the transmitted signal. However, it has already been found that the performance of the optical fibre communication system largely depends on the modulation format [26]-[28], [105]-[107]. In fact, the best modulation format is dictated by many system parameters such as system length, fibre type, dispersion management and the optical bandwidth [5]. In general, the carrier-suppressed return-to-zero (CSRZ) modulation format, which has been proposed in recent years, can deliver excellent transmission performance due to its high tolerance to nonlinear effects and chromatic dispersion compared to that of the conventional non-return-to-zero (NRZ) and return-to-zero (RZ) formats [3]. The CSRZ reduces the main carrier component of the signal, which carries most of the power in the NRZ and RZ formats but contains no useful information. This results in that the input power into the fibre is reduced, allowing the use of optical amplifiers in transmission with lower nonlinear effects. Furthermore, the CSRZ also narrows the optical spectrum, thus the signal becomes more tolerant to chromatic dispersion with higher spectral efficiency [108]. For WDM applications, CSRZ offers better performance because it is less sensitive to four-wave-mixing (FWM) caused by the WDM channels interaction [109]. However, CSRZ signal generation is more complex than the conventional NRZ and RZ since at least one additional modulator is required [110]. This modulator can be a $LiNbO_3$ MZ modulator which is an electro-optic device. Recently, electro-optic devices have been thought to be replaced by all-optical devices which have been considered to be of key importance in future all-optical networks where the signal remains in the optical domain all over the network without being converted to electronics [111]. This indeed can increase the cost effectiveness of the WDM network. As a result of this, all-optical signal processing including switching, demultiplexing, signal regeneration and format conversion have

received much interest in the recent research, where this chapter will consider the all-optical format conversion from NRZ and RZ to CSRZ due to the advantages mentioned above. The chapter is actually designated to examine the transmission performance of a CSRZ signal after all-optical format conversion. The performance must be compared with that of the unconverted NRZ and RZ signals, so any improvement resulted on the converted CSRZ may encourage using the all-optical converters in place of the conventional electro-optic modulators that exist in the current WDM communication systems.

The work of this chapter has been done as a collaborative work with Mohammad Halim Wahid who is one of the Aston Photonics Research Group members, doing research in all-optical devices and applications. He was therefore responsible for the converter while I was responsible for the transmission work.

5.1.1 All-optical format conversion

The conversion from NRZ and RZ to CSRZ is conventionally implemented as shown in figure 5.1 [112], where the electro-optic MZ modulator is biased at the minimum power transmission point. An electrical clock with half the data frequency is inserted into the modulator to modulate the input NRZ or RZ optical data. As a result, the optical field changes the polarity for every other pulse, i.e. the phase alternates systematically between 0 and π from pulse to pulse. Therefore, the time-averaged optical field is zero, and the spectrum shows no carrier where the two characteristic frequency components will be at $\pm v$; since v is half the frequency of the data [105], [112].

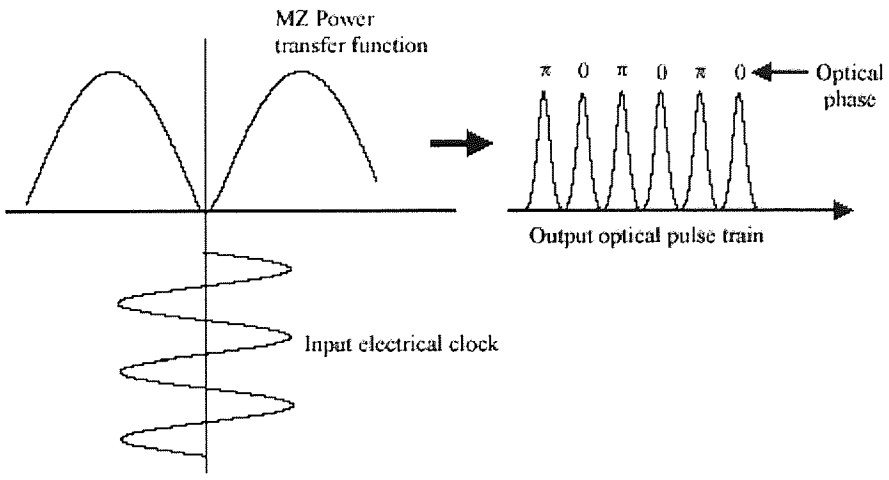

Figure 5.1 CSRZ conversion principle.

The all-optical conversion from NRZ and RZ to CSRZ was first shown in [113] using a semiconductor optical amplifier based nonlinear optical loop mirror (SOA-NOLM) or sometimes referred to as SLALOM: semiconductor laser amplifier in a loop mirror [114]. The all-optical conversion is implemented as shown in figure 5.2, which applies to 10Gbit/s data. The SOA-NOLM is biased at around 2π, i.e. the phase difference between the clockwise and counter-clockwise signals is 2π. A control pulse, which is a sinusoidal optical clock at half the data channel clock frequency i.e. 5GHz, is injected to saturate the SOA hence modulates the refractive index of the SOA's active region periodically. At the output of the loop mirror, when the clockwise and the counter clockwise signals are recombined, their phase modulation is converted into amplitude modulation. Thus, the output data is alternating between 0 and π at adjacent bits; hence the input NRZ or RZ data signal is converted into CSRZ format. Paper [113] has also shown the conversion of a CSRZ back to the original NRZ and RZ by following the same principle. However, if the control pulse is absent, the clockwise and counter-clockwise signals will destructively interfere at the output of the loop mirror. If the phase difference is adjusted from 2π to π, the interference will be constructive, thus the input NRZ or RZ signal is switched out of the SOA-NOLM without changing its modulation format [115].

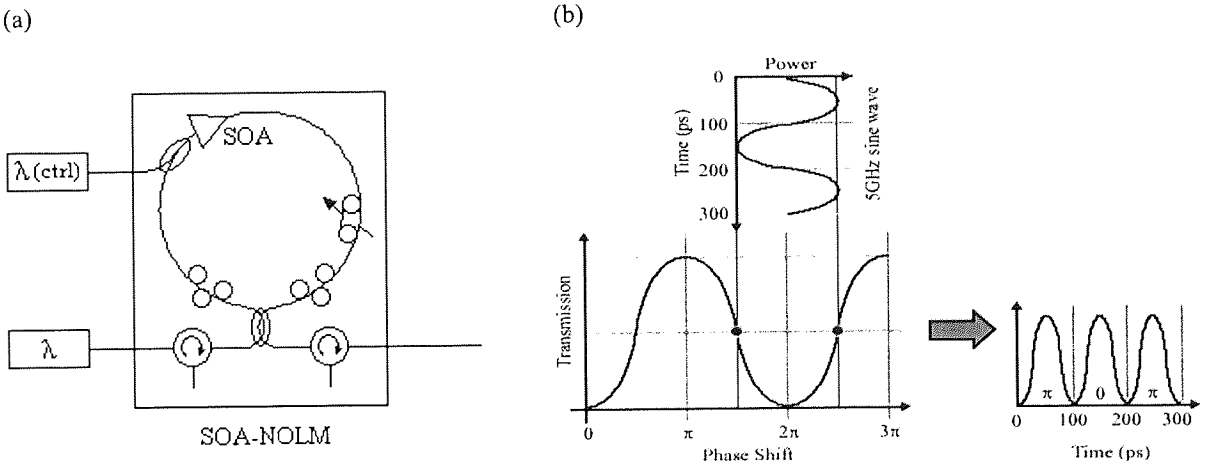

Figure 5.2 (a) SOA-NOLM converter. (b) All-optical conversion.

This chapter investigates the feasibility of such SOA-NOLM device in converting single-channel (as in [113]) and 4×10Gbit/s WDM channels. For single-channel, the new contribution would be that the BER performance over long transmission distance for the converted CSRZ signal against its original NRZ and RZ counterparts is presented. For WDM, which has totally

not been shown elsewhere, the available optical conversion bandwidth for this device and its limitations are explored. Moreover, the BER performance for the converted WDM signals is compared with that of the original unconverted signals after short transmission distance.

5.2 Single-channel experiment

5.2.1 Conversion results

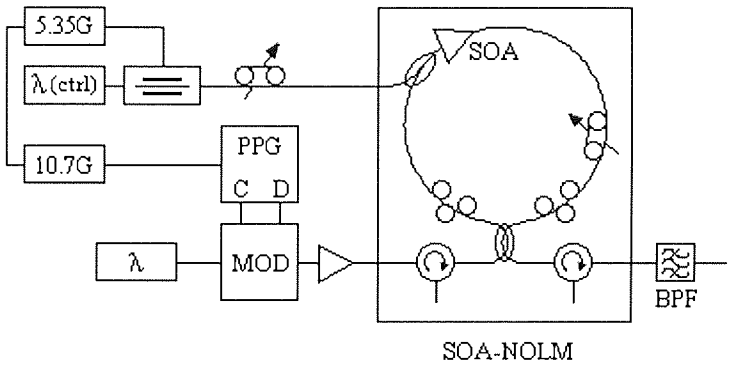

Figure 5.3 Experimental setup for the SOA-NOLM converter.

Figure 5.3 shows the experimental setup for the SOA-NOLM converter for single-channel. The optical data signal is generated in the same way discussed in previous chapters, where a CW laser source at 1555.2nm is applied with a $2^{31}-1$ PRBS via one $LiNbO_3$ modulator for the NRZ format, and two $LiNbO_3$ modulators for the RZ format. The data signal therefore has a much longer bit sequence than that used in paper [113] which was $2^{7}-1$. Again, the pulse pattern generator generating the PRBS sequence is driven by an external clock reference of 10.7GHz, where no forward error correction is applied. The resultant data stream is amplified and launched into the converter. The SOA-NOLM comprises of a 50/50 coupler with polarisation controllers (PCs) on each arm, a 50/50 coupler on the clockwise path and an SOA being offset from the centre by a 140ps on counter-clockwise direction using variable optical delay line on the clockwise arm. The SOA provides a peak fibre-to-fibre gain of 20dB, and a saturation output power of 3.85dBm when biased at 200mA. For the control pulse, a CW DFB laser with a wavelength of 1542.3nm is modulated at 5.35GHz, delayed and coupled via a 50/50 coupler into the SOA-NOLM at a power of 3.2dBm. A variable optical delay line, to adjust the control pulse arrival time relative to the data, controls the phase seen by the clockwise and counter clockwise

data at the SOA. On the output of the SOA-NOLM a tunable grating band-pass filter with a 0.24nm 3dB bandwidth and a 7dB insertion loss is used to pass the data traffic signal while the 1542.3nm control wavelength is filtered out. Two circulators are used within the system; one before the SOA-NOLM to prevent its reflected signal from interfering with the incoming data, and one after the SOA-NOLM to prevent any reflected light from re-entering the loop mirror that can change the whole characteristics of the device.

Having propagated NRZ and RZ signals through the converter, the results can be shown in figure 5.4. The figure shows the spectrum and corresponding eye diagram for the original NRZ signal at (a) and its converted CSRZ signal at (b), and the original RZ signal at (c) and its converted CSRZ signal at (d). It can be clearly seen that the main component of the NRZ and RZ signal is suppressed after conversion, where the main two characteristic components are at ~±0.04 (±5GHz) from the central wavelength component. It is also seen that the spectrum of both signals slightly narrows after conversion, where the new signal is narrower by almost 0.015nm in both cases if measured at -40dBm which is just above the noise floor (note that this value depends on the resolution bandwidth of the OSA).

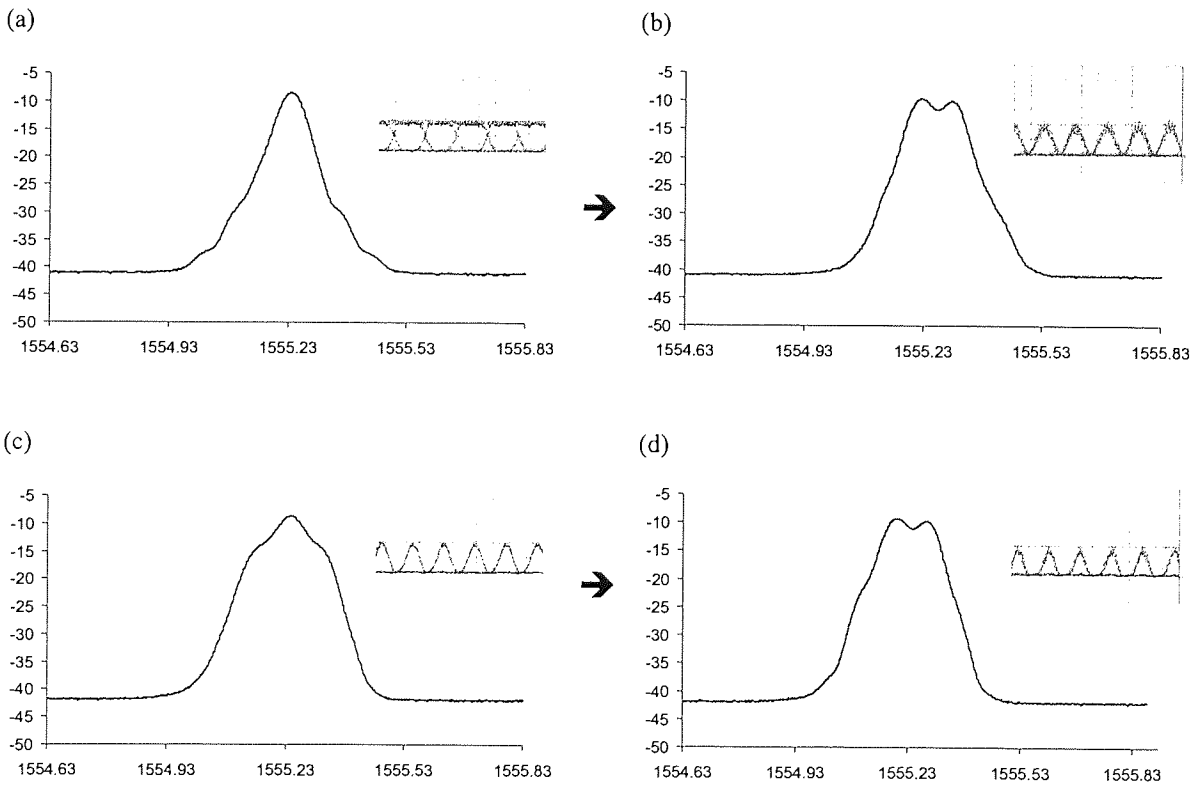

Figure 5.4 Spectrum (OSA resolution bandwidth: 0.06nm) and corresponding eye diagram. (a) NRZ signal; (b) CSRZ signal converted from NRZ; (c) RZ signal; (d) CSRZ signal converted from RZ.

Figure 5.5 shows the BER measurements for the converted CSRZ signal at the output of the SOA-NOLM for different input RZ signal power. The dynamic range of the input RZ signal for RZ to CSRZ format conversion with acceptable BER is found between -18 and -14dBm for this converter. The optimum input power for RZ signal can be between -16 and -15dBm, where the BER is at 10^{-10}. Similar results have been achieved with input NRZ signal for NRZ to CSRZ conversion.

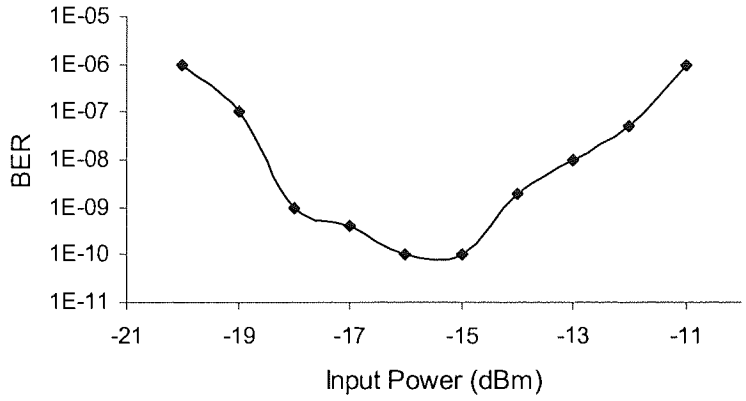

Figure 5.5 BER measurements for the CSRZ at different input RZ signal power.

5.2.2 Transmission results

Having achieved the all-optical conversion from NRZ and RZ to CSRZ, a transmission experiment can be performed to examine the performance of the converted signal in comparison with that of the original signals. The whole experimental setup for this test can be shown in figure 5.6. The figure depicts both the transmitter, including the data source and the SOA-NOLM converter, the transmission link which is a 194.9km recirculating loop and the receiver.

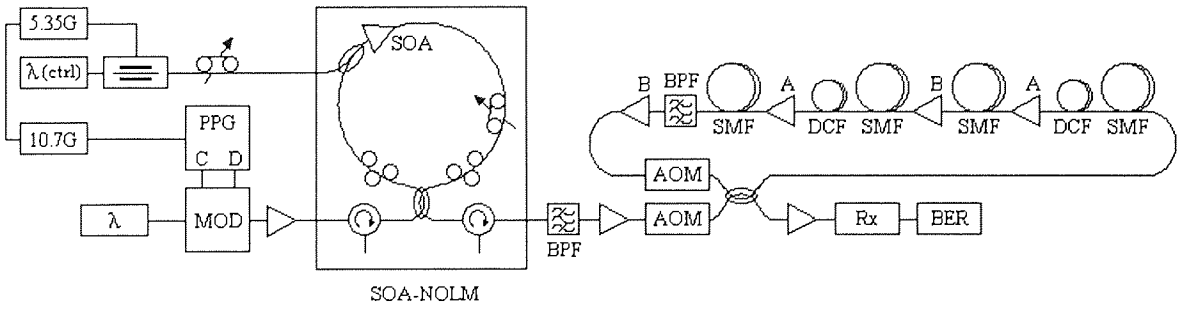

Figure 5.6 Experimental setup, depicting the SOA-NOLM converter and 194.9km recirculating loop.

The converted CSRZ signal that has passed through the band-pass filter is amplified by a booster to reach the required level which is here 6.4dBm at the input to the fibre spans. This power has been chosen to allow nonlinear operation that can be useful in comparing the tolerance of the converted and unconverted signals towards nonlinear effects. The optimum power for the system was found at around 2dBm, giving that the launched power used here is approximately 4dB higher than the optimum. This should lead to significant nonlinearity which will have a considerable affect on the system performance. The amplified signal is then propagated through a 194.9km recirculating loop, which is similar to that used in chapter 3 and shown in figure 3.32. Again, the loop consists of two nearly symmetric fibre sections; the first consisting of 40.7km of SMF, 16.5km of DCF with -1383ps/nm and 41.8km of SMF. The second section has 42.9km SMF, 15.2km DCF with -1387ps/nm and 38km SMF. The SMFs have 0.2dB/km attenuation coefficient and dispersion of 17ps/nm/km at 1550nm. The losses are compensated using two C-band erbium-doped fibre amplifier (EDFA) repeaters in each span. The EDFA denoted A in the figure has a 30dB maximum small signal gain and the EDFA denoted B has a 40dB maximum small signal gain. The noise figure is ~5dB for each EDFA, where no GFF is used here. A tunable band-pass filter with a 1.4nm 3dB bandwidth and an insertion loss of 2.5dB is used in place of the ASE filter to remove the whole accumulative ASE noise outside the signal band including the gain peak at 1530nm. At the receiver, the data signal is pre-amplified and then isolated by a 10GHz clock recovery unit for error detection at the BERT.

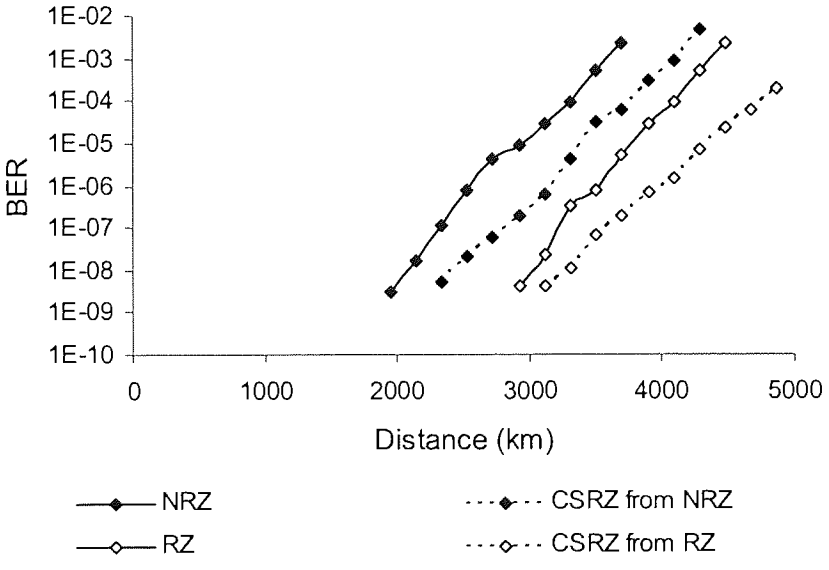

Figure 5.7 BER versus transmission distance for all formats.

Having run the experiment for back-to-back, it was found that the CSRZ always has large penalty compared to the original NRZ/RZ formats, thus worse performance would be expected after transmission. This is basically because the SOA-NOLM deteriorates the quality of the converted signal due to the ASE and other noise introduced by the SOA in addition to some other undesired nonlinear effects, i.e. cross-gain modulation and four-wave mixing, existing in the SOA. These effects all together cause some instability and distortion on the output signal. Therefore, for consistency, the comparisons were all performed with the loop mirror, i.e. all signals pass through the SOA-NOLM thus they have the same environmental condition where any impairment introduced by the loop mirror is common to all measurements. This means that in the case of unconverted NRZ/RZ signal, the signal is passed through the SOA-NOLM, with absence of the control pulse and bias at π, before being transmitted over the fibre in the recirculating loop. The SOA-NOLM switches the input NRZ or RZ signal out without changing its modulation format as explained earlier.

Doing this, the BER performance versus transmission distance for the converted CSRZ signals against their original NRZ/RZ formats can be shown in figure 5.7. Obviously, the SOA-NOLM limits the transmission distance in all formats due to the SOA effects mentioned above. Considering this in addition to the other limiting factors that appear during transmission, i.e. dispersion, noise and self-phase modulation (SPM), the maximum distance achieved with 10^{-9} BER is ~1800km for NRZ and ~2300km for its converted CSRZ, and ~2800km for RZ and ~3000km for its converted CSRZ. This means in other words that the converted CSRZ signal shows less BER for given transmission distance in both cases. Nevertheless, it is still necessary to ensure that the improvement is only caused due to the signal being converted to CSRZ. Note that the OSNR and extinction ratio were nearly equalised for all formats before transmission. The other possible reason for the improvement can be that either the converted or unconverted signal is being chirped somewhere within the loop mirror, while the other signal is not being affected. It also could be that the signals are chirped differently thus they have different performance after transmission. To examine this, the SOA-NOLM output signals have been passed through three lengths of SMF, where the broadening of signal is compared as shown in figure 5.8. The figure shows the results for RZ and its converted CSRZ. In fact, if one signal is positively chirped, it will broaden more rapidly than the other during propagation thus its performance is worse. In contrast, if it is negatively chirped, it will see negative dispersion at the beginning of transmission until its pre-chirp and the dispersion-induced chirp along the fibre cancel each other. This results in that the signal starts broadening later than the un-chirped signal [43] hence better performance

is expected. Figure 5.8 shows similar broadening evolution for the converted CSRZ and unconverted RZ pulse, giving that there is no improvement caused by chirp. The converted CSRZ pulse is shown slightly narrower than its unconverted RZ which has also been seen ealier in figure 5.4.

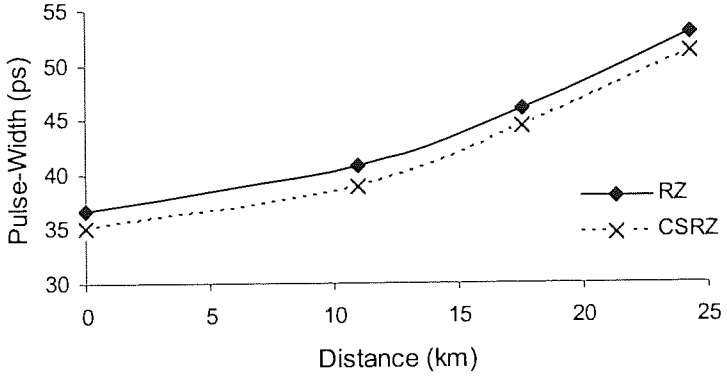

Figure 5.8 Pulse-width versus distance for the RZ and its converted CSRZ after three different fibre lengths: 11km, 17.6km and 24.2km, respectively.

5.3 WDM experiment

5.3.1 Conversion results

This section investigates the feasibility of the SOA-NOLM converter in converting 4×10Gbit/s WDM signals from NRZ/RZ to CSRZ formats. The experimental setup for such investigation is shown in figure 5.9.

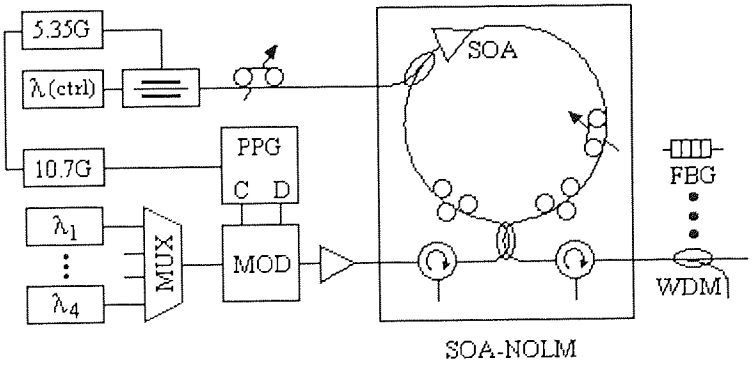

Figure 5.9 Experimental setup for the WDM conversion.

The SOA-NOLM setup is exactly the same as that used for single-channel conversion. The data source has four CW laser sources, starting at 1554.7nm with an even separation of 100GHz. Again, these wavelengths are applied with a $2^{31}-1$ PRBS via one $LiNbO_3$ modulator for the NRZ format, and two $LiNbO_3$ modulators for the RZ format as done for single-channel. The pattern generator is also driven by an external clock reference of 10.7GHz. The resultant 4×10Gbit/s WDM data stream is amplified and launched into the converter. On the output of the SOA-NOLM a WDM coupler, whose characteristics are shown in figure 5.10, is used to extract the 1542.3nm control wavelength whilst allowing the WDM data to propagate along the fibre. It is seen from figure 5.10 that the control signal can be suppressed by approximately 37dB through the WDM coupler while the whole WDM data pass without considerable attenuation.

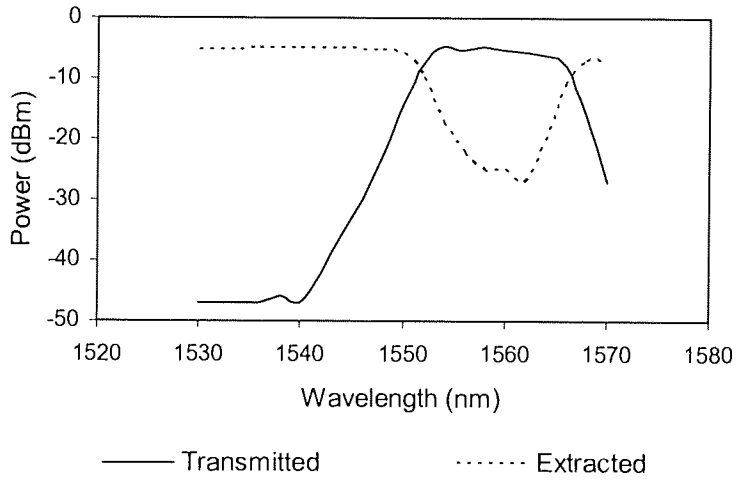

Figure 5.10 WDM coupler spectrum, depicting transmitted and extracted wavelengths.

Figure 5.11 shows the spectra and corresponding eye diagrams for the whole WDM signals before and after conversion in both NRZ and RZ cases. The suppression of the carrier frequency component is clearly shown and the difference between the new main components in the converted CSRZ is 0.08nm (10GHz) in all signals. It can also be seen that the converted signals are slightly broadened and distorted compared to the original signals and that again can be due to the ASE noise and some other undesired nonlinear effects such as cross-gain modulation and FWM exist in the SOA, which are more of consideration in WDM conversion.

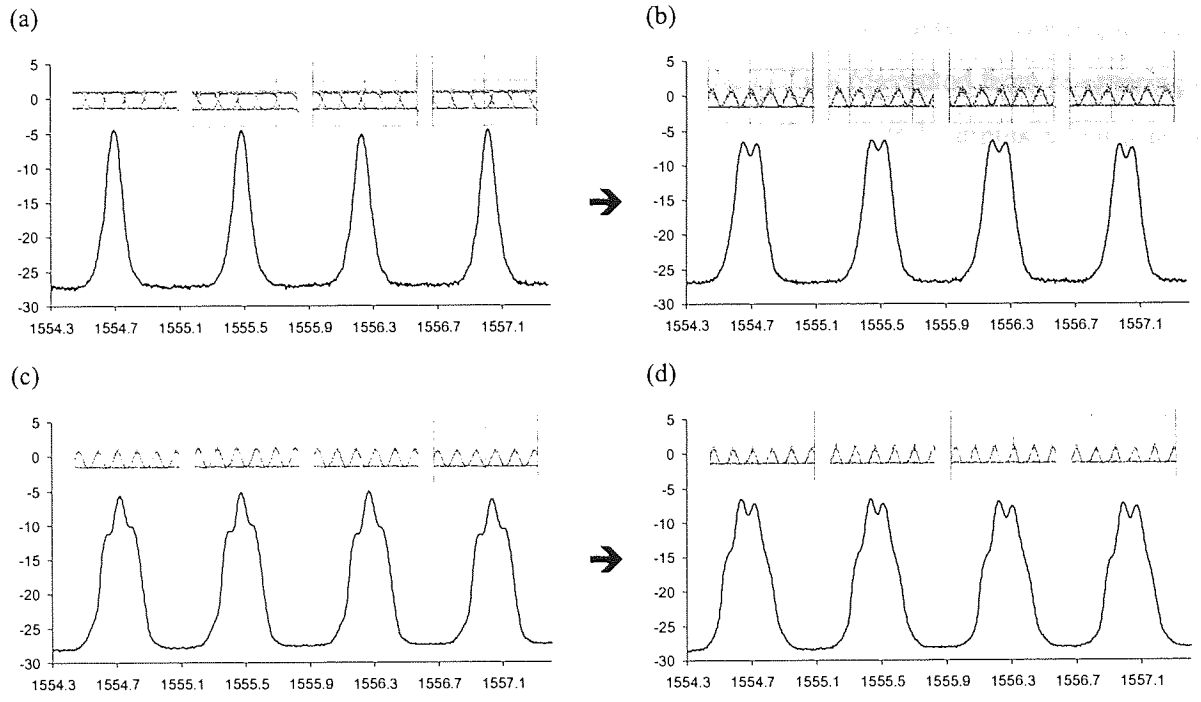

Figure 5.11 Spectra (OSA resolution bandwidth: 0.06nm) and corresponding eye diagrams for WDM signals. (a) NRZ; (b) CSRZ converted from NRZ; (c) RZ; (d) CSRZ converted from RZ.

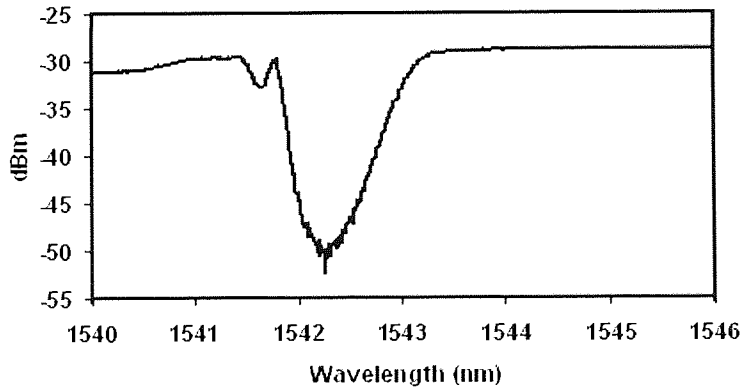

Figure 5.12 Spectrum of the fibre Bragg grating.

Having achieved a conversion for the WDM signals, it is necessary to explore the maximum bandwidth of such converter. This enables determining the maximum number of WDM channels that can be converted via this device without considerable penalty. For this experiment, the WDM coupler was replaced by a fibre Bragg grating (FBG) with 3dB a bandwidth of ~1.1nm and isolation of ~19.8dB as shown in figure 5.12 to reflect the control wavelength at 1542.3nm. The reason for using the FBG is that the transmission bandwidth of the WDM coupler used before is a small fraction of that for the whole C-band wavelength region.

This basically allows some wavelengths to pass through which in turn disables finding the entire conversion bandwidth. Again, the reflected signal from the FBG is prevented from re-entering the SOA-NOLM by the second circulator. Figure 5.13 depicts the spectral outputs taken after the SOA-NOLM for four arbitrary wavelengths spanning the available conversion bandwidth of the converter for RZ to CSRZ conversion.

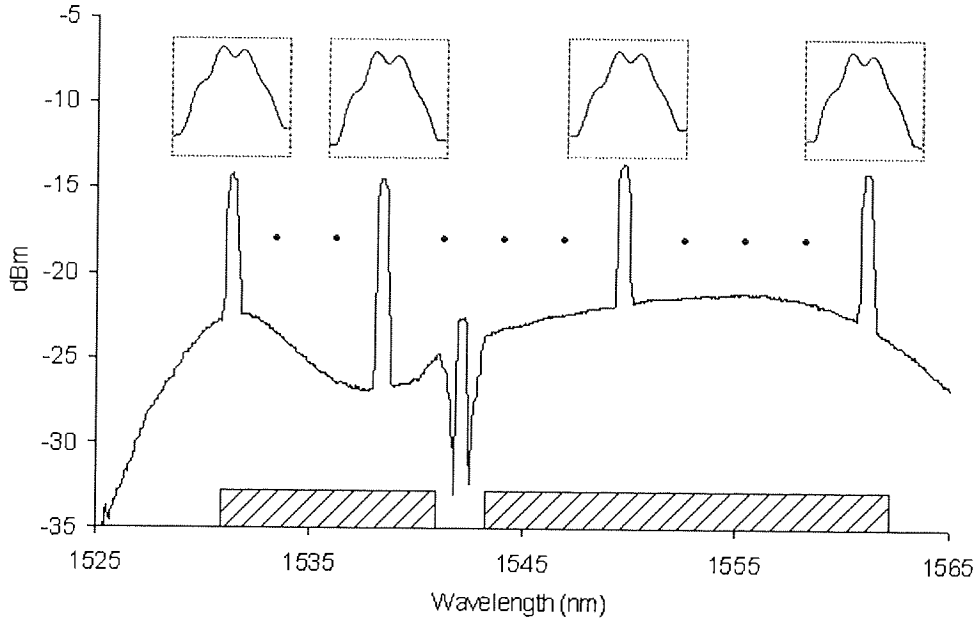

Figure 5.13 The spectral outputs taken after the SOA-NOLM for four arbitrary wavelengths spanning the available conversion bandwidth of the converter for RZ to CSRZ conversion.

The lowest and the highest wavelengths at which the signal is fully converted to CSRZ with BER $\leq 10^{-9}$ are 1531.4 nm and 1562.2 nm, respectively. This means that the signal will be either unconverted fully or converted with considerable error-rate ($>10^{-9}$) outside this region. In fact, this bandwidth is limited by the active region of the SOA as well as the wavelength of the control pulse used to saturate the SOA in the SOA-NOLM. So even with the 19.8dB isolation provided by the fibre Bragg grating, a peak 2dB above the noise floor at 1542.3nm can be clearly seen in the spectrum. This partial suppression of the switching signal reduces the conversion region by approximately 1nm either side of the control signal resulting in a total available bandwidth of 28.8nm (depicted as a lined block in figure 5.13). However, the WDM coupler which was used in place of the fibre FBG earlier can increase the suppression of the control pulse by an additional 17.2dB albeit at the expense of available bandwidth, as the 3dB cut-off for the transmission port on the WDM is at 1551nm. Ideally a device with the suppression performance of the WDM

coupler but with the bandwidth of the fibre Bragg grating could be used to increase the bandwidth of the SOA-NOLM converter by at least 2nm.

5.3.2 Transmission results

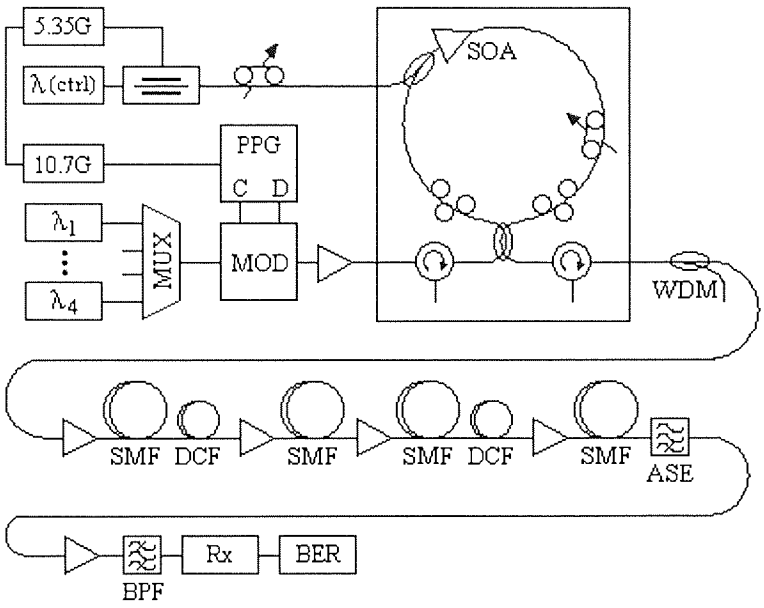

Figure 5.14 Experimental setup for WDM transmission, depicting the SOA-NOLM converter and 194.9km fibre link.

After conversion, the WDM data signals propagate along a 194.9km in-line fibre span as shown in figure 5.14. The fibre span is the same as that used in the recirculating loop for single-channel transmission. It therefore consists of two dispersion-managed sections of SMF-DCF-SMF. All parameters of the fibres and corresponding EDFAs have already been mentioned with single-channel experiment. The main difference to single-channel setup is that there is no recirculating loop, thus no additional components such as AOMs and coupler. This means that the EDFA operating conditions, specifically of the first and the last amplifiers, are different because the system saves approximately 9dB of loss compared to 1-recirculation in the recirculating loop system. The other change is that an ASE filter is used again after the last fibre span in place of the band-pass filter that was locked to the single-channel wavelength. Therefore, the fibre link becomes again similar to that used in the recirculating loop of figure 3.32. At the receiver, the WDM signals are demultiplexed by a tunable band-pass grating filter with a 0.24nm

3dB bandwidth and a 7dB insertion loss. The individual channels are then isolated by a 10GHz clock recovery unit and detected by the BERT.

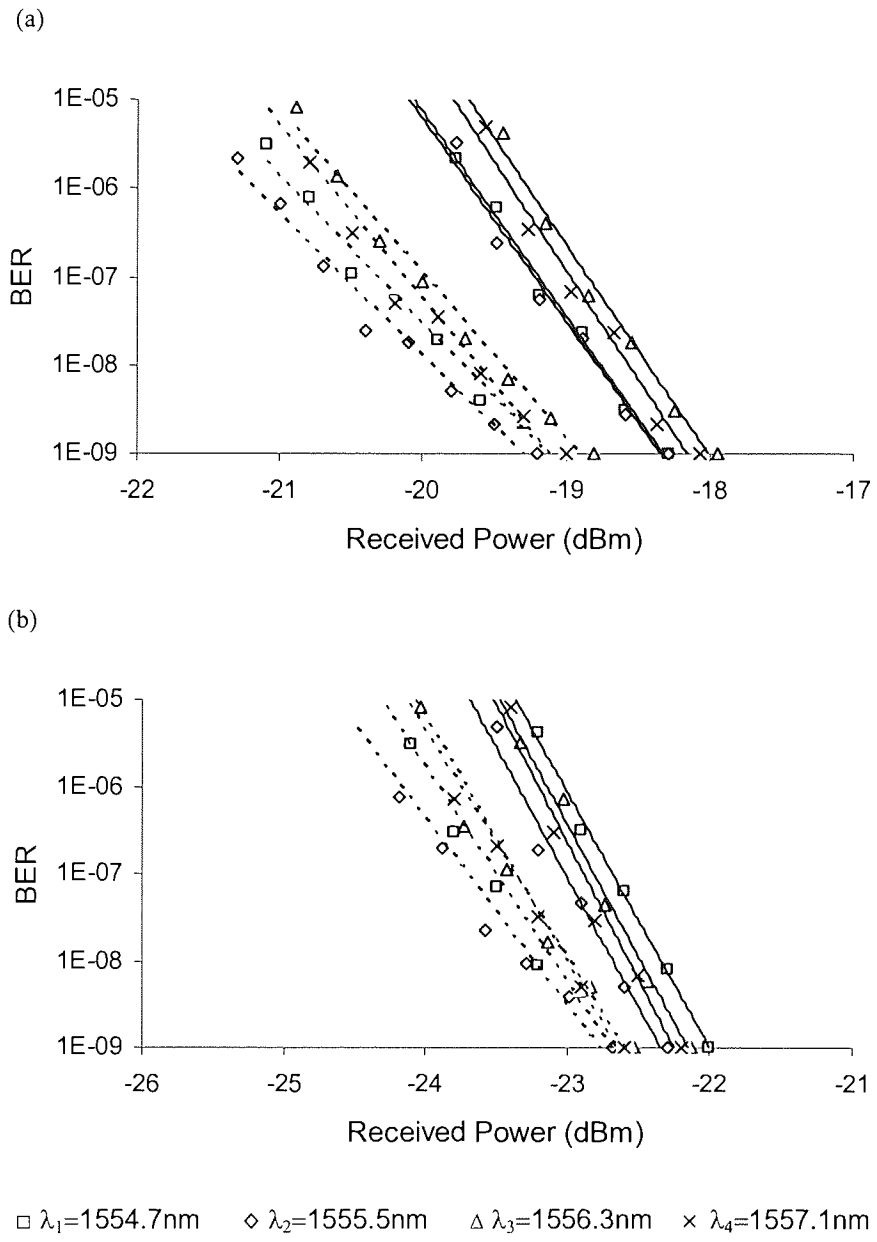

Figure 5.15 BER versus received power after 194.9km transmission for: (a) NRZ (Solid) and its converted CSRZ (Dashed); (b) RZ (Solid) and its converted CSRZ (Dashed).

The experiment uses 4.6dBm per channel, to ensure nonlinear effects during transmission. Figure 5.15 shows the BER performance versus received power after transmission over the 194.9km span for the four WDM channels in both NRZ and its converted CSRZ (top graph), and RZ and its converted CSRZ (bottom graph). Again, the original NRZ and RZ signals are passed

through the SOA-NOLM, without a control pulse and bias at π, before being transmitted over the fibre span. This is to keep the same transmitter impairments in all formats for comparison purpose. As a result, a received power of -17.9dBm per channel is required to achieve a BER of 10^{-9} for the NRZ format, whereas the converted format required a lower power of -18.8dBm to attain the same error-rate. For the RZ case, the received power required for 10^{-9} BER is -22dBm, while for the converted format it is -22.5dBm. The slope of the BER-power curve for both converted carrier-suppressed formats decays slower than that of their original counterparts. Therefore, at a BER of 10^{-5}, the improvement in required received power can increase from 0.9dB to 1.2dB for NRZ case and from 0.5dB to 0.9dB for RZ. This would imply that the receiver sensitivity improvement at 10^{-9} BER could be further increased if forward error correction (FEC) is used to correct errors at 10^{-5} error-rate. However, the larger improvement in the NRZ case was due to the entire change of data format, i.e. NRZ to RZ with the carrier being suppressed. In RZ to CSRZ case, the signal is still return-to-zero after conversion but its carrier was suppressed. This implies that in NRZ case, part of the improvement was attained before transmission just because the NRZ has become CSRZ. In fact, the receiver sensitivities at the output of the SOA-NOLM were measured (by Mohammad Halim Wahid) without transmission for all formats using single-channel at 1555.2 nm. It was found that in the case of NRZ to CSRZ, the received power required for the converted CSRZ for 10^{-9} BER was less than that for the unconverted NRZ by 0.5 dB. In the case of RZ to CSRZ, the converted and unconverted formats had almost the same required power for 10^{-9} BER. This implies that the transmission improved the sensitivity of the CSRZ format by 0.4 dB in the case of NRZ, and 0.5 dB in the case of RZ format.

Although the impairments of the SOA-NOLM converter limits the performance of all formats, the results can still be useful as relative comparisons for the converted and unconverted signals in transmission. Further work must therefore involve optimising the performance of the loop mirror by using better SOA. However, as this particular system configuration presented 194.9km strongly dispersion-managed fibre link with ~40km maximum accumulated dispersion and 100GHz channel spacing; it did not present huge transmission penalties for the formats studied. This can be understood as the majority of the nonlinear contribution comes from self-phase modulation (SPM) of the individual signals. More considerable improvement would be expected if the transmission configuration is modified to demonstrate significant four-wave mixing (FWM) by using lower local dispersion, e.g. DSF, or higher inter-channel crosstalk by using lower channel spacing.

5.4 Summary

This chapter has presented one possible technique that can be used to enhance the performance of the single and WDM transmission system through choosing a suitable modulation format. The chapter has particularly considered the CSRZ format that, in general, is expected to deliver excellent performance due to its high tolerance to nonlinear effects and chromatic dispersion compared to the conventional NRZ and RZ formats. More specifically, the chapter has intended to examine the performance of a CSRZ format after all-optical conversion from NRZ and RZ formats using a semiconductor laser amplifier based nonlinear optical loop mirror (SOA-NOLM). This is because of the recent interest that has been received by the all-optical devices which are considered to be of key importance in future all-optical networks. The chapter started by discussing the main principle of the conversion from NRZ/RZ to CSRZ format using a conventional electro-optic modulator. It then explained the principle of the all-optical format conversion using an SOA-NOLM. After that, the experimental work of this chapter has been presented. It was divided into two parts: single-channel and WDM channels, where both parts have presented conversion and transmission results.

For single-channel, the SOA-NOLM converter setup and conversion results have been shown for a 10Gbit/s signal being converted from both NRZ and RZ to CSRZ. The optimum power range of the input RZ signal for good conversion to CSRZ format has been shown. Then, a transmission results for the converted CSRZ and original NRZ/RZ signals over long distance has been demonstrated using a recirculating loop. The BER performance versus distance for the converted signal was compared with that for the original signals. The comparisons were all performed with the loop mirror in place so that any signal or noise degradation introduced by the SOA-NOLM was common to all measurements. The CSRZ signal has shown superiority to the unconverted signals during transmission using relatively high launch power. The SOA-NOLM has shown no chirp introduced to any input signal that can be the reason for such improvement in one format than the other.

For WDM channels, the SOA-NOLM converter setup and conversion results have been shown for 4×10Gbit/s WDM signals with 100GHz spacing. The optical conversion bandwidth and limitations for the all-optical converter device have also been presented. Then, a transmission results over a 194.9km in-line fibre span for the all-optical converted CSRZ signal and its original NRZ/RZ have been demonstrated. The receiver sensitivity for the converted four wavelengths was compared with the sensitivity for the original NRZ and RZ counterparts. It has been shown that the power required for 10^{-9} BER is less for the converted CSRZ format in all

signals. More significant improvement should be expected if the system uses fibres with low local dispersion, or less channel spacing so more inter-channel interaction is induced.

In general, the SOA-NOLM converter limits the performance of all formats in both single and WDM experiments, but the results can still be used to show relative performance for the converted and unconverted signals in transmission. This would imply that further work must be performed on optimising the performance of the loop mirror by using better characteristics in the SOA. Having achieved an all-optical converter with the same quality of the normal electro-optic converters (which has never been shown in any all-optical application due to the instability problem), the WDM networks can replace the existing electro-optic converters with the all-optical ones so the networks can save a lot of electronics hence become more cost-effective.

Chapter 6

Conclusions and future work

This thesis has investigated WDM communication systems as applied to legacy communication links. The research has presented a development of line monitoring technique that can be used to monitor the WDM communication link. It has also compared different techniques involving: transmitter designs, bit patterning and modulation formats. All these studies can be used for upgrading the legacy optical fibre communication systems that now exist.

The first chapter has given an introduction to optical fibre communications presenting the main features of using optical fibres in the systems. It has also discussed the main system components which involved the design of the transmitter, fibre link and receiver. The chapter has then presented the main problems that limit the performance of the optical fibre communication system and their solutions. The problems involved the fibre loss, dispersion, nonlinear effects (that arise at high launch power) and birefringence. The solutions included discussions about optical amplifiers (particularly EDFAs) that compensate for the fibre losses, and dispersion-compensating fibres (DCFs) that compensate for the dispersion of single-mode fibres (SMFs).

The second chapter has demonstrated the basic experimental techniques that can be used in laboratories to simulate the real optical fibre communication systems. It included the main principles of generating and detecting different optical data signals involving single-channel, WDM and OTDM signals. Results of generating 10Gbit/s data using single and WDM channels have been presented as well as 40Gbit/s data using OTDM. After that, the main principles of designing and operating the recirculating loop which is used to simulate long-haul optical transmission link have been presented. This has included the main design issues such as power and dispersion management of the loop. All measurements techniques that are used for characterising the performance of the recirculating loop system have been demonstrated. Experimental results for dispersion, Q-value and OSNR measurements have been presented.

The first experimental investigation of this thesis has demonstrated a line monitoring equipment (LME) that can be suitable for monitoring the optically amplified long-haul undersea systems. The technique is based on setting up a simple, passive, low cost high-loss optical loopback circuit after each amplifier. This loopback circuit provides a connection between the existing two undersea fibres and can be used to find fault location. Fault location is defined by transmitting a low power supervisory signal (referred to as LME signal) along with the WDM data signals where a portion of the overall light is attenuated and returned to the transmit terminal

by the loopback circuit. An LME receiver extracts the weakly returned LME signal and analyse it. An oscilloscope can show different LME pulses corresponding to different optical amplifiers, where the degradation in any amplifier will be observed on its corresponding LME signal. The chapter started by comparing the proposed high-loss loopback LME system with other line monitoring techniques, specifically the OTDR. It has said that the OTDR method is relatively expensive as it is based on optical coherent detection rather than electrical coherent detection. It also tends to be used out-of-service in the case of a fibre break because it requires high optical power levels which can badly affect the in-service signals performance. The proposed LME technique therefore has low cost as well as it can be performed in-service and out-of-service. The chapter has then presented two different approaches for the proposed high-loss loopback LME system. The first approach uses an in-band LME signal where the supervisory signal is a modulated signal that is superimposed by the data traffic signals, and the second approach uses an out-of-band LME signal, where the supervisory signal has its own wavelength. The LME experiment has employed the out-of-band LME signal and the system can be referred to as "out-of-band LME system" or "pulsed LME system". The performance analysis of this LME system, including OSNR and measurement time of the received LME signal, has been presented. It has been found that the measurement time for the out-of-band LME signal is reduced from an order of 3 hours as in the in-band LME signal to 1 minute. The system prototype for the out-of-band LME has been demonstrated, including the architecture of the LME transmitter and receiver as well as the basic setup of the high-loss loopback circuit that connects between forward and backward paths. The forward path used a recirculating loop for long-haul transmission while the backward path used only noise source and backward data traffic. This of course allowed examining the LME over single direction through the forward path. The whole LME experimental setup based on such prototype has then been demonstrated using two WDM data signals plus the LME signal in the forward path, and two similar WDM data signals in the backward path. The forward and backward data signals had different wavelengths where the separation between the adjacent signals including the LME was 1nm. The forward direction recirculating loop had 200km dispersion-managed fibre spans using SMF-DCF configuration. The experiment started by measuring the performance of the recirculating loop including dispersion and OSNR. It was found that the dispersion of the loop was not fully managed where it had a total dispersion of 0.5ps/nm/km at 1550nm. Nevertheless, this loop setup was still usable for the first experimental part which was designated to test the feasibility of the proposed LME receiver in recovering the LME signal after 45dB loopback attenuation and after long

transmission distance. This decision was based on that the LME pulse was wide enough (500μs) so that the dispersion effect can be negligible. The experiment had low LME power at the start so the receiver was able to detect the LME signal after 36dB loopback attenuation at most. The LME power was increased until the receiver became able to recover the LME signal after the aimed 45dB loopback attenuation. The effect of the optical notch filter bandwidth to the LME performance has also been presented, showing that the narrower the bandwidth; the more loopback attenuation can be used. The recovered LME signal has been analysed through the electrical signal-to-noise ratio (eSNR) measurements. The chapter has then shown a study of the effect of the LME signal to the co-propagating data traffic signals. For this investigation, the recirculating loop had further dispersion management such that the overall dispersion became around 0ps/nm/km in the operating wavelength region. Moreover, the performance of the loop was further improved by changing the loop configuration from periodic dispersion map to symmetric dispersion map thus an additional SPM effect has been avoided. As a result, it was shown that the LME signal would have no considerable effect to the adjacent data signals even when its power becomes comparable to the data signals power. The opposite effect has also been studied i.e. the effect of the data signals to the co-propagating LME signal. It was found that a considerable degradation in the LME eSNR would appear if the spacing between the LME signal and its adjacent signals is less than 0.6nm, although the LME signal was still being detected until 0.4nm spacing. The last investigation for the LME has involved studying the effect of the receiver averaging to the eSNR performance of the LME signal. A gain-flattening filter (GFF) has been added to the recirculating loop at the time of this stage so the system performance has been further improved. This part has proven that the performance of the LME signal improves linearly as the number of the receiver averages increases. This enabled a recovery of the LME signal after ~5400km distance and ~45dB attenuation in the loopback circuit while the LME signal was lower than the WDM data signals by ~10dB. Future work on the LME can involve examining the LME performance over a full dual-path system by setting two symmetric recirculating loops as shown in figure 6.1. This will require that the two loops are triggered by single digital delay generator, so that both paths have the same distance at one experimental run. This will of course increase the similarity between the experiment and the real system where the LME can be tested on each path individually. Having provided two LME sets, i.e. LME transmitter and receiver, the system can monitor both directions simultaneously where one LME signal will be transmitted over each path. Furthermore, the LME experiment can be performed

using larger number of WDM data traffic signals, e.g. 5×10Gbit/s WDM signal or more, so the experiment simulates systems of larger capacity.

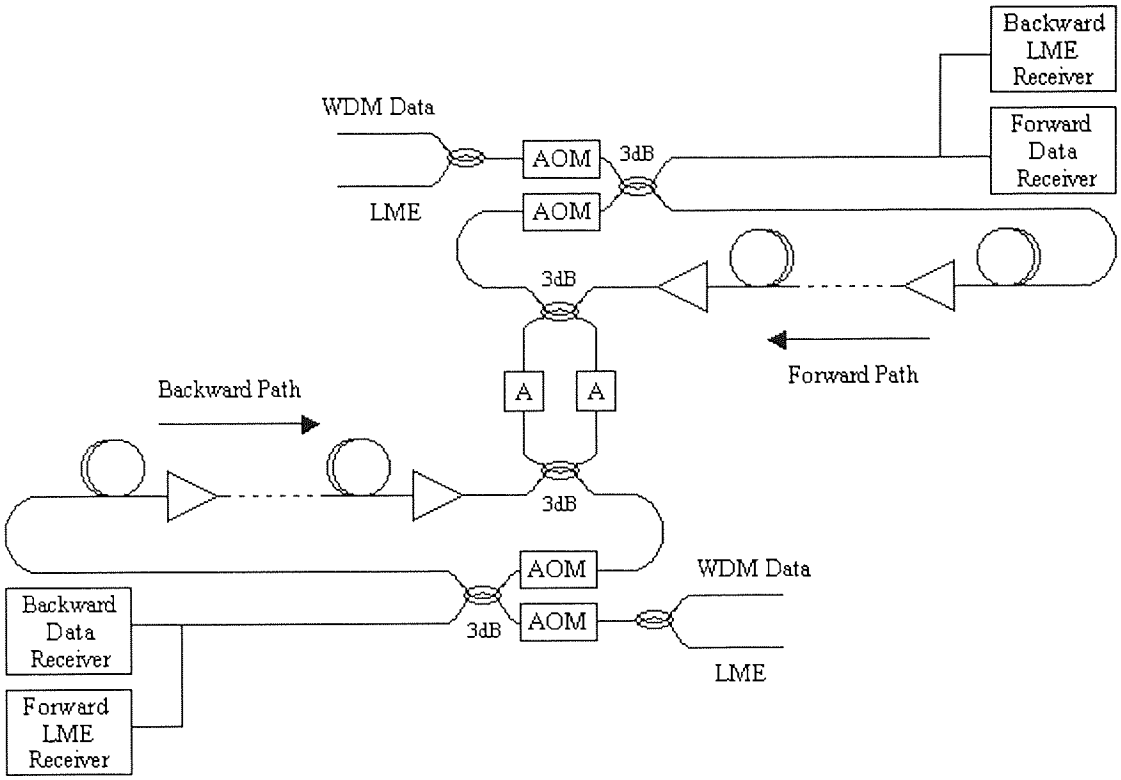

Figure 6.1 Dual-path LME system.

Chapter 4 has investigated a patterning effect, specifically by changing the number of the 1s and 0s in random data, to the performance of a WDM communication system. This study was based on one concept of the information theory which says that the probability of errors in the 1 and 0 bits is different for linear and nonlinear optical transmission systems. In linear system, if the noise is additive at the receiver the probability of errors in the 1 and 0 bits is almost the same. This gives that the ideal proportion of the 1s and 0s in linear transmission can be 50%, which is indeed good selection as it represent the maximum possible information transmitted and simplifies the receiver design. In practice, the probability of errors in the 1 is larger than that of the 0 during transmission due to a larger ASE contribution on the 1, which is known as signal-spontaneous beat noise. This means that 50% is not necessarily the best selection for linear transmission if the difference in the probabilities is too large. In nonlinear system, the 1-bits have much larger probability of errors due to nonlinear interaction while the noise effect is negligible, giving that 50% (theoretically) cannot be ideal for nonlinear transmission. For instance, if the

number of 1s increases at the transmitter, the pulse energy at the input to fibre spans will decrease because the amplifiers' output power is constant. This will reduce the nonlinear impairments during transmission thus the system performance improves. In contrast, if the number of 1s decreases, opposite results would be expected as the pulse energy will increase i.e. more nonlinearities will be introduced. However, forward error correction (FEC) technique has been given as an example for the applications that can use this study. In FEC, additional information are transmitted along with the original data which can be used at the receiver to correct errors occurred during transmission. Therefore, if the input data to the FEC encoder was balanced i.e. had approximately 50% 1s, the extra bits would increase the bit-rate of the data and unbalance fraction of the 1s and 0s. This is usually solved by adding a digital scrambler which re-balances the data back to 50% before transmission. This can be useful for systems operating near the linear regime and there is no strong difference in the noise contribution between the 1s and 0s. The main investigation was therefore performed to prove that such additional scrambler would not be required if the system operates in the nonlinear regime in case that the output of the FEC encoder has more than 50% of 1s. The experiment of this chapter has actually been split into two parts; linear and nonlinear experiments. For linear experiment, the objective was to show if the 50% fraction is the ideal selection or considerable improvement can be attained with different fractions of 1s and 0s due to different error probabilities. Both linear and nonlinear experiments used 5×10Gbit/s WDM signals propagating through SMFs and DCFs in a recirculating loop. The linear experiment used 52km recirculating loop, including SMFs and DCFs, with sufficiently low launch power to ensure linear operation. The OSNR and Q-value performance of the loop have been presented for 50% 1s. Then, this performance has been compared with that for highly unbalanced data, i.e. 25% and 75, where the results have shown little change in the system performance. Since the unbalancing in FEC coding is much smaller than the fractions presented, no considerable effect would be expected in the overall system performance. Again, the above results were all assuming constant power over the fibre link. Therefore, for comparison, experimental results have been presented if the pulse energy was kept constant, i.e. the total average power was larger for more 1s and smaller for more 0s. The results have shown better performance for more 1s due to an improvement in the OSNR hence Q-value, and worse performance for less 1s due to a degradation in the OSNR. For nonlinear experiment, the loop used 194.9km recirculating loop, using SMFs and DCFs as well. The optimum power has been measured to define the nonlinear power region. The OSNR and BER performance of the system have been presented for 50% 1s with the optimum power. The launch power was then increased

by 3dB to ensure high nonlinearities during transmission. The performance has been shown for 50%, 25% and 75% 1s using constant power into the loop fibres. The results have shown considerable improvement for more 1s due to the decrease in the pulse energy hence less nonlinear interaction, and considerable degradation for more 0s due to the increase in the pulse energy hence more nonlinear interaction. Because of that, the experiment was run with small changes of the fraction, e.g. 47%, 53%, to simulate the FEC coding effect. It has been shown that the performance improved almost linearly with more 1s and degraded with more 0s. This was due to an increase and decrease in the nonlinear interaction, respectively. It has been shown that the signals had distortion and spectral broadening with less 1s i.e. higher pulse energy. The majority of this nonlinear effect can be from SPM because the system used high local dispersion fibres and large channel spacing, thus the XPM and FWM contribution can be negligible. As a result, the above results can be used in FEC encoders that adds more 1s to the data, thus the additional scrambler can be saved if the system is using high power. This is basically because the more 1s in the transmitted data; the better performance, thus there is no need for re-balancing the data back to 50%. If the encoder adds more 0s, the data can be inversed for transmission and then re-inversed back to the original bit stream at the receiver, thus the scrambler is also saved. Again, for comparison purpose, the transmission results have been shown where the pulse energy was fixed at the input to the fibres. The performance has improved as the fraction increases until 65%. Although the OSNR keeps increasing, the large fractions had interaction between the pulses because they had more successive 1s in the data. Future work on this chapter can involve using fibres with low local dispersion, e.g. DSF, or less channel spacing (as applied to DWDM systems) to allow more inter-channel interaction such as FWM. In this case, the above patterning effect would be more considerable. Furthermore, the same work can be performed with using more bit-rates i.e. 40Gbit/s data. Other patterning effects can also be examined such as using specific data patterns rather than random data. An example of this has already been shown in [99] where the data has used different triplets i.e. 101, 110, 001. Experimental results of this would be expected to show different performance for different triplets due to inter-symbol interference (ISI) and nonlinear effects. For example, the pattern 101 would, in principle, have larger error contribution to the 0-bits due to the overlap between the 1s during transmission. This effect will be significant if the system uses high bit-rate such as 40Gbit/s or more.

Chapter 5 has presented single and WDM transmission results after all-optical format conversion between NRZ and RZ to CSRZ using semiconductor optical amplifier in nonlinear optical loop mirror (SOA-NOLM). The reason for using CSRZ format was that the signal can be

more tolerant to nonlinear effects and chromatic dispersion than the conventional NRZ and RZ signals. This is basically because the main frequency component is suppressed thus the power is reduced into the fibre which in turn reduces nonlinearities during transmission. Chromatic dispersion can be avoided where the CSRZ has narrower spectrum than that of the NRZ and RZ formats. This of course increases the spectral efficiency of the transmission along the fibre. The chapter has particularly considered all-optical converter due to the recent attention that has been given to the all-optical devices that will be the fundamental components for the future all-optical networks. The main principle of the NRZ and RZ format conversion to CSRZ has been discussed based on the conventional electro-optic $LiNbO_3$ MZ modulator. Then the principle for the same conversion using all-optical converter i.e. SOA-NOLM has been shown. The experiment of this chapter has firstly demonstrated the all-optical conversion results for single-channel using 10Gbit/s PRBS data with 2^{31}-1 length. The dynamic range of the input RZ signal for RZ to CSRZ format conversion with BER $\leq 10^{-9}$ has been defined. The transmission results for the converted CSRZ and its original NRZ/RZ signals over long distance have then been presented using 194.9km dispersion managed fibre in a recirculating loop. Since the converted signal had large penalty due to the SOA-NOLM impairments such as ASE noise of the SOA and some other factors, all signals were allowed to pass through the NOLM before being transmitted around the loop. This was in order to ensure the same environment for all measurements. Having considered this, the BER performance versus propagation distance for the converted CSRZ signal has been compared with that for the original NRZ/RZ signals, using relatively high launch power in all formats. The CSRZ signals have been able to propagate for further distance with acceptable error-rate compared to the unconverted signals. This can be realised as a more tolerance to nonlinear effects induced by the signal itself through SPM where the system used single-channel. It has been shown that the converted and unconverted signals passed through the NOLM had similar broadening behaviour, giving that there was no chirp introduced to one format which could have been the reason for improvement. The WDM experiment has then been demonstrated using 4×10Gbit/s signals with an even separation of 100GHz. The SOA-NOLM converter has shown ability to convert the whole WDM signals with acceptable performance, i.e. BER $\leq 10^{-9}$. The converter has also shown good conversion over wide-band, i.e. ~29nm. This optical bandwidth for the converter was mainly limited by the SOA active region. It was also limited by additional 2dBs around the control wavelength due to incomplete removal of the control signal by the available fibre Bragg grating. The transmission results for the whole WDM signals have been demonstrated through BER versus received power after a 194.9km distance. The receiver

sensitivity for the converted four wavelengths was therefore compared with the sensitivity of the original NRZ and RZ signals. It has been shown that the CSRZ had sensitivity improvement of about 0.9dB if converted from NRZ, and 0.5 if converted from RZ format. Future work on this part must therefore involve minimising the penalty of the converter so that the output CSRZ can be compared with NRZ/RZ signals generated directly from the source rather than switched out of the loop mirror. This can be achieved by using an SOA with better characteristics, hence more stability on the output signal. Furthermore, for more significant evaluation of the converter performance, the same experiment must be performed using fibres with low local dispersion and small channel spacing, so that more significant nonlinear interactions, e.g. FWM, can be demonstrated. Moreover, the different formats of the WDM signals can be examined over long distance through a recirculating loop as done for single-channel. This was disabled in this chapter due to the high instability caused by the ASE noise and the nonlinear effects in the SOA such as cross-gain modulation and FWM, which were much more considerable in WDM operation.

As an overall conclusion, the performance of legacy WDM communication systems can be enhanced using different techniques such as the techniques discussed in this thesis. These techniques are mainly based on changing the transmitter design or transmitted signals parameters, but nothing to do with the legacy transmission link itself. This was clearly seen in chapters 4 and 5 while changing the patterns and modulation formats of the transmitted data. It was also seen in the LME work, where a supervisory transmitter/receiver were set up at the original WDM transmit terminal. Although the LME requires a high-loss loopback circuit being set up at every repeater of the transmission link, it should not change the fundamental configuration of the legacy fibre link. In addition, since the loopback circuits have passive components, they are expected to last for very long time assuming good protection. This implies that no more installation is required after the initial set up unless in the event of fault where instant upgrading is required. Other techniques can be used to upgrade legacy systems using the same principle (i.e. changes are only made at the terminals) such as using different filters at the transmitter or receiver.

In principle, the techniques discussed here can all be mixed up for further improving the legacy system. For instance, the transmitter can employ FEC technique using the advantage of the patterning effect discussed here as well as a CSRZ modulation format for more nonlinearity/dispersion tolerance. Line monitoring can also be used in association with the other techniques so that the system is being provided with continuous monitoring during operation. However, using all-optical CSRZ generation can be employed only if the all-optical device is

perfectly stable, which has not been achieved here nor elsewhere. This gives that the legacy systems cannot employ such a device but can sill use electro-optic modulators for generating CSRZ signal or any other suitable format. This in fact can apply to the other all-optical processing such as demultiplexing or signal regeneration where the conventional electro-optic devices can still be used. However, other modulation formats such as CRZ or duobinary can also be used in upgrading legacy WDM systems depending on the system parameters such as system length, fibre type and capacity.

References

[1] S. Yoshida, S. Kuwano, M. Yamada, T. Kanamori, N. Takachio, and K. Iwashita, "10 Gbit/s×10 channel transmission experiment over 600 km with 100 km repeater spacing employing cascaded fluoride-based erbium doped fibre amplifiers". *Electronics Letters*, **31**, 1678-1679 (1995).

[2] S. Aisawa, N. Takachio, and K. Iwashita, "A 10 Gb/s 8 channel transmission experiment over 480 km with 120 km repeater spacing using frequency modulated RZ pulse format". *Optical Communication (ECOC '96)- 22nd European Conference*, **2**, 137-140 (1996).

[3] Y. Miyamoto, A. Hirano, K.Yonenaga, A.Sano, H.Toba, K. Murata, and O. Mitomi, "320 Gbit/s (8×40 Gbit/s) WDM transmission over 367 km with 120 km repeater spacing using carrier-suppressed return-to-zero format". *Electronics Letters*, **35**, 2041-2042 (1999).

[4] T. Miyakawa, N. Edagawa, and M.Suzuki, "210 Gbit/s (10.7 Gbit/s×21 WDM) transmission over 1200 km with 200 km repeater spacing for the festoon undersea cable system". *Optical Fibre Communication Conference (OFC 2000)*, **4**, 44-46 (2000).

[5] I. P. Kaminow, T. Li, *Optical fibre telecommunications IVB: systems and impairments*, Academic Press, San Diego, London, 2002.

[6] T. E. Stern, and K. Bala, *Multiwavelength optical networks*, Addison Wesley, Reading, MA, 1999.

[7] K. M. Sevalingam, and S. Subramaniam, Eds., *Optical WDM networks: principles and practice*, Kluwer Academic, Norwell, MA, 2000.

[8] M. T. Fatehi, and M. Wilson, *Optical networking with WDM*, McGraw-Hill, New York, 2001.

[9] A. D. Ellis, D. M. Patrick, D. Flannery, R. J. Manning, D. A. O. Davies, and D. M. Spirit, "Ultra-high-speed OTDM networks using semiconductor amplifier-based processing nodes". *Journal of Lightwave Technology*, **13**, 761-770 (1995).

[10] V. W. S. Chan, K. L. Hall, E. Modiano, and K. A. Rauschenbach, "Architectures and technologies for high-speed optical data networks". *Journal of Lightwave Technology*, **16**, 2146-2168 (1998).

[11] J. Gower, *Optical communication systems*, 2nd ed., Prentice-Hall, Upper Saddle River, NJ, 1993.

[12] G. P. Agrawal, Ed., *Semiconductor lasers: past, present, and future*, AIP Press, Woodbury, NY, 1995.

[13] W. Franz, *Z. Naturforschung*, **13A**, 484-489 (1958).

[14] A. B. Miller, D. S. Chemia, T. C. Damen, A. C. Gossard, W. Wiegmann, T. H. Wood, and C. A. Burrus, "Band-edge electroabsorption in quantum well structures: the quantum-confined Stark effect". *Physical Review Letters*, **53**, 2173-2176 (1984).

[15] M. Aoki, M. Suzuki, H. Sano, T. Kawano, T. Ido, T. Taniwatari, K. Uomi, and A. Takai, "InGaAs/InGaAsP MQW electroabsorption modulator integrated with a DFB laser fabricated by band-gap energy control selective area MOCVD". *IEEE Journal of Quantum Electronics*, **29**, 2088-2096 (1993).

[16] J. E. Cunningham "Recent developments and applications in electroabsorption semiconductor modulators". *Materials Science and Engineering*, **25**, 155-194 (1999).

[17] S. Kaneko, M. Noda, Y. Miyazaki, H. Watanabe, K. Kasahara, and T. Tajime, "An electroabsorption modulator module for digital and analog applications". *Journal of Lightwave Technology*, **17**, 669-676 (1999).

[18] Y. Kim, S. K. Kim, J. Lee, Y. Kim, J. Kang, W. Choi, and J. Jeong, "Characteristics of 10Gb/s electroabsorption modulator integrated distributed feedback lasers for long-haul optical transmission systems". *Optical Fibre Technology*, **7**, 84-100 (2001).

[19] H. Fukano, T. Yamanaka, M. Tamura, Y. Kondo, and T. Saitoh, "Very low driving-voltage InGaAlAs/InAlAs electroabsorption modulators operating at 40Gbit/s".*Electronics Letters*, **41**, 211-212 (2005).

[20] L. Thylen, "Integrated optics in $LiNbO_3$: recent developments in devices for telecommunications". *Journal of Lightwave Technology*, **6**, 847-861 (1988).

[21] K. Noguchi, H. Miyazawa, and O. Mitomi, "75 GHz broadband Ti:$LiNbO_3$ optical modulator with ridge structure". *Electronis Letters*, **30**, 949-951 (1994).

[22] K. Noguchi, O. Mitomi, and H. Miyazawa, "Millimeter-wave Ti:$LiNbO_3$ optical modulators". *Journal of Lightwave Technology*, **16**, 615-619 (1998).

[23] M. M. Howerton, R. P. Moeller, A. S. Greenblatt, and R. Krähenbühl, "Fully packaged, broad-band $LiNbO_3$ modulator with low drive voltage". *IEEE Photonics Technology Letters*, **12**, 792-794 (2000).

[24] G. L. Li, and P. K. L. Yu, "Optical intensity modulators for digital and analogue applications". *Journal of Lightwave Technology*, **21**, 2010-2030 (2003).

[25] E. L. Wooten, K. M. Kissa, A. Yi-Yan, E. J. Murphy, D. A. Lafaw, P. F. Hallemeier, D. Maack, D. V. Attanasio, D. J. Fritz, G. J. McBrien, and D. E. Bossi, "A review of lithium niobate modulators for fibre-optic communications systems". *IEEE Journal of Selected Topics in Quantum Electronics*, **6**, 69-82 (2000).

[26] T. Matsuda, A. Naka, and S. Saito, "Comparison between NRZ and RZ signal formats for in-line amplifier transmission in the zero-dispersion regime". *Journal of Lightwave Technology*, **16**, 340-348 (1998)

[27] C. Caspar, H.-M. Foisel, A. Gladisch, N. Hanik, F. Kuppers, R. Ludwig, A. Mattheus, W. Pieper, B. Strebel, and H. G. Weber, "RZ versus NRZ modulation format for dispersion compensated SMF-based 10Gb/s transmission with more than 100km amplifier spacing". *IEEE Photonics Technology Letters*, **11**, 481-483 (1999)

[28] R. Ludwig, U. Fieste, E. Dietrich, H. G. Weber, D. Breuer, M. Martin, and F. Kuppers, "Experimental comparison of 40Gbit/s RZ and NRZ transmission over standard singlemode fibre". *Electronics Letters,* **35**, 2216-2218 (1999).

[29] M. Nakazawa, H. Kubata, K. Suzuki, E. Yamada, and A. Sahara, "Ultrahigh-speed long-distance TDM and WDM soliton transmission technologies". *IEEE Journal of Selected Topics in Quantum Electronics*, **6**, 363-396 (2000).

[30] O. V. Sinkin, J. Zweck, and C. R. Menyuk, "A comparative study of pulse interactions in optical fibre transmission systems with different modulation formats". *Conference of Lasers and Electro-Optics Society (LEOS 2001)*, **1**, 216-217 (2001).

[31] L. W. Couch, *Modern communication systems: principles and applications*, 4th ed., Prentice Hall, Upper Saddle River, NJ, 1995.

[32] A. Hodžic´, B. Konrad, and K. Petermann, "Alternative modulation formats in N X 40Gb/s WDM standard fibre RZ-transmission systems". *Journal of Lightwave Technology*, **20**, 598-607 (2002).

[33] L. N. Binh, and Z. Csematony, "Double-sideband carrier suppressed RZ and NRZ modulation formats for ultra-high capacity 40Gb/s optical communications systems". *Technical Report* (*MECSE*-23-2003), *Monash University, Australia*, 2003.
http://www.ds.eng.monash.edu.au/techrep/reports/2003/MECSE-23-2003.pdf.

[34] H. Kim, and C. Yu, "Optical duobinary transmission system featuring improved receiver sensitivity and reduced optical bandwidth". *IEEE Photonics Technology Letters*, **14**, 1205-1207 (2002).

[35] G. Bosco, A. Carena, Member, V. Curri, R. Gaudino, and P. Poggiolini, "Modulation formats suitable for ultrahigh spectral efficient WDM systems". *IEEE Journal of Selected Topics in Quantum Electronics*, **10**, 321-328 (2004).

[36] X. Gu, and L. C. Blank, "10 Gbit/s unrepeatered three-level optical transmission over 100km of standard fibre". *Electronics Letters*, **29**, 2209-2211 (1993).

[37] W. Kaiser, T. Wouth, M. Wichers and W. Rosenkranz, "A simple system upgrade from binary to duobinary". *National Fibre Optic Engineers Conference (NFOEC)*, Proc. pp1043-1050 (2001).

[38] G. Katsaros, P. M. Lane, M. Murphy, M. Green, and P. Jiang "Experimental demonstration of the reduction of FWM with duobinary modulation". *European Conference on Optical Communication (ECOC 99)*, (1999).

[39] M. born, and E. Wolf, *Principles of optics*, 7th ed., Cambridge University Press, New York, 1999.

[40] G. E. Keiser, *Optical fibre communications*, 3rd ed., McGraw-Hill, New York, 2000.

[41] M. Cvijetic, *Optical transmission systems engineering*, Artech House, London, 2003

[42] R. Tricker, *Optoelectronics and fibre optic technology*, Newnes, Oxford, 2002

[43] G. P. Agrawal, *Fibre-optic communication systems*, 3rd ed., Wiley, New York, 2001.

[44] A. M. Vengsarkar, "Dispersion compensating fibres". *Optical Fibre Communication Conference and Exhibit (OFC 97)*, Proc. pp233-234 (1997).

[45] S. N. Knudsen, "Design and manufacture of dispersion compensating fibres and their performance in systems". *Optical Fibre Communication Conference and Exhibit (OFC 2002)*, Proc. pp330-332 (2002).

[46] I. C. Goyal, A. K. Ghatak, and R. K. Varshney, "Dispersion compensating fibres". *Transparent Optical Networks Conference 2002*, **1**, 20-23 (2002).

[47] L. G. Nielsen, S. N. Knudsen, B. Edvold, T. Veng, D. Magnussen, C. C. Larsen, and H. Damsgaard, "Dispersion compensating fibres". *Optical Fibre Technology*, **6**, 164-180 (2000).

[48] G. P. Agrawal, *Nonlinear fibre optics*, 3rd ed., San Diego, Harcourt, 2001.

[49] R. W. Boyd, *Nonlinear optics*, Academic Press, San Diego, CA, 1992.

[50] A. R. Charplyvy, D. Marcuse, and P. S. Henry, "Carrier-induced phase noise in angle-modulated optical-fibre systems". *Journal of Lightwave Technology*, **2**, 6-10 (1984).

[51] C. DeCusatis, *Fibre optic data communication: technology advances and futures*, Academic Press, San Diego, CA, 2002.

[52] S. Tsuda, A. J. Lucero, and V. L. da Silva, "DWDM transmission in high capacity optical systems using large effective area NZ-DSF LEAF fibre". *Microwave and Optoelectronics Conference (IMOC 99)*, **1**, 73-74 (1999).

[53] A. Ghatak, K. Thyagaajan, *Introduction to fibre optics*, Cambridge University Press, Cambridge, 1998.

[54] P. C. Becker, N. A. Olsson, and J. R. Simpson, *Erbium-doped fibre amplifiers: fundamentals and technology*, Academic Press, San Diego, London, 1999.

[55] E. Desurvire, *Erbium-doped fibre amplifiers: principles and applications*, Wiley, New York, 2002.

[56] T. Naito, N. Shimojoh, T. Tanaka, H. Nakamoto, M. Doi, T. Ueki, M. Suyama, "1 Tbit/s WDM transmission over 10000 km". *European Conference on Optical Communications (ECOC 99)*, post-deadline paper PD2-1 (1999).

[57] O. Gautheron, and M. Suyama "Submarine cable networks". *Optical telecommunications*, **4**, 115-126 (2003).

[58] Y. Matsui, H. Murai, S. Arahira, S. Kutsuzawa, and Y. Ogawa, "30GHz bandwidth 1.55μm strained-compensated InGaAlAs-InGaAsP MQW laser," *IEEE Photonics Technology Letters*, **9**, 25-27 (1997).

[59] O. Kjebon, R. Schatz, S. Lourdudoss, S. Nilsson, B. Stalnacke, and L. Backbom, "30GHz direct modulation bandwidth in detuned loaded In-GaAsP DBR lasers at 1.55μm wavelength". *Electronics Letters*, **33**, 488-489 (1997).

[60] M. Aoki, M. Suzuki, H. Sano, T. Kawano, T. Ido, T. Taniwatari, K. Uomi, and A. Takai, "InGaAs/InGaAsP MQW electroabsorption modulator integrated with a DFB laser fabricated by band-gap energy control selective area MOCVD". *IEEE Journal of Quantum Electronics*, **29**, 2088-2096 (1993).

[61] C. DeCusatis, *Fibre optic data communications*, Academic Press, San Diego, CA, 2002.

[62] B. Razavi, *Design of integrated circuits for optical communications*, McGraw-Hill, Boston, London, 2003.

[63] I. P. Kaminow, T. Li, *Optical fibre telecommunications IVA: components*, Academic Press, San Diego, London, 2002.

[64] K. H. Liu, *IP over WDM*, Chichester, Wiley, New York, 2002.

[65] R. Ramaswami, K. N. Sivarajan, *Optical networks: a practical perspective*, 2nd ed., Morgan Kaufmann, San Francisco Publishers, London, 2002.

[66] http://www.pritel.com.

[67] I. S. Penketh, "Experimental transmission of dispersion managed solitons" *PhD Thesis*, Department of Electronic Engineering and Applied Physics, Aston University, Birmingham, 2000.

[68] I. D. Phillips, A. Gloag, D. G. Moodie, N. J. Doran, I. Bennion, and A. D. Ellis, "Simultaneous demultiplexing and clock recovery using a single electroabsorption modulator in a novel bi-directional configuration". *Optics Communications*, **150**, 101-105 (1998).

[69] V. Kaman, Y. J Chiu, T. Liljeberg, S. Z. Zhang, and J. E. Bowers, "Compact 40Gbit/s demultiplexing receiver based on integrated tandem electroabsorption modulators". *Electronics Letters*, **36**, 1943-1944 (2000).

[70] V. Kaman, A. J. Keating, S. Z. Zhang, and J. E. Bowers, "Simultaneous OTDM demultiplexing and detection using an electroabsorption modulator". *IEEE Photonics Technology Letters*, **12**, 711-713 (2000).

[71] T. Tanifuji, and M. Ikeda, "Pulse circulation measurement of transmission characteristics in long optical fibre". *Applied Optics*, **16**, 2175-2179 (1977).

[72] D. J. Malyon, T. Widdowson, E. G. Bryant, S. F. Carter, J. V. Wright, and W.A. Stallard, "Demonstration of optical pulse propagation over 10000km of fibre using recirculating loop". *Electronics Letters*, **27**, 120-121 (1991).

[73] H. Taga, M. Suzuki, Y. Yoshida, S. Yamamoto, and H. Wakabayashi, "Bit-error-rate characterization of IM-DD ultralong-distance optical communication systems with Er-doped fibre amplifiers using a recirculating loop". *Journal of Lightwave Technology*, **11**, 2100-2104 (1993).

[74] K. Ogawa, "10Gb/s long-haul experimental systems". *Conference of Lasers and Electro-Optics Society (LEOS 94)*, **1**, 201-202 (1994).

[75] N. S. Bergano, and C. R. Davidson, "Circulating loop transmission experiments for the study of long-haul transmission systems using erbium-doped fibre amplifiers". *Journal of Lightwave Technology*, **13**, 879-888 (1995).

[76] N. Kikuchi, S. Sasaki, K. Sekine, "10Gbit/s dispersion-compensated transmission over 2245km conventional fibres in a recirculating loop". *Electronics Letters*, **31**, 375-377 (1995).

[77] N. S. Bergano, and C. R. Davidson, "High capacity long-haul transmission experiments". *Conference of Integrated Optics and Optical Fibre Communications*, **1**, 1 - 6 (1997).

[78] http://www.neostech.com/new_content.asp?content=AO_Introduction.

[79] http://www.brimrose.com/pictures/fploop.pdf.

[80] P. Harper, "Long distance dispersion managed soliton transmission experiments". *PhD Thesis*, Department of Electronic Engineering and Computer Science, Aston University, Birmingham, 1997.

[81] http://www.testequity.com/products/1098.

[82] J. P. King, D. F. Smith, K. Richards, P. Timson, R. E. Epworth, and S. Wright, "Development of a coherent OTDR instrument". *Journal of Lightwave Technology*, **5**, 616-624 (1987).

[83] Y. Horiuchi, S. Ryu, K. Mochizuki, and H. Wakabayashi, "Novel coherent heterodyne optical time domain reflectometry for fault localization of optical amplifier submarine cable systems". *IEEE Photonics Technology Letters*, **2**, 291-293 (1990).

[84] Y. Sato, and K. Aoyama, "OTDR in optical transmission systems using Er-doped fibre amplifiers containing optical circulators". *IEEE Photonics Technology Letters*, **3**, 1001-1003 (1991).

[85] Y. Sato, and K. Aoyama, "Optical time domain reflectometry in optical transmission lines containing in-line Er-doped fibre amplifiers". *Journal of Lightwave Technology*, **10**, 78-83 (1992).

[86] J. C. MacKichan, J. A. Kitchen, and C. W. Pitt, "Innovative approach to interspan fibre break location in fibre amplifier repeatered communication systems", *Electronics Letters*, **28**, 626-628 (1992).

[87] M. Sumida, S. I. Furukawa, K. Tanaka, and M. Aiki, "High-accurate fault location technology using FSK-ASK probe backscattering reflectometry in optical amplifier submarine systems". *Journal of Lightwave Technology*, **14**, 2108-2116 (1996).

[88] P. Kim, H. Yoon, N. Park,a, J. Seo, K. Jeong, K. Ryoo, K. Lee, J. Blow, and S. Fleming, "Novel in-service supervisory scheme for the amplified WDM link with modified optical time domain reflectometry". *Optical Fibre Technology*, **8**, 139-145 (2002).

[89] J. Prat, and S. Ruiz-Moreno, "Transparent supervision of optically amplified fibre links with received signal and ASE monitoring". *Optics Communications*, **183**, 65-71 (2000).

[90] C. K. Chan, L. K. Chen, F. Tong, and D. Lam, "A novel in-service surveillance scheme for optically amplified transmission systems". *IEEE Photonics Technology Letters*, **9**, 1520-1522 (1997).

[91] C. Yeh, and S. Chi, "Fibre-fault monitoring technique for passive optical networks based on fibre Bragg gratings and semiconductor optical amplifier". *Optics Communications*, **257**, 306-310 (2006).

[92] C. D. Anderson, "Supervisory apparatus for optical transmission system", U.S. Patent 5,825,515, filed May 1996.

[93] "Performance analysis of passive high loss loopback system", *Internal Azea Technical Report.*

[94] "Performance analysis of pulsed high loss loopback system", *Internal Azea Technical Report.*

[95] "Prototype of pulsed high loss loopback system", *Internal Azea Technical Report.*

[96] http://www.home.agilent.com/USeng/nav/-536891689.536883077/pd.html.

[97] A. G. Striegler, and B. Schmauss, "Compensation of intrachannel effects in symmetric dispersion-managed transmission systems". *Journal of Lightwave Technology*, **22**, 1877-1882 (2004).

[98] C. E. Shannon, "A mathematical Theory of Communication". *The Bill System Technical Journal (BSTJ)*, **27**, 379-423 (1948).

[99] E. G. Shapiro, M. P. Fedoruk, and S. K. Turitsyn "Direct modelling of error statistics at 40Gbit/s rate in SMF/DCF link with strong bit overlapping". *Electronic Letters*, **40**, 22, 2004.

[100] O. A. Sab, "Forward error correction techniques". *Optical Fibre Communications Conference (OFC 2003)*, **1**, 391 (2003).

[101] N. Ramanujam, A. B. Puc, G. Lenner, H. D. Kidorf, C. R. Davidson, I. Hayee, J. -X Cai. M. Nissov, A. Pilipetskii, C. Rivers, and N. S. Bergano, "Forward error correction (FEC) techniques in long-haul optical transmission systems", *Lasers and Electro-Optics Society (LEOS)*, **2**, 405-406 (2000).

[102] J. Dunlop, D. G. Smith, *Telecommunications engineering*, 3rd ed., Chapman & Hall, London, 1994.

[103] D. G. Leeper, "A universal digital data scrambler". *The Bill System Technical Journal (BSTJ)*, **52**, 1851-1865 (1973).

[104] A. R. Chraplyvy, J. A. Nagel, and R. W. Tkach, "Equalization in amplified WDM lightwave transmission systems". *IEEE Photonics Technology Letters*, **4**, 920-922 (1992).

[105] O. A. Sab, H. Bissessur, "Signal formats and error correction in optical transmission". *Optical Telecommunications*, **4**, 95-104 (2003).

[106] B. Bakhshi, M. Vaa, E. A. Golovchenko, W. W. Patterson, R. L. Maybach, and N. S. Bergano, "Comparison of CRZ, RZ and NRZ modulation formats in a 64 /spl times/ 12.3 Gb/s WDM transmission experiment over 9000 km". *Optical Fibre Communication Conference and Exhibit (OFC 2001)*, **3**, Proc. ppWF4-1-WF4-3 (2001).

[107] D. Breuer, and K. Petermann, "Comparison of NRZ- and RZ-modulation format for 40-Gb/s TDM standard-fibre systems". *IEEE Photonics Technology Letters,* **9**, 398-400 (1997).

[108] A. Hodzic, B. Konrad, and K. Petermann, "Alternative modulation formats in N×40 Gb/s WDM standard fibre RZ-transmission systems". *Journal of Lightwave Technology*, **20**, 598-607 (2002).

[109] T. Tokle, C. Peucheret, and P. Jeppesen, "Advanced modulation formats in 40Gbit/s optical communication systems with 80-km fibre spans". *Optics Communications*, **225**, 79-87 (2003).

[110] J. Yan , M. Chen, S. Xie, and B. Zhou, "Performance comparison of standard FEC in 40Gbit/s optical transmission systems with NRZ, RZ and CS-RZ modulation formats" *Optics Communications*, **231**, 175-180 (2004).

[111] B. Mukherjee, *Optical communication networks*, McGraw-Hill, New York, 1997.

[112] R. Hui, S. Zhang, A. Ganesh, C. Allen, and K. Demarest, "40Gb/s Optical Transmission System Testbed". *Technical Report*, Information and Telecommunication Technology Centre, The University of Kansas, 2004.

[113] W. Li, M. Chen, Y. Dong, and S. Xie, "All-optical format conversion from NRZ to CSRZ and between RZ and CSRZ using SOA-based fibre loop mirror". *IEEE Photonics Technology Letters*, **16**, 203-205 (2004).

[114] M. Eiselt, W. Pieper, and H. G. Weber, "SLALOM: Semiconductor laser amplifier in a loop mirror". *Journal of Lightwave Technology*, **13**, 2099-2112, (1995).

[115] R. J. Manning, A. D. Ellis, A. J. Poustie, and K. J. Blow, "Semiconductor laser amplifier for ultrafast all-optical signal processing". *Journal of the Optical Society of America*, **B14**, 3204-3216 (1997).

List of Publications

1. M. M. Nahas, R. A. Ibbotson, and K. J. Blow, "5 × 10Gb/s WDM transmission system performance using different number of one's and zero's in PRBS data". *Nonlinear Optics in Communications Meeting*, Institute of Physics, London, June 2004.

2. M. M. Nahas, R. A. Ibbotson, and K. J. Blow, "5 ×10Gb/s WDM transmission system performance using different number of one's and zero's in PRBS data". *Networks & Optical Communications Conference (NOC 2005)*, Proc. pp 471-475, UCL, London, July 2005.

3. M. M. Nahas, M. H. A. Wahid, R. A. Ibbotson, and K. J. Blow, "10Gbit/s transmission over long distance after all-optical NRZ and RZ to CSRZ format conversion using SLALOM". *Nonlinear Guided Waves Conference (NLGW 2005)*, Proc. ppWB7, Dresden, Germany, September 2005.

4. M. H. A. Wahid, M. M. Nahas, R. A. Ibbotson, and K. J. Blow, "WDM transmission after All-Optical NRZ to CSRZ and RZ to CSRZ format conversion using an SOA-NOLM". *Optics Communications Letters*, resubmitted after revision, May 2006.

Note: due to the high privacy and confidentiality nature of industrial projects, it has not been possible to publish any results from the LME work presented in chapter 3, which was done exclusively for Azea Networks.

Appendix A

Low Power Mixer 3 V Receiver IF Subsystem

AD607

FEATURES

Complete Receiver-on-a-Chip: Monoceiver® Mixer
- −15 dBm 1 dB Compression Point
- −8 dBm Input Third Order Intercept
- 500 MHz RF and LO Bandwidths

Linear IF Amplifier
- Linear-in-dB Gain Control
- Manual Gain Control

Quadrature Demodulator
- On-Board Phase-Locked Quadrature Oscillator
- Demodulates IFs from 400 kHz to 12 MHz
- Can Also Demodulate AM, CW, SSB

Low Power
- 25 mW at 3 V
- CMOS Compatible Power-Down

Interfaces to AD7013 and AD7015 Baseband Converters

APPLICATIONS

GSM, CDMA, TDMA, and TETRA Receivers
Satellite Terminals
Battery-Powered Communications Receivers

PIN CONFIGURATION

20-Lead SSOP
(RS Suffix)

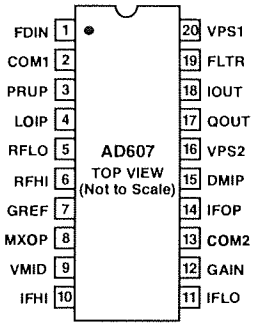

GENERAL DESCRIPTION

The AD607 is a 3 V low power receiver IF subsystem for operation at input frequencies as high as 500 MHz and IFs from 400 kHz to 12 MHz. It consists of a mixer, IF amplifiers, I and Q demodulators, a phase-locked quadrature oscillator, and a biasing system with external power-down.

The AD607's low noise, high intercept mixer is a doubly balanced Gilbert cell type. It has a nominal −15 dBm input referred 1 dB compression point and a −8 dBm input referred third order intercept. The mixer section of the AD607 also includes a local oscillator (LO) preamplifier, which lowers the required LO drive to −16 dBm.

In MGC operation, the AD607 accepts an external gain-control voltage input from an external AGC detector or a DAC.

The I and Q demodulators provide in-phase and quadrature baseband outputs to interface with Analog Devices' AD7013 (IS54, TETRA, MSAT) and AD7015 (GSM) baseband converters. A quadrature VCO phase-locked to the IF drives the I and Q demodulators. The I and Q demodulators can also demodulate AM; when the AD607's quadrature VCO is phase-locked to the received signal, the in-phase demodulator becomes a synchronous product detector for AM. The VCO can also be phase-locked to an external beat-frequency oscillator (BFO), and the demodulator serves as a product detector for CW or SSB reception. Finally, the AD607 can be used to demodulate BPSK using an external Costas Loop for carrier recovery.

REV. C

One Technology Way, P.O. Box 9106, Norwood, MA 02062-9106, U.S.A.
Tel: 781/329-4700 www.analog.com
Fax: 781/326-8703

AD607—SPECIFICATIONS (@ T_A = 25°C, Supply = 3.0 V, IF = 10.7 MHz, unless otherwise noted.)

Model	Conditions	AD607ARS Min	Typ	Max	Unit
DYNAMIC PERFORMANCE					
MIXER					
Maximum RF and LO Frequency Range	For Conversion Gain > 20 dB		500		MHz
Maximum Mixer Input Voltage	For Linear Operation; Between RFHI and RFLO		±54		mV
Input 1 dB Compression Point	RF Input Terminated in 50 Ω		–15		dBm
Input Third-Order Intercept	RF Input Terminated in 50 Ω		–5		dBm
Noise Figure	Matched Input, Max Gain, f = 83 MHz, IF = 10.7 MHz		14		dB
	Matched Input, Max Gain, f = 144 MHz, IF = 10.7 MHz		12		dB
Maximum Output Voltage at MXOP	Z_{IF} = 165 Ω, at Input Compression		±1.3		V
Mixer Output Bandwidth at MXOP	–3 dB, Z_{IF} = 165 Ω		45		MHz
LO Drive Level	Mixer LO Input Terminated in 50 Ω		–16		dBm
LO Input Impedance	LOIP to VMID		1		kΩ
Isolation, RF to IF	RF = 240 MHz, IF = 10.7 MHz, LO = 229.3 MHz		30		dB
Isolation, LO to IF	RF = 240 MHz, IF = 10.7 MHz, LO = 229.3 MHz		20		dB
Isolation, LO to RF	RF = 240 MHz, IF = 10.7 MHz, LO = 229.3 MHz		40		dB
Isolation, IF to RF	RF = 240 MHz, IF = 10.7 MHz, LO = 229.3 MHz		70		dB
IF AMPLIFIERS					
Noise Figure	Max Gain, f = 10.7 MHz		17		dB
Input 1 dB Compression Point	IF = 10.7 MHz		–15		dBm
Output Third-Order Intercept	IF = 10.7 MHz		18		dBm
Maximum IF Output Voltage at IFOP	Z_{IF} = 600 Ω		±560		mV
Output Resistance at IFOP	From IFOP to VMID		15		Ω
Bandwidth	–3 dB at IFOP, Max Gain		45		MHz
GAIN CONTROL	(See Figures 23 and 24)				
Gain Control Range	Mixer + IF Section, GREF to 1.5 V		90		dB
Gain Scaling	GREF to 1.5 V		20		mV/dB
	GREF to General Reference Voltage V_R		$75/V_R$		dB/V
Gain Scaling Accuracy	GREF to 1.5 V, 80 dB Span		±1		dB
Bias Current at GAIN			5		μA
Bias Current at GREF			1		μA
Input Resistance at GAIN, GREF			1		MΩ
I AND Q DEMODULATORS					
Required DC Bias at DMIP			VPOS/2		V dc
Input Resistance at DMIP	From DMIP to VMID		50		kΩ
Input Bias Current at DMIP			2		μA
Maximum Input Voltage	IF > 3 MHz		±150		mV
	IF ≤ 3 MHz		±75		mV
Amplitude Balance	IF = 10.7 MHz, Outputs at 600 mV p-p, F = 100 kHz		±0.2		dB
Quadrature Error	IF = 10.7 MHz, Outputs at 600 mV p-p, F = 100 kHz		–1.2		Degrees
Phase Noise in Degrees	IF = 10.7 MHz, F = 10 kHz		–100		dBc/Hz
Demodulation Gain	Sine Wave Input, Baseband Output		18		dB
Maximum Output Voltage	R_L ≥ 20 kΩ		±1.23		V
Output Offset Voltage	Measured from I_{OUT}, Q_{OUT} to VMID	–150	+10	+150	mV
Output Bandwidth	Sine Wave Input, Baseband Output		1.5		MHz
PLL					
Required DC Bias at FDIN			VPOS/2		V dc
Input Resistance at FDIN	From FDIN to VMID		50		kΩ
Input Bias Current at FDIN			200		nA
Frequency Range			0.4 to 12		MHz
Required Input Drive Level	Sine Wave Input at Pin 1		400		mV
Acquisition Time to ±3°	IF = 10.7 MHz		16.5		μs
POWER-DOWN INTERFACE					
Logical Threshold	For Power Up on Logical High		2		V dc
Input Current for Logical High			75		μA
Turn-On Response Time	To PLL Locked		16.5		μs
Standby Current			550		μA
POWER SUPPLY					
Supply Range		2.92		5.5	V
Supply Current	Midgain, IF = 10.7 MHz		8.5		mA
OPERATING TEMPERATURE					
T_{MIN} to T_{MAX}	Operation to 2.92 V Minimum Supply Voltage	–25		+85	°C
	Operation to 4.5 V Minimum Supply Voltage	–40		+85	°C

Specifications subject to change without notice.

ABSOLUTE MAXIMUM RATINGS[1]

Supply Voltage VPS1, VPS2 to COM1, COM2 ..... 5.5 V
Internal Power Dissipation[2] ..... 600 mW
2.92 V to 5.5 V Operating Temperature Range
..... −25°C to +85°C
4.5 V to 5.5 V Operating Temperature Range
..... −40°C to +85°C
Storage Temperature Range ..... −65°C to +150°C
Lead Temperature Range (Soldering 60 sec) ..... 300°C

NOTES

[1] Stresses above those listed under Absolute Maximum Rating may cause permanent damage to the device. This is a stress rating only; functional operation of the device at these or any other conditions above those indicated in the operational section of this specification is not implied. Exposure to absolute maximum rating conditions for extended periods may affect device reliability.

[2] Thermal Characteristics: 20-lead SSOP Package: θ_{JA} = 126°C/W.

ORDERING GUIDE

Model	Temperature Range	Package Description	Package Option
AD607ARS	−25°C to +85°C for 2.92 V to 5.5 V Operation; −40°C to +85°C for 4.5 V to 5.5 V Operation	20-Lead Plastic SSOP	RS-20

CAUTION

ESD (electrostatic discharge) sensitive device. Electrostatic charges as high as 4000 V readily accumulate on the human body and test equipment and can discharge without detection. Although the AD607 features proprietary ESD protection circuitry, permanent damage may occur on devices subjected to high energy electrostatic discharges. Therefore, proper ESD precautions are recommended to avoid performance degradation or loss of functionality.

PIN FUNCTION DESCRIPTIONS

Pin	Mnemonic	Reads	Function
1	FDIN	Frequency Detector Input	PLL Input for I/Q Demodulator Quadrature Oscillator, ±400 mV Drive Required from External Oscillator. Must be biased at $V_P/2$.
2	COM1	Common #1	Supply Common for RF Front End and Main Bias
3	PRUP	Power-Up Input	3 V/5 V CMOS compatible power-up control; logical high = powered-up; max input level = VPS1 = VPS2.
4	LOIP	Local Oscillator Input	LO input, ac-coupled ±54 mV LO input is required (–16 dBm for 50 Ω input termination).
5	RFLO	RF "Low" Input	Usually Connected to AC Ground
6	RFHI	RF "High" Input	AC-Coupled, ±56 mV, Max RF Input for Linear Operation
7	GREF	Gain Reference Input	High Impedance Input, typically 1.5 V, sets gain scaling.
8	MXOP	Mixer Output	High Impedance, Single-Sided Current Output, ±1.3 V Max Voltage Output (±6 mA Max Current Output)
9	VMID	Midsupply Bias Voltage	Output of the Midsupply Bias Generator (VMID = VPOS/2)
10	IFHI	IF "High" Input	AC-Coupled IF Input, ±56 mV Max Input for Linear Operation
11	IFLO	IF "Low" Input	Reference Node for IF Input; Auto-Offset Null
12	GAIN	Gain Control Input	High Impedance Input, 0 V–2 V Using 3 V Supply, Max Gain at V = 0
13	COM2	Common #2	Supply Common for IF Stages and Demodulator
14	IFOP	IF Output	Low Impedance, Single-Sided Voltage Output, 5 dBm (±560 mV) Max
15	DMIP	Demodulator Input	Signal input to I and Q demodulators has a ±150 mV max input at IF > 3 MHz for linear operation; ±75 mV max input at IF < 3 MHz for linear operation. Must be biased at $V_P/2$.
16	VPS2	VPOS Supply #2	Supply to High Level IF, PLL, and Demodulators
17	QOUT	Quadrature Output	Low Impedance Q Baseband Output; ±1.23 V Full Scale in 20 kΩ Min Load; AC-Coupled
18	IOUT	In-Phase Output	Low Impedance I Baseband Output; ±1.23 V Full Scale in 20 kΩ Min Load; AC-Coupled
19	FLTR	PLL Loop Filter	Series RC PLL Loop Filter, Connected to Ground
20	VPS1	VPOS Supply #1	Supply to Mixer, Low Level IF, PLL, and Gain Control

PIN CONNECTION
20-Lead SSOP (RS-20)

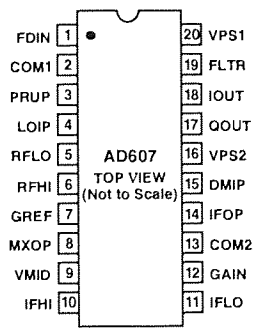

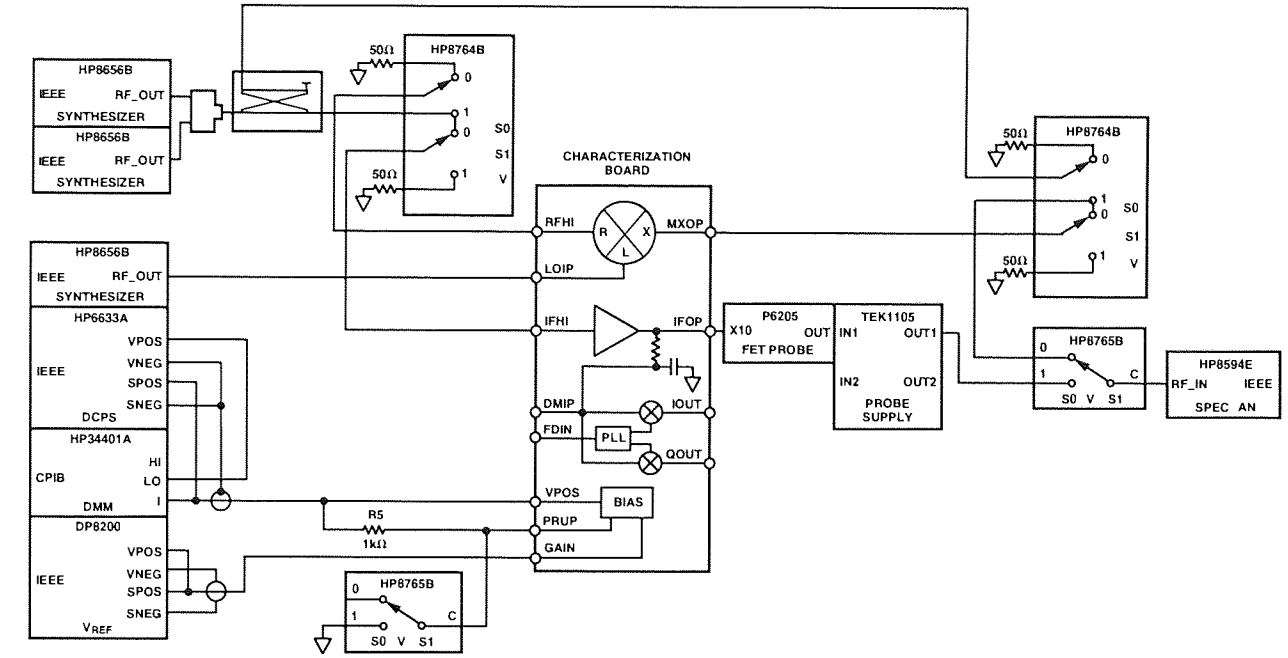

Figure 1. Mixer/Amplifier Test Set

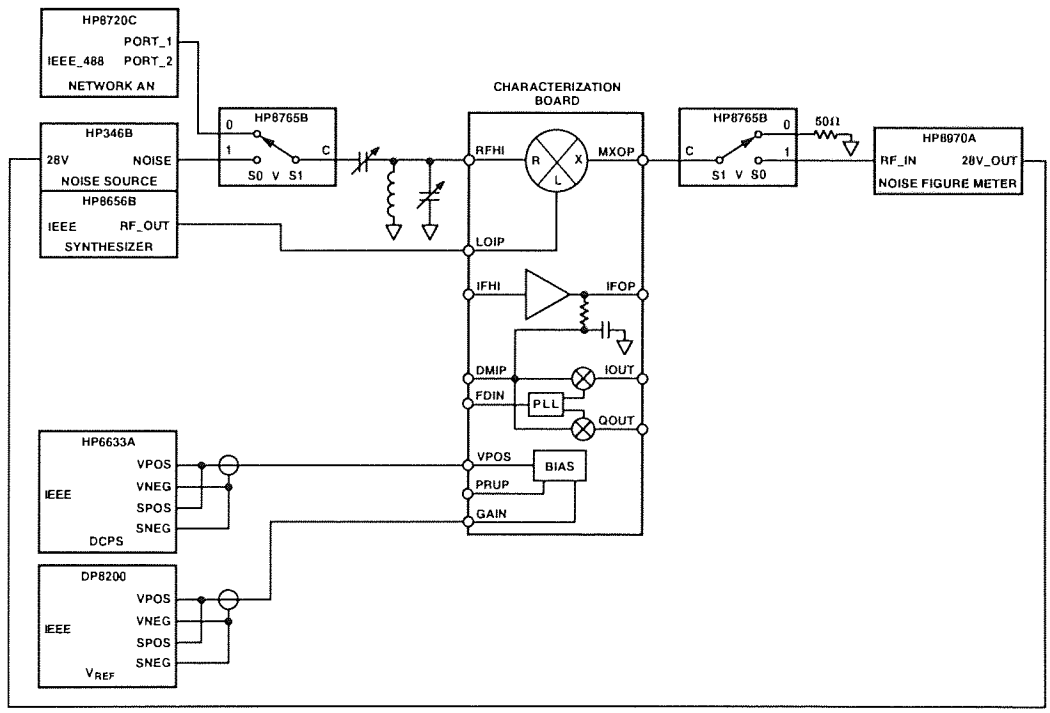

Figure 2. Mixer Noise Figure Test Set

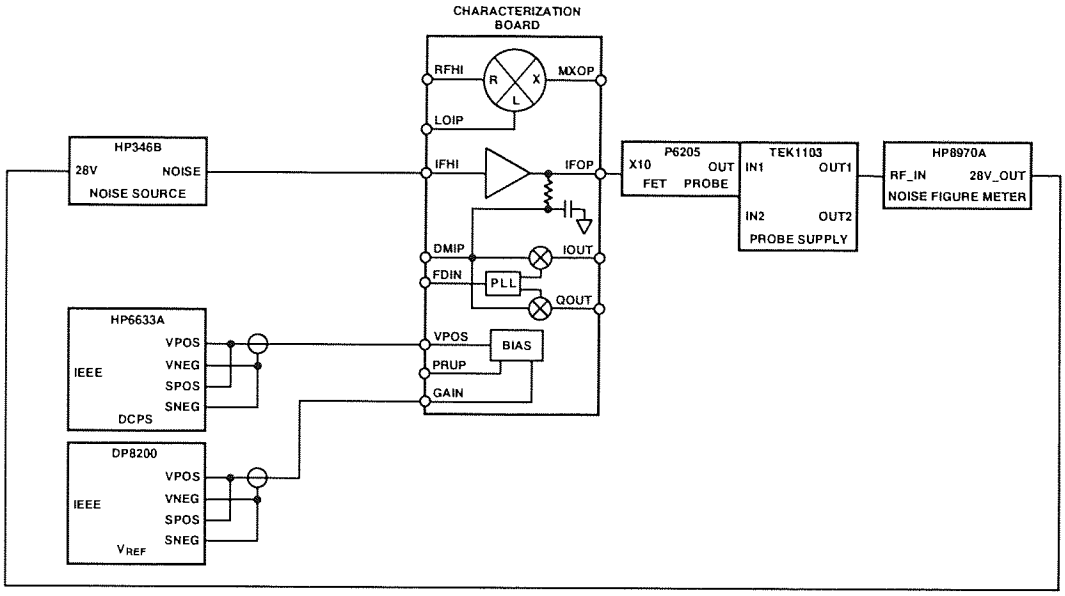

Figure 3. IF Amp Noise Figure Test Set

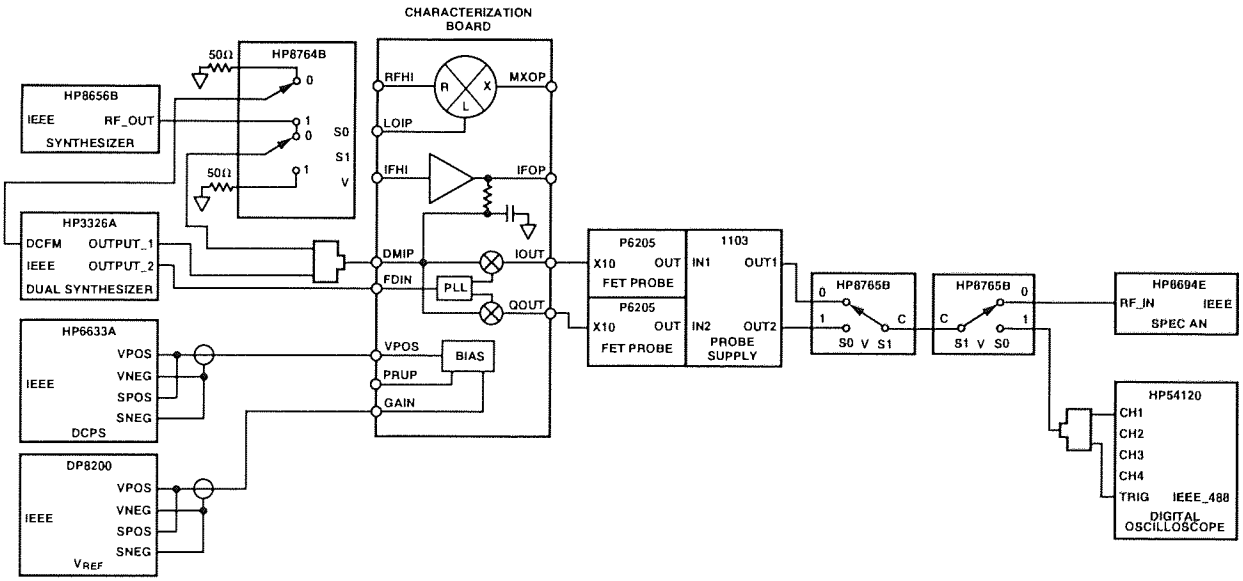

Figure 4. PLL/Demodulator Test Set

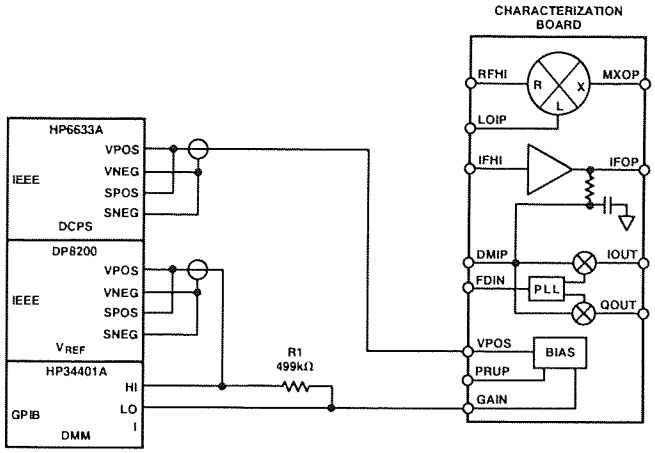

Figure 5. GAIN Pin Bias Test Set

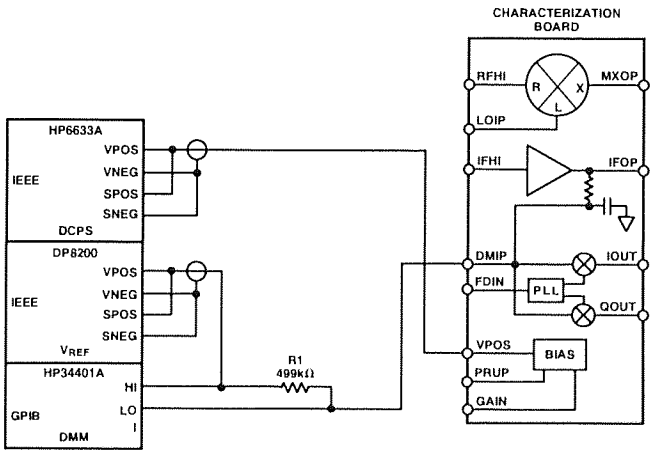

Figure 6. Demodulator Bias Test Set

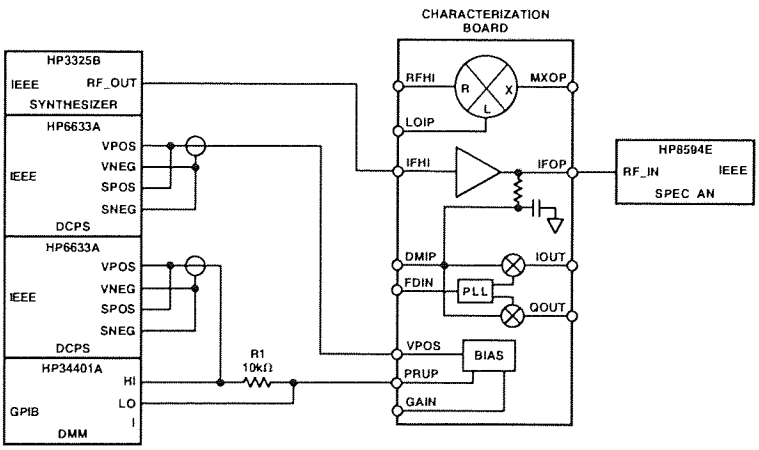

Figure 7. Power-Up Threshold Test Set

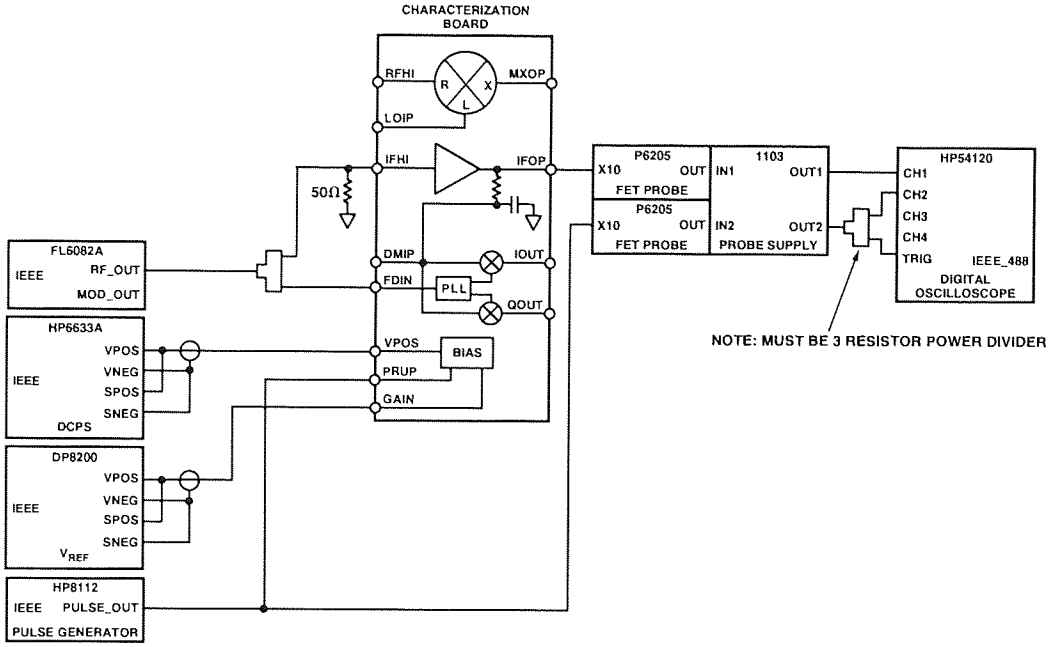

Figure 8. Power-Up Test Set

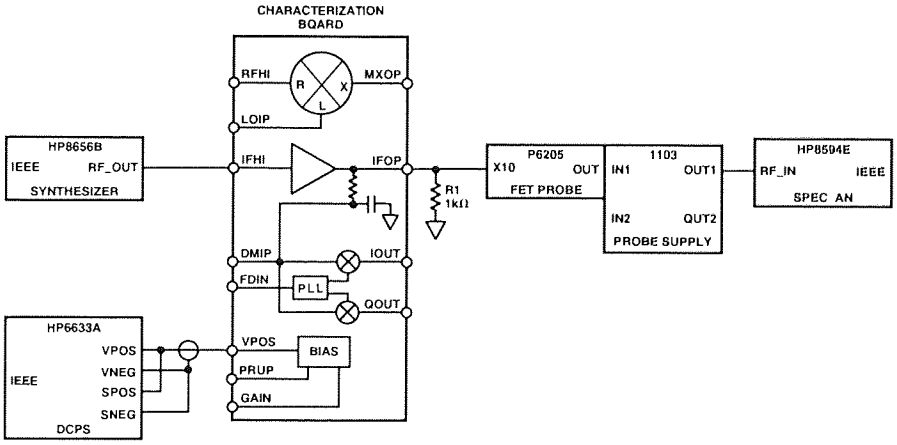

Figure 9. IF Output Impedance Test Set

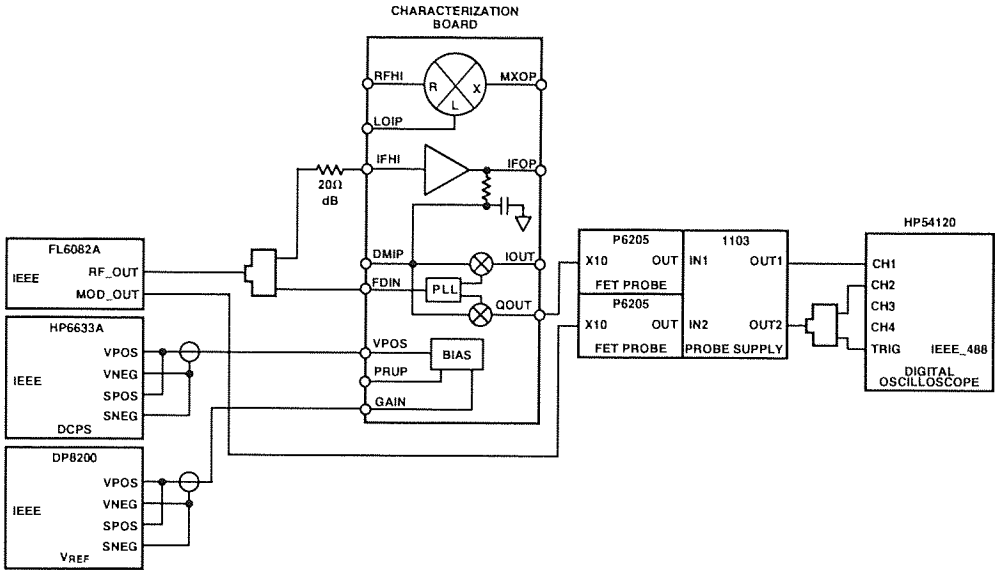

Figure 10. PLL Settling Time Test Set

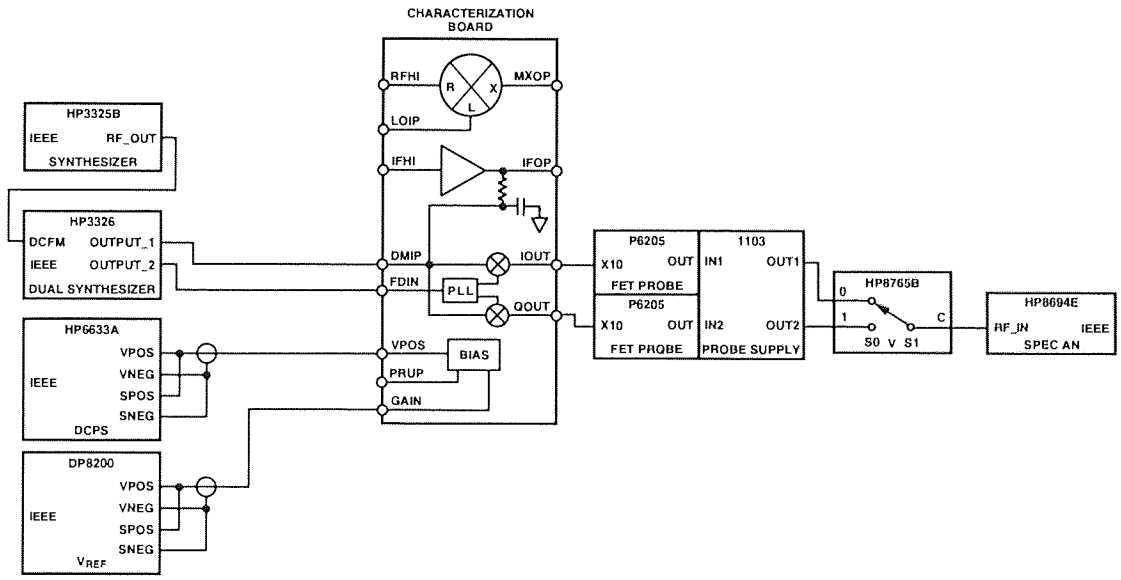

Figure 11. Quadrature Accuracy Test Set

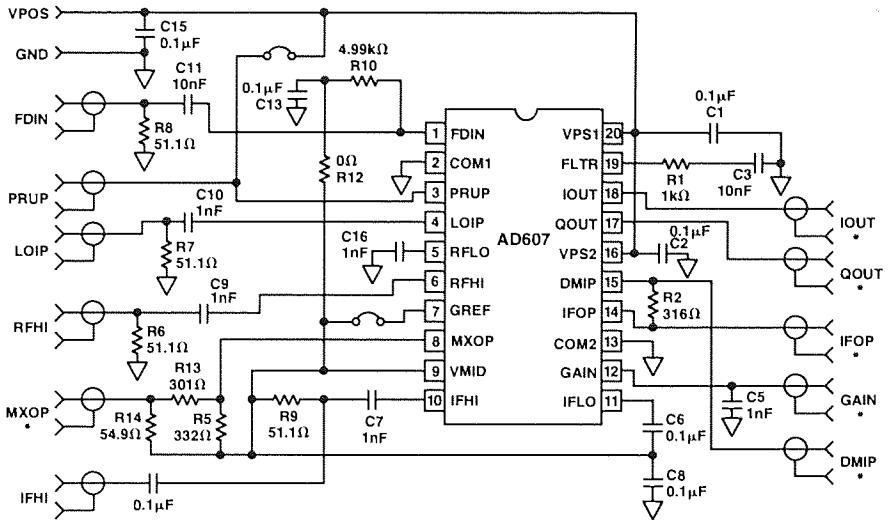

*CONNECTIONS ARE DC-COUPLED.

Figure 12. Characterization Board

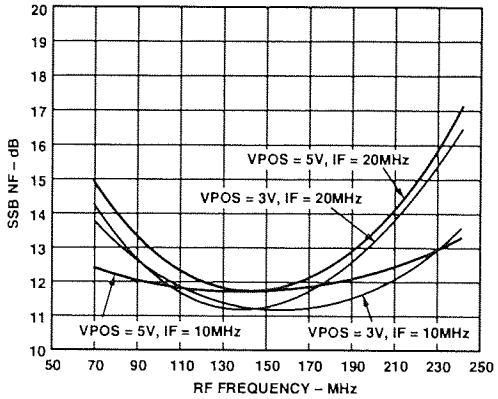

TPC 1. Mixer Noise Figure vs. Frequency

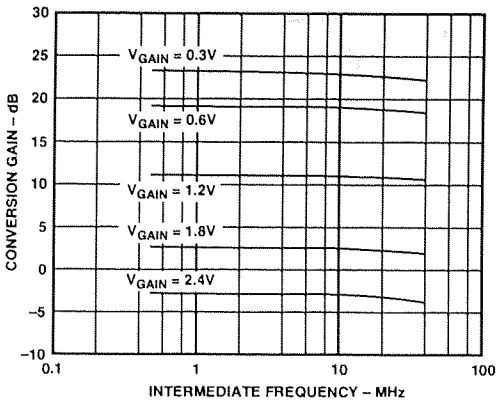

TPC 4. Mixer Conversion Gain vs. IF, T = 25°C, VPOS = 3 V, VREF = 1.5 V

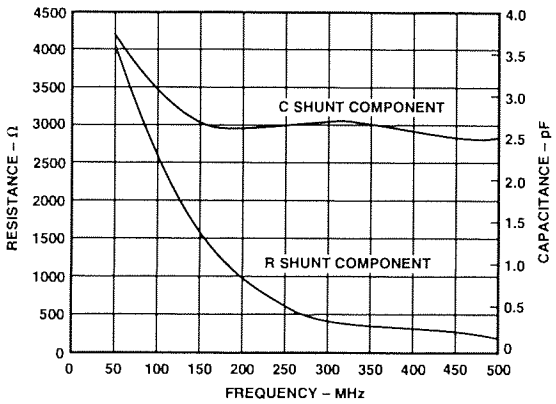

TPC 2. Mixer Input Impedance vs. Frequency, VPOS = 3 V, V GAIN = 0.8 V

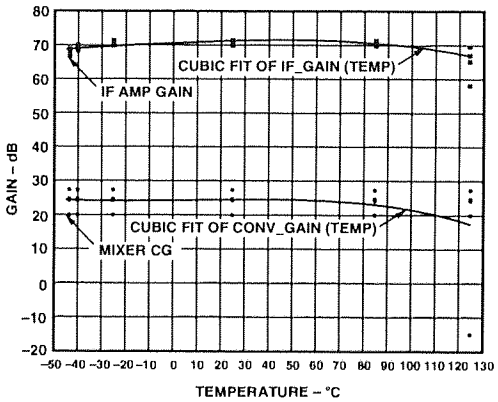

TPC 5. Mixer Conversion Gain and IF Amplifier Gain vs. Temperature, VPOS = 3 V, VGAIN = 0.3 V, VREF = 1.5 V, IF = 10.7 MHz, RF = 250 MHz

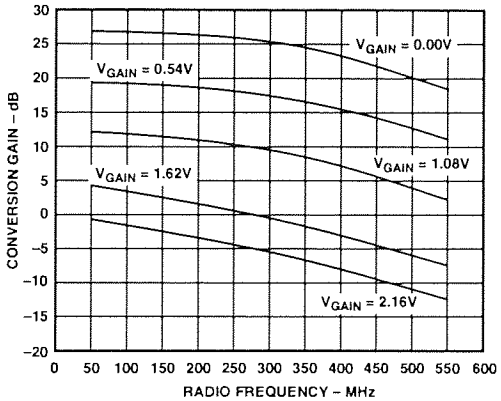

TPC 3. Mixer Conversion Gain vs. Frequency, T = 25°C, VPOS = 2.92 V, VREF = 1.35 V, IF = 10.7 MHz

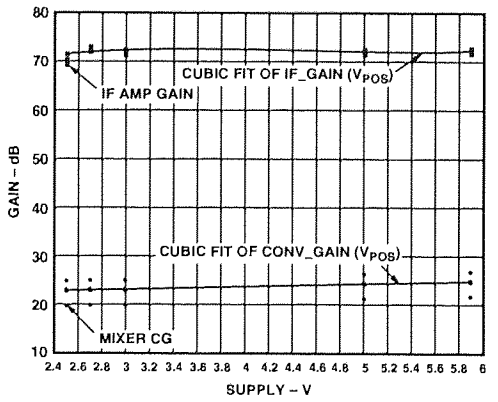

TPC 6. Mixer Conversion Gain and IF Amplifier Gain vs. Supply Voltage, T = 25°C, VGAIN = 0.3 V, VREF = 1.5 V, IF = 10.7 MHz, RF = 250 MHz

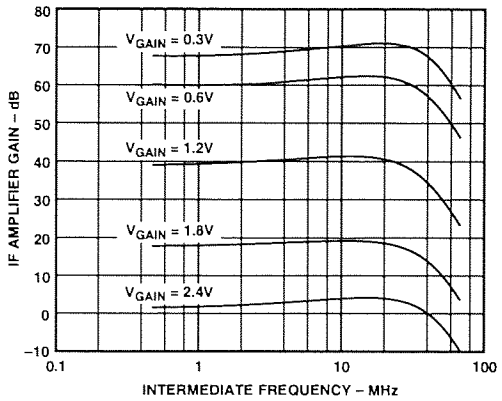

TPC 7. IF Amplifier Gain vs. Frequency, T = 25°C, VPOS = 3 V, VREF = 1.5 V

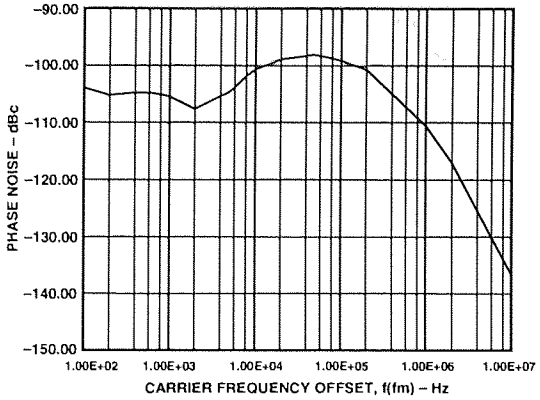

TPC 10. PLL Phase Noise L (F) vs. Frequency, VPOS = 3 V, C3 = 0.1 µF, IF = 10.7 MHz

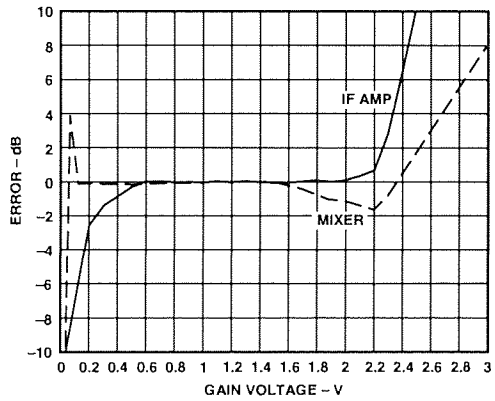

TPC 8. Gain Error vs. Gain Control Voltage, Representative Part

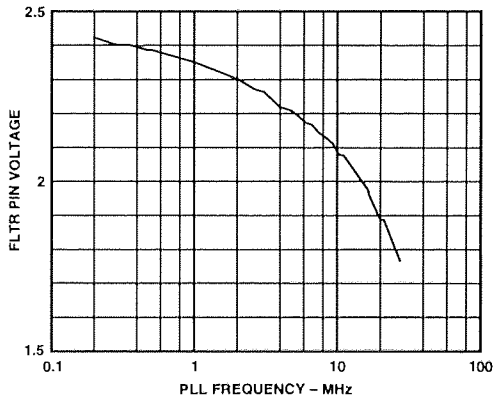

TPC 11. PLL Loop Voltage at FLTR (K_{VCO}) vs. Frequency

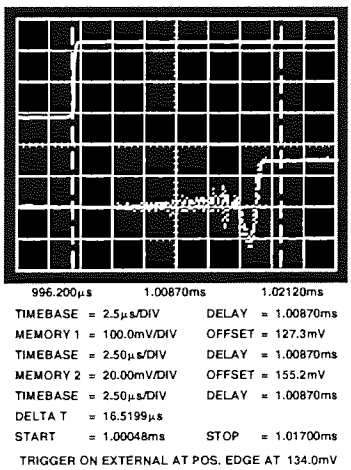

TPC 9. PLL Acquisition Time

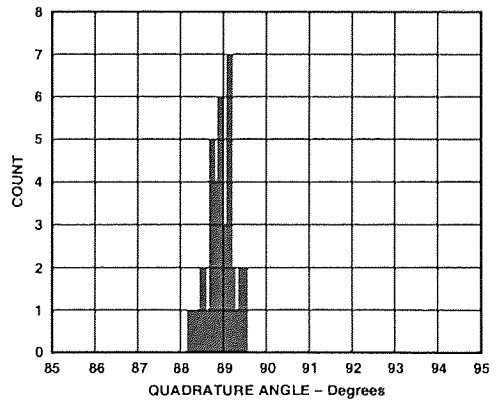

TPC 12. Demodulator Quadrature Angle, Histogram, T = 25°C, VPOS = 3 V, IF = 10.7 MHz

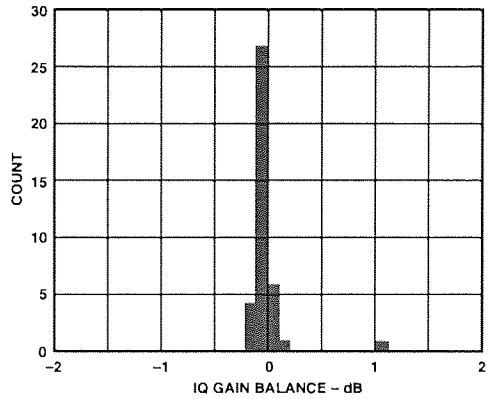

TPC 13. Demodulator Gain Balance, Histogram, T = 25°C, VPOS = 3 V, IF = 10.7 MHz

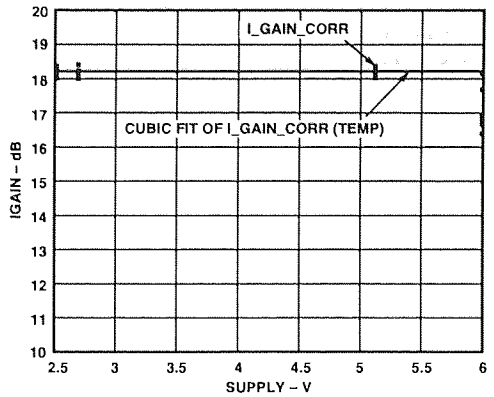

TPC 16. Demodulator Gain vs. Supply Voltage

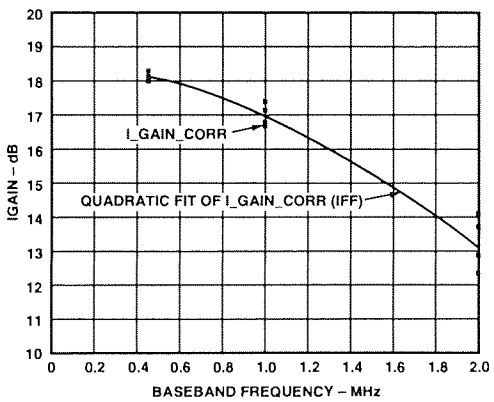

TPC 14. Demodulator Gain vs. Frequency

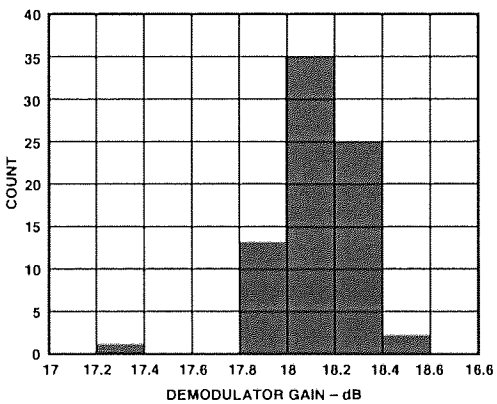

TPC 17. Demodulator Gain Histogram, T = 25°C, VPOS = 3 V, IF = 10.7 MHz

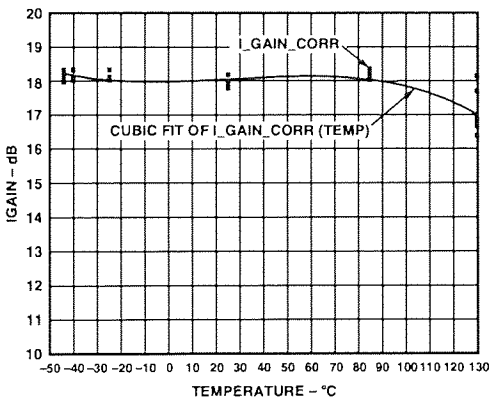

TPC 15. Demodulator Gain vs. Temperature

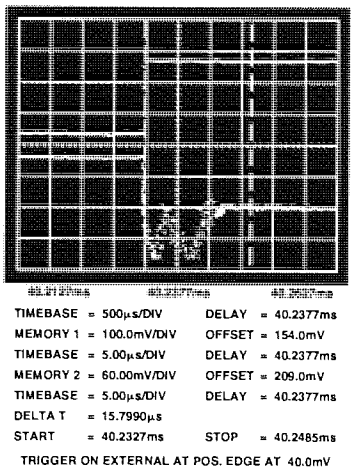

TPC 18. Power-Up Response Time to PLL Stable

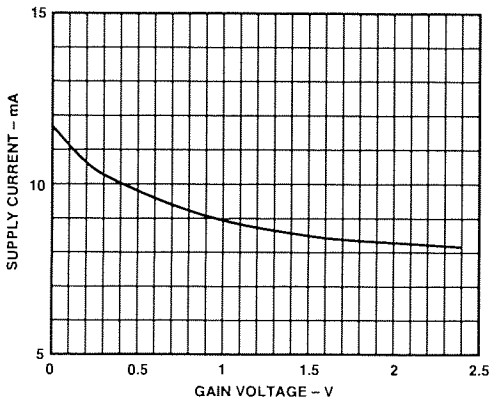

TPC 19. Power Supply Current vs. Gain Control Voltage, GREF = 1.5 V

PRODUCT OVERVIEW

The AD607 provides most of the active circuitry required to realize a complete low power, single-conversion superheterodyne receiver, or most of a double-conversion receiver, at input frequencies up to 500 MHz, and an IF from 400 kHz to 12 MHz. The internal I/Q demodulators and their associated phase-locked loop, which can provide carrier recovery from the IF, support a wide variety of modulation modes, including n-PSK, n-QAM, and AM. A single positive supply voltage of 3 V is required (2.92 V minimum, 5.5 V maximum) at a typical supply current of 8.5 mA at midgain. In the following discussion, V_P will be used to denote the power supply voltage, which will be assumed to be 3 V.

Figure 13 shows the main sections of the AD607. It consists of a variable gain UHF mixer and linear four-stage IF strip, which together provide a voltage controlled gain range of more than 90 dB; dual demodulators, each comprising a multiplier followed by a two-pole, 2 MHz low-pass filter; and a phase-locked loop providing the inphase and quadrature clocks. A biasing system with CMOS compatible power-down completes the AD607.

Mixer

The UHF mixer is an improved Gilbert cell design, and can operate from low frequencies (it is internally dc-coupled) up to an RF input of 500 MHz. The dynamic range at the input of the mixer is determined at the upper end by the maximum input signal level of ±56 mV between RFHI and RFLO up to which the mixer remains linear, and at the lower end by the noise level. It is customary to define the linearity of a mixer in terms of the 1 dB gain-compression point and third order intercept, which for the AD607 are –15 dBm and –8 dBm, respectively, in a 50 Ω system.

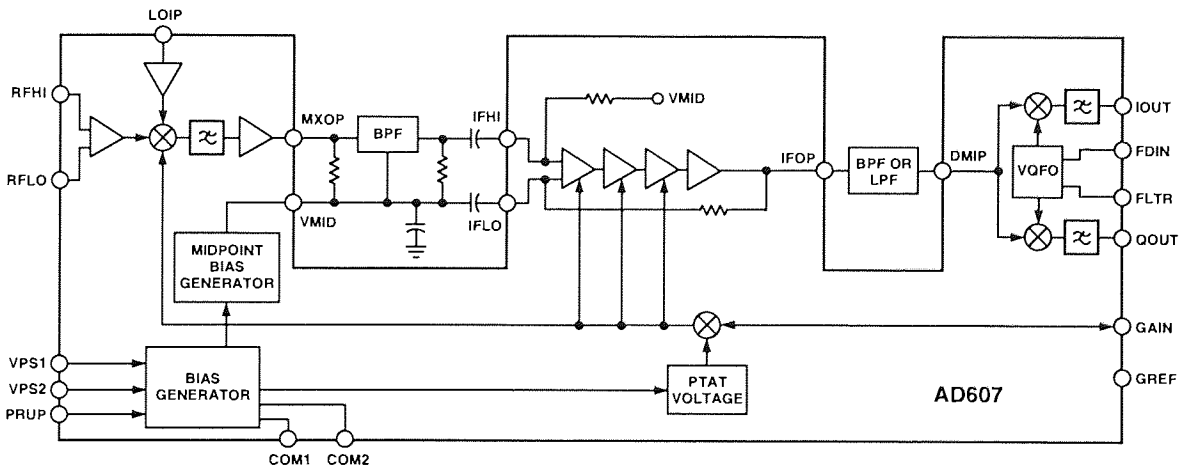

Figure 13. Functional Block Diagram

The mixer's RF input port is differential, that is, pin RFLO is functionally identical to RFHI, and these nodes are internally biased; we will generally assume that RFLO is decoupled to ac ground. The RF port can be modeled as a parallel RC circuit as shown in Figure 14.

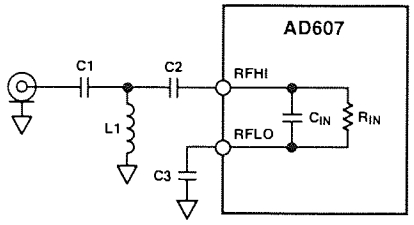

C1, C2, L1: OPTIONAL MATCHING CIRCUIT
C3: COUPLES RFLO TO AC GROUND

Figure 14. Mixer Port Modeled as a Parallel RC Network; an Optional Matching Network Is also Shown

The local oscillator (LO) input is internally biased at $V_P/2$ via a nominal 1000 Ω resistor internally connected from pin LOIP to VMID. The LO interface includes a preamplifier that minimizes the drive requirements, thus simplifying the oscillator design and reducing LO leakage from the RF port. Internally, this single-sided input is actually differential; the noninverting input is referenced to Pin VMID. The LO requires a single-sided drive of ±50 mV, or −16 dBm in a 50 Ω system.

The mixer's output passes through both a low-pass filter and a buffer, which provides an internal differential to single-ended signal conversion with a bandwidth of approximately 45 MHz. Its output at Pin MXOP is in the form of a single-ended current. This approach eliminates the 6 dB voltage loss of the usual series termination by replacing it with shunt terminations at both the input and the output of the filter. The nominal conversion gain is specified for operation into a total IF band-pass filter (BPF) load of 165 Ω, that is, a 330 Ω filter doubly-terminated as shown in Figure 14. Note that these loads are connected to bias point VMID, which is always at the midpoint of the supply (that is, $V_P/2$).

The conversion gain is measured between the mixer input and the input of this filter, and varies between 1.5 dB and 26.5 dB for a 165 Ω load impedance. Using filters of higher impedance, the conversion gain can always be maintained at its specified value or made even higher; for filters of lower impedance, of say Z_O, the conversion gain will be lowered by 10 $\log_{10}(165/Z_O)$. Thus, the use of a 50 Ω filter will result in a conversion gain that is 5.2 dB lower. Figure 15 shows filter matching networks and Table I lists resistor values.

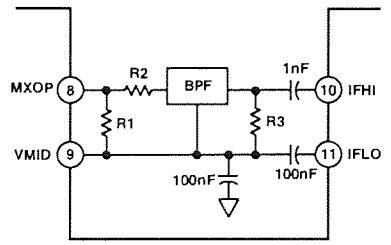

Figure 15. Suggested IF Filter Matching Network. The Values of R1 and R2 Are Selected to Keep the Impedance at Pin MXOP at 165 Ω

Table I. Filter Termination Resistor Values for Common IFs

IF	Filter Impedance	Filter Termination Resistor Values* for 24 dB of Mixer Gain		
		R1	R2	R3
450 kHz	1500 Ω	174 Ω	1330 Ω	1500 Ω
455 kHz	1500 Ω	174 Ω	1330 Ω	1500 Ω
6.5 MHz	1000 Ω	215 Ω	787 Ω	1000 Ω
10.7 MHz	330 Ω	330 Ω	0 Ω	330 Ω

*Resistor values were calculated such that R1+ R2 = Z_{FILTER} and R1‖ (R2 + Z_{FILTER}) = 165 Ω.

The maximum permissible signal level at MXOP is determined by both voltage and current limitations. Using a 3 V supply and VMID at 1.5 V, the maximum swing is about ±1.3 V. To attain a voltage swing of ±1 V in the standard IF filter load of 165 Ω requires a peak drive current of about ±6 mA, which is well within the linear capability of the mixer. However, these upper limits for voltage and current should not be confused with issues related to the mixer gain, already discussed. In an operational system, the AGC voltage will determine the mixer gain, and hence the signal level at the IF input Pin IFHI; it will always be less than ±56 mV (−15 dBm into 50 Ω), which is the limit of the IF amplifier's linear range.

IF Amplifier

Most of the gain in the AD607 arises in the IF amplifier strip, which comprises four stages. The first three are fully differential and each has a gain span of 25 dB for the nominal AGC voltage range. Thus, in conjunction with the mixer's variable gain, the total gain exceeds 90 dB. The final IF stage has a fixed gain of 20 dB, and it also provides differential to single-ended conversion.

The IF input is differential, at IFHI (noninverting relative to the output IFOP) and IFLO (inverting). Figure 16 shows a simplified schematic of the IF interface. The offset voltage of this stage would cause a large dc output error at high gain, so it is nulled by a low pass feedback path from the IF output, also shown in TPC 13. Unlike the mixer output, the signal at IFOP is a low-impedance single-sided voltage, centered at $V_P/2$ by the dc feedback loop. It may be loaded by a resistance as low as 50 Ω, which will normally be connected to VMID.

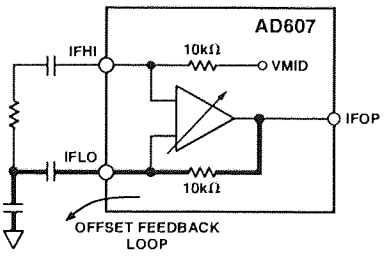

Figure 16. Simplified Schematic of the IF Interface

The IF's small-signal bandwidth is approximately 45 MHz from IFHI and IFLO through IFOP. The peak output at IFOP is ±560 mV at V_P = 3 V and ±400 mV at the minimum V_P of 2.92 V. This allows some headroom at the demodulator inputs (Pin DMIP), which accept a maximum input of ±150 mV for IFs > 3 MHz and ±75 mV for IFs ≤ 3 MHz (at IFs ≤ 3 MHz, the drive to the demodulators must be reduced to avoid saturating the output amplifiers with higher order mixing products that are no longer removed by the on-board low pass filters).

Since there is no band-limiting in the IF strip, the output-referred noise can be quite high; in a typical application and at a gain of 75 dB, it is about 100 mV rms, making post-IF filtering desirable. IFOP may be also used as an IF output for driving an A/D converter, external demodulator, or external AGC detector. Figure 17 shows methods of matching the optional second IF filter.

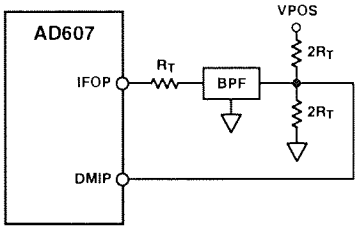

a. Biasing DMIP from Power Supply (Assumes BPF AC-Coupled Internally)

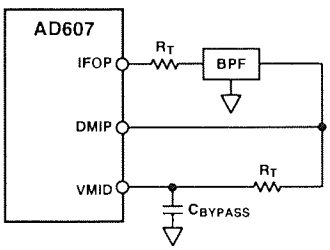

b. Biasing DMIP from VMID (Assumes BPF AC-Coupled Internally)

Figure 17. Input and Output Matching of the Optional Second IF Filter

Gain Scaling and RSSI

The AD607's overall gain, expressed in decibels, is linear-in-dB with respect to the AGC voltage V_G at Pin GAIN. The gain of all sections is maximum when V_G is zero, and reduces progressively up to V_G = 2.2 V (for V_P = 3 V; in general, up to a limit V_P – 0.8 V). The gain of all stages changes in parallel. The AD607 features temperature compensation of the gain scaling. The gain control scaling is proportional to the reference voltage applied to the Pin GREF. When this pin is tied to the midpoint of the supply (VMID), the scale is nominally 20 mV/dB (50 dB/V) for V_P = 3 V. Under these conditions, the lower 80 dB of gain range (mixer plus IF) corresponds to a control voltage of 0.4 V ≤ V_G ≤ 2.0 V. The final centering of this 1.6 V range depends on the insertion losses of the IF filters used. More generally, the gain scaling using these connections is V_P/150 (volts per dB), so scale becomes 33.3 mV/dB (30 dB/V) using a 5 V supply, with a proportional change in the AGC range, to 0.33 V ≤ V_G ≤ 3 V.

Table II lists gain control voltages and scale factors for power supply voltages from 2.92 V to 5.5 V

Alternatively, Pin GREF can be tied to an external voltage reference (V_R) from, for example, an AD1582 (2.5 V) or AD1580 (1.21 V) voltage reference, to provide supply-independent gain scaling of V_R/75 (volts per dB). When using the Analog Devices' AD7013 and AD7015 baseband converters, the external reference may also be provided by the reference output of the baseband converter (Figure 18). For example, the AD7015 baseband converter provides a V_R of 1.23 V; when connected to GREF, the gain scaling is 16.4 mV/dB (60 dB/V). An auxiliary DAC in the AD7015 can be used to generate the MGC voltage. Since it uses the same reference voltage, the numerical input to this DAC provides an accurate RSSI value in digital form, no longer requiring the reference voltage to have high absolute accuracy.

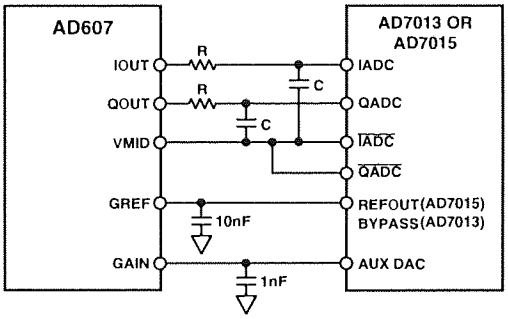

Figure 18. Interfacing the AD607 to the AD7013 or AD7015 Baseband Converters

I/Q Demodulators

Both demodulators (I and Q) receive their inputs at Pin DMIP. Internally, this single-sided input is actually differential; the noninverting input is referenced to Pin VMID. Each demodulator comprises a full-wave synchronous detector followed by a 2 MHz, two-pole low-pass filter, producing single-sided outputs at pins IOUT and QOUT. Using the I and Q demodulators for IFs above 12 MHz is precluded by the 400 kHz to 12 MHz response of the PLL used in the demodulator section. Pin DMIP requires an external bias source at V_P/2; Figure 19 shows suggested methods.

Outputs IOUT and QOUT are centered at V_P/2 and can swing up to ±1.23 V even at the low supply voltage of 2.92 V. They can therefore directly drive the RX ADCs in the AD7015 baseband converter, which require an amplitude of 1.23 V to fully load them when driven by a single-sided signal. The conversion gain of the I and Q demodulators is 18 dB (X8), requiring a maximum input amplitude at DMIP of ±150 mV for IFs > 3 MHz.

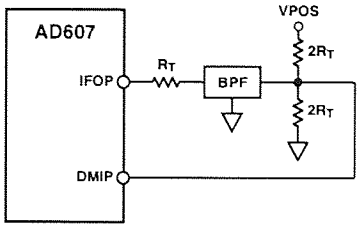

a. Biasing DMIP from Power Supply (Assumes BPF AC-Coupled Internally)

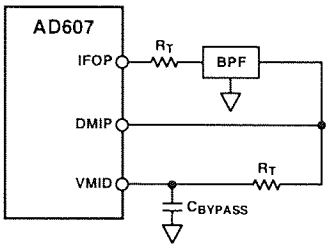

b. Biasing DMIP from VMID (Assumes BPF AC-Coupled Internally)

Figure 19. Suggested Methods for Biasing Pin DMIP at $V_P/2$

For IFs < 3 MHz, the on-chip low-pass filters (2 MHz cutoff) do not attenuate the IF or feedthrough products. Thus, the maximum input voltage at DMIP must be limited to ±75 mV to allow sufficient headroom at the I and Q outputs for not only the desired baseband signal, but also the unattenuated higher-order demodulation products. These products can be removed by an external low-pass filter. In the case of IS54 applications using a 455 kHz IF and the AD7013 baseband converter, a simple one-pole RC filter with its corner above the modulation bandwidth is sufficient to attenuate undesired outputs.

Phase-Locked Loop

The demodulators are driven by quadrature signals that are provided by a variable frequency quadrature oscillator (VFQO), phase-locked to a reference signal applied to Pin FDIN. When this signal is at the IF, in-phase and quadrature baseband outputs are generated at IOUT and QOUT, respectively. The quadrature accuracy of this VFQO is typically –1.2°C at 10.7 MHz. The PLL uses a sequential-phase detector that comprises low power emitter-coupled logic and a charge pump (Figure 20).

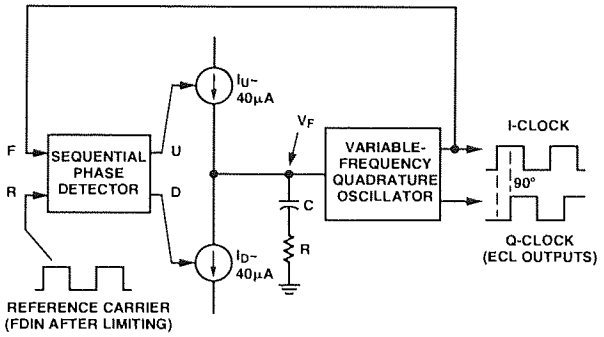

Figure 20. Simplified Schematic of the PLL and Quadrature VCO

The reference signal may be provided from an external source in the form of a high level clock, typically a low level signal (±400 mV) since there is an input amplifier between FDIN and the loop's phase detector. For example, the IF output itself can be used by connecting DMIP to FDIN, which will then provide automatic carrier recover for synchronous AM detection and take advantage of any post-IF filtering. Pin FDIN must be biased at $V_P/2$; Figure 22 shows suggested methods.

The VFQO operates from 400 kHz to 12 MHz and is controlled by the voltage between VPOS and FLTR. In normal operation, a series RC network forming the PLL loop filter is connected from FLTR to ground. The use of an integral sample-hold system ensures that the frequency-control voltage on Pin FLTR remains held during power-down, so reacquisition of the carrier typically occurs in 16.5 µs.

In practice, the probability of a phase mismatch at power-up is high, so the worst-case linear settling period to full lock needs to be considered in making filter choices. This is typically 16.5 µs at an IF of 10.7 MHz for a ±100 mV signal at DMIP and FDIN.

Table II. AD607 Gain and Manual Gain Control Voltage vs. Power Supply Voltage

Power Supply Voltage (V)	GREF (= VMID) (V)	Scale Factor (dB/V)	Scale Factor (mV/dB)	Gain Control Voltage Input Range (V)
3.0	1.5	50.00	20.00	0.400–2.000
3.5	1.75	42.86	23.33	0.467–2.333
4.0	2.0	37.50	26.67	0.533–2.667
4.5	2.25	33.33	30.00	0.600–3.000
5.0	2.5	30.00	33.33	0.667–3.333
5.5	2.75	27.27	36.67	0.733–3.667

Maximum gain occurs for gain control voltage = 0 V.

Bias System

The AD607 operates from a single supply, V_P, usually of 3 V, at a typical supply current of 8.5 mA at midgain and T = 27°C, corresponding to a power consumption of 25 mW. Any voltage from 2.92 V to 5.5 V may be used.

The bias system includes a fast-acting active-high CMOS-compatible power-up switch, allowing the part to idle at 550 µA when disabled. Biasing is proportional-to-absolute temperature (PTAT) to ensure stable gain with temperature.

An independent regulator generates a voltage at the midpoint of the supply ($V_P/2$) that appears at the VMID pin at a low impedance. This voltage does not shut down, ensuring that the major signal interfaces (e.g., mixer-to-IF and IF-to-demodulators) remain biased at all times, thus minimizing transient disturbances at power-up and allowing the use of substantial decoupling capacitors on this node. The quiescent consumption of this regulator is included in the idling current.

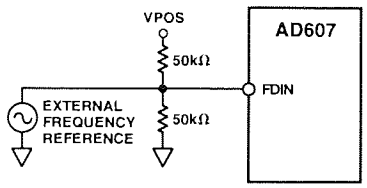

a. Biasing FDIN from Supply when Using External Frequency Reference

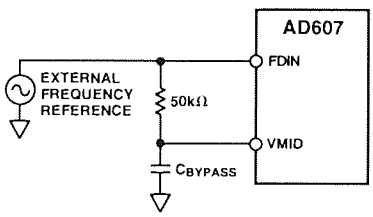

b. Biasing FDIN from VMID when Using External Frequency Reference

Figure 21. Suggested Methods for Biasing Pin FDIN at $V_P/2$

USING THE AD607

In this section, we will focus on a few areas of special importance and include a few general application tips. As is true of any wideband high gain component, great care is needed in PC board layout. The location of the particular grounding points must be considered with due regard to the possibility of unwanted signal coupling, particularly from IFOP to RFHI or IFHI or both.

The high sensitivity of the AD607 leads to the possibility that unwanted local EM signals may have an effect on the performance. During system development, carefully-shielded test assemblies should be used. The best solution is to use a fully-enclosed box enclosing all components, with the minimum number of needed signal connectors (RF, LO, I, and Q outputs) in miniature coax form.

The I and Q output leads can include small series resistors (about 100 Ω) inside the shielded box without significant loss of performance, provided the external loading during testing is light (that is, a resistive load of more than 20 kΩ and capacitances of a few picofarads). These help to keep unwanted RF emanations out of the interior.

The power supply should be connected via a through-hole capacitor with a ferrite bead on both inside and outside leads. Close to the IC pins, two capacitors of different value should be used to decouple the main supply (V_P) and the midpoint supply pin, VMID. Guidance on these matters is also generally included in applications schematics.

Gain Distribution

As in all receivers, the most critical decisions in effectively using the AD607 relate to the partitioning of gain between the various subsections (Mixer, IF Amplifier, Demodulators) and the placement of filters so as to achieve the highest overall signal-to-noise ratio and lowest intermodulation distortion.

Figure 22 shows the main RF/IF signal path at maximum and minimum signal levels.

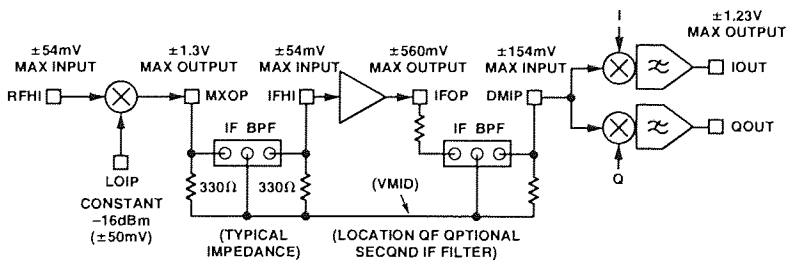

Figure 22. Signal Levels for Minimum and Maximum Gain

As noted earlier, the gain in dB is reduced linearly with the voltage V_G on the GAIN pin. Figure 23 shows how the mixer and IF strip gains vary with V_G when GREF is connected to VMID (1.5 V) and a supply voltage of 3 V is used. Figure 24 shows how these vary when GREF is connected to a 1.23 V reference.

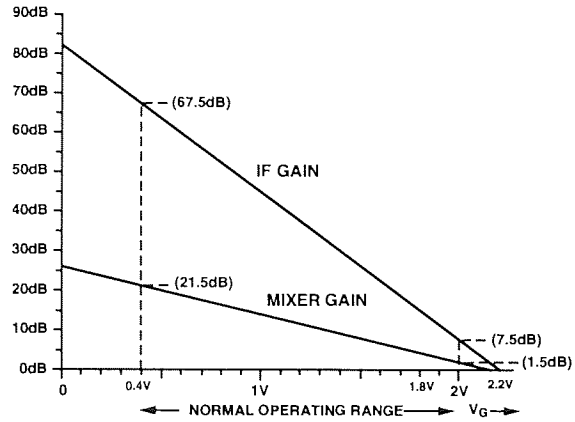

Figure 23. Gain Distribution for GREF = 1.5 V

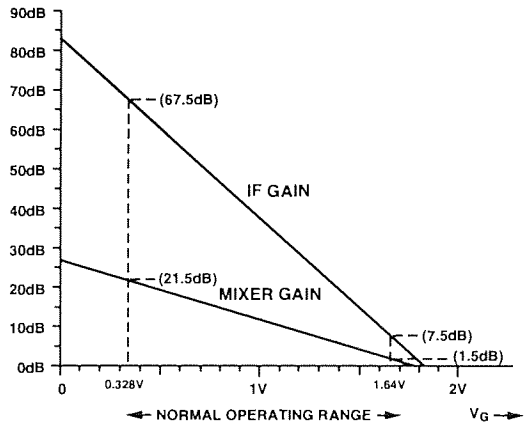

Figure 24. Gain Distribution for GREF = 1.23 V

Using the AD607 with a Fast PRUP Control Signal

If the AD607 is used in a system in which the PRUP signal (Pin 3) is applied with a rise time less than 35 µs, anomalous behavior occasionally occurs. The problem is intermittent, so it will not occur every time the part is powered up under these conditions. It does not occur for any other normal operating conditions when the PRUP signal has a rise time slower than 35 µs. Symptoms of operation with too fast a PRUP signal include low gain, oscillations at the I or Q outputs of the device, or no valid data occurring at the output of the AD607. The problem causes no permanent damage to the AD607, so it will often operate normally when reset.

Fortunately, there is a very simple solution to the fast PRUP problem. If the PRUP signal (Pin 3) is slowed down so that the rise time of the signal edge is greater than 35 µs, the anomalous behavior will not occur. This can be realized by a simple RC circuit connected to the PRUP pin, where R = 4.7 kΩ and C = 1.5 nF. This circuit is shown in Figure 25.

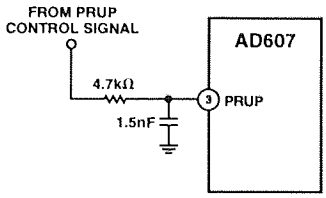

Figure 25. Proper Configuration of AD607 PRUP Signal

All designs incorporating the AD607 should include this circuitry.

Note that connecting the PRUP pin to the supply voltage will not eliminate the problem, since the supply voltage may have a rise time faster than 35 µs. With this configuration, the 4.7 kΩ series R and 1.5 nF shunt C should be placed between the supply and the PRUP pin as shown in Figure 25.

AD607 EVALUATION BOARD

The AD607 evaluation board (Figures 26 and 27) consists of an AD607, ground plane, I/O connectors, and a 10.7 MHz bandpass filter. The RF and LO ports are terminated in 50 Ω to provide a broadband match to external signal generators to allow a choice of RF and LO input frequencies. The IF filter is at 10.7 MHz and has 330 Ω input and output terminations; the board is laid out to allow the user to substitute other filters for other IFs.

The board provides SMA connectors for the RF and LO port inputs, the demodulated I and Q outputs, the manual gain control (MGC) input, the PLL input, and the power-up input. In addition, the IF output is also available at an SMA connector; this may be connected to the PLL input for carrier recovery to realize synchronous AM and FM detection via the I and Q demodulators, respectively. Table III lists the AD607 Evaluation Board's I/O Connectors and their functions.

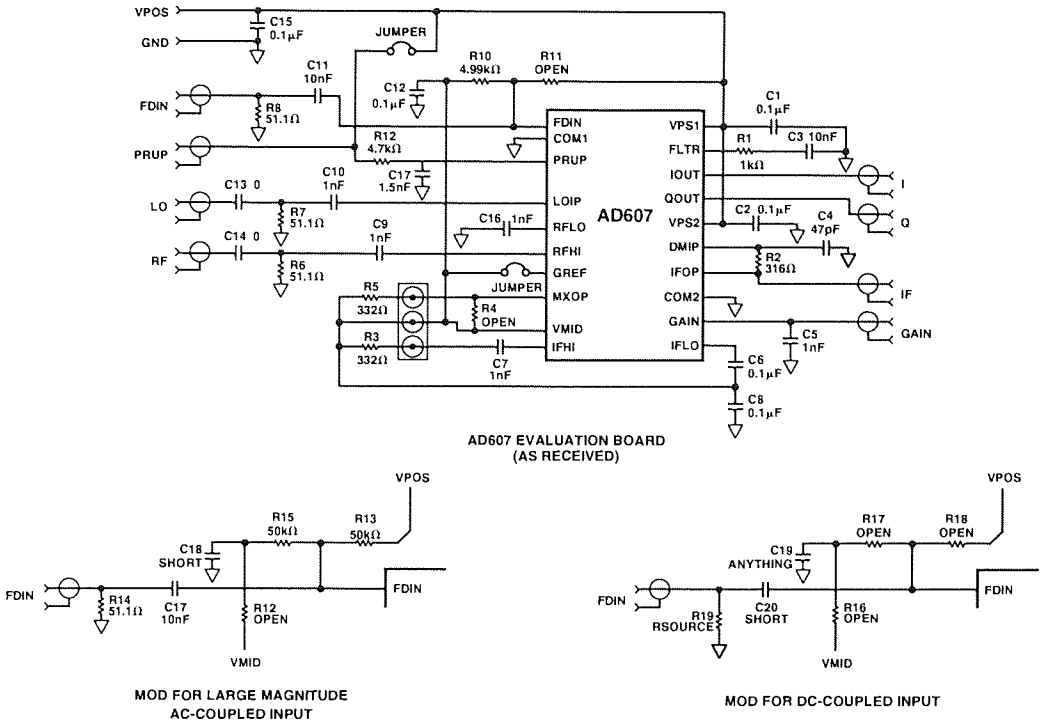

Figure 26. Evaluation Board

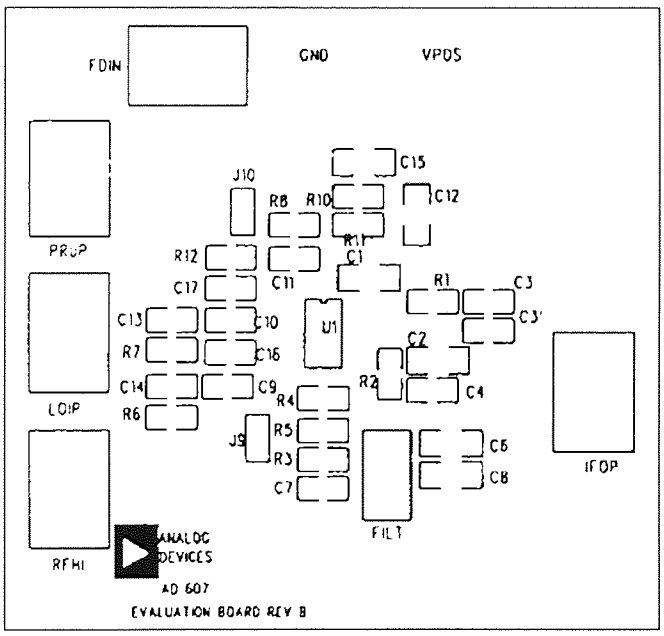

Figure 27a. Evaluation Board Layout, Topside

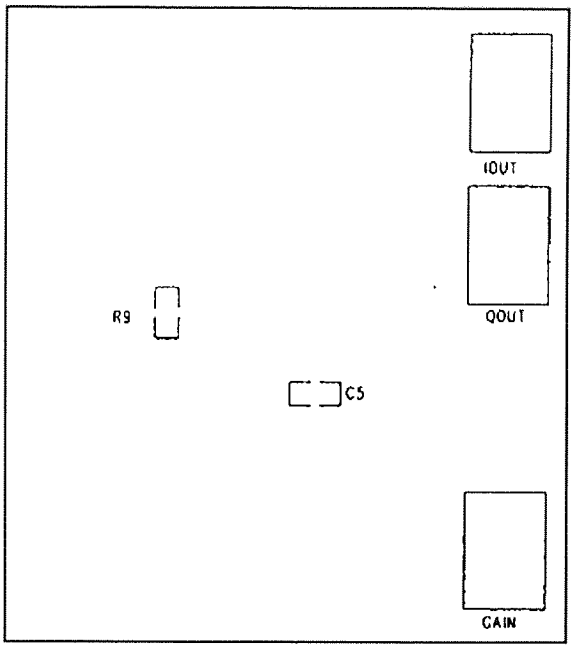

Figure 27b. Evaluation Board Layout, Bottom Side

Table III. AD607 Evaluation Board Input and Output Connections

Reference Designation	Connector Type	Description	Coupling	Approximate Signal Level	Comments
J1	SMA	Frequency Detector Input	DC	±400 mV	This pin needs to be biased at VMID and ac-coupled when driven by an external signal generator.
J2	SMA	Power-Up	DC	CMOS Logic Level Input	Tied to Positive Supply by Jumper J10
J3	SMA	LO Input	AC	−16 dBm (±50 mV)	Input is terminated in 50 Ω.
J4	SMA	RF Input	AC	−15 dBm max (±54 mV)	Input is terminated in 50 Ω.
J5	SMA	MGC Input	DC	0.4 V to 2.0 V (3 V Supply) (GREF = VMID)	Jumper is set for manual gain control input; see Table I for control voltage values.
J6	SMA	IF Output	AC	NA	This signal level depends on the AD607's gain setting.
J7	SMA	Q Output	AC	NA	This signal level depends on the AD607's gain setting.
J8	SMA	I Output	AC	NA	This signal level depends on the AD607's gain setting.
J9	Jumper	Ties GREF to VMID	NA	NA	Sets gain-control scale factor (SF); SF = 75/VMID in dB/V, where VMID = VPOS/2.
J10	Jumper	Ties Power-Up to Positive Supply	NA	NA	Remove to test power-up/-down.
T1	Terminal Pin	Power Supply Positive Input (VPS1, VPS2)	DC	DC	2.92 V to 5.5 V Draws 8.5 mA at midgain connection.
T2	Terminal Pin	Power Supply Return (GND)	DC	0 V	

In operation (Figure 28), the AD607 evaluation board draws about 8.5 mA at midgain (59 dB). Use high impedance probes to monitor signals from the demodulated I and Q outputs and the IF output. The MGC voltage should be set such that the signal level at DMIP does not exceed ±150 mV; signal levels above this will overload the I and Q demodulators. The insertion loss between IFOP and DMIP is typically 3 dB if a simple low-pass filter (R8 and C2) is used, and higher if a reverse-terminated band-pass filter is used.

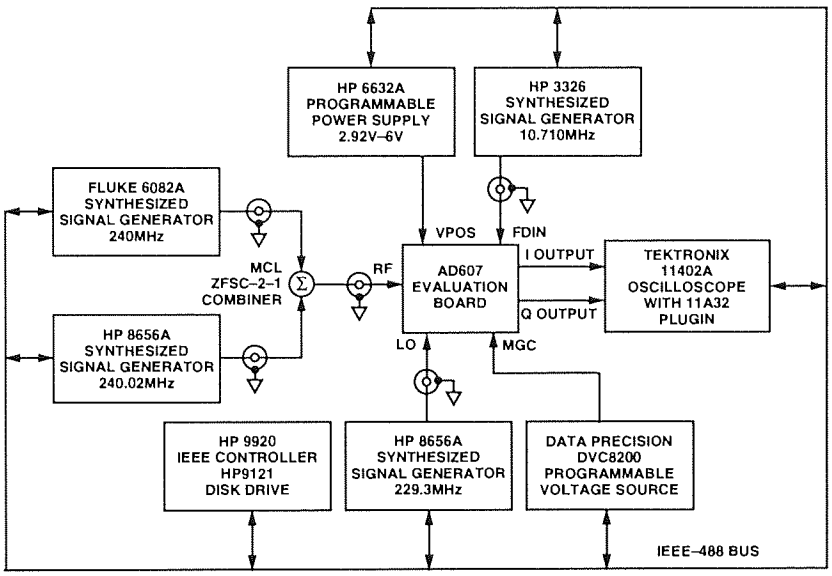

Figure 28. Evaluation Board Test Setup

OUTLINE DIMENSIONS

20-Lead Shrink Small Outline Package [SSOP]
(RS-20)

Dimensions shown in millimeters

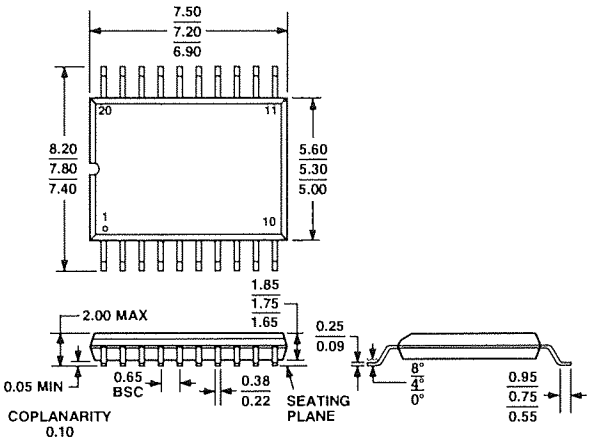

COMPLIANT TO JEDEC STANDARDS MO-150AE

Revision History

Location	Page
11/02—Data Sheet changed from REV. B to REV. C.	
Edits to SPECIFICATIONS	2
Edits to ABSOLUTE MAXIMUM RATINGS	3
Edits to ORDERING GUIDE	3
Changes to TPC 3	11
Edits to PRODUCT OVERVIEW	14
Edits to IF Amplifier section	15
Edits to Gain Scaling and RSSI section	16
Edits to I/Q Demodulators section	16
Edits to Table II	17
Edits to Bias System	18
Edits to Table III	21
Edits to Figure 28	22
OUTLINE DIMENSIONS Updated	23

C00543–0–11/02(C)

PRINTED IN U.S.A.

Appendix B

VPI Transmission Maker

VPI Transmission Maker has been developed for modelling all types of photonics systems and networks, from single-channel TDM systems, to several-hundred channel WDM systems. The graphical user interface (GUI) allows the user to create new or open an existing schematic diagram, place icons representing modules, link the modules together, run the simulation, and display results. A typical view of the simulator is shown in figure B1.

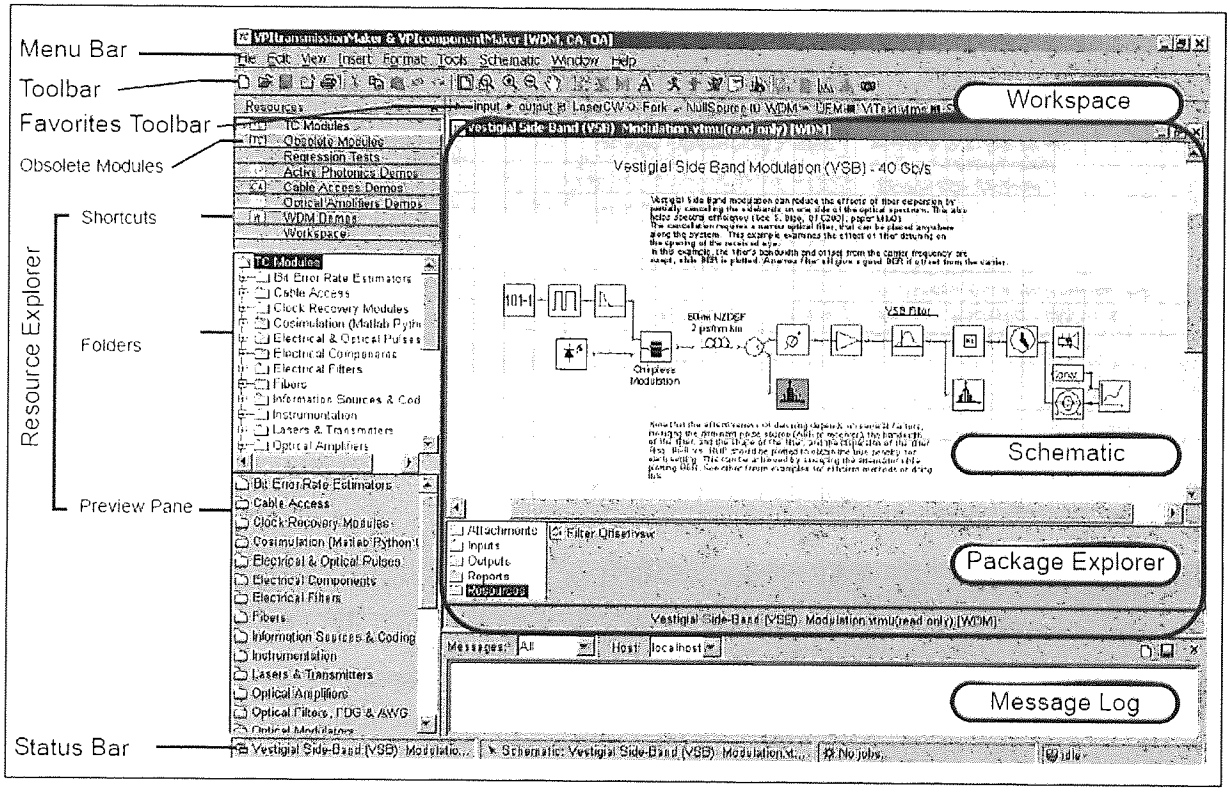

Figure B1 VPI Transmission Maker.

There are many levels of abstraction that can be used for each type of component. At one extreme, each component could be represented by a detailed physical model based on material and structural parameters of the device. This would require intensive computation. Alternatively, the user could choose to represent the component by a Black-Box model, where the parameters are derived solely from external measurements on that device. This is useful at a systems level of modelling. The different levels of abstraction available are shown in figure B2.

VPI Transmission Maker offers a wide range of powerful signal representations. A mixture of these signal representation is used to give a balance between computation speed and accuracy. Block mode signals are used to cover the spectral region where large interactions occur between channels, and where it is necessary to analyze optical data in modulated optical carriers. Parameterised signals represent only the powers of signals, and Noise Binds represent wide-band noise in a system using a coarse frequency grid. The signal representations available are shown in figure B3.

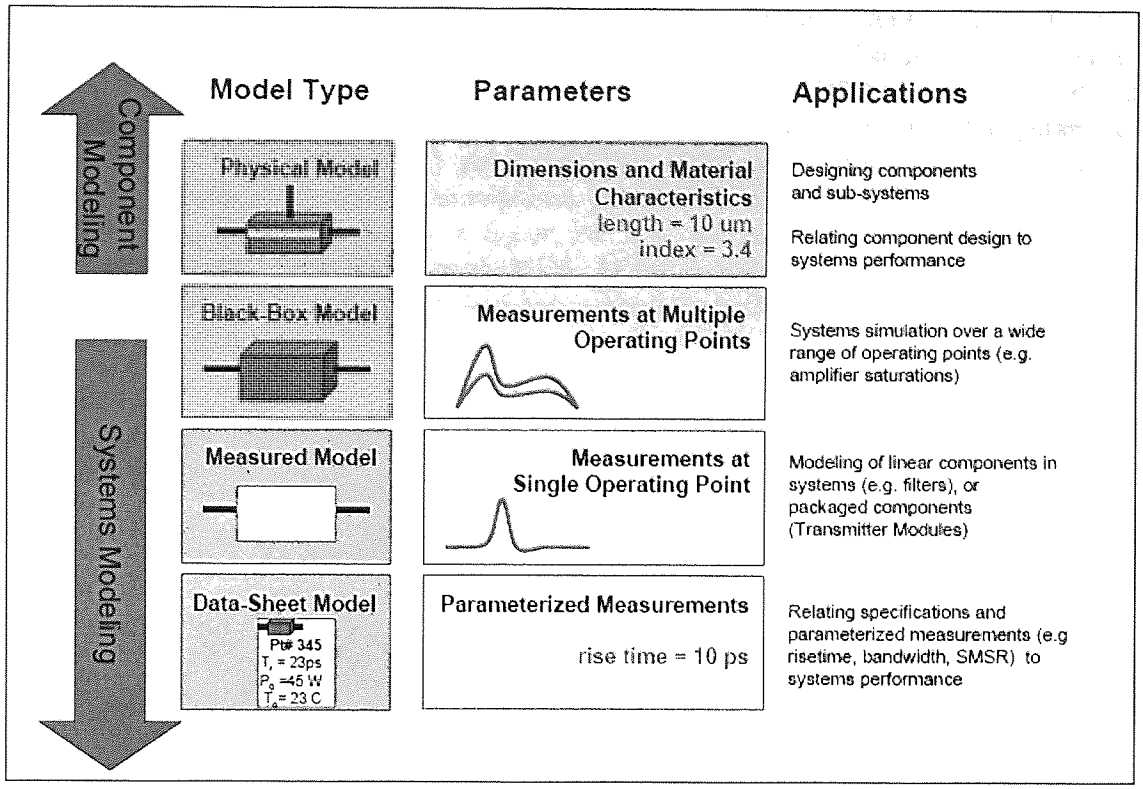

Figure B2 Different levels of abstraction.

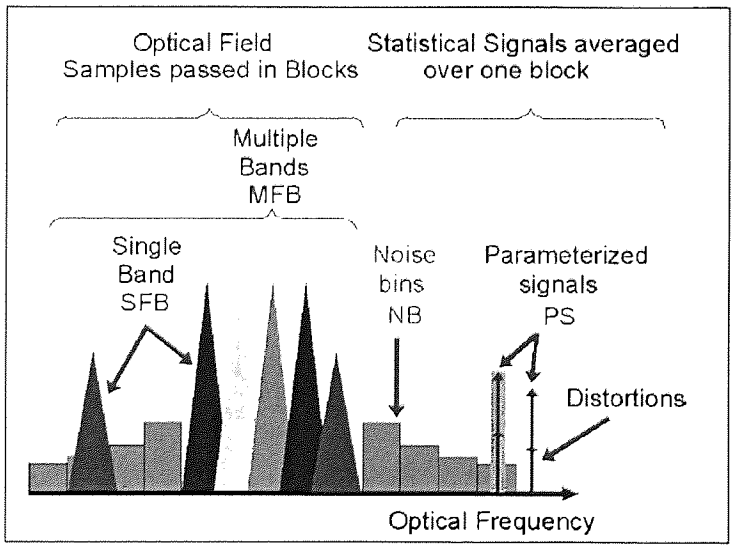

Figure B3 Different signal representations – Block Mode and Parameterised signals.

In the LME simulations, the LME pulse is represented in block mode while the ASE is represented by Noise Bins. The transmitter is modulated by a PRBS generator with a CW laser source as the optical carrier. The signal is then propagated into the fibre modules, which are based on the split-step Fourier method. The split-step Fourier method divides the fiber into

alternate sections of two types. The first type represents the dispersion in the frequency domain, the second represents the nonlinearity in the time domain. The choice of step-size is crucial in achieving a balance between computation time and accuracy. The EDFA module simulates a system-level amplifier with a wavelength-independent gain and Noise Figure. By parameter selection the module may act in a (a) gain-controlled, (b) output power-controlled, or (c) saturation (uncontrolled) mode. In the simulations, the EDFA is operated in saturation mode where the gain characteristics is shown in figure B4. The Saturation Power P_{sat} specifies the optical power at the 3 dB-optical-gain-compression. At the receiver end, the signal is optically filtered, detected, clock-recovered, and analysed by visualiser modules such as BER estimators, sampling scopes and optical spectrum analysers.

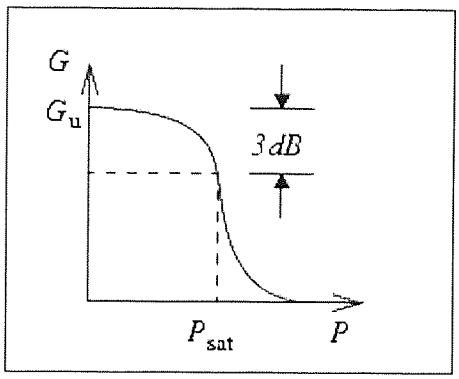

Figure B4 Gain characteristics of an EDFA.